INVESTIGATING THE INHIBITION MECHANISM OF L,D-TRANSPEPTIDASE 5 FROM *MYCOBACTERIUM TUBERCULOSIS* USING COMPUTATIONAL METHODS

BY: GIDEON FEMI TOLUFASHE
216076453

Submitted in fulfilment of the requirements for the degree of Doctor of Philosophy in

Pharmaceutical Chemistry

School of Health Sciences, College of Health Sciences, University of KwaZulu-Natal, Durban, South

Africa.

2018

PREFACE

The work described in this thesis was conducted at the Catalysis and Peptide Research Unit, Westville Campus, University of KwaZulu-Natal, Durban, South Africa, under the supervision of Dr Bahareh Honarparvar, Prof. H.G. Kruger and Dr G.E.M. Maguire.

This work has not been submitted in any form for any degree or diploma to any institution, where use has been made of the work of others, it is duly acknowledged in the text.

Supervisors:

Dr B. Honarparvar_____   Date <u>30/10/2018</u>

Prof. H. G. Kruger_____   Date _____

Dr. G.E.M Maguire_____   Date _____

As candidate's supervisor I agree to the submission of this thesis.

DECLARATION
DECLARATION I- PLAGIARISM

I, **Gideon Femi Tolufashe** declare that

(i). The research reports in this thesis, except where otherwise indicated, is my original work.

(ii). This thesis has not been submitted for any degree or examination at any other university.

(iii). This thesis does not contain other person's data, pictures, graphs or other information, unless specifically acknowledged as being sourced from other persons.

(iv). This thesis does not contain other person's writing, unless specifically acknowledged as being sourced from other researchers. Where other written sources have been quoted, then:

a. Their words have been re-written, but the general information attributed to them has been referenced.

b. Where their exact words have been used, then their writing has been placed in italics and inside quotation marks, and referenced.

(v). This thesis does not contain text, graphics or tables copied and pasted from the internet, unless specifically acknowledged, and the source being detailed in the thesis and in the references sections.

Signed …………………………

DECLARATION II-PUBLICATION

List of publications included in this Thesis

1. **Gideon F. Tolufashe,** Victor T. Sabe, Colins U. Ibeji, Thandokuhle Ntombela, Thavendran Govender, Glenn E. M. Maguire, Hendrik G. Kruger, Gyanu Lamichhane, and Bahareh Honarparvarar. (2018). **Structure and function of L,D- and D,D-transpeptidase family enzymes from** *Mycobacterium tuberculosis*. *Current Medicinal Chemistry*. DOI: 10.2174/0929867326666181203150231

Contributions:

Tolufashe, G.F: Main author- contributed to the project by performing all literature reviews, manuscript preparation and writing.

Sabe, V.T, Ibeji, C.U, Ntombela, T., Govender, T., Lamichhane, G.: Helped with technical, experimental and financial supports.

Honarparvar, B.: Supervisor

Kruger, H. G. and Maguire, G. E.: co-supervisors with academic contribution

2. **Gideon F. Tolufashe,** Thavendran Govender, Amit K. Halder, Collins U. Ibeji1, Monsurat M. Lawal, Thandokuhle Ntombela, Glenn E. M. Maguire, Gyanu Lamichhane, Hendrik G. Kruger, and Bahareh Honarparvar. **Inhibition of** *Mycobacterium tuberculosis* **L,D-transpeptidase 5 by carbapenems: MD and QM/MM Mechanistic Studies,** *ChemistrySelect* **2018, 3, 1-11. DOI:** 10.1002/slct.20180318

Contributions:

Tolufashe, G.F: Main author- contributed to the project by performing all literature reviews, manuscript preparation and writing.

Halder, A.K., Ibeji, C.U, Lawal, M.M., Ntombela, T., Govender, T., Lamichhane, G.: Provided assistance with technical, experimental and financial supports.

Honarparvar, B.: Supervisor

Kruger, H. G. and Maguire, G. E.: co-supervisors with academic contribution

3. Victor T. Sabe**, Gideon F. Tolufashe** , Collins U. Ibeji, Sibusiso B. Maseko, Thavendran Govender , Glenn E. M. Maguire, Gyanu Lamichhane, Bahareh Honarparvar and Hendrik G. Kruger. **Identification of potent L,D-transpeptidase 5 inhibitors for** *Mycobacterium tuberculosis* **as potential anti-TB leads: Virtual Screening and Molecular Dynamics Simulations**
Manuscript Submitted to *Journal of molecular modelling* **on 5 October 2018**

Contributions:

Victor T. Sabe: Principal investigator in the design of this project and first author responsible for writing and preparation of this manuscript.

Gideon F. Tolufashe and Collins U. Ibeji: Provided technical assistance on the project. He did part of the calculations and writing of the manuscript.

Sibusiso Maseko: Performed experimental work.

Thavendran Govender and Gyanu Lamichhane: Provided technical and experimental assistance in the overall project.

Bahareh Honarparvar: Supervisor.

Hendrik G. Kruger and Glenn E. M. Maguire: Co-supervisors.

4. **Gideon F. Tolufashe,** Victor T. Sabe, Collins U. Ibeji, Monsurat M. Lawal, Thavendran Govender, Glenn E. M. Maguire, Gyanu Lamichhane, Hendrik G. Kruger and Bahareh Honarparvar. (2018) **Inhibition Mechanism of L,D-transpeptidase 5 in presence of the β-lactams using ONIOM Method.** *Journal of molecular graphics and modelling*, 87, 204-210. DOI: 10.1016/j.jmgm.2018.11.009

Contributions:

Victor T. Sabe: Principal investigator in the contextualisation and design of the project.

Gideon F. Tolufashe: Responsible for the calculations, writing and preparation of the manuscript.

Collins U. Ibeji and Monsurat M. Lawal: Provided technical assistance to the project.

Bahareh Honarparvar: Supervisor.

Hendrik G. Kruger and Glenn E. M. Maguire: Co-supervisors.

Publication not included in this Thesis

Ibeji, Collins U., **Gideon F. Tolufashe**, Thandokuhle Ntombela, Thavendran Govender, Glenn EM Maguire, Gyanu Lamichhane, Hendrik G. Kruger, and Bahareh Honarparvar. "The catalytic role of water in the binding site of L, D-Transpeptidase 2 within acylation mechanism: A QM/MM (ONIOM) modeling." *Tuberculosis* (2018).

RESEARCH OUTPUTS
CONFERENCE PRESENTATIONS

1. Poster presentation "Binding free energy calculations of carbapenem inhibitors against L,D-transpeptidase 5 using molecular dynamics(MD) simulation", **CHPC National Meeting & Conference,** East London, 4-9 December 2016.

2. Oral presentation "Inhibition mechanism of L,D-Transpeptidase 5 from Mycobacterium Tuberculosis in presence of Carbapenems: Molecular Dynamics study", **College of Health Sciences Annual Research Symposium**, Nelson Mandela Medical School, K-RITH Building, 5-6 October 2017.

DEDICATION

This thesis is dedicated to God Almighty, my ever-supporting father, loving wife and daughter.

ACKNOWLEDGEMENTS

TABLE OF CONTENTS

LIST OF FIGURES

CHAPTER ONE

CHAPTER TWO

CHAPTER THREE

CHAPTER FOUR

CHAPTER FIVE

LIST OF TABLES
CHAPTER TWO

CHAPTER THREE

CHAPTER FOUR

CHAPTER FIVE

ABBREVIATIONS

Tuberculosis	TB
Mycobacterium tuberculosis	*Mtb*
L,D-transpeptidase 5	Ldt_{Mt5}
Transition state	TS
Molecular dynamics	MD
Quantum mechanics	QM
Density functional theory	DFT
Molecular mechanics	MM
Hybrid quantum mechanics/molecular mechanics	QM/MM
Ertapenem	ERT
Imipenem	IMI
Meropenem	MERO
Natural substrate	SUB
World Health Organization's	WHO
Millennium Development Goals	MDGs
Sustainable Development Goals	SDGs
Peptidoglycan	PGN
N-acetylglucosamine	GlcNAc
N-acetylmuramic acid	MurNAc
Meso-diaminopimelic acid	mDAP
Penicillin binding proteins	PBPs
Food and Drug Administration	FDA
Protein data bank	PDB
Monte Carlo	MC

Generalized Born	GB
Polarisable Continuum Models	PCM
Virtual screening	VS
High-throughput screening	HTS
Isothermal titration calorimetry	ITC
Molecular Mechanics-Generalized Born Surface Area	MM-GBSA
Principal component analysis	PCA
L,D-transpeptidases	DDT
L,D-transpeptidases	LDT
Root mean square deviation	RMSD
Root mean square fluctuation	RMSF
Intrinsic reaction coordinates	IRC
Glide simple precision	SP
Glide extra precision	XP
Glide extra precision	XP
General AMBER force field	GAFF
Partial Mesh Ewald	PME
Highest occupied molecular orbitals	HOMOs
Lowest unoccupied molecular orbitals	LUMOs

ABSTRACT

Tuberculosis (TB) is one of the world's deadliest diseases caused by the bacterium, *Mycobacterium tuberculosis* (*Mtb*). Peptidoglycan is the exoskeleton of bacterial cells and is required for their survival and growth including *Mtb*. For *Mtb*, a mycobacterium, the final step of peptidoglycan synthesis involves the generation of 4→3 and 3→3 transpeptide crosslinks catalyzed by D,D-transpeptidase and L,D-transpeptidase (Ldt) enzymes, respectively. Unlike in most other bacteria, for *Mtb*, the majority of the cross-links are generated by L,D-transpeptidases. *Mtb* genome encodes five Ldt paralogs, namely Ldt_{Mt1} to Ldt_{Mt5}.

Any *Mtb* strain that lacks a functional copy of an Ldt, namely L,D-transpeptidase 5 (Ldt_{Mt5}), displays aberrant growth phenotype and is more susceptible to killing by cell wall perturbing agents including carbapenems which are considered the last resort antibiotics to treat resistant bacterial infections in humans. Carbapenems inactivate L,D-transpeptidases by acylation, although differences in antibiotic side chains modulate drug binding and acylation rates. However, it is known that carbapenems do not show any reasonable inhibitory activities against Ldt_{Mt5} and also an adduct of meropenem exhibited slow acylation.

The inhibition mechanism of L,D-transpeptidase 5 against carbapenems were investigated using molecular dynamics and transition state (TS) structural models. Virtual screening of new compounds was also carried out in this present study. The investigation was adopted to clarify the acylation process of carbapenems, compute their activation energies and propose new *β*-lactams inhibitors with lower activation energies in comparison to the known FDA approved carbapenems.

Molecular dynamics (MD), Quantum mechanics (QM) methods which include density functional theory (DFT) models, molecular mechanics (MM), hybrid QM/MM and virtual screening methods were used together to probe and give a better understanding on this topic. To understand the macromolecular structure-to-function relationships, molecular dynamics simulations were proposed. The complexes [ertapenem (ERT), imipenem (IMI) and meropenem (MERO) with Ldt_{Mt5}] were simulated and trajectory analyses were carried out using CPPTRAJ module implemented in Amber 14 package. To further understand the catalytic reaction mechanism of Ldt_{Mt5} with the selected carbapenems, the possible reaction pathways (thermodynamics and kinetics) were investigated using a two-layered ONIOM [B3LYP/6-31+g(d,p):Amber] model. Due to the high activation energies calculated for meropenem and imipenem, which correspond to experimental observations, the need for screening of potential inhibitors against Ldt_{Mt5} arises.

Herein, we have aimed to find new compounds with better binding free energies for Ldt_{Mt5}. The automated docking process was performed using Autodock Vina and Schrödinger Maestro programs to screen the

libraries of compounds. Subsequently, the molecular dynamics of compounds with best binding affinities were simulated to calculate the binding free energies of the drug-enzyme precomplexes. Thereafter, the catalytic mechanism of six β-lactams within the enzyme was studied using hybrid QM/MM; Our own N-layered Integrated molecular Orbital and Molecular mechanics (ONIOM) method. Activation energies for these drugs were calculated.

The study on the molecular interactions of carbapenems with Ldt_{Mt5} confirms that the computational inhibitor-enzyme precomplex model for transpeptidases correctly reflects experimental observations in terms of the activity and binding energies. In addition, the high free energies of activation ($\Delta G^{\#}$) for meropenem and imipenem, explain the reason behind inefficient binding of these carbapenems to Ldt_{Mt5} (**Chapter 3**). One of the first aims of this study was to find new β-lactams compounds that will potentially inhibit Ldt_{Mt5}. This was achieved *via* virtual screening, molecular dynamics and calculation of activation energies of a six-membered cyclic TS in the active pocket of the enzyme. Out of the 12766 compounds tested against Ldt_{Mt5}, 37 compounds showed favourable docking scores (**Chapter 4**). These compounds were further analysed to determine the activation energies. It was also observed that several of the compounds showed an improved and lower activation free energies when compared to the previously calculated for imipenem and meropenem for the acylation step for Ldt_{Mt5} (**Chapter 5**). Finally, the last chapter (Chapter 6) gathers the conclusion of the work. The outcome of this study provides insight into the design of a potential novel leads for Ldt_{Mt5}.

Keywords: *Mycobacterium tuberculosis* (*Mtb*); L,D-transpeptidase 5 (Ldt_{Mt5}); Carbapenems; Molecular dynamics (MD); quantum mechanics/molecular mechanics (QM/MM), Catalytic mechanism; Virtual Screening.

CHAPTER ONE

INTRODUCTION

1.1 Tuberculosis

Mycobacterium tuberculosis (*Mtb*) is the causative organism responsible for TB[1]. TB is transmitted through droplet infection and starts when an infected person coughs or spits, which results in the bacterium going into the air and being inhaled by a new host. If infection occurs the bacteria will later develop in the host. TB can occur as latent infection where someone has been infected with the bacteria but does not have any symptoms of the active disease. Pulmonary TB can affect the lungs and causes symptoms, or as extrapulmonary TB which occur outside the lungs[2-4].

The World Health Organization's (WHO) target to halt and reverse TB incidence from 2011 to 2015 supported the UN Millennium Development Goals (MDGs) of stopping and beginning to reverse the epidemic by 2015. In addition, statistics showed that the overall TB death rate in 2015 was 47% less than what was reported in 1990 and that the objective of a 50% decrease was not achieved. The objectives were achieved in some regions, excluding African, Europe and in a few high burden countries[5, 6]. WHO has gone one step further and set a 2035 target of 95% reduction in deaths and a 90% decline in TB incidence – like the current levels in low TB incidence countries today[7].

Statistics show that approximately 10 million persons were regarded as being infected with TB in 2017, of whom 5.8, 3.2 and 1.0 million were men, women and children respectively, with 9% being HIV-positive worldwide[7]. In order to reduce the growing burden of new TB cases, discovering and treatment gaps must be targeted, funding gaps closed, and novel techniques established.

It has been five decades since the introduction of effective antibiotics to combat TB[8]. As a result of the endemic and persistent occurrence of TB, the United Nations adopted the Sustainable Development Goals (SDGs) in 2015 to be achieved in 2030 to set the pace for a new direction to end the global TB prevalence. The targets are a 90% decrease in TB mortality and an 80% decrease in the TB occurrence rate by 2030, related to 2015[9]. The inability to curb TB prevalence is a result of *Mtb* mutants that have become drug-resistant toward the age-long traditional anti-mycobacterial drugs. For example, isoniazid and rifampicin, among the early therapies are no longer effective against drug resistant TB, therefore there is a need for immediate development of new and potent antibacterial drugs[10].

1.2 Peptidoglycan synthesis in Mycobacterium tuberculosis

The peptidoglycan (PGN) is one of three major layers linked to the cytoplasmic membrane, the others being mycolic acids and arabinogalactan, all of which are inside the *Mtb* cell wall[11, 12]. PGN is accountable for major cellular mechanisms of *Mtb*, for example, cell growth and division, and revitalization from inactivity. The bacteria can endure hostile physical and chemical environments or nutrient starvation[13], especially in its metabolically inactive state. This microbial inactive state is the cause of the dormant infection affecting one-third of the world's population. Thus, peptidoglycan is a crucial 'organelle' that is needed for the survival and growth of *Mtb* [14, 15].

PGN biosynthesis starts with the addition of 1–4-linked-N-acetylglucosamine (GlcNAc) and N-acetylmuramic acid (MurNAc) cross-linked by tiny peptidoglycan stems (**Figure 1.1**). PGN in *Mtb* is categorized as meso-diaminopimelic acid (mDAP)-type, as it contains a DAP residue at the third position of the peptidoglycan stem. The UDP-MurNAc-pentapeptide is produced by adding L-alanine to the lactate moiety of the UDP-MurNAc, and the following chronological addition of D-glutamic acid, DAP and D-alanyl-D-alanine dipeptide to form UDP-MurNAc pentapeptide[11]. The transmission of the phospho-MurNAc-pentapeptide moiety of the nucleotide to the lipid carrier and the addition of GlcNAc occurs at the membrane step of peptidoglycan synthesis. The whole antecedent related to the lipid carrier is translocated via the membrane and is polymerized by glycosyltransferases and D,D-transpeptidase activity. The cleavage of the D-Ala^4-D-Ala^5 bond belonging to the pentapeptide donor is achieved by these enzymes, therefore linking the carbonyl atom of D-Ala^4 to the side chain amine of mDap at the third location of an acceptor stem (4→3 cross-linkage). β-Lactam antibiotics are structural equivalents of the D-Ala^4-D-Ala^5 extreme of the antecedents and act as suicide substrates of the penicillin binding proteins (PBPs). The mDap^3-D-Ala^4 bond of a tetrapeptide donor is cleaved by L,D-transpeptidases and links the carbonyl of mDap3 to the acceptor stem (3→3 cross linkages)[16].

The peptidoglycan of *Mtb* exhibits 80% occurrence of 3→3 cross linkages made by L,D-transpeptidation[16], whereas the 4→3 peptidoglycan cross linkages are predominantly generated by PBPs throughout the exponential period of growth[17].
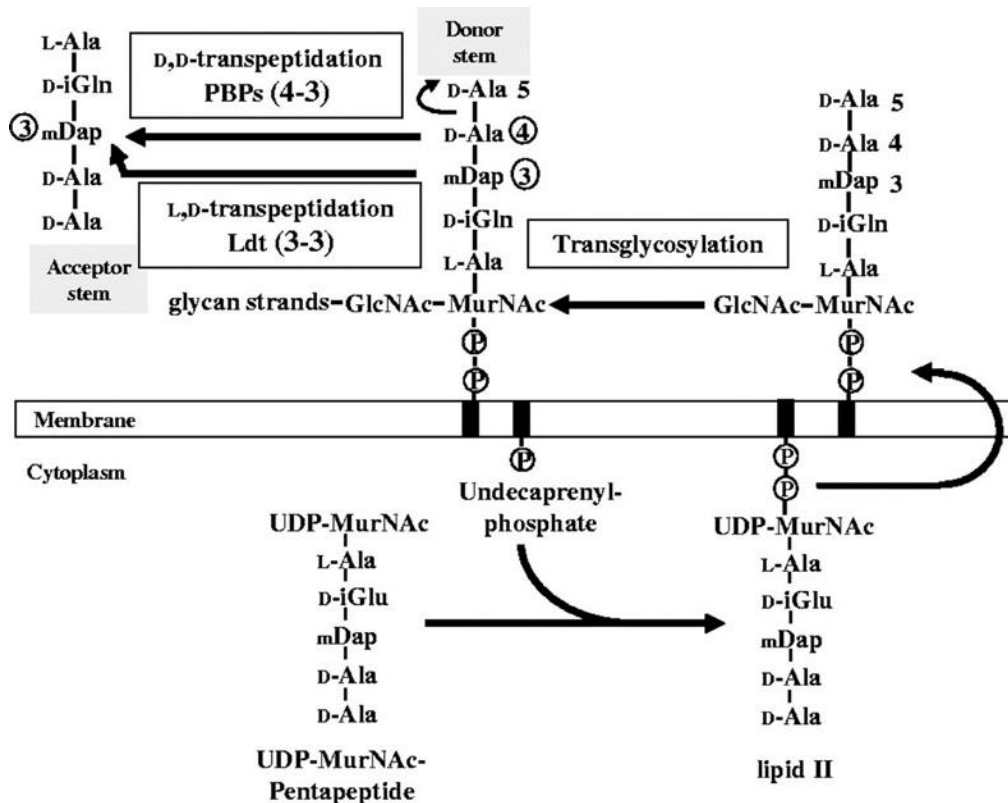
Figure 1.1 Illustration of peptidoglycan synthesis[16]

Both L,D and D,D transpeptidase enzymes should be inhibited simultaneously to inhibit biosynthesis of the peptidoglycan layer and, consequently, kill the bacteria[18].

1.2.1 L,D-transpeptidases from Mycobacterium tuberculosis

L,D-transpeptidation was first reported in wild-type strains of *Enterococcus faecium* and linked with a side catalytic process of D,D-transpeptidases needed in PGN production[19]. It was reported that *Enterococcus faecium* was 3% 3→4 cross-linked, making it insignificant, while *Mtb* showed 80% 3→3 cross-linkages, making L,D-transpeptidase an attractive target[20]. This family of enzymes utilize cysteine in its active site, while serine fulfils the same role for D,D-transpeptidases[21, 22].

The genome of *Mtb* contains five mutants of L,D-transpeptidases (Ldt$_{Mt1}$, Ldt$_{Mt2}$, Ldt$_{Mt3}$, Ldt$_{Mt4}$ and Ldt$_{Mt5}$), with 1 and 2 being reported to be responsible for in vitro peptidoglycan cross-linkage assay[17, 23]. Ldt$_{Mt1}$ is believed to show a distinct function in peptidoglycan adaptation to the non-replicative form of the bacillus[16]. Ldt$_{Mt2}$ is known to be essential for virulence in a mouse model of acute infection[23], while Ldt$_{Mt5}$ performs a major and distinct role in the good maintenance of *Mtb* cell wall integrity[21].

1.2.2 Carbapenem derivatives as inhibitors of L,D-transpeptidases

Carbapenem antibiotics were initially developed from thienamycin[24, 25], a naturally occurring product discovered in culture filtrates of *Streptomyces cattleya*[26]. The *β*-lactams were discovered in the 1920s[27] and

first used as therapeutic agents in the 1940s[28] against an enzyme from the bacteria. Since then, this family of drugs has played a major role in antibiotherapies[29]. These compounds are thus one of the most important antibiotic groups, which include cephalosporins monobactams, penicillin derivatives, β-lactamase, and carbapenems inhibitors. Among the aforementioned categories, carbapenems have proven to exhibit the widest range of bioactivities and they provide safe and effectual treatments in dealing with dangerous infections triggered by Gram-positive, Gram-negative and anaerobic microbial pathogens[30, 31].

In 1985, the USA Food and Drug Administration (FDA) organization approved imipenem, the first commonly used carbapenem drug for the treatment of serious bacterial infections. Application of meropenem for human use was endorsed in 1995, thereafter ertapenem in 2001, while doripenem became available in 2007. Apart from imipenem, all carbapenems are stable against the mammalian kidney dehydropeptidase[32]. The weight-dosage adjustment of imipenem is required to minimize the chance of seizures[33]. Ertapenem and doripenem can be given once per day due to their high target affinity and circulating stability[31, 34]. Possible side effects can be reduced if smaller effective doses of the latter drugs are used, as well as the development of resistance[35]. Presently, complex intra-abdominal and urinary tract infections are treated with ertapenem and doripenem [36,37].

The first study to explore the kinetics and processes of inactivation of some selected carbapenems and cephalosporins against L,D-transpeptidase Ldt$_{Mt1}$ in Mtb was conducted by Dubee et al[17]. The study revealed that the families of drugs form covalent adducts with Ldt$_{Mt1}$, while the acylation with cephalosporins is not fast, and resulted in the removal of one of their side chains. The evaluation of the kinetic rate constants for drug binding, acylation and acyl enzyme hydrolysis indicated that carbapenems and cephems can be employed together to inhibit peptidoglycan biosynthesis in Mtb[17].

In another study, the structure of Ldt$_{Mt2}$, an L,D-transpeptidase inherent in $Mtb,$ was crystallized by Böth and co-workers. They used mass-spectrometric analysis to demonstrate that Ldt$_{Mt2}$(Cys354) forms covalent adducts with the β-lactam antibiotics imipenem and ampicillin[22]. In addition to the previously reported binding of imipenem and meropenem to Ldt$_{Mt2}$ using ITC[38], they suggested that Ldt$_{Mt2}$ can identify and bind a variety of β-lactam antibiotics.

1.2.3 Catalytic mechanism of L,D-transpeptidases

The catalytic mechanism of L,D-transpeptidases from $Mtb,$ and the atomistic details of their transition states provide useful information for the design of new antituberculosis drugs[39]. So far, two catalytic mechanism proposals have been reported for these enzymes in Mtb. Biarrote-Sorin and co-workers[40] reported on two reaction pathways to the catalytic cysteine, one for the acyl donor and the other for the acyl-acceptor substrates. Erdemli et $al.$[38] gave the most recent proposal for the catalytic process, which was also based on cysteine proteases process. Erdemli's approach provides an easier pathway for the catalytic process in comparison to the Biarrotte-Sorin approach[18]. Here, the L,D-transpeptidase will undergo various

configurational variations within the flap region in order to enable the natural substrates to enter and to discharge the adducts with the binding site channel[40]. The catalytic mechanism proposed for Ldt_{Mt2}[38] (**Figure 2**) happens in two steps. In the first step (acylation), the formation of the catalytic Cys354 thiolate by hydrogen removal is followed by an attack on the carbonyl carbon of the natural substrate, resulting in a tetrahedral intermediary. The addition of hydrogen to His336 imidazolium group results in the D-Ala being given away after the intermediary thioester is formed. In the second step (deacylation), an additional peptidoglycan stem goes in the binding site and binds to active site residues using the side chain amide of the m-A2pm3′ residue. His336 serves as a catalytic base by removing a hydrogen atom from the amine group of the mA2pm3′ residue, although the same amine group does a nucleophilic attack on the carbonyl carbon of acyl-enzyme[18, 38].

A computational approach was carried out using QM/MM MD simulations on Ldt_{Mt2} with substrate[18] on the aforementioned described catalytic mechanism as presented in **Figure 1.2.**
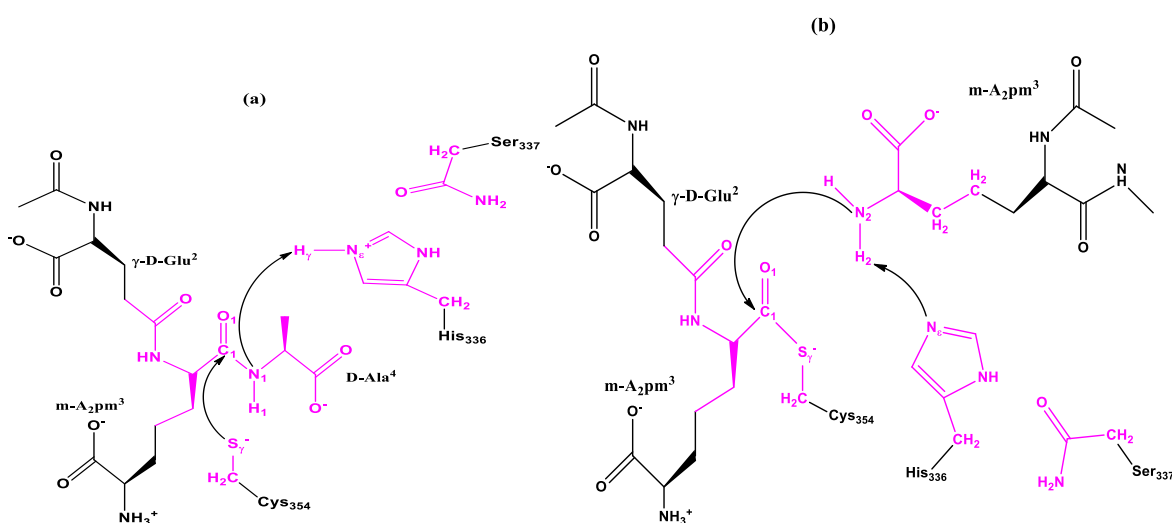
Figure 1.2 (a) The acylation step and (b) Deacylation step process in the binding site of Ldt_{Mt2}. Diagram was adapted from Silva et al.[18]

The free energy results derived from the PMF data revealed that in the entire binding process of a four-membered ring transition state, the rate-limiting stage occurs at the acylation stage. This supports the experimental observation[18] of the acylation step proposed by Erdemli[38]. In a more recent study in our group, the process of nucleophilic attack by Cys354 thiol in Ldt_{Mt2} to the acyl carbon of the β-lactam, followed by concerted proton transmission to the β-lactam nitrogen atom via a four (without the involvement of water) and water aided six-membered ring transition state models[41] was investigated.

5

Papain[42, 43], another cysteine protease family, also revealed a similar acylation stage in which the first step is proposed to be a proton transfer to form a zwitterionic form (i.e. Cys-S−/His-H+ ion-pair), and the second step is the nucleophilic attack on the carboxyl carbon of the substrate accompanied by the dissociation of 4-nitroanilide[42].

1.2.4 Structural and functional behaviour of L,D-transpeptidase 5

L,D-transpeptidase 5 creates 3→3 cross-links in the peptidoglycan, catalysing the joining of the mDap(3)-D-Ala(4) bond of a tetrapeptide donor stem, and the formation of a bond between the carbonyl of mDap(3) of the donor stem and the side chain of mDap(3) of the acceptor stem[21]. L,D-transpeptidase 5 is peculiar for donor substrates containing a tetrapeptide stem, as it cannot use pentapeptide stems. The free and meropenem bound crystal structures of an *N*-terminally shortened Ldt_{Mt5} protein lacking the hydrophobic domain was predicted to be a membrane anchor for this protein. The structures were determined using X-ray crystallography with resolution solved to 2.8 Å. RMSD[21]. The shortened enzyme showed a large degree of sequence similarity to Ldt_{Mt2} (31%) when compared to the full-length enzyme of Ldt_{Mt5} (28%). Ldt_{Mt5} comprises of a proline-rich extension of the *C*-terminal subdomain (amino acids 417-451) that are not present in all other *Mtb* L,D-transpeptidases[21]. The free enzyme and meropenem bound crystals to have a $P6_222$ space group with comparable cell dimensions and one molecule in the asymmetric unit[21]. The structures are available in the protein data bank (PDB) with the accession codes 4Z7A (Free Ldt_{Mt5}) and 4ZFQ (Meropenem-Ldt_{Mt5})[21].

1.3 Molecular modelling approaches to study drug-enzyme interactions

An overview of computer modelling and simulation methods that play an increasing role in drug design[44] will be presented in this section: computational chemistry, molecular mechanics, molecular dynamics, force fields, hybrid quantum molecular/molecular mechanics and virtual screening.

1.3.1 Computational chemistry

Computational chemistry is, in its widest sense, the use of computers to elucidate and understand chemical and biological phenomena, that is, the behaviour and properties of atoms, molecules, protein-ligand and solids[45]. Vast progress in computational chemistry has been accomplished, our review demonstrates that the field of rational drug design with the aid of molecular modelling has matured in the past decade, and it is now realized that an integrated experimental and theoretical approach is essential for optimum impact[48,46]. Theoretical methods, which include quantum mechanics, molecular dynamics, and statistical mechanics, have been effectively used to describe chemical systems and build new materials, drugs and chemicals[47]. Comprehensive reviews on the combined method to structure-based enzymatic drug design is readily available in the literature[48-50], on which this study is based.

1.3.2 Molecular mechanics

Molecular Mechanics (MM) is one of the best computational chemistry approaches for protein and also biological molecules simulations, and useful in studying their conformational flexibility[51, 52]. The underlying model for a molecular mechanics calculation, as well as classical atomistic Molecular dynamics (MD) or Monte Carlo (MC) simulations, is that the energy of a molecule can be described in terms of a function called the force field that depends only on the atomic positions, a highly simplifying assumption. This function must provide a good description of the forces acting within the molecule[53, 54]. MM is vital in most of the computational structure-based drug discovery projects, due to the significance of protein flexibility in drug binding[51]. The use of semiempirical approaches has received much attention[55], although has severe constraints on the simulation time. MM force fields, approximate the quantum mechanical energy surface with a classical mechanical model, thereby reducing the computational cost of simulations on the large system by orders of magnitude[51].

1.3.4 Force fields

Force fields are the combination of mathematical functions that describe parameters used in molecular mechanics or dynamics calculations in order to evaluate the conformations, flexibility and interactions of molecules[56]. These various force fields are created for application to biologically fascinating molecules. These could be due to the greater difficulty of the interactions, which include the ionic and polar groups in aqueous solution, and the struggle to obtain a clear test set to appraise such force fields. Many of these force fields were established prior to 1987, which were defined temporarily by McCammon and Harvey[57]. The conformations of the molecule are stable at low energy regions of the potential energy function, and the forces on the individual atoms are related to the gradient of this potential energy function. So, such functions are commonly known as "force fields"[58]. In addition, the force field is a collection of equations and associated constants designed to reproduce molecular geometry and selected properties of the tested structures. For an atomistic force field, one needs parameters for every type of atom. The parameters are usually derived from experimental data or quantum mechanical calculations. The potential energy function can be divided into bonded and non-bonded interaction energies, and these can be split up again:

$$E_{total} = \underbrace{E_{bonds} + E_{angle} + E_{dihedral}}_{\text{bonded interactions}} + \underbrace{E_{vdW} + E_{coulomb}}_{\text{non-bonded interactions}}$$

With such a potential energy function we can calculate the force on each atom (via $F\sim = -\Delta E_{total}$) and with that the position and velocity for each time step[59].

Force fields, including AMBER[60, 61], are commonly used for proteins and DNA. CHARMM[62] is mostly applicable for both molecules and macromolecules. CHARMM is used for various systems ranging from isolated molecules to solvated complexes of large biological macromolecules[63] CVFF[64] is used for molecules and macromolecules. GROMOS[65] can be applied to aqueous or apolar solutions of proteins, nucleotides, sugars, and lipids simulation. For a gas phase system, simulation of isolated molecules is available as OPLS[66] and ECEPP/2[67, 68] as a free energy force field. However, the use of OPLS is not limited to simulation in the gas phase. The advent of these force fields has gained increasing success in studying compounds of biochemical and organic chemical significance, with the aid of computer-based models. As a result of their significance, ample effort has been invested in considering both the functional form and the parameters that must be developed to use such force fields[69].

1.3.3 Molecular dynamics

MD has been a useful tool in areas of physics and chemistry due to advances in algorithms and computer technology. The basic idea behind MD simulations is the representation of the energy of the molecule as a function of its atomic coordinates. The first molecular dynamics simulation methods were introduced by Alder, Wainwright, and Rahman between 1950s and 1960s, which were applied to the dynamics of liquids. Later, in the 1970s, MD was broadly applied to determine the structure and dynamics of proteins and protein in complex with ligands. In addition, MD is largely used to simulate complex structures that are designed at the atomic level. MD obeys the equations of motion, which are explained numerically to mirror the time evolution of the system, permitting the solving of the kinetic and thermodynamic properties of interest by means of computer testing. Temperature control algorithms (Constant total energy classical dynamics, Constant temperature, using the weak-coupling algorithm, Andersen temperature coupling scheme, Langevin dynamics, Optimized Isokinetic Nose-Hoover chain ensemble (OIN), and Stochastic Isokinetic Nose-Hoover RESPA integrator)[71] are an important component of many molecular dynamics simulations. Using a method to enforce constant temperature is necessary to compare simulation results with laboratory experiments conducted at a constant temperature and either constant pressure or volume[70, 71]. A molecular dynamics thermostat couples a fictitious heat bath to the system or some portion of the system, such that the time-averaged instantaneous kinetic energy of the coupled degrees of freedom corresponds to a target temperature[72]. The result is that conformational constraints are overcome at a high enough simulation temperature. The properties of biologically active large molecules (structure and dynamics), and their surroundings are normally calculated using MD simulation approaches. While quantum MD was reported by Car and Parrinello,[73] this approach explicitly considers the significant nature of the chemical bond required in the activity. The valence electrons that take part in the bonding of the system is calculated using quantum equations, while the dynamics of ions are measured classically. While important information on

some biological problems is best derived using Quantum MD simulations, as it was designed to consider the important system alone over the classical approach, they have high computational cost[62, 74].

1.3.5 Hybrid quantum molecular/molecular mechanics

The use of hybrid potentials in a system is sectioned in different regions, which are then modelled by different levels of approximation[75]. The concept is to apply a QM method to the region, where the chemical reaction occurs and treat the rest of the system using the MM method. The QM and MM generally interact, so it is not possible to write the total energy of the entire system simply as the sum of the energies of the subsystems[76]. As computational methods improve, the need for accuracy must still be tempered with practicality. When calculating how molecules interact in solution, treating solute molecules quantum mechanically and the surrounding solvent molecules classically combine accuracy with computational efficiency[77]. Quantitative prediction of thermodynamic properties of solute molecules requires an accurate description of the solvent[78]. Distinct solvent models may refer to either explicit (TIP3P, TIP4P, TIP5P, and SPC/E) solvent molecules or an implicit (Generalized Born (GB)[79] and Polarisable Continuum Models (PCM)) description of the solvent environment[78]. Explicit-solvent methods, without further approximations, treat solvent molecules explicitly, i.e., interactions between all pairs of solute and solvent atoms are explicitly computed[80, 81]. Implicit-solvent methods, on the other hand, speed up atomistic simulations by approximating the discrete solvent as a continuum, thus drastically reducing the number of particles to keep track of in the system[79, 81].

Warshel and Levitt in 1976 presented the concept of QM/MM to the study of chemical reactions in lysozyme[82] treated semi-empirically. The method has spread over the last 20 years, and many review articles have dealt with both the advance of the QM/MM methods and their application in the biomolecular field.

Essential to the QM/MM idea is the partition (**Figure 1.3**) of the system into QM (inner) and MM (outer) regions that are defined by a force field. Morokuma *et al.*[83, 84] developed Our own N-layered Integrated molecular Orbital and Molecular mechanics (ONIOM) Hybrid Method. ONIOM is one of the approaches used to understand the mechanisms of enzymatic reactions[85] in proteins, DNA/RNA, carbohydrates, and artificial enzymes.
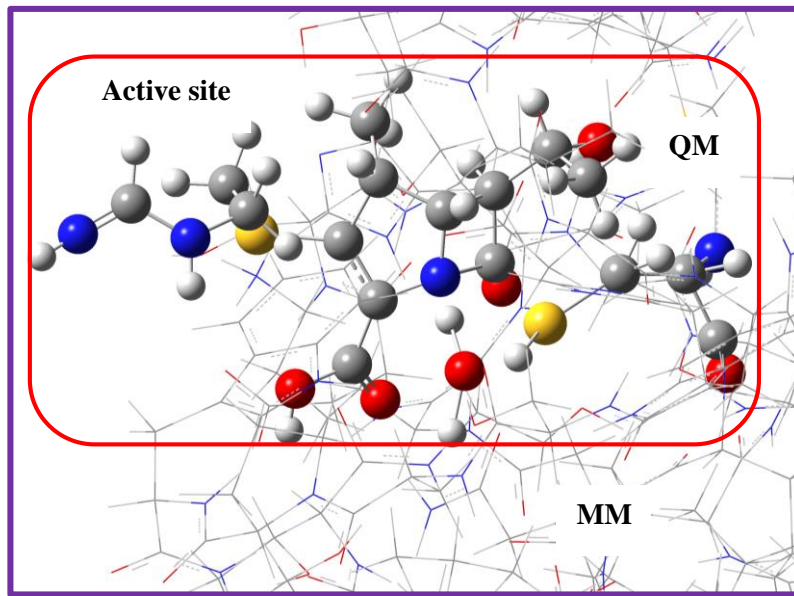
Figure 1.3 A QM/MM model[86]. The active site, water and inhibitor are in ball and stick (QM region) while rest protein-solvent environment (MM region) is in line format.

ONIOM has been widely used to describe the bond formation and breaking processes, which cannot be treated by MM methods, and involve systems that are too large and computationally demanding for the QM methods[85, 87]. In a two partition ONIOM calculation, the total energy of the system is derived from three independent calculations:

$$E^{ONIOM(QM:MM)} = E_{model}^{QM} + E_{real}^{MM} - E_{model}^{MM} = E_{model}^{high} + E_{real}^{high} - E_{model}^{low}$$

Where, E_{model}^{QM} is energy othe f the QM model region, E_{real}^{MM} is the energy of the MM real region, E_{model}^{MM} is the energy of the MM model region, E_{model}^{high} is energy of the high layer model the the region, E_{real}^{high} is energy of the high layer for the modelthe region, and E_{model}^{low} is energy of the low layer model region. The entire system encompasses all the atoms and is derived only at the MM level[88, 89]. The model system comprises the part of the system treated at the QM level, along with the linked atoms between the QM and the MM regions[88, 89].

1.3.6 Virtual Screening Techniques

The journey of drug discovery starts from virtual screening (VS) of libraries of compounds against the target before conducting wet-lab experiments[90]. VS is an approach used in automated docking for a larger set of drug-like compounds, small molecules, or fragments/scaffolds of known biologically active compounds inside the binding site of a protein, and ranking their binding affinities[48, 91]. Methods applied in VS are divided into two categories: structure- or ligand-based approaches[92]. Structure- or receptor-based approaches have been reported to be more efficient than the old-style way of drug discovery. This is aimed

at understanding the molecular origin of a disease, thereby applying the knowledge of the three-dimensional (3D) structure of the biological target-derived. The 3D structure can be retrieved from experimental data (X-ray, NMR or neutron scattering spectroscopy), by homology modelling, or from molecular dynamics (MD) simulations[93]. Information derived from the 3D structure is used to dock each library of compounds into the binding pocket of the relevant enzyme associated with the disease using a docking program[93]. Thereafter, important underlying molecular interactions utilized in ligand-protein binding can be deduced to provide explanations to experimental results at an atomic-level[93]. In the same manner, identifying and developing potential ligands to a particular protein target form the basis in the drug discovery process[94, 95]. Compounds/drugs with known activities are used as a reference in ligand-based virtual screening in order to find filters that are closely related experimental data or possess a pharmacophore or substructure similar to the potent drug/compound[96]. Ligand-based approaches are built on the concept of likeness, that is, compounds that are alike are assumed to yield comparable bioactivity. Using this approach, if one or more potent compounds are identified, we can search the databases for comparable and more active molecules[97]. Generally, structure- and ligand-based virtual screening procedures are combined in a serial in order to meet the demanding search algorithms[98]. At the moment, numerous software tools are available for enzyme-ligand docking, for example, AutoDock Vina[99], Glide[100], FlexX[101], GOLD[102] and DOCK[103]. Equally, several methods have been developed to enhance the speed of executing the job[104]. The use of virtual screening has advanced the field forward, although with the shortcomings of scoring functions and the magnitude of having to dock millions of ligands into any given target or several possible targets. Accurately calculated binding energies and scores are not qualitative for meaningful compound selection. Finding active compounds in the shortlist is, however, critically important. Appropriate selection strategies, therefore, compensate for methodological shortcomings, while deselection of inappropriate compounds reduces the risk of taking a non-promising candidate through a drug-discovery campaign[105]. Albeit docking methods have contributed enormously to rational drug design, it should be noted that there are still some major challenges to be addressed. These include docking into flexible receptors. In this case, the same protein adopts different conformations depending on which ligand it binds to[106-108]. Water molecules often play a key role in protein-ligand recognition[109], in most cases, solvent effects are neglected, and real dynamic movement of the inhibitor-enzyme complex is not possible[48]. Also, docking techniques were designed to provide an estimation of the binding affinity of the inhibitor upon finding the best fit inside the active enzymatic pocket. Scoring failures in docking indicate the inaccuracy of the energy function to fit in the most compatible score to a correct sampled conformation out of the generated ensemble. Now the choice of a more accurate energy function implemented in the software may improve the overall results. The effectiveness of the docking algorithm decreases as a function of the number of rotatable bonds[110]. Another challenge in docking is accounting for the various tautomeric and protomeric states the molecules

can adopt. In many databases, molecules such as acids or amines are deposited in their neutral forms. Seeing that they are ionized under physiological conditions it is necessary to ionize them prior to docking. One approach to this would be to generate all possible forms, subsequently to dock all of them and to choose the relevant form based on the scores[109]. In addition, since most docking software (for example AutoDock) remove the protons of the enzyme and inhibitors, more useful information can be obtained from MD studies where the protons (and water molecules as the solvent) are considered[48].

1.4 Databases of potential bio-active compounds

Free databases of commercially available compounds for virtual screening are crucial in the journey to drug discovery[111-113]. The compounds deposited in the databases have been assigned their biologically relevant information. These include the appropriate protonation states, and characteristics that include molecular weight, calculated LogP, and a number of rotatable bonds[111, 114]. Each molecule in the database has merchant and procuring information, and is available for docking using a number of common docking programs[111]. The concept of a drug-like molecules[115, 116] has existed for many years[117], and include optimized parameters for physicochemical properties as well as the functional groups to be avoided. This concept starts with finding a lead-like[115] instead of a drug-like[117], and then to hit-like[118] molecules, which are tailored toward providing true positive results in high-throughput screening (HTS) assays and thereby yielding a basis for lead generation[117]. The structures of the receptors/enzymes are generated through X-ray crystallography, NMR or homology modelling, which are then deposited in the Protein data bank (PDB)[48, 119]. Similarly, the structures of compounds with different biological properties have been deposited into databases, where they can be retrieved for virtual screening purpose. These include PubChem[120], ZINC[121], ChEMBL[122], NCI[123], ChemDB[124], ChemSpider[125], BindingDB[126], PDB-Bind[127], PDBeChem[128], KEGG[129], HMDB[130], SMPDB[131], BIAdb[132], DrugBank[133], HIT[134], SuperNatural[135], NPACT[136], TTD[137], PharmaGKB[138] and SuperDrug[139] among others. For this study, we have selected ZINC database, which is a commercially free database with 21 million compounds available for virtual screening[111].

1.5 Novelty and significance of the study

Tuberculosis remains a general health threat affecting people in all nations of the world. The drug resistance strains of *Mtb* have weakened the capability to respond effectually to this threat[23]. Five Ldt paralogues have been identified in *Mtb*, Ldt$_{Mt1}$ to Ldt$_{Mt5}$, four of these, with the exception of Ldt$_{Mt3}$, being active in vitro peptidoglycan cross-linking assays, whereas all but Ldt$_{Mt5}$ are inhibited by carbapenems[140].

Recently, Brammer and co-workers[21] reported the crystal structures of apo- and meropenem-bound Ldt$_{Mt5}$ for the first time. An experimental study using isothermal titration calorimetry (ITC) demonstrated that the interaction of meropenem with Ldt$_{Mt5}$ is not associated with significant heat exchange[21]. Similar results[46] were observed for other tested carbapenems, with no adduct being detected by mass spectrometry after five

hours incubation of meropenem and Ldt$_{Mt5}$. It was concluded that meropenem will acylate Ldt$_{Mt5}$ over an extended incubation period that is required for co-crystallization due to the meropenem—adduct crystal formation, which suggests the very slow acylation of Ldt$_{Mt5}$ over many days[21]. They did not rule out the possibility that Ldt$_{Mt5}$ is more rapidly inactivated by this class of *β*-lactams *in vivo*, particularly in the event of Ldt$_{Mt5}$ requiring a protein-protein interaction for productive catalysis[21]. In conclusion, since carbapenems do not show any reasonable inhibitory activities against Ldt$_{Mt5}$ and also an adduct of meropenem exhibited slow acylation requires more investigation theoretically, which would serve as a lead for experimental findings.

1.6 Aims and Objectives

1. Literature review on structure and function of L,D- and D,D-transpeptidase family enzymes from Mycobacterium tuberculosis. To accomplish this, the following objectives were outlined: (Chapter two)

1.1 To summarize recent findings and observations regarding the structure and function of the LDTs and DDTs of *Mtb.*

1.2 To provide bioactivities of known *Mtb* drugs against these targets both experimentally and computationally.

2. To theoretically study carbapenems inactivation against L,D-transpeptidase 5 from *Mycobacterium tuberculosis* using MD and QM/MM Mechanistic methods. To accomplish this, the following objectives were outlined: (Chapter three)

2.1 To study the conformation of carbapenems in the binding site of Ldt$_{Mt5}$ by docking.

2.2 To explore the inactivation of Ldt$_{Mt5}$ in complexation with the selected carbapenems upon ligand binding using 60 ns MD simulations in explicit solvent.

2.3 To identify the conformational changes in terms of opening and closing of the *β*-hairpin flap and the Lc loop upon binding, using distance metrics.

2.4 To qualitatively understand the divergent effects of different inhibitors on the dominant motion of each enzyme residue using Principal component analysis (PCA).

2.5 To assess the binding free energies of the considered complexes and to characterize the participation of the key residues to the total binding free energies using Molecular Mechanics-Generalized Born Surface Area (MM-GBSA).

3. To identify new potent inhibitor against Ldt$_{Mt5}$ from Mycobacterium tuberculosis with the known classes of antituberculosis drugs using virtual screening. To accomplish this, the following objectives were outlined: (Chapter Four)

3.1 To retrieve libraries of compounds with similar scaffolds with *β*-lactam, Diarylquinoline, Oxazolidinone, Rifamycin, and Quinolone classes of TB antibiotics from the ZINC database.

3.2 To select compounds from the ZINC database with drug-like properties using Lipinski and Weber's rules.

3.3 To study the conformation of the refined libraries of compounds into the active pocket of Ldt_{Mt5} using virtual screening techniques implemented in the Glide and AutoDock Vina.

3.4 To rank the scoring functions of the docked poses based on compounds with more negative binding affinity and by visual inspection.

3.5 To study the dynamics of the complexes using molecular dynamics.

4. To determine the mechanistic acylation step of β-lactam derivatives from virtual screening study against Ldt_{Mt5} from *Mycobacterium tuberculosis.* To accomplish this, the following objectives were outlined: (Chapter Five)

4.1 To obtain a favourable and lowest energy conformation of the β-lactam-Ldt_{Mt5} complexes by full geometry optimization of the system using the ONIOM method.

4.2 To determine the thermodynamics and energetics of the reaction path, a geometry optimization to transition state model using a two multilayer ONIOM model.

4.3 To determine the relative energies of the stationary points (reactant, transition and product) using a single-point calculation and employing electronic embedding scheme.

1.7 Thesis outline

The thesis is presented in a paper format in which each chapter is dedicated to addressing one or two research questions. In the first and last chapters, a general introduction and an overall conclusion are provided, respectively, for the entire study. The outline is therefore highlighted.

Chapter one: General introduction to the disease and applications used in the study was first highlighted in the dissertation.

Chapter Two: Literature review on structure and function of D,D and L,D-transpeptidase receptors from *Mycobacterium tuberculosis.*

Chapter Three: Inhibition of *Mycobacterium tuberculosis* L,D-transpeptidase 5 by carbapenems: MD and QM/MM mechanistic studies.

Chapter Four: Identification of potent L,D-transpeptidase 5 inhibitors for Mycobacterium tuberculosis as potential anti-TB leads: Virtual Screening and Molecular Dynamics Simulations.

Chapter Five: Investigating the reaction mechanism of L,D-transpeptidase 5 by β-lactams using ONIOM Method.

Chapter Six

The overall conclusion of the research outcome.

1.8 References

[1] Organization, W. H. (2010) *Global tuberculosis control: WHO report 2010*, World Health Organization.

[2] Lee, J. Y. (2015) Diagnosis and treatment of extrapulmonary tuberculosis, *Tuberculosis and respiratory diseases 78*, 47-55.

[3] Sharma, S., and Mohan, A. (2004) Extrapulmonary tuberculosis, *Indian Journal of Medical Research 120*, 316-353.

[4] Barrios-Payán, J., Saqui-Salces, M., Jeyanathan, M., Alcántara-Vazquez, A., Castañon-Arreola, M., Rook, G., and Hernandez-Pando, R. (2012) Extrapulmonary locations of Mycobacterium tuberculosis DNA during latent infection, *The Journal of infectious diseases 206*, 1194-1205.

[5] Organization, W. H. (2008) *Global tuberculosis control: surveillance, planning, financing: WHO report 2008*, Vol. 393, World Health Organization.

[6] Organization, W. H. (2015) *Global tuberculosis report 2015*, World Health Organization.

[7] Organization, W. H. (2018) Global tuberculosis report 2017. 2017, *Google Scholar*.

[8] Netto, E., Dye, C., and Raviglione, M. (1999) Progress in global tuberculosis control 1995–1996, with emphasis on 22 high-incidence countries, *The International Journal of Tuberculosis and Lung Disease 3*, 310-320.

[9] Organization, W. H. (2016) Global tuberculosis report 2016.

[10] Koul, A., Arnoult, E., Lounis, N., Guillemont, J., and Andries, K. (2011) The challenge of new drug discovery for tuberculosis, *Nature 469*, 483-490.

[11] Squeglia, F., Ruggiero, A., and Berisio, R. (2018) Chemistry of Peptidoglycan in Mycobacterium tuberculosis Life Cycle: An off-the-wall Balance of Synthesis and Degradation, *Chemistry–A European Journal 24*, 2533-2546.

[12] Alderwick, L. J., Harrison, J., Lloyd, G. S., and Birch, H. L. (2015) The Mycobacterial cell wall—Peptidoglycan and arabinogalactan, *Cold Spring Harbor perspectives in medicine*, a021113.

[13] Correale, S., Ruggiero, A., Capparelli, R., Pedone, E., and Berisio, R. (2013) Structures of free and inhibited forms of the L, D-transpeptidase LdtMt1 from Mycobacterium tuberculosis, *Acta Crystallographica Section D: Biological Crystallography 69*, 1697-1706.

[14] Alderwick, L., Birch, H., Mishra, A., Eggeling, L., and Besra, G. (2007) Structure, function and biosynthesis of the Mycobacterium tuberculosis cell wall: arabinogalactan and lipoarabinomannan assembly with a view to discovering new drug targets, Portland Press Limited.

[15] Hett, E. C., and Rubin, E. J. (2008) Bacterial growth and cell division: a mycobacterial perspective, *Microbiology and Molecular Biology Reviews 72*, 126-156.

[16] Lavollay, M., Arthur, M., Fourgeaud, M., Dubost, L., Marie, A., Veziris, N., Blanot, D., Gutmann, L., and Mainardi, J.-L. (2008) The peptidoglycan of stationary-phase Mycobacterium tuberculosis predominantly contains cross-links generated by L, D-transpeptidation, *Journal of Bacteriology 190*, 4360-4366.

[17] Dubée, V., Triboulet, S., Mainardi, J.-L., Ethève-Quelquejeu, M., Gutmann, L., Marie, A., Dubost, L., Hugonnet, J.-E., and Arthur, M. (2012) Inactivation of Mycobacterium tuberculosis L, D-transpeptidase LdtMt1 by carbapenems and cephalosporins, *Antimicrobial agents and chemotherapy 56*, 4189-4195.

[18] Silva, J. R. r. A., Roitberg, A. E., and Alves, C. u. N. (2014) Catalytic mechanism of L, D-transpeptidase 2 from Mycobacterium tuberculosis described by a computational approach: insights for the design of new antibiotics drugs, *Journal of Chemical Information and Modeling 54*, 2402-2410.

[19] Mainardi, J.-L., Fourgeaud, M., Hugonnet, J.-E., Dubost, L., Brouard, J.-P., Ouazzani, J., Rice, L. B., Gutmann, L., and Arthur, M. (2005) A novel peptidoglycan cross-linking enzyme for a β-lactam-resistant transpeptidation pathway, *Journal of Biological Chemistry 280*, 38146-38152.

[20] Lamichhane, G., Freundlich, J. S., Ekins, S., Wickramaratne, N., Nolan, S. T., and Bishai, W. R. (2011) Essential metabolites of Mycobacterium tuberculosis and their mimics, *MBio 2*, e00301-00310.

[21] Brammer, B. L., Ghosh, A., Pan, Y., Jakoncic, J., Lloyd, E., Townsend, C., Lamichhane, G., and Bianchet, M. (2015) Loss of a Functionally and Structurally Distinct ld-Transpeptidase, LdtMt5, Compromises Cell Wall Integrity in Mycobacterium tuberculosis, *The Journal of Biological Chemistry 290*, 25670-25685.

[22] Böth, D., Steiner, E. M., Stadler, D., Lindqvist, Y., Schnell, R., and Schneider, G. (2013) Structure of LdtMt2, an L, D-transpeptidase from Mycobacterium tuberculosis, *Acta Crystallographica Section D: Biological Crystallography 69*, 432-441.

[23] Gupta, R., Lavollay, M., Mainardi, J.-L., Arthur, M., Bishai, W. R., and Lamichhane, G. (2010) The Mycobacterium tuberculosis protein LdtMt2 is a nonclassical transpeptidase required for virulence and resistance to amoxicillin, *Nature Medicine 16*, 466-469.

[24] Kahan, J., Kahan, F., Goegelman, R., Currie, S., Jackson, M., Stapley, E., Miller, T., Miller, A., Hendlin, D., and Mochales, S. (1979) Thienamycin, a new β-lactam antibiotic I. Discovery, taxonomy, isolation and physical properties, *The Journal of antibiotics 32*, 1-12.

[25] Spratt, B. G., Jobanputra, V., and Zimmermann, W. (1977) Binding of thienamycin and clavulanic acid to the penicillin-binding proteins of Escherichia coli K-12, *Antimicrobial agents and chemotherapy 12*, 406-409.

[26] Birnbaum, J., Kahan, F. M., Kropp, H., and Macdonald, J. S. (1985) Carbapenems, a new class of beta-lactam antibiotics: discovery and development of imipenem/cilastatin, *The American journal of medicine 78*, 3-21.

[27] Bennett, J. W., and Chung, K.-T. (2001) Alexander Fleming and the discovery of penicillin, *Advances in applied microbiology 49*, 163-184.

[28] Chain, E., Florey, H., Adelaide, M., Gardner, A., Heatley, N., Jennings, M., Orr-Ewing, J., and Sanders, A. (1993) Penicillin as a chemotherapeutic agent, *Clinical Orthopaedics and Related Research® 295*, 3-7.

[29] Walsh, C. (2003) Where will new antibiotics come from?, *Nature Reviews Microbiology 1*, 65-70.

[30] Mandell, L. (2009) Doripenem: a new carbapenem in the treatment of nosocomial infection, *Clinical Infectious Diseases 49*, S1-S3.

[31] Baughman, R. P. (2009) The use of carbapenems in the treatment of serious infections, *Journal of intensive care medicine 24*, 230-241.

[32] Livermore, D. M. (2001) Of Pseudomonas, porins, pumps and carbapenems, *Journal of Antimicrobial Chemotherapy 47*, 247-250.

[33] Calandra, G., Lydick, E., Carrigan, J., Weiss, L., and Guess, H. (1988) Factors predisposing to seizures in seriously III infected patients receiving antibiotics: experience with imipenem/cilastatin, *The American journal of medicine 84*, 911-918.

[34] Bhavnani, S. M., Hammel, J. P., Cirincione, B. B., Wikler, M. A., and Ambrose, P. G. (2005) Use of pharmacokinetic-pharmacodynamic target attainment analyses to support phase 2 and 3 dosing strategies for doripenem, *Antimicrobial agents and chemotherapy 49*, 3944-3947.

[35] Lynch, M., Drusano, G., and Mobley, H. (1987) Emergence of resistance to imipenem in Pseudomonas aeruginosa, *Antimicrobial agents and chemotherapy 31*, 1892-1896.

[36] Behera, B., Mathur, P., Das, A., and Kapil, A. (2009) Ertapenem susceptibility of extended spectrum beta-lactamase-producing Enterobacteriaceae at a tertiary care centre in India, *Singapore Med J 50*, 628-632.

[37] Paterson, D. L., and DePestel, D. D. (2009) Doripenem, *Clinical infectious diseases 49*, 291-298.

[38] Erdemli, S. B., Gupta, R., Bishai, W. R., Lamichhane, G., Amzel, L. M., and Bianchet, M. A. (2012) Targeting the cell wall of Mycobacterium tuberculosis: structure and mechanism of L, D-transpeptidase 2, *Structure 20*, 2103-2115.

[39] Calixto, A. R., Brás, N. r. F., Fernandes, P. A., and Ramos, M. J. (2014) Reaction mechanism of human renin studied by quantum mechanics/molecular mechanics (QM/MM) calculations, *Acs Catalysis 4*, 3869-3876.

[40] Biarrotte-Sorin, S., Hugonnet, J.-E., Delfosse, V., Mainardi, J.-L., Gutmann, L., Arthur, M., and Mayer, C. (2006) Crystal structure of a novel β-lactam-insensitive peptidoglycan transpeptidase, *Journal of molecular biology 359*, 533-538.

[41] Fakhar, Z., Govender, T., Lamichhane, G., Maguire, G. E., Kruger, H. G., and Honarparvar, B. (2017) Computational model for the acylation step of the β-lactam ring: Potential application for l, d-transpeptidase 2 in mycobacterium tuberculosis, *Journal of Molecular Structure 1128*, 94-102.

[42] Wei, D., Huang, X., Tang, M., and Zhan, C.-G. (2013) Reaction pathway and free energy profile for papain-catalyzed hydrolysis of N-acetyl-Phe-Gly 4-nitroanilide, *Biochemistry 52*, 5145.

[43] Janowski, R., Kozak, M., Jankowska, E., Grzonka, Z., and Jaskolski, M. (2004) Two polymorphs of a covalent complex between papain and a diazomethylketone inhibitor, *The Journal of peptide research 64*, 141-150.

[44] Lesyng, B., and McCammon, J. A. (1993) Molecular modeling methods. Basic techniques and challenging problems, *Pharmacology & therapeutics 60*, 149-167.

[45] Council, N. r. (2003) *Beyond the molecular frontier: Challenges for chemistry and chemical engineering*, National Academies Press.

[46] Caflisch, A., Walchli, R., and Ehrhardt, C. (1998) Computer-aided design of thrombin inhibitors, *Physiology 13*, 182-189.

[47] Leszczynski, J. (2003) *Computational chemistry: reviews of current trends*, Vol. 8, World Scientific.

[48] Honarparvar, B., Govender, T., Maguire, G. E., Soliman, M. E., and Kruger, H. G. (2013) Integrated approach to structure-based enzymatic drug design: molecular modeling, spectroscopy, and experimental bioactivity, *Chemical reviews 114*, 493-537.

[49] Brown, R. D., and Martin, Y. C. (1996) Use of structure− activity data to compare structure-based clustering methods and descriptors for use in compound selection, *Journal of Chemical Information and Computer Sciences 36*, 572-584.

[50] Chica, R. A., Doucet, N., and Pelletier, J. N. (2005) Semi-rational approaches to engineering enzyme activity: combining the benefits of directed evolution and rational design, *Current opinion in biotechnology 16*, 378-384.

[51] Vanommeslaeghe, K., and Guvench, O. (2014) Molecular mechanics, *Current pharmaceutical design 20*, 3281-3292.

[52] Vanommeslaeghe, K., and MacKerell, A. (2015) CHARMM additive and polarizable force fields for biophysics and computer-aided drug design, *Biochimica et Biophysica Acta (BBA)-General Subjects 1850*, 861-871.

[53] Burkert, U., and Allinger, N. (1982) Molecular Mechanics American Chemical Society, *Washington, DC*.

[54] Aped, P., and Allinger, N. (1992) A molecular mechanics study of cyclopropanes within the MM2 and MM3 force fields, *Journal of the American Chemical Society 114*, 1-16.

[55] Liu, H., Elstner, M., Kaxiras, E., Frauenheim, T., Hermans, J., and Yang, W. (2001) Quantum mechanics simulation of protein dynamics on long timescale, *Proteins: Structure, Function, and Bioinformatics 44*, 484-489.

[56] Halgren, T. A. (1996) Merck molecular force field. I. Basis, form, scope, parameterization, and performance of MMFF94, *Journal of computational chemistry 17*, 490-519.

[57] McCammon, J. A., and Harvey, S. C. (1988) *Dynamics of proteins and nucleic acids*, Cambridge University Press.

[58] Oostenbrink, C., Villa, A., Mark, A. E., and Van Gunsteren, W. F. (2004) A biomolecular force field based on the free enthalpy of hydration and solvation: the GROMOS force-field parameter sets 53A5 and 53A6, *Journal of computational chemistry 25*, 1656-1676.

[59] Ilse, S. E. (2016) Classical Atomistic Force Fields for Single-and Double-Stranded DNA, *Institute for Computational Physics-University of Stuttgart*.

[60] Weiner, P. K., and Kollman, P. A. (1981) AMBER: Assisted model building with energy refinement. A general program for modeling molecules and their interactions, *Journal of Computational Chemistry 2*, 287-303.

[61] Weiner, S. J., Kollman, P. A., Case, D. A., Singh, U. C., Ghio, C., Alagona, G., Profeta, S., and Weiner, P. (1984) A new force field for molecular mechanical simulation of nucleic acids and proteins, *Journal of the American Chemical Society 106*, 765-784.

[62] Brooks, B. R., Bruccoleri, R. E., Olafson, B. D., States, D. J., Swaminathan, S., and Karplus, M. (1983) CHARMM: a program for macromolecular energy, minimization, and dynamics calculations, *Journal of computational chemistry 4*, 187-217.

[63] Momany, F. A., and Rone, R. (1992) Validation of the general purpose QUANTA® 3.2/CHARMm® force field, *Journal of Computational Chemistry 13*, 888-900.

[64] Kitson, D. H., and Hagler, A. T. (1988) Theoretical studies of the structure and molecular dynamics of a peptide crystal, *Biochemistry 27*, 5246-5257.

[65] Van Gunsteren, W., and Berendsen, H. (1987) Groningen molecular simulation (GROMOS) library manual, *Biomos, Groningen 24*, 13.

[66] Jorgensen, W. L., and Pranata, J. (1990) Importance of secondary interactions in triply hydrogen bonded complexes: guanine-cytosine vs uracil-2, 6-diaminopyridine, *Journal of the American Chemical Society 112*, 2008-2010.

[67] Momany, F., McGuire, R. F., Burgess, A., and Scheraga, H. A. (1975) Energy parameters in polypeptides. VII. Geometric parameters, partial atomic charges, nonbonded interactions, hydrogen bond interactions, and intrinsic torsional potentials for the naturally occurring amino acids, *The Journal of Physical Chemistry 79*, 2361-2381.

[68] Nemethy, G., Pottle, M. S., and Scheraga, H. A. (1983) Energy parameters in polypeptides. 9. Updating of geometrical parameters, nonbonded interactions, and hydrogen bond interactions for the naturally occurring amino acids, *The Journal of Physical Chemistry 87*, 1883-1887.

[69] Cornell, W. D., Cieplak, P., Bayly, C. I., Gould, I. R., Merz, K. M., Ferguson, D. M., Spellmeyer, D. C., Fox, T., Caldwell, J. W., and Kollman, P. A. (1996) A second generation force field for the simulation of proteins, nucleic acids, and organic molecules j. am. chem. soc. 1995, 117, 5179-5197, *Journal of the American Chemical Society 118*, 2309-2309.

[70] Berger, O., Edholm, O., and Jähnig, F. (1997) Molecular dynamics simulations of a fluid bilayer of dipalmitoylphosphatidylcholine at full hydration, constant pressure, and constant temperature, *Biophysical journal 72*, 2002-2013.

[71] Cadena, C., Zhao, Q., Snurr, R. Q., and Maginn, E. J. (2006) Molecular modeling and experimental studies of the thermodynamic and transport properties of pyridinium-based ionic liquids, *The Journal of Physical Chemistry B 110*, 2821-2832.

[72] Basconi, J. E., and Shirts, M. R. (2013) Effects of temperature control algorithms on transport properties and kinetics in molecular dynamics simulations, *Journal of chemical theory and computation 9*, 2887-2899.

[73] Meller, J. (2001) Molecular dynamics, *eLS*.

[74] Brooks, C. L. (1998) Simulations of protein folding and unfolding, *Current opinion in structural biology 8*, 222-226.

[75] Svensson, M., Humbel, S., and Morokuma, K. (1996) Energetics using the single point IMOMO (integrated molecular orbital+ molecular orbital) calculations: Choices of computational levels and model system, *The Journal of chemical physics 105*, 3654-3661.

[76] Senn, H. M., and Thiel, W. (2007) QM/MM studies of enzymes, *Current opinion in chemical biology 11*, 182-187.

[77] Gao, J., and Furlani, T. R. (1995) Simulating solvent effects in organic chemistry: Combining quantum and molecular mechanics, *IEEE Computational Science and Engineering 2*, 24-33.

[78] Zhang, J., Zhang, H., Wu, T., Wang, Q., and van der Spoel, D. (2017) Comparison of Implicit and Explicit Solvent Models for the Calculation of Solvation Free Energy in Organic Solvents, *Journal of chemical theory and computation 13*, 1034-1043.

[79] Onufriev, A., Bashford, D., and Case, D. A. (2000) Modification of the generalized Born model suitable for macromolecules, *The Journal of Physical Chemistry B 104*, 3712-3720.

[80] Schlick, T. (2010) *Molecular modeling and simulation: an interdisciplinary guide: an interdisciplinary guide*, Vol. 21, Springer Science & Business Media.

[81] Anandakrishnan, R., Drozdetski, A., Walker, R. C., and Onufriev, A. V. (2015) Speed of conformational change: comparing explicit and implicit solvent molecular dynamics simulations, *Biophysical journal 108*, 1153-1164.

[82] Warshel, A., and Levitt, M. (1976) Theoretical studies of enzymic reactions: dielectric, electrostatic and steric stabilization of the carbonium ion in the reaction of lysozyme, *Journal of molecular biology 103*, 227-249.

[83] Dapprich, S., Komáromi, I., Byun, K. S., Morokuma, K., and Frisch, M. J. (1999) A new ONIOM implementation in Gaussian98. Part I. The calculation of energies, gradients, vibrational frequencies and electric field derivatives, *Journal of Molecular Structure: THEOCHEM 461*, 1-21.

[84] Vreven, T., and Morokuma, K. (2006) Hybrid methods: Oniom (qm: mm) and qm/mm, *Annual reports in computational chemistry 2*, 35-51.

[85] Chung, L. W., Sameera, W., Ramozzi, R., Page, A. J., Hatanaka, M., Petrova, G. P., Harris, T. V., Li, X., Ke, Z., and Liu, F. (2015) The ONIOM method and its applications, *Chemical reviews 115*, 5678-5796.

[86] Lin, H., and Truhlar, D. G. (2007) QM/MM: what have we learned, where are we, and where do we go from here?, *Theoretical Chemistry Accounts 117*, 185.

[87] Fisher, J. F., Meroueh, S. O., and Mobashery, S. (2005) Bacterial resistance to β-lactam antibiotics: compelling opportunism, compelling opportunity, *Chemical reviews 105*, 395-424.

[88] Maseras, F., and Morokuma, K. (1995) IMOMM: A new integrated ab initio+ molecular mechanics geometry optimization scheme of equilibrium structures and transition states, *Journal of Computational Chemistry 16*, 1170-1179.

[89] Humbel, S., Sieber, S., and Morokuma, K. (1996) The IMOMO method: Integration of different levels of molecular orbital approximations for geometry optimization of large systems: Test for n-butane conformation and SN 2 reaction: RCl+ Cl−, *The Journal of chemical physics 105*, 1959-1967.

[90] Zhu, T., Cao, S., Su, P.-C., Patel, R., Shah, D., Chokshi, H. B., Szukala, R., Johnson, M. E., and Hevener, K. E. (2013) Hit identification and optimization in virtual screening: practical recommendations based on a critical literature analysis: miniperspective, *Journal of medicinal chemistry 56*, 6560-6572.

[91] Jaghoori, M. M., Bleijlevens, B., and Olabarriaga, S. D. (2016) 1001 ways to run AutoDock Vina for virtual screening, *Journal of computer-aided molecular design 30*, 237-249.

[92] Kurczyk, A., Warszycki, D., Musiol, R., Kafel, R., Bojarski, A. J., and Polanski, J. (2015) Ligand-based virtual screening in a search for novel anti-HIV-1 chemotypes, *Journal of chemical information and modeling 55*, 2168-2177.

[93] Lionta, E., Spyrou, G., K Vassilatis, D., and Cournia, Z. (2014) Structure-based virtual screening for drug discovery: principles, applications and recent advances, *Current topics in medicinal chemistry 14*, 1923-1938.

[94] Koh, J. T. (2003) Making virtual screening a reality, *Proceedings of the National Academy of Sciences 100*, 6902-6903.

[95] Evers, A., and Klebe, G. (2004) Ligand-Supported Homology Modeling of G-Protein-Coupled Receptor Sites: Models Sufficient for Successful Virtual Screening, *Angewandte Chemie International Edition 43*, 248-251.

[96] Vidal, D., Thormann, M., and Pons, M. (2006) A novel search engine for virtual screening of very large databases, *Journal of chemical information and modeling 46*, 836-843.

[97] Lengauer, T., Lemmen, C., Rarey, M., and Zimmermann, M. (2004) Novel technologies for virtual screening, *Drug discovery today 9*, 27-34.

[98] Kitchen, D. B., Decornez, H., Furr, J. R., and Bajorath, J. (2004) Docking and scoring in virtual screening for drug discovery: methods and applications, *Nature reviews. Drug discovery 3*, 935.

[99] Trott, O., and Olson, A. J. (2010) AutoDock Vina: improving the speed and accuracy of docking with a new scoring function, efficient optimization, and multithreading, *Journal of computational chemistry 31*, 455-461.

[100] Friesner, R. A., Banks, J. L., Murphy, R. B., Halgren, T. A., Klicic, J. J., Mainz, D. T., Repasky, M. P., Knoll, E. H., Shelley, M., and Perry, J. K. (2004) Glide: a new approach for rapid, accurate docking and scoring. 1. Method and assessment of docking accuracy, *Journal of medicinal chemistry 47*, 1739-1749.

[101] Kramer, B., Rarey, M., and Lengauer, T. (1999) Evaluation of the FLEXX incremental construction algorithm for protein–ligand docking, *Proteins: Structure, Function, and Bioinformatics 37*, 228-241.

[102] Jones, G., Willett, P., and Glen, R. C. (1995) Molecular recognition of receptor sites using a genetic algorithm with a description of desolvation, *Journal of molecular biology 245*, 43-53.

[103] Ewing, T. J., Makino, S., Skillman, A. G., and Kuntz, I. D. (2001) DOCK 4.0: search strategies for automated molecular docking of flexible molecule databases, *Journal of computer-aided molecular design 15*, 411-428.

[104] Zhang, S., Kumar, K., Jiang, X., Wallqvist, A., and Reifman, J. (2008) DOVIS: an implementation for high-throughput virtual screening using AutoDock, *Bmc Bioinformatics 9*, 126.

[105] Yuriev, E. (2014) Challenges and advances in structure-based virtual screening, *Future medicinal chemistry 6*, 5-7.

[106] Murray, C. W., Baxter, C. A., and Frenkel, A. D. (1999) The sensitivity of the results of molecular docking to induced fit effects: application to thrombin, thermolysin and neuraminidase, *Journal of computer-aided molecular design 13*, 547-562.

[107] Teague, S. J. (2003) Implications of protein flexibility for drug discovery, *Nature reviews Drug discovery 2*, 527.

[108] Plewczynski, D., Łaźniewski, M., Augustyniak, R., and Ginalski, K. (2011) Can we trust docking results? Evaluation of seven commonly used programs on PDBbind database, *Journal of computational chemistry 32*, 742-755.

[109] Kroemer, R. T. (2007) Structure-based drug design: docking and scoring, *Current protein and peptide science 8*, 312-328.

[110] Mukherjee, S., Balius, T. E., and Rizzo, R. C. (2010) Docking validation resources: protein family and ligand flexibility experiments, *Journal of chemical information and modeling 50*, 1986-2000.

[111] Irwin, J. J., and Shoichet, B. K. (2005) ZINC–a free database of commercially available compounds for virtual screening, *Journal of chemical information and modeling 45*, 177.

[112] Forli, S. (2015) Charting a path to success in virtual screening, *Molecules 20*, 18732-18758.

[113] Glanzer, J. G., Byrne, B. M., McCoy, A. M., James, B. J., Frank, J. D., and Oakley, G. G. (2016) In silico and in vitro methods to identify ebola virus VP35-dsRNA inhibitors, *Bioorganic & medicinal chemistry 24*, 5388-5392.

[114] Lipinski, C. A., Lombardo, F., Dominy, B. W., and Feeney, P. J. (1997) Experimental and computational approaches to estimate solubility and permeability in drug discovery and development settings, *Advanced drug delivery reviews 23*, 3-25.

[115] Chuprina, A., Lukin, O., Demoiseaux, R., Buzko, A., and Shivanyuk, A. (2010) Drug-and lead-likeness, target class, and molecular diversity analysis of 7.9 million commercially available

organic compounds provided by 29 suppliers, *Journal of chemical information and modeling 50*, 470-479.

[116] Ajay, Walters, W. P., and Murcko, M. A. (1998) Can we learn to distinguish between "drug-like" and "nondrug-like" molecules?, *Journal of medicinal chemistry 41*, 3314-3324.

[117] Huggins, D. J., Venkitaraman, A. R., and Spring, D. R. (2011) Rational methods for the selection of diverse screening compounds, *ACS chemical biology 6*, 208.

[118] Keserű, G. M., and Makara, G. M. (2006) Hit discovery and hit-to-lead approaches, *Drug discovery today 11*, 741-748.

[119] Berman, H. M., Westbrook, J., Feng, Z., Gilliland, G., Bhat, T. N., Weissig, H., Shindyalov, I. N., and Bourne, P. E. (2006) The protein data bank, 1999–, In *International Tables for Crystallography Volume F: Crystallography of biological macromolecules*, pp 675-684, Springer.

[120] Bolton, E. E., Wang, Y., Thiessen, P. A., and Bryant, S. H. (2008) PubChem: integrated platform of small molecules and biological activities, *Annual reports in computational chemistry 4*, 217-241.

[121] Irwin, J. J., and Shoichet, B. K. (2005) ZINC− A free database of commercially available compounds for virtual screening, *Journal of chemical information and modeling 45*, 177-182.

[122] Gaulton, A., Bellis, L. J., Bento, A. P., Chambers, J., Davies, M., Hersey, A., Light, Y., McGlinchey, S., Michalovich, D., and Al-Lazikani, B. (2011) ChEMBL: a large-scale bioactivity database for drug discovery, *Nucleic acids research 40*, D1100-D1107.

[123] Ihlenfeldt, W.-D., Voigt, J. H., Bienfait, B., Oellien, F., and Nicklaus, M. C. (2002) Enhanced CACTVS browser of the Open NCI Database, *Journal of chemical information and computer sciences 42*, 46-57.

[124] Chen, J., Swamidass, S. J., Dou, Y., Bruand, J., and Baldi, P. (2005) ChemDB: a public database of small molecules and related chemoinformatics resources, *Bioinformatics 21*, 4133-4139.

[125] Pence, H. E., and Williams, A. (2010) ChemSpider: an online chemical information resource, ACS Publications.

[126] Chen, X., Liu, M., and Gilson, M. K. (2001) BindingDB: a web-accessible molecular recognition database, *Combinatorial chemistry & high throughput screening 4*, 719-725.

[127] Liu, T., Lin, Y., Wen, X., Jorissen, R. N., and Gilson, M. K. (2006) BindingDB: a web-accessible database of experimentally determined protein–ligand binding affinities, *Nucleic acids research 35*, D198-D201.

[128] Dimitropoulos, D., Ionides, J., and Henrick, K. (2006) Using MSDchem to search the PDB ligand dictionary, *Current Protocols in Bioinformatics*, 14.13. 11-14.13. 21.

[129] Kanehisa, M., and Goto, S. (2000) KEGG: kyoto encyclopedia of genes and genomes, *Nucleic acids research 28*, 27-30.

[130] Wishart, D. S., Tzur, D., Knox, C., Eisner, R., Guo, A. C., Young, N., Cheng, D., Jewell, K., Arndt, D., and Sawhney, S. (2007) HMDB: the human metabolome database, *Nucleic acids research 35*, D521-D526.

[131] Frolkis, A., Knox, C., Lim, E., Jewison, T., Law, V., Hau, D. D., Liu, P., Gautam, B., Ly, S., and Guo, A. C. (2009) SMPDB: the small molecule pathway database, *Nucleic acids research 38*, D480-D487.

[132] Singla, D., Sharma, A., Kaur, J., Panwar, B., and Raghava, G. P. (2010) BIAdb: a curated database of benzylisoquinoline alkaloids, *BMC pharmacology 10*, 4.

[133] Wishart, D. S., Knox, C., Guo, A. C., Shrivastava, S., Hassanali, M., Stothard, P., Chang, Z., and Woolsey, J. (2006) DrugBank: a comprehensive resource for in silico drug discovery and exploration, *Nucleic acids research 34*, D668-D672.

[134] Charifson, P. S., Corkery, J. J., Murcko, M. A., and Walters, W. P. (1999) Consensus scoring: A method for obtaining improved hit rates from docking databases of three-dimensional structures into proteins, *Journal of medicinal chemistry 42*, 5100-5109.

[135] Dunkel, M., Fullbeck, M., Neumann, S., and Preissner, R. (2006) SuperNatural: a searchable database of available natural compounds, *Nucleic acids research 34*, D678-D683.

[136] Mangal, M., Sagar, P., Singh, H., Raghava, G. P., and Agarwal, S. M. (2012) NPACT: naturally occurring plant-based anti-cancer compound-activity-target database, *Nucleic acids research 41*, D1124-D1129.

[137] Chen, X., Ji, Z. L., and Chen, Y. Z. (2002) TTD: therapeutic target database, *Nucleic acids research 30*, 412-415.

[138] Klein, T. E., Chang, J. T., Cho, M. K., Easton, K. L., Fergerson, R., Hewett, M., Lin, Z., Liu, Y., Liu, S., and Oliver, D. (2001) Integrating genotype and phenotype information: an overview of the PharmGKB project, *The pharmacogenomics journal 1*, 167-170.

[139] Goede, A., Dunkel, M., Mester, N., Frommel, C., and Preissner, R. (2005) SuperDrug: a conformational drug database, *Bioinformatics 21*, 1751-1753.

[140] Cordillot, M., Dubée, V., Triboulet, S., Dubost, L., Marie, A., Hugonnet, J.-E., Arthur, M., and Mainardi, J.-L. (2013) In vitro cross-linking of Mycobacterium tuberculosis peptidoglycan by l, d-transpeptidases and inactivation of these enzymes by carbapenems, *Antimicrobial agents and chemotherapy 57*, 5940-5945.

CHAPTER TWO
LITERATURE REVIEW

The manuscript in chapter two has been published in Current Medicinal Chemistry

Structure and function of L,D- and D,D-transpeptidase family enzymes from
Mycobacterium tuberculosis

Gideon F. Tolufashe,[a] Victor T. Sabe,[a] Colins U. Ibeji, Thandokuhle Ntombela,

Thavendran Govender, Glenn E. M. Maguire,[a,b] Hendrik G. Kruger,[a] and Gyanu

Lamichhane,[c] and Bahareh Honarparvar[a*]

[a]Catalysis and Peptide Research Unit, School of Health Sciences, University of KwaZulu-Natal, Durban 4001, South Africa.

[b]School of Chemistry and Physics, University of KwaZulu-Natal, 4001 Durban, South Africa.

[c]Division of Infectious Diseases, School of Medicine, Johns Hopkins University, Baltimore, MD 21287, USA.

*Corresponding authors: Honarparvarb@ukzn.ac.za (Dr Bahareh Honarparvar), (Prof. Hendrik G. Kruger) kruger@ukzn.ac.za, Telephone: + 27 31 2601845, Fax: +27 31 2603091, Catalysis and Peptide Research Unit, School of Health Sciences, University of KwaZulu-Natal, Durban 4041, South Africa.

Table of Contents

Abstract

Peptidoglycan, the exoskeleton of the bacterial cell and an essential barrier that protects the cell, is synthesized by a pathway whose final steps are catalysed by transpeptidases, including *M.tuberculosis*. Knowledge of the structure and function of these vital enzymes that generate this macromolecule in *M. tuberculosis* could facilitate the development of potent lead compounds against tuberculosis. This review summarizes the experimental and computational studies to date on these aspects of transpeptidases in *M. tuberculosis* that have been identified and validated. The reported structures of L,D- and D,D-transpeptidases, as well as their functionalities, are reviewed and the proposed enzymatic mechanisms for L,D-transpeptidases are summarized. In addition, we provide bioactivities of known *M. tuberculosis* drugs against these enzymes based on both experimental and computational approaches. Advancing knowledge about these prominent targets in *M. tuberculosis* supports the development of new drugs with novel inhibition mechanisms overcoming to address the current need for new drugs against tuberculosis.

Keywords: *Mycobacterium tuberculosis* (*Mtb*); Peptidoglycan, L,D-transpeptidase, D,D-transpeptidase.

2.1 Introduction

The first genome sequence of the H37Rv strain of *Mycobacterium tuberculosis* (*Mtb*) was completed in 1998[1]. This major breakthrough greatly facilitated molecular studies of the biology, metabolism, and evolution of this dangerous pathogen, and thereby ushering tuberculosis research into a new era. TB occurrence has the highest incidence in Africa, while a large fraction of recent cases has been reported in six Asian countries, namely, Bangladesh, China, India, Indonesia, Pakistan and the Philippines[2, 3]. The ability of a sub-population of *Mtb* to persist, or survive for long durations even in the presence of otherwise lethal actions of antibiotics, requires several months of therapy with multiple drugs or drug regimes and therefore contributes to the overall burden of treating TB [4, 5]. This long duration of treatment has been associated with poor compliance and the selection of multidrug-resistant strains, which characterize a growing segment of TB cases in much of the world[6]. Although various antibiotics are effective in treating *Mtb* infections, they only target a small number of essential functions in the cell[7]. Identifying the pathways required for *Mtb*'s survival and growth would provide many new targets for designing more effective agents that could be active against drug-resistant strains[8]. Peptidoglycan (PG) is required for its vital cellular stages, which include cell growth and division, and recovery from latency. *Mtb* often remains in a metabolically non-replicating condition that favours its survival during adverse physio-chemical circumstances or nutrient starvation[9]. Bacilli in a metabolically non-replicating state have been proposed to the sub-population that produce clinically latent infection. It is estimated that one-third of the world's population harbours latent *Mtb* infection[10] Polymerization and regrowth of the PG is a prerequisite for *Mtb* to resuscitate from non-replicating persistence, to elongate its cell, divide and proliferate and to cause the active disease.

The PG of *Mtb* is unique: two distinct families of transpeptidases catalyse the polymerization of PG subunits, the classical D,D-transpeptidases (DDT), also known as penicillin binding proteins (PBP), [11, 12 13] and the recently discovered L,D-transpeptidases (LDT) [14, 15 16 17]. These enzyme families are evolutionarily unrelated as their amino acid sequences share no similarity and their structures are different. While DDTs use serine as the catalytic residue, a conserved cysteine serves this role in the LDTs[9, 18]. The LDTs and DDTs also differ in their substrate with the former using tetrapeptide[19] in contrast to the pentapeptide[20] substrate that is a requirement for the latter[19]. Emerging evidence shows that the PG of *Mtb* is distinct from that in Gram-positives and negatives, and is not represented by the historical model of PG[21, 22]. According to the model, which was developed largely from studies using *E. coli,* the final step of PG synthesis is catalysed by one enzyme, DDTs[19], which generate transpeptide linkages between the 4th amino acid of one step peptide and 3rd amino acid of another (4→3 linkages). It was documented in 1974 that PG of *Mtb* consists predominantly of cross-links between the 3rd amino acid of one step peptide and the 3rd amino acid

of another (3→3 linkages)[23, 24]. These unusual 3→3 linkages, which are not included in the historical model of the PG, not only distinguish *Mtb* PG from others, it also has direct relevance to the antibiotics whose mechanism is based on inhibiting PG synthesis. Emerging evidence shows that *Mtb* LDTs that generate these linkages are uniquely susceptible to the carbapenem subclass of *β*-lactams[17, 25-29]. In this review, we summarize recent findings and observations regarding the structure and function of the LDTs and DDTs of *Mtb*. Knowledge of these enzymes and their bioactivities could serve to facilitate the discovery of antibiotics in targeting this key component of *Mtb*.

2.2 Structure and function of D,D- and L,D-transpeptidases

The *Mtb* genome encodes two classes of DDTs, two class A (ponA1 and ponA2), two class B (PBPA and PBPB) and a lipoprotein (PBP-lipo) with common motifs as class B PBPs[30]. There are additional six class C proteins, one categorized as type-4 (PBP4), one type-5 (PBP5), one type-7 (PBP7) and three putative type AmpH; PBP (Rv0907), PBP and PBP (Rv1367c)[31, 32]. Among these PBPs, only PBPA, PonA1 and PonA2 have reported crystal structures[11, 12]. There are five LDT paralogs in *Mtb,* namely: Ldt_{Mt1}, Ldt_{Mt2}, Ldt_{Mt3}, Ldt_{Mt4} and Ldt_{Mt5}[33] and have been outlined in Table 2.1. No crystal structures for Ldt_{Mt3} and Ldt_{Mt4} have been reported yet.

Table 2.1. Summary of the *Mtb* transpeptidases whose structures have been determined.

Target	Target protein	Type of transpeptidases in PG synthesis	Reported structure (PDB Code)
Cell wall	PBPA	D,D-transpeptidase	3LO7 (wild-type)[11], 3UN7 (mutant)[12], 3UPN (PBPA-imipenem)[12], 3UP0 (PBPA-penicillin G)[12] and 3UPP (PBPA-ceftriazone)[12]
	PonA1	D,D-transpeptidase	5CRF (mutant)[34] and 5CXW (PonA1-penicillin V)[34]
	PonA2	D,D-transpeptidase	1QMF (PBP2x-cefuroxime), 1QME (wild-type) [35],2KUI (mutant)[35], 2MQV (mutant)[35]
	L,D-transpeptidase (Ldt$_{Mt1}$)	L,D-transpeptidase	4JMN (mutant)[14] and 4JMX (imipenem)[14]
	L,D-transpeptidase (Ldt$_{Mt2}$)	L,D-transpeptidase	3VYP (Ldt$_{Mt2}$-meropenem)[15], 3VYN (mutant)[15], 3VYO (mutant)[15], 4HU2 (wild-type) [16], 4HUC (wild-type) [16], 3U1Q (Ldt$_{Mt2}$-2-mercaptoethanol), 3TX4 (mutant)[17], 3U1P (Ldt$_{Mt2}$-β-mercaptoethanol)[17], 3VAE (mutant)[17], 3TUR(mutant)[17], 4GSQ(mutant)[36], 4GSR(mutant)[36], 4GSU(Ldt$_{Mt2}$-meropenem)[36], 5DU7 (mutant)[29], 5DUJ (Ldt$_{Mt2}$-faropenem) [29], 5DVP (Ldt$_{Mt2}$-doripenem)[29], 5E5L (mutant)[29], 5E51 (Ldt$_{Mt1}$-faropenem)[29], 5DZJ (mutant)[29] 5DZP (mutant)[29], 5E1G (mutant) [29], (mutant) 5E1I (mutant) [29], 5K69 (mutant) [29], 5D7H (mutant) [37], 5DCC (Ldt$_{Mt2}$-biapenem) [37], 5DC2 (LdtMt2-tebipenem)[26], 5LB1(mutant) [26], 5LBG (mutant)[26], 4QR7 (Ldt$_{Mt2}$-Se-meropenem)[38], 4QTF (Ldt$_{Mt2}$-imipenem)[38], 4QRA (wild-type)[38], 4QRB (mutant)[38]
	L,D-transpeptidase (Ldt$_{Mt5}$)	L,D-transpeptidase	4ZFQ (Ldt$_{Mt5}$-meropenem)[39], 4Z7A (mutant)[39]

The first structure of a DDT of *Mtb* was reported by Fedarovich *et al.* in 2010 [11]. PBPA from *Mycobacterium tuberculosis* is a class B penicillin-binding protein which is important for cell division[11]. The crystal structure of PBPA from H37Rv was resolved at 2.05 Å resolution and refined to an R-factor of 21.7% with excellent stereochemistry. The alignment with the class B PBPs shows that the SxN motif of PBPA occupies a position that is farther from the core of the binding site than that observed in other PBPs, which places Ser281 beyond hydrogen-bonding distance with residues of the SxxK and KTG motifs[11]. Later, this same group determined the second crystal structure of PBPA, also in the apo form, and compared it with their earlier structure[11]. Significant structural differences in the active site region were apparent, including increased ordering of a *β*-hairpin loop and a shift of the SxN active site motif such that it occupied a position that appears catalytically competent.

The second-order acylation rate constants for some selected antibiotics, imipenem, penicillin G and ceftriaxone were assayed against PBPA. Among these antibiotics, only imipenem demonstrated anti-tubercular activity with maximum acylation efficiency. Different conformational behaviour was observed in the complexation of PBPA with the same antibiotics in the *β*5-α11 loop near the active site, but these varied for each *β*-lactam and the two molecules in the crystallographic asymmetric unit. In general, it was revealed that the *β*5-α11 loop of PBPA has a flexible region that appears important for acylation and provides further indication that the PBPs in the apo form can occupy different conformational forms[12].

In another study, the crystal structure of the PonA1 transpeptidase domain from the *Mtb* strain H37Rv in the apo form and bound to penicillin V was reported. PonA1 is a class A penicillin-binding protein, that is required for maintaining physiological cell wall synthesis and cell shape during growth in the mycobacteria[34]. The general structural detail and the penicillin-binding site were characterized. The crystallized PonA1 structure (residues 249–643) contains the transpeptidase domain and one small adjacent domain at the N terminus of the transpeptidase enzyme. The first 156 residues that form part of the N-terminal glycosyltransferase domain and 33 residues at the C terminus of the PonA1 were not observed in the protein structure. These modifications could be due to protein degradation and/or structural disorder. The PonA1 X-ray structure has a unique unstructured C terminus that contains a proline-rich region. This region forms an exposed long hydrophobic tail, suggesting that it may be involved in the protein-protein interactions that have been suggested by previous studies[40]. It was concluded from their study that the structural comparison of inhibitor-free and inhibitor-bound states of PonA1 indicates that binding of penicillin V induces conformational changes of the loop *β*4-α3 leading to a widening of the penicillin-binding pocket.[34].

PonA2 is the second enzyme of the class A PBP in *Mtb*[35], which is involved in the adaptation of *Mtb* to non-replicating persistency, an ability that has been attributed to the presence of a C-terminal PBP and Serine/Threonine kinase Associated (PASTA) domain. The PASTA domains are typically considered as

β-lactam antibiotic binding domains and were previously proposed to act as sensors of muropeptides and mediate complex mechanisms bacterial revival from the non-replicating state[41, 42]. Calvanase and co-workers[35] determined the solution structure of the PASTA domain from the PonA2[35] and analyzed the binding characteristics against a plethora of possible binders, as well as *β*-lactam antibiotics, two distinctive muropeptide mimics, and polymeric peptidoglycan. Their study showed that, despite a high structural similarity with other PASTA domains, the corresponding domain of PonA2 displays varying binding characteristics, as it is not able to bind any of the ligands tested. The findings revealed that the role of the PASTA domains cannot be generalized, as their specific binding characteristics largely depend on surface residues, which are usually variable[35]. The DDT activity of PBPs is catalysed by a common PB domain, which binds *β*-lactam antibiotics. The latter inhibits the enzymatic DDT activity of the PB domain, based on the structural similarity between penicillin and the D-ala-D-ala dipeptide that forms the terminus of the natural substrate of PBPs [L-ala D-glu L-lys D-ala D-ala (UDP-MurNAc-pentapeptide[43])], the penta-peptide precursors of the PG[31].

Nuclear Magnetic Resonance (NMR) was used to solve the structure of the PonA2-PASTA domain and explored its binding properties toward the *β*-lactam antibiotics cefuroxime and cefotaxime, the muropeptides L-Ala-gamma-D-Glu-mDAP and MurNAc-L-Ala-gamma-D-Glu-mDAP, and polymeric peptidoglycan (PGN). The 1H-15N heteronuclear single quantum coherence (HSQC) spectrum of the 15N-labeled PonA2-PASTA domain shows a good dispersion of signals, indicative of a well-folded structure and consistent with UV circular dichroism (CD) data[35]. Triboulet *et al.*[28], performed NMR chemical shift perturbation experiments to explore the structural and thermodynamics basis for this specificity, and identify *β*-lactam features that are critical for efficient L,D-transpeptidase inactivation. In a study where LDT (LdtfmC442A) was incubated with increasing *β*-lactam concentrations up to the drug solubility limit in order to observe the formation of noncovalent complexes, it was observed that a fast exchange occurred between free enzymes and the protein-beta-lactam complex. The residues that were affected by drug binding were mostly located at the surface of the protein in the vicinity of the LdtfmC442A catalytic cavity indicating specific binding of the drugs[28]. In 2010, Kastrinsky *et al.*[44] performed the synthesis of labeled meropenem to identify the protein targets of the carbapenems in whole cells of *Mtb*, using two labeled forms of meropenem to use as probes for transpeptidases. The use of radiolabeled meropenem synthesis that relied on the introduction of a labeled amine, served as an advantage to introduce an alternative label in a similar fashion with the only constraints that the label is compatible with the carbapenem nucleus and not impart any significant steric demand. The synthesized ^{14}C labeled meropenems offer useful tools to identify and characterize the targets of the carbapenems in other organisms.

The overexpression, purification and biochemical characterization of a class A high-molecular-mass penicillin-binding protein, PBP1* and its soluble derivative from *Mtb* were earlier studied by Sanjib Bhakta and Joyoti Basu[13]. The study was the first report of the complete genome sequence of *Mtb*[1] with the presence of two open reading frames (ORFs), Rv3682 and Rv0050, which encodes the two putative class A high-molecular-mass PBPs. They found that *Mtb* PBP1* has a similar sequence to *M.leprae* PBP1*. The sequence similarity and sensitivity of *Mtb* PBP1* to *β*-lactam antibiotics suggests that it is the counterpart of *M.leprae* PBP1*[13]. No crystal data was reported for this study.

Lavollay and co-workers[20] reported a new structure of *Mtb* PG from a stationary-phase culture that showed an unusually high content (80%) of 3-3 cross-linkage created by L,D-transpeptidation. The X-ray crystallographic study of one of the LDTs (Ldt_{Mt1}) (**Figure 2.1**) from *Mtb* was performed by Correale *et al.* in 2012[14]. Analysis of the protein families (PFAM) database[45] showed that Ldt_{Mt1} comprises of two domains, the *N*-terminal domain, the structure of which cannot clearly be predicted, and the *C*-terminal LDT catalytic domain. The catalytic domain of Ldt_{Mt1} shares 29% sequence identity with that of the LDT from *Enterococcus faecium*[46]. The catalytic residues of Ldt_{Mt1} are Cys226, His208, and Ser209. In a further study by Correale *et al.* in 2013[9], the crystal structures of LDT Ldt_{Mt1} from *Mtb* in the apo form and imipenem-bound were reported. They used X-ray crystallography, spectroscopic and calorimetric assays to investigate the structural features of Mtb Ldt_{Mt1} in both a ligand-free form and in complex with the carbapenem imipenem. The crystal structure of Ldt_{Mt1} showed that the catalytic site is located in a tiny tunnel, the results suggesting a high specificity of Ldt_{Mt1} for its substrates, as was observed for the LDT from *Enterococcus faecium*[47]. Additionally, the structure of the imipenem inactivated Ldt_{Mt1} gives a detailed molecular view of the interactions between the carbapenem drug and Ldt_{Mt1}.

Ldt_{Mt1} is upregulated 17-fold during the stationary phase and is believed to perform a role in bacterial adaptation to the non-replicating state[48]. Furthermore, Ldt_{Mt1} is believed to perform an important role in PG metabolism to the non-replicative state of the bacilli[20].
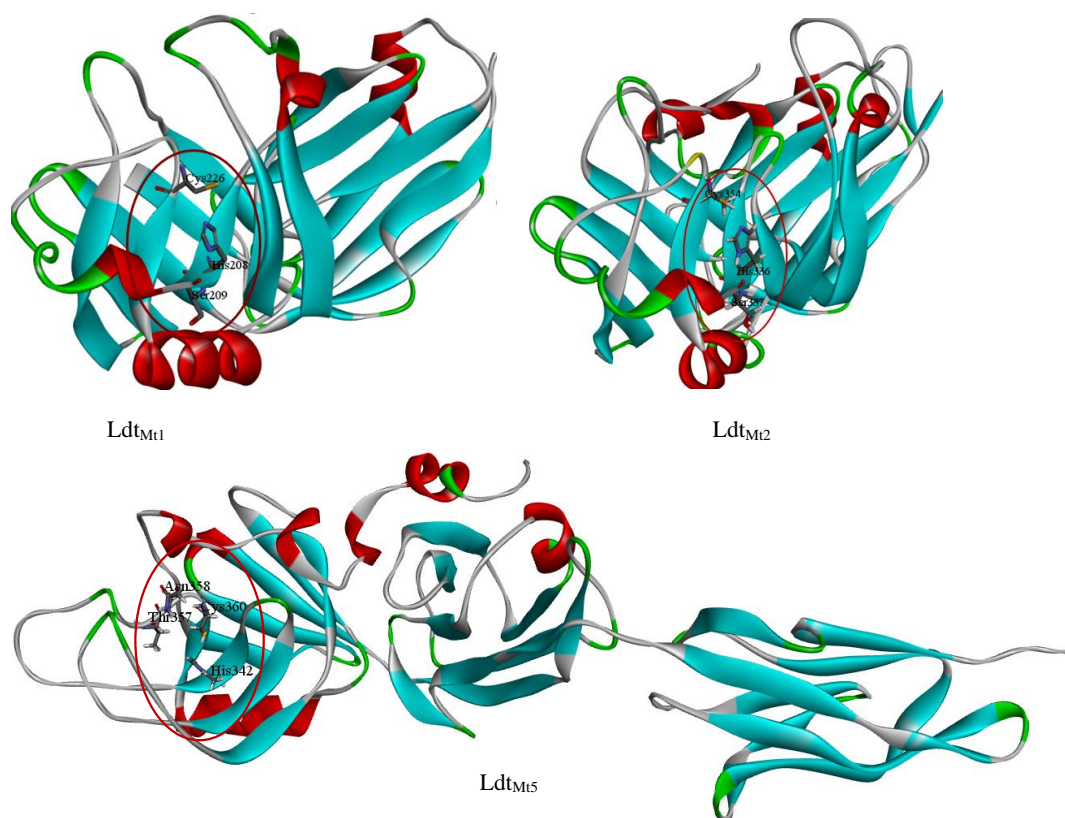
Figure 2.1 Structure of Mtb Ldt$_{Mt1}$[14], Ldt$_{Mt2}$[17], and Ldt$_{Mt5}$[39]. Residues of the active sites are represented as sticks within the enzyme. On aligning the sequences of Ldt$_{Mt1}$, Ldt$_{Mt2}$ and Ldt$_{Mt5}$, the important regions of these enzymes such as the catalytic domains, the BIgA and BIgB interfaces and loop LD, are presented in Figure 2.

In 2012, Erdemli *et al.* reported the first crystal structure of *Mtb* LDT (Ldt$_{Mt2}$) containing a bound PG fragment. The holo-enzyme structure information provides the catalytic site organization as well as the substrate identification by the enzyme. Added to the description of the structure of Ldt$_{Mt2}$ is the characterization of the extracellular portion of the enzyme as comprising of two domains. The *N*-terminus possesses immunoglobulin-like domains and the *C*-terminus harbours the catalytic ErfK/YbiS/YhnG domain. The catalytic residues of Ldt$_{Mt2}$ are Cys354, His336, His352 and Ser337[16, 17, 36] In comparison to Ltd$_{Mt1}$, the catalytic domain is located at the C-terminus. On the basis of this structure, comparative modelling of the identified *Mtb* homologs suggested[49] that the[20] *N*-terminal domain fold, and that the enzyme's overall conformation differentiate this category from other structurally characterized ErfK/YbiS/YhnG domain-containing proteins such as *Bacillus subtilis* ykuD[49] and *E. faecium* LDT Ldt$_{fm}$[46]. An *Mtb* strain deficient of Ldt$_{Mt2}$ loses virulence and has weakened growth during the chronic phase of the disease[33]. Also, this strain lacking Ldt$_{Mt2}$ is more susceptible to the therapeutic combination of amoxicillin

and clavulanic acid[33], suggesting that the 3-3 transpeptidation activity is a major contributor to β-lactam resistance.

Also in 2012, Böth et al. [16], investigated the structure of Ldt$_{Mt2}$ from *Mtb* and reported its three-dimensional structure of Ldt$_{Mt2}$ based on the X-ray crystal structures of two fragments of Ldt$_{Mt2}$ representing the extracellular part of the protein. Their structural analysis disclosed that Ldt$_{Mt2}$ folds into three domains, i.e., two domains in the N-terminal portion, both of which display an immunoglobulin-related fold, and the C-terminal transpeptidase domain. This domain composition is different from the two-domain structure of the extramembrane part of the Ldt$_{Mt2}$ proposed recently[17]. The crystal structures of the Ldt$_{Mt2}$[16] constructs allow for modelling of the full-length extramembrane part of the enzyme (residues 55–408), providing an estimate of the maximal distance of the catalytic site from the membrane and thereby the approximate distance at which 3–3 cross-links that are formed in the PG layer. Additionally, they used mass-spectrometric analysis to demonstrate that Ldt$_{Mt2}$ (Cys354) forms covalent adducts with the β-lactam antibiotics imipenem and ampicillin.

Several X-ray crystal structures of an *N*-terminal-truncated Ldt$_{Mt2}$ (**Figure 2.1**) were reported by Li et al. in 2013[50]. Apart from the free enzyme (apo), these included a trypsin-degraded fragment of Ldt$_{Mt2}$ and the complex of Ldt$_{Mt2}$ with meropenem, at 2.5, 1.8 and 1.4 Å resolutions, respectively. The authors indicated that these structures disclose the inhibition mechanism of meropenem against Ldt$_{Mt2}$ (**Figure 2.2**). The apo Ldt$_{Mt2}$ structure[50] showed a linear arrangement of the two *N*-terminal β-barrel domains (residues 60-148 and 149-250) and the *C*-terminal YkuD domain (residues 251-408). The two *N*-terminal β-barrel domains, both of which adopt an IgG-like fold, contain one three-stranded and one four-stranded sheet, respectively. It was concluded that these two IgG-like domains act as a spacer arm for the YkuD catalytic domain[50].
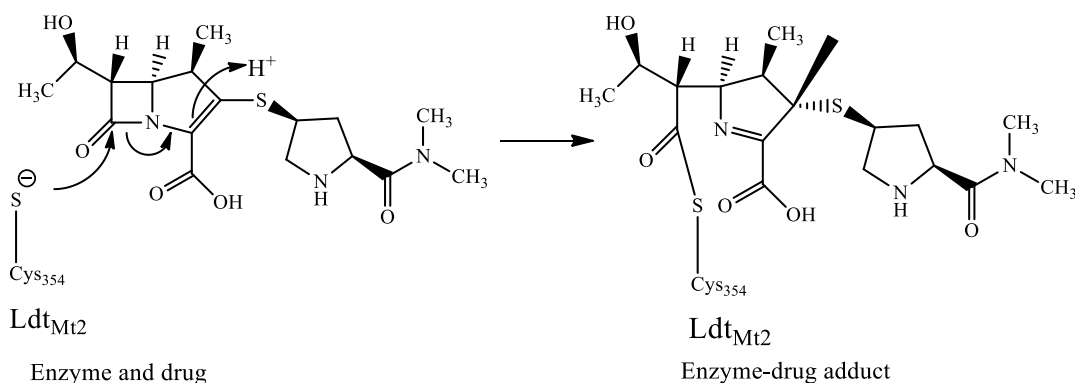
Figure 2.2 Molecular structure of the Cys354-meropenem adduct formed with Ldt$_{Mt2}$[50]

The most recent study[37] on the X-ray crystal structures of Ldt$_{Mt2}$ bound with either biapenem or tebipenem, showed that even with significant variations of the carbapenem sulfur side chains, biapenem (**Figure 2.3**)

and tebipenem eventually form similar adducts that bind to the outer cavity of Ldt$_{Mt2}$. The sulfur atom of Cys354 forms a covalent bond with the carbonyl group of the β-lactam ring in carbapenems. This study differs from other Ldt$_{Mt2}$ studies described previously[17], where binding occurs within the inner cavity. The study proposed that this common adduct is an enzyme catalysed the decomposition of the carbapenem adduct by a mechanism similar to the S-conjugate elimination by β-lyases[37]. The apo-Ldt$_{Mt2}$ structure and the previously solved apo-Ldt$_{Mt2}$ structure (3VYN[50]) have an RMSD of 0.7 Å among 347 Cα atoms superimposed on each other. Therefore, the catalytic residues of Ldt$_{Mt1}$ and Ldt$_{Mt2}$ behave similarly while that of Ldt$_{Mt5}$ is different as represented in **Figure 2.2**. The earlier study by Correale *et al.*[9] gave clarification on the structural features of Ldt$_{Mt1}$ and disclosed analogies and differences between the two key transpeptidases of *Mtb*, the Ldt$_{Mt1}$ and Ldt$_{Mt2}$.
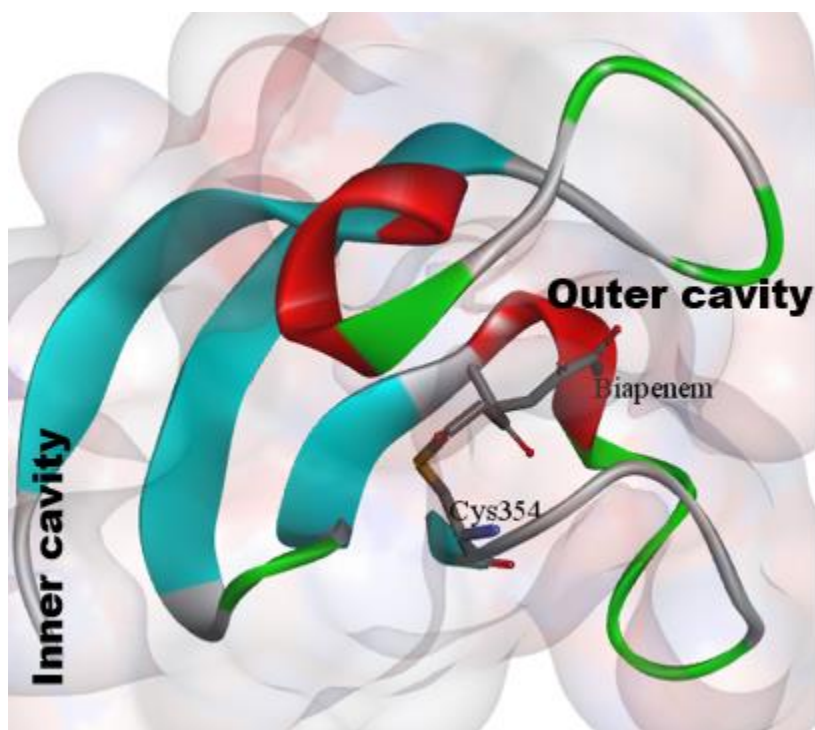
Figure 2.3 The description of the Cys354 adduct formation of biapenem with Ltd$_{Mt2}$ showing where the inner and outer cavities[37].

Brammer *et al* [39] reported the first crystal structures of Ldt$_{Mt5}$ (**Figure 2.1**) in apo form and as a meropenem complex. It was observed that *Mtb* with deletion of Ldt$_{Mt5}$, exhibits abnormal growth, and is more vulnerable to killing by crystal violet, osmotic shock, and select carbapenem antibiotics. Consequently, they concluded that Ldt$_{Mt5}$ is not a functionally redundant LDT, but that it serves a unique role in maintaining the integrity of the *Mtb* cell wall. The catalytic residues of Ldt$_{Mt5}$ are Cys360, His342, Thr357 and Asn358. The Ldt$_{Mt5}$ has two variations in the conserved motif; a motif alternative Thr357 of Ldt$_{Mt5}$

replaces the Ldt$_{Mt2}$ serine (Ser351) and Asn358 replaces the characteristic motif histidine (His352 in Ldt$_{Mt2}$)[39].
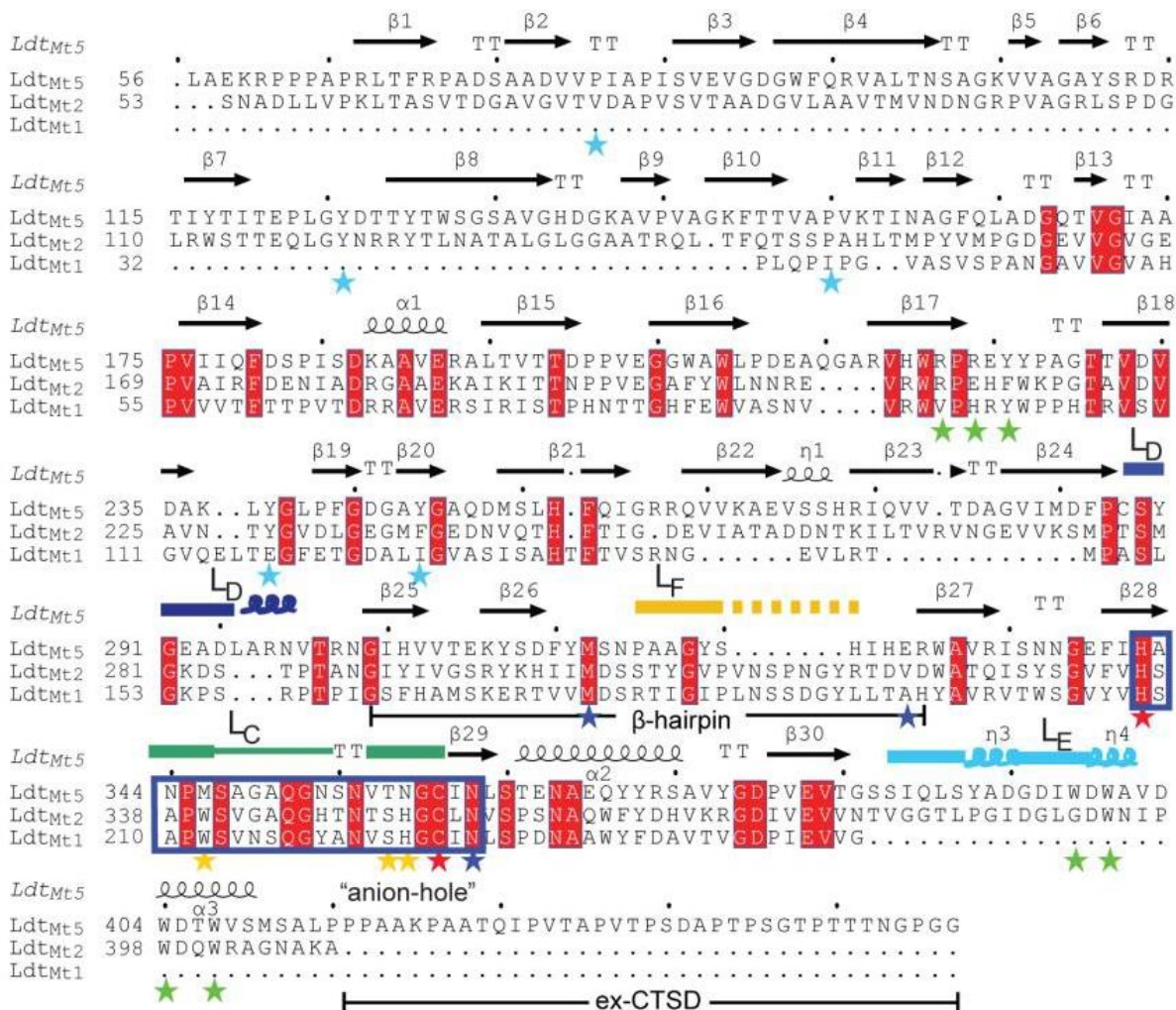
Figure 2.4 The sequence alignment based on the structural superposition of Ldt$_{Mt1}$[14], Ldt$_{Mt2}$[17] and Ldt$_{Mt5}$[39]. The observed secondary structures are noted above the amino acid sequences. red: catalytic residues; yellow: loop LD).

Recently, Gokulan *et al.*[38] reported the full length crystal structures of the periplasmic region of Ldt$_{Mt2}$ apo form, in complex with meropenem and imipenem and a calcium bound dimeric structure. In their observations, it was revealed that the periplasmic region of the LDT folds into three domains and that the catalytic residues are situated in the *C*-terminal domain. The acylation reaction occurs, as before, between carbapenem antibiotics and the catalytic Cys-354, forming a covalent complex. The adduct formed mimics the acylation of LDT with the donor PG-stem. It is interesting to note that in both the apo form and the carbapenem complexes, the *N*-terminal domain has a muropeptide unit non-covalently bound to it. Another

interesting observation is that the calcium complex crystallized as a dimer through head and tail interactions between the monomers. It was concluded that a fragment of the PG-stem binds with the *N*-terminal domain of LDT, which was not observed in the earlier reported structures[9, 14, 16, 17, 28, 51].

2.3 Mechanistic pathway of transpeptidases

The benefit of understanding the possible reaction mechanisms of the transpeptidases (**Figure 2.5**) required for the growth and metabolism of *Mtb* PG is more in the context of developing new drugs against TB[52-54]. The *β*-lactam antibiotics act as a suicide substrate of the DDTs, as the active-site serine residue attacks the carbonyl of the *β*-lactam ring[31]. However, the resulting ester bond is hydrolysed at a very slow rate, typically 2–10 h^{-1}, with the formation of the acyl enzyme is, therefore, being considered to lead to irreversible inactivation of the enzyme at a physiologically relevant time scale. The active-site cysteine residues of LDTs similarly form thioester bonds with the *β*-lactam ring[55]. The enzymes display narrow substrate specificity as this reaction occurs preferentially with *β*-lactams of the carbapenem and penem subclasses.
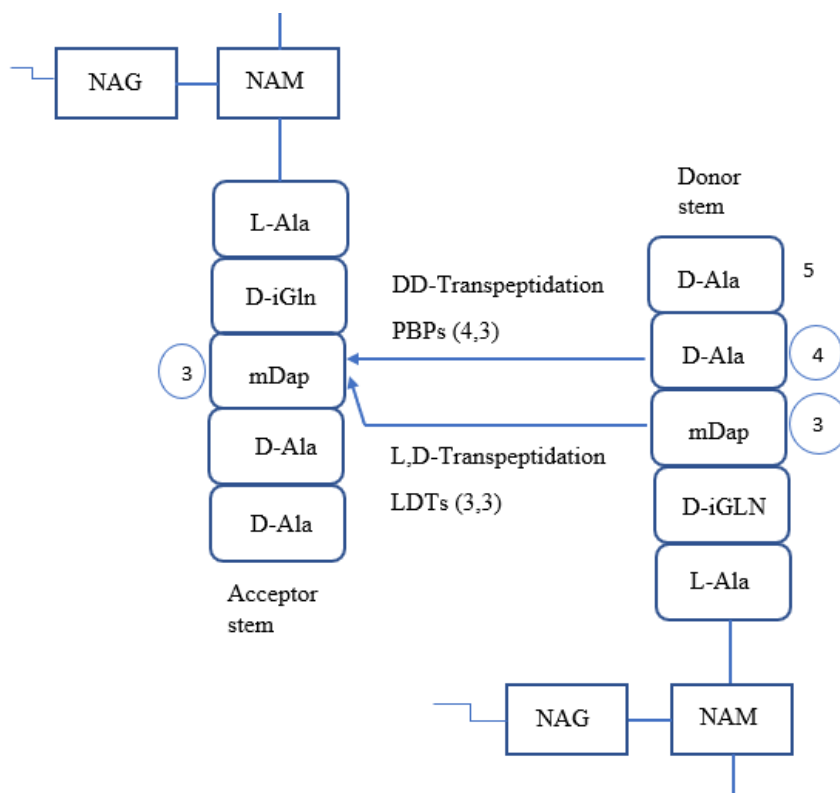
Figure 2.5 Diagrammatic illustration of peptidoglycan transpeptidation. D,D-transpeptidases (4-3) while L,D-transpeptidases (3-3) linkages, redrawn from literature[9].

Two different catalytic reaction mechanisms were proposed for the LDTs. The first one was offered by Biarrote-Sorin and colleagues[46], who proposed that in LDT, the two pathways to the catalytic cysteine (Cys442) are used: one for the acyl donor and the other for the acyl-acceptor substrates. The buried pocket also contains Asp422, Ser439, His440 and a conserved His421. By comparison of the cysteine and serine proteases[56], the $N^{\varepsilon 2}$ of His421 will capture the S^{γ} hydrogen released by Cys442 to assist nucleophilic attack of the carbonyl of the L-Lys3-D-Ala4 peptide bond. The position of the imidazole ring of His421 is stabilized by a hydrogen bond involving $N^{\delta 1}$ and the main-chain carbonyl oxygen of Asp422. The hydrogen bond interaction[56] is expected to increase the pKa of His421 to a lesser extent than the $N^{\delta 1}$-carboxylate interaction in the classical Ser-His-Asp triad found in serine proteases. The latest and more simplified proposal was suggested by Erdemli and colleagues[17] for LDT which is based on a cysteine proteases mechanism. In the cysteine protease proposal for Ldt$_{Mt2}$ (**Figure 2.6**), the catalytic mechanism occurs in two stages. First, (acylation step), the catalytic Cys352 thiolate (upon proton abstraction) attacks the acyl carbon of the substrate to form a tetrahedral intermediate (EI^{ox}). After the intermediate thioester formation and protonation by the His336 imidazolium group, D-Ala is released. In the second stage (deacylation step), another peptide stem enters the catalytic site, also through the external vestibule and binds to the catalytic site residues with the side chain amide of the m-A2pm3′ residue (which is isomorphic to D-Ala and also has a D chiral centre). In this step, the His336 acts as a catalytic base by abstracting a proton from the amine group of the mA2pm3′ residue, while the same amine group performs a nucleophilic attack into the carbonyl carbon of acyl-enzyme[17]. Subsequent theoretical studies by Silva *et al.*[57, 58] investigated the inhibition reaction of *Mtb* Ldt$_{Mt2}$ in the presence of carbapenems. The activation energies ($\Delta G^{\ddagger}_{cal}$) values obtained for the whole reaction (acylation and deacylation steps, **Figure 2.4**) at M06-2X-D3/MM level are 17.41 and 20.00 kcal mol^{-1} for the first and second steps (Figure 4), respectively, which is in agreement with experimental data[15].
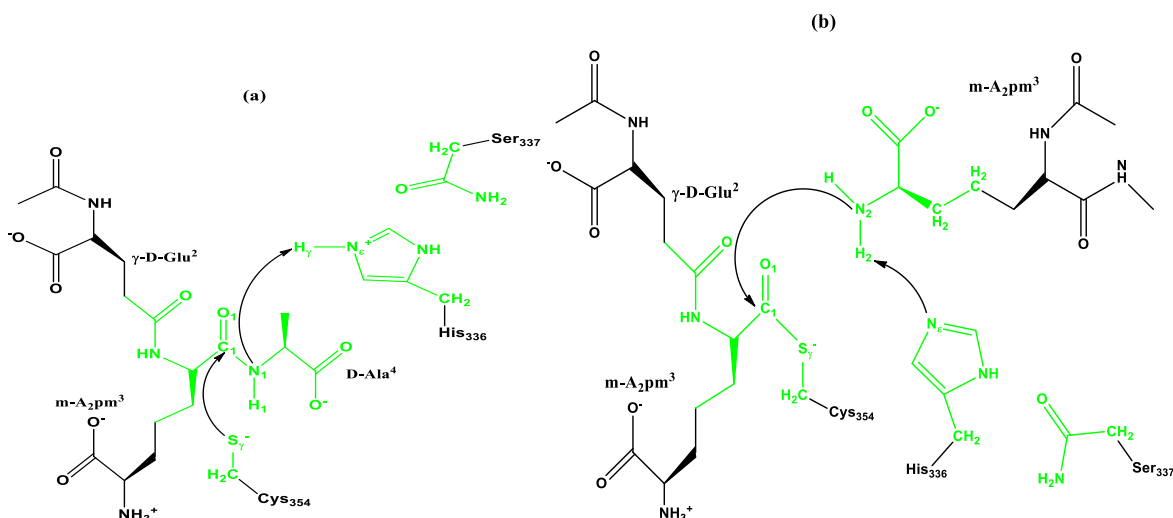
Figure 2.6. Reaction mechanism for (a) Acylation Step and (b) Deacylation Step in the active site of the Ldt$_{Mt2}$ enzyme[58].

2.4 Drugs for Mtb transpeptidase inactivation

The development of TB drugs started with streptomycin with the isolation of the antibiotic reported in a paper in January 1944. The first human clinical trials of streptomycin were administered on November 20th, 1944 [59]. The treatment occurred a few weeks after the first patient received an oral dose of Para-Aminosalicylic Acid (PAS) as the derivatives of aspirin in October 1944[60]. Later, in 1951, isoniazid was discovered and found to be ten times more potent than either streptomycin or PAS and it appeared to be nontoxic[61, 62]. Combined therapy with isoniazid (INH), streptomycin, and PAS turned out to be the typical triplicate drugs used for more than a decade. The usage of the first line antimycobacterial drugs began with the inclusion of pyrazinamide (PZA), rifampicin (RIF) and ethambutol (EMB) in 1952, 1957 and 1962 respectively[63].

The combination of INH, PZA, RIF, and EMB form the four regimens for treating TB at the intensive phase of treatment, which is for two months. Thereafter, at the continuation phase, only INH and RIF are used for either four or seven months of the therapy period[64, 65]. Drug-resistance to frontline anti-TB drugs has become a major public health problem. The treatment of MDR and XDR tuberculosis according to the results of drug vulnerability testing is achieved using both first and second-line drugs together. Second-line drugs comprise of aminoglycosides (kanamycin and amikacin), cycloserine, terizidone, ethionamide, protionamide, capreomycin, aminosalicylic acid, and fluoroquinolones (together with ofloxacin, levofloxacin, gatifloxacin, and moxifloxacin)[66].

Carbapenems were recently introduced to treat TB[67, 68]. These antibiotics were initially created from thienamycin, a natural product found in the culture filtrates of *Streptomyces cattleya*[69]. Four carbapenems have been approved thus far for human use, these being imipenem, meropenem, ertapenem, and

doripenem[70]. Imipenem was the first carbapenem endorsed by the FDA in 1985 and is the most extensively used one of this family. The use of meropenem was endorsed in 1995, with ertapenem and doripenem being approved in 2001 and 2007, respectively[71]. Carbapenems kill *Mtb*, at least in the active phase[72], and the addition of a *β*-lactamase inhibitor is recommended[72, 73] as it inhibits 3,3-transpeptidases. Despite the general success of *β*-lactam antibiotics[74], faropenem has been approved in Japan and is currently available as an orally administered sodium salt, Farom®: while in the USA, faropenem is in Phase III clinical trials as the ester prodrug, faropenem medoxomil. Faropenem is a penem and is structurally similar to the carbapenems, which include the clinically available drugs imipenem, meropenem, doripenem and ertapenem, it differed by a sulfur atom[75].

2.5 Experimental case studies

In this section, we highlight the bioactivities of known and approved TB drugs that function by targeting LDTs and DDTs.

The first bioactivity assay of the PonA1[34] against penicillin V and meropenem was elucidated by Filippova *et al.* in 2016[34]. They applied site-directed mutagenesis, antibiotic profiling experiments, and fluorescence thermal shift assays to quantify PonA1's sensitivity to different classes of *β*-lactams. Their results showed that the structural comparison of the PonA1 apo-form and the antibiotic-bound form indicated that the binding of penicillin V induces conformational changes in the position of the loop *β*40-α3 that surrounds the penicillin-binding site. In addition, their antibiotic profiling experiments indicated that the transpeptidase activity of PonA1 in both *Mtb* mediates tolerance to specific cell wall-targeting antibiotics, particularly to penicillin V and meropenem. Fluorescence thermal shift (FTS) data revealed that formation of the acyl-enzyme by compounds such as carbenicillin or penicillin V result in positive thermal (Tm) shifts, while others such as clavulanate or meropenem give negative Tm shifts, indicating that they induce a more destabilized conformation of PonA1. The conformational changes showed that both antibiotics bind to the enzyme. Meanwhile, the binding of clavulanate or meropenem induced a more destabilized conformation of PonA1. It was concluded that as *Mtb* is an important human pathogen, the structural data provided could serve as a template for designing novel transpeptidase inhibitors to treat tuberculosis infections.

In 2010, Gupta *et al.*[33] reported that Ldt_Mt2 from *Mtb* is a non-classical transpeptidase that is essential for virulence and resistance to amoxicillin. They isolated a *Mtb* mutant lacking Ldt_Mt2 resulting from the inactivation of gene encoding it, by screening a group of 5,100 unique transposon insertion mutants for growth attenuation. It was hypothesized that the deletion of Ldt_Mt2 may compromise the mutant's ability to adapt during the chronic phase of infection, a crucial stage in the pathogenesis of tuberculosis. They tested this hypothesis by assessing the susceptibility of the Ldt_Mt2 mutant to amoxicillin. The deletion of Ldt_Mt2 showed increased susceptibility to amoxicillin/clavulanate combination. Their result showed that

deletion of this protein leads to the altered cell surface and colony morphology, loss of virulence and increased vulnerability to amoxicillin-clavulanate during the chronic phase of infection. It was concluded that inhibiting LDTs aids in targeting persisting bacilli during the chronic phase of *Mtb* infection.

Dubee and colleagues in 2012[76] investigated the inactivation of Ldt_{Mt1} with carbapenems and cephalosporins. Using mass spectrometry and stopped-flow fluorimetry they explored the kinetics and mechanisms of inactivation of the prototypic Ldt_{Mt1} with some selected carbapenems, while cephalosporins were explored using mass spectrometry and stopped-flow fluorimetry. Inactivation happened through noncovalent drug binding and acylation of the catalytic cysteine of Ldt_{Mt1}, which was eventually followed by hydrolysis of the resulting acyl enzyme. Meropenem quickly inhibited Ldt_{Mt1}, with a binding rate constant of 0.08 μM^{-1} min^{-1}. By comparing the kinetic constants for drug binding, it was concluded that acylation and acyl enzyme hydrolysis indicated that carbapenems and cephems can both be tailored to optimize PG synthesis inhibition in *Mtb*.

The *in vitro* cross-linking of *Mtb* PG by LDTs, and the inactivation of these enzymes using carbapenems was studied by Cordillot and co-workers[15] in 2013. They purified five LDT paralogues of *Mtb* (Ldt_{Mt1} to 5) and compared their activities with those of peptidoglycan fragments and carbapenems. The five LDTs were functional *in vitro* as they were active in assays of PG cross-linking(Ldt_{Mt5}), β-lactam acylation(Ldt_{Mt3}), or both (Ldt_{Mt1}, Ldt_{Mt2} and Ldt_{Mt4}). Ldt_{Mt3} was the only LDTs that was inactive in the crosslinking assay, suggesting that this enzyme might be involved in other cellular functions, such as anchoring proteins to peptidoglycan, as shown in *Escherichia coli*. Inactivation of LDTs by carbapenems is a two-step reaction consisting of a reversible formation of a tetrahedral intermediate, the oxyanion, followed by irreversible rupture of the β-lactam ring, which leads to the formation of a stable acyl enzyme. It was concluded that imipenem could inactivate LDTs more rapidly than ertapenem and that both drugs were more efficient than meropenem and doripenem, signifying that modification of the carbapenem side chain could be used to optimize their antimycobacterial activity[15].

In 2014[77], Schoonmaker *et al*., generated and studied *Mtb* strains deleted for Ldt_{Mt1} or both Ldt_{Mt1} and Ldt_{Mt2}. The study defined the cellular phenotypes linked with deletion of these LDTs. They used an *Mtb* mutant of CDC1551 without a functional replica of Ldt_{Mt2} (strain M2)[33] which represents the parent strain for producing a double knockout strain missing in both Ldt_{Mt2} and Ldt_{Mt1}. The cell surface morphologies of *Mtb* strains at exponential and stationary phases of growth was processed for field emission scanning electron microscopy(FESEM) analysis. Strains lacking Ldt_{Mt1}, Ldt_{Mt2}, or both Ldt_{Mt1} and Ldt_{Mt2} (M12), were studied. Unlike the parent wild-type *Mtb* strain, whose cell length was 1.8 µm, mutants lacking both Ldt_{Mt1} and Ldt_{Mt2} were consistently shorter, with an average cell length of 1.0 µm. Complementation of this double mutant with wild-type copies of Ldt_{Mt1} and Ldt_{Mt2} restored the cell length phenotype. However,

the minimum inhibitory concentrations (MICs) of imipenem, meropenem and ertapenem tested against the strains of Ldt_{Mt1}, Ldt_{Mt2} and M12 showed a trend similar to the burden in mice infected with wild-type *Mtb*. They concluded that the *Mtb* strain without both Ldt_{Mt1} and Ldt_{Mt2} shows changed cellular morphology, size, physiology, and *in vitro* and *in vivo* growth, as well as enhanced vulnerability to amoxicillin-clavulanate and a glycopeptide drug, vancomycin.

In 2015, Kaushik and co-workers[78] investigated the synergy of carbapenems and rifampin against *Mtb*. They determined the potencies of a number of carbapenems; ertapenem, meropenem, imipenem, doripenem, biapenem, tebipenem, panipenem and faropenem against *Mtb* by determining the minimum bactericidal concentration (MIC) and minimum bactericidal concentrations (MBC). They also examined if carbapenems and isoniazid or rifampin, the two drugs that form the pillars of TB treatment, show any synergy, indifference, or antagonism in activity. In addition, they compared the rates of spontaneous resistant mutants when *Mtb* is exposed to either rifampin or faropenem or a combination of these two drugs. Finally, they studied antimicrobial activities of combinations containing rifampin and carbapenems against drug-resistant clinical *Mtb* isolates. They concluded that faropenem or biapenem, doripenem, meropenem (carbapenems), and rifampin, act with synergy when combined.

In 2015, Dhar *et al.*[79] performed *in vitro* analysis to compare the potency of faropenem and meropenem to inhibit the LDTs, which is involved in the last cross-linking step of PG synthesis. In this study, a kinetic analysis of LDT inactivation through faropenem and *β*-lactams hydrolysis was made using spectrophotometry. The results showed that faropenem inactivated Ldt_{Mt1} 14-fold more efficiently than meropenem, as deduced from the k_{inact}/K_{app} ratio. The comparison of inactivation of the other LDTs by meropenem and faropenem revealed that the latter drug was also more efficient for inactivation of Ldt_{Mt2} (22-fold), Ldt_{Mt3} (6-fold), and Ldt_{Mt4} (9-fold). The acylated adducts of Ldt_{Mt1} were identified by mass spectrometry. All acyl enzymes were stable, while the rate constants were slightly higher for faropenem, except for Ldt_{Mt4}. Ldt_{Mt5} was not acylated by meropenem or faropenem. It was also concluded that the target LDT enzymes are inactivated more efficiently by faropenem than by meropenem, mainly due to a more favourable catalytic constant for the chemical step of the acylation reaction[79].

In 2015, Brammer *et al*[39]., performed the MIC studies to evaluate whether or not the loss of Ldt_{Mt5} would affect the susceptibility of *Mtb* to carbapenems. The MICs were determined using the standard broth dilution method[80] The Ldt_{Mt5} strain reproducibly showed modestly enhanced susceptibility to doripenem and faropenem (a penem) compared to wild-type, but neither strain is susceptible to ertapenem or meropenem under the conditions that were tested.

The study by Kumar *et al.* in 2017[29] characterized the inhibitory interactions of faropenem and carbapenems with Ldt$_{Mt1}$ and Ldt$_{Mt2}$ using biochemical and biophysical approaches. Multiple crystal structures of faropenem and carbapenems with the Ldt$_{Mt1}$ and Ldt$_{Mt2}$) were resolved. The penem and carbapenems were tested against these enzymes in a preclinical mouse model of TB treatment. Their result showed that while each carbapenem gave a unique adduct when reacting separately with the LDTs, acylation by faropenem was the only adduct detected in the competition assays with the carbapenem mixture. This suggests that Ldt$_{Mt1}$ and Ldt$_{Mt2}$ enzymes preferentially bind to faropenem. In addition, the MIC values of meropenem, doripenem, tebipenem and faropenem varied by only 2- to 8-fold between the two strains. They concluded that carbapenems are particularly effective not only because they inhibit DDTs and are not regularly inactivated by β-lactamases, but mainly because they also inhibit the LDTs which create most of the linkages in the PG of *Mtb*.

2.6 Computational case studies

The first computational report of a transpeptidase enzyme from *Mtb* was unveiled in 2014 by Silva and co-workers[58], who investigated the catalytic mechanism of L,D-transpeptidase 2. This group employed an umbrella sampling technique to produce the free energy profile connected with the catalytic mechanism of Ldt$_{Mt2}$. The Cys354-thiolate/His336-imidazolium pair of Ldt$_{Mt2}$ formed the starting point to drive the acylation step. Thereafter, the attack of Cys354 on the carbonyl carbon of the substrate happened in a single step to form a covalent intermediate. This step was found to be rate-limiting, which agrees with experimental data[17] for cysteine proteases. In the de-acylation step to complete the mechanism processes, the amine group of the second substrate attacks the acyl-enzyme complex, after which the 3→3 peptide bond is formed. In 2015, Silva and co-workers[57] explored the inhibition reaction of the Ldt$_{Mt2}$ with carbapenems and calculated the binding free energy that was used to describe the inactivation of Ldt$_{Mt2}$. They used QM/MM[81] and PMF approaches to determine a new reaction mechanism for the two carbapenems, and their theoretical findings agree in principle with experimental data. Silva *et al.*[82], in another study, investigated the non-covalent interaction of imipenem and meropenem with Ldt$_{Mt2}$ that targeted the cell wall of *Mtb* using the MM/GBSA[83] and SIE[84] approaches. These methods reproduced the same order of binding energies as experimentally observed for imipenem and meropenem.

Our research group has investigated the mechanistic study of the acylation step of the β-lactam ring with LDT$_{Mt2}$ was performed by Fakhar *et al.*[85] using DFT methods. Four possible reaction pathways with different transition states (TS) models were proposed as four membered-ring (TS-4, TS-4-His and TS-4-water) and a six-membered ring (TS-6-water). The obtained thermochemical quantities for the proposed models indicated that the activation barrier of TS-6-water model was considerably lower and therefore more favourable than the other models. Fakhar *et al.* recently studied the flap dynamics of Ldt$_{Mt2}$[86], and the

impact of the induced conformational changes of the flap region to the binding process was studied using molecular dynamics simulations in explicit solvent. Dynamic cross-correlation matrix (DCCM) analysis demonstrated significant anti-correlated motions in the imipenem/LDT$_{Mt2}$ flap, whereas ertapenem and meropenem binding induced a shift to correlation movement within the flap units. The MM-GBSA method revealed a lower value of ΔG_{bind} for MERO-Ldt$_{Mt2}$ and ERT-Ldt$_{Mt2}$ than IMI-Ldt$_{Mt2.}$

The *in silico* screening of synthetic compounds against *Mtb* LDTs was carried out by Billones *et al.*, is aimed at finding potent anti-tuberculosis drugs. In their study, they used structure-based pharmacophore screening, molecular docking, and *in silico* toxicity assays to screen compounds from a database of synthetic compounds[87]. Out of the 4.5 million compounds they screened, 18 were found to have better binding energies than meropenem and satisfactory *in silico* ADMET properties[87, 88]. Two of the 18 compounds that were tested *in vitro*, with one compound being found to have an excellent bioactivity against *Mtb* H37Ra. In 2017, Baldin *et al.* built a full-atom model of Ldt$_{Mt2}$ for screening new inhibitors[89]. They performed molecular modelling of the enzyme binding with the tetrapeptide fragment of peptidoglycan, as well as with *β*-lactam compounds, and built a full-atom model of Ldt$_{Mt2}$ for screening and optimizing the inhibitor structures. They observed that binding of the *N*- and *C*-terminal fragments of the growing PG chain in various tunnels is responsible for the different steps of the catalytic mechanism at the formation of non-classical 3-3 cross-linkages in peptidoglycan. They concluded that to simulate Ldt$_{Mt2}$ interaction with *β*-lactam inhibitors to inactivate the enzyme through the formation of stable acyl enzymes, it is necessary to consider the binding of potential inhibitors in tunnel C of the active site.

Recently, the non-covalent interactions between carbapenems and Ldt$_{Mt2}$ were investigated by Ntombela *et al.*[90] using the ONIOM approach. The binding interactions of Ldt$_{Mt2}$ in complexed with four carbapenems (biapenem, imipenem, meropenem, and tebipenem) was elucidated, where the carbapenems, together with catalytic triad active site residues of Ldt$_{Mt2}$ (His187, Ser188 and Cys205), were treated with QM [B3LYP/6-31+G(d)]. The remaining part of the complexes was treated at the MM level (AMBER force field), for the first time, an explicit water molecule was placed in the enzymatic pocket (as suggested by X-ray structures). The Gibbs free energy (ΔG), enthalpy (ΔH) and entropy (ΔS) for all complexes showed that the carbapenems exhibit reasonable binding interactions towards Ldt$_{Mt2}$. The water molecule increased the number of hydrogen bond interactions in the QM layer which showed a significant impact on the binding interaction energy differences and the stabilities of the carbapenems inside the active pocket of Ldt$_{Mt2}$. The study concluded[90] that the theoretical binding free energies obtained reflected the same trend as that of the experimental observations.

2.7 Conclusive remarks and perspectives

Understanding the structure and function of transpeptidases in the *Mtb* responsible for its survival, especially in its non-replicating form, is essential for the development of anti-TB agents to permanently inactivate it. Two biosynthetic pathways have been reported to inactivate both penicillin binding proteins and the non-classical transpeptidase in the presence of a *β*-lactam class of antibiotics via the serine and cysteine catalytic sites, respectively. Studies have shown that most of the cross-links were generated by LDTs when compared to that created by penicillin binding proteins, thereby making the former a major target to impede the biosynthesis of *Mtb* peptidoglycan. The transpeptidases enzymes are required to catalyze the polymerization of peptidoglycan (PG) cell wall of Mycobacterium tuberculosis. Since *Mtb* cannot survive without PG, inhibiting its synthesis can be a powerful way to kill *Mtb*. Indeed, there is a powerful precedent to this approach. More than 50% of antibiotics used today to treat bacterial infections in humans belong to the *β*-lactam class. The *β*-lactams exert their activity by inhibiting PG synthesis by inhibiting the classical transpeptidases, namely DDTs. Unlike in other bacteria where DDTs play a major role, the LDTs play dominant role in the synthesis of PG in *Mtb*. Therefore, if inhibition of DDTs has resulted in 50% of antibiotics in use today, one can be hopeful that inhibiting LDTs can also produce effective drugs to treat bacterial infections, especially to treat *Mtb* infections. Equally important is that since *β*-lactams have not been routinely used to treat TB, even the MDR-XDR strains are susceptible to this class of drugs. The main conclusion of the landmark paper by Hugonnet et al, in 2009[91] in the journal Science was the carbapenems were effective against MDR and XDR-TB strains. Now we know that carbapenems are effective largely because they inhibit the unique LDTs in *Mtb*. Also, it is highly relevant here to note that in a recent publication Cohen et al[92] demonstrated the MDR-XDR strains are paradoxically susceptible to *β*-lactams. The first set of anti-mycobacterial antibiotics such as isoniazid and rifampicin are no longer effective in combating *Mtb* strains that are multidrug resistant. This has led to the urgent need to elucidate the survival mechanisms of these enzymes inherent in *Mtb*. The mechanism of inactivation of this *mycobacterium* using *β*-lactam derivatives drugs (carbapenems) involves the acylation of the serine and cysteine catalytic sites for DDTs and LDTs respectively. However, it seems that only Ldt_{Mt2} has been well studied in terms of the bioactivities using its natural substrate and FDA approved drugs. Crystallography structures have been deposited in a protein data bank for further investigation computationally, which could advance the course of drug design. It is important to note that relatively few crystal structures have been reported for both TB enzymes (10 for DDTs and 36 for LDTs), which limits the theoretical development of new TB drugs. Thus, in order to permanently inactivate *Mtb,* all targets required for their survival needs to be investigated which could proffer adequate information leading to the development of potent anti-TB drugs.

Abbreviations

ADMET	Absorption, distribution, metablism, excretion and toxicity
DCCM	Dynamic cross correlation marix
EMB	Ethambutol
FDA	Food and Drug Administration
FTICR	Fourier transform ion cyclotron resonance
INH	Isoniazid
LDTs	L,D-transpeptidases
Mtb	*Mycobacterium tuberculosis*
MBCs	Minimum bactericidal concentrations
MDR	Multi-drug resistant
MIC	Minimum inhibitory concentration
MM/GBSA	Molecular mechanics generalized born surface area
PAS	Para-Aminosalicylic Acid
PASTA	PBP and Serine/Threonine kinase Associated
PBPs	Penicillin-binding proteins
PDB	Protein data bank
PG	Peptidoglycan
PMF	Potential of mean force
PZA	Pyrazinamide
QM/MM	Quantum mechanics/Molecular mechanics
RIF	Rifampicin
RNA	Ribonucleic acid
RT-PCR	Reverse transcription polymerase chain reaction
SIE	Solvation Interaction Energy
TB	Tuberculosis
XDR	Extensively drug-resistant
NTD	N terminal domain
FTS	Fluorescence thermal shift

Competing interests

The authors declare no competing interests.

Acknowledgements

References

[1] Cole, S., Brosch, R., Parkhill, J., Garnier, T., Churcher, C., Harris, D., Gordon, S., Eiglmeier, K., Gas, S., and II III, C. B. (1998) Erratum: Deciphering the biology of Mycobacterium tuberculosis from the complete genome sequence, *Nature 396*, 190.

[2] Petersen, P. E., Bourgeois, D., Ogawa, H., Estupinan-Day, S., and Ndiaye, C. (2005) The global burden of oral diseases and risks to oral health, *Bulletin of the World Health Organization 83*, 661-669.

[3] Organization, W. H. (2017) Global tuberculosis report 2017, In *Global tuberculosis report 2017*.

[4] Connolly, L. E., Edelstein, P. H., and Ramakrishnan, L. (2007) Why is long-term therapy required to cure tuberculosis?, *PLoS medicine 4*, e120.

[5] Kerantzas, C. A., and Jacobs, W. R. (2017) Origins of combination therapy for tuberculosis: lessons for future antimicrobial development and application, *MBio 8*, e01586-01516.

[6] Nachega, J. B., and Chaisson, R. E. (2003) Tuberculosis drug resistance: a global threat, *Clinical Infectious Diseases 36*, S24-S30.

[7] Lamichhane, G., and Bishai, W. (2007) Defining the'survivasome'of Mycobacterium tuberculosis, *Nature medicine 13*, 280.

[8] Sassetti, C. M., Boyd, D. H., and Rubin, E. J. (2003) Genes required for mycobacterial growth defined by high density mutagenesis, *Molecular microbiology 48*, 77-84.

[9] Correale, S., Ruggiero, A., Capparelli, R., Pedone, E., and Berisio, R. (2013) Structures of free and inhibited forms of the L, D-transpeptidase LdtMt1 from Mycobacterium tuberculosis, *Acta Crystallographica Section D: Biological Crystallography 69*, 1697-1706.

[10] Organization, W. H. (2016) *World malaria report 2015*, World Health Organization.

[11] Fedarovich, A., Nicholas, R. A., and Davies, C. (2010) Unusual conformation of the SxN motif in the crystal structure of penicillin-binding protein A from Mycobacterium tuberculosis, *Journal of molecular biology 398*, 54-65.

[12] Fedarovich, A., Nicholas, R. A., and Davies, C. (2012) The role of the β5–α11 loop in the active-site dynamics of acylated penicillin-binding protein A from Mycobacterium tuberculosis, *Journal of molecular biology 418*, 316-330.

[13] Bhakta, S., and Joyoti, B. (2002) Overexpression, purification and biochemical characterization of a class a high-molecular-mass penicillin-binding protein (PBP), PBP1∗ and its soluble derivative from Mycobacterium tuberculosis, *Biochemical Journal 361*, 635-639.

[14] Correale, S., Ruggiero, A., Pedone, E., and Berisio, R. (2013) Expression, purification, crystallization and preliminary X-ray crystallographic analysis of the L, D-transpeptidase LdtMt1 from Mycobacterium tuberculosis, *Acta Crystallographica Section F: Structural Biology and Crystallization Communications 69*, 253-256.

[15] Cordillot, M., Dubée, V., Triboulet, S., Dubost, L., Marie, A., Hugonnet, J.-E., Arthur, M., and Mainardi, J.-L. (2013) In vitro cross-linking of Mycobacterium tuberculosis peptidoglycan by l, d-transpeptidases and inactivation of these enzymes by carbapenems, *Antimicrobial agents and chemotherapy 57*, 5940-5945.

[16] Böth, D., Steiner, E. M., Stadler, D., Lindqvist, Y., Schnell, R., and Schneider, G. (2013) Structure of LdtMt2, an L, D-transpeptidase from Mycobacterium tuberculosis, *Acta Crystallographica Section D: Biological Crystallography 69*, 432-441.

[17] Erdemli, S. B., Gupta, R., Bishai, W. R., Lamichhane, G., Amzel, L. M., and Bianchet, M. A. (2012) Targeting the cell wall of Mycobacterium tuberculosis: structure and mechanism of L, D-transpeptidase 2, *Structure 20*, 2103-2115.

[18] Mattoo, R., Lloyd, E. P., Kaushik, A., Kumar, P., Brunelle, J. L., Townsend, C. A., and Lamichhane, G. (2017) LdtMav2, a nonclassical transpeptidase and susceptibility of Mycobacterium avium to carbapenems, *Future microbiology 12*, 595-607.

[19] Mainardi, J.-L., Fourgeaud, M., Hugonnet, J.-E., Dubost, L., Brouard, J.-P., Ouazzani, J., Rice, L. B., Gutmann, L., and Arthur, M. (2005) A novel peptidoglycan cross-linking enzyme for a β-lactam-resistant transpeptidation pathway, *Journal of Biological Chemistry 280*, 38146-38152.

[20] Lavollay, M., Arthur, M., Fourgeaud, M., Dubost, L., Marie, A., Veziris, N., Blanot, D., Gutmann, L., and Mainardi, J.-L. (2008) The peptidoglycan of stationary-phase Mycobacterium tuberculosis predominantly contains cross-links generated by L, D-transpeptidation, *Journal of Bacteriology 190*, 4360-4366.

[21] Story-Roller, E., and Lamichhane, G. Have we realized the full potential of β-lactams for treating drug-resistant TB?, *IUBMB Life*.

[22] Pavelka, M. S., Mahapatra, S., and Crick, D. C. (2014) Genetics of peptidoglycan biosynthesis, In *Molecular Genetics of Mycobacteria, Second Edition*, pp 513-533, American Society of Microbiology.

[23] Wietzerbin, J., Das, B. C., Petit, J. F., Lederer, E., Leyh-Bouille, M., and Ghuysen, J. M. (1974) Occurrence of D-alanyl-(D)-meso-diaminopimelic acid and meso-diaminopimelyl-meso-diaminopimelic acid interpeptide linkages in the peptidoglycan of Mycobacteria, *Biochemistry 13*, 3471-3476.

[24] Sanders, A. N., Wright, L. F., and Pavelka Jr, M. S. (2014) Genetic characterization of mycobacterial L, D-transpeptidases, *Microbiology 160*, 1795-1806.

[25] Behera, B., Mathur, P., Das, A., and Kapil, A. (2009) Ertapenem susceptibility of extended spectrum beta-lactamase-producing Enterobacteriaceae at a tertiary care centre in India, *Singapore Med J 50*, 628-632.

[26] Steiner, E. M., Schneider, G., and Schnell, R. (2017) Binding and processing of β-lactam antibiotics by the transpeptidase LdtMt2 from Mycobacterium tuberculosis, *The FEBS journal 284*, 725-741.

[27] Triboulet, S., Arthur, M., Mainardi, J.-L., Veckerlé, C., Dubée, V., NGuekam-Moumi, A., Gutmann, L., Rice, L. B., and Hugonnet, J.-E. (2011) Inactivation kinetics of a new target of β-lactam antibiotics, *Journal of Biological Chemistry 286*, 22777-22784.

[28] Triboulet, S., Dubée, V., Lecoq, L., Bougault, C., Mainardi, J.-L., Rice, L. B., Ethève-Quelquejeu, M., Gutmann, L., Marie, A., and Dubost, L. (2013) Kinetic features of L, D-transpeptidase inactivation critical for β-lactam antibacterial activity, *PLoS One 8*, e67831.

[29] Kumar, P., Kaushik, A., Lloyd, E. P., Li, S.-G., Mattoo, R., Ammerman, N. C., Bell, D. T., Perryman, A. L., Zandi, T. A., and Ekins, S. (2017) Non-classical transpeptidases yield insight into new antibacterials, *Nature chemical biology 13*, 54.

[30] Goffin, C., and Ghuysen, J.-M. (2002) Biochemistry and comparative genomics of SxxK superfamily acyltransferases offer a clue to the mycobacterial paradox: presence of penicillin-susceptible target proteins versus lack of efficiency of penicillin as therapeutic agent, *Microbiology and molecular biology reviews 66*, 702-738.

[31] Sauvage, E., Kerff, F., Terrak, M., Ayala, J. A., and Charlier, P. (2008) The penicillin-binding proteins: structure and role in peptidoglycan biosynthesis, *FEMS microbiology reviews 32*, 234-258.

[32] Goffin, C., and Ghuysen, J.-M. (1998) Multimodular penicillin-binding proteins: an enigmatic family of orthologs and paralogs, *Microbiology and Molecular Biology Reviews 62*, 1079-1093.

[33] Gupta, R., Lavollay, M., Mainardi, J.-L., Arthur, M., Bishai, W. R., and Lamichhane, G. (2010) The Mycobacterium tuberculosis protein LdtMt2 is a nonclassical transpeptidase required for virulence and resistance to amoxicillin, *Nature Medicine 16*, 466-469.

[34] Filippova, E. V., Kieser, K. J., Luan, C. H., Wawrzak, Z., Kiryukhina, O., Rubin, E. J., and Anderson, W. F. (2016) Crystal structures of the transpeptidase domain of the Mycobacterium tuberculosis penicillin-binding protein PonA1 reveal potential mechanisms of antibiotic resistance, *The FEBS journal 283*, 2206-2218.

[35] Calvanese, L., Falcigno, L., Maglione, C., Marasco, D., Ruggiero, A., Squeglia, F., Berisio, R., and D'Auria, G. (2014) Structural and binding properties of the PASTA domain of PonA2, a key penicillin binding protein from Mycobacterium tuberculosis, *Biopolymers 101*, 712-719.

[36] Kim, H. S., Kim, J., Im, H. N., Yoon, J. Y., An, D. R., Yoon, H. J., Kim, J. Y., Min, H. K., Kim, S.-J., and Lee, J. Y. (2013) Structural basis for the inhibition of Mycobacterium tuberculosis L, D-transpeptidase by meropenem, a drug effective against extensively drug-resistant strains, *Acta Crystallographica Section D: Biological Crystallography 69*, 420-431.

[37] Bianchet, M. A., Pan, Y. H., Basta, L. A. B., Saavedra, H., Lloyd, E. P., Kumar, P., Mattoo, R., Townsend, C. A., and Lamichhane, G. (2017) Structural insight into the inactivation of Mycobacterium tuberculosis non-classical transpeptidase Ldt Mt2 by biapenem and tebipenem, *BMC biochemistry 18*, 8.

[38] Gokulan, K., Khare, S., Cerniglia, C. E., Foley, S. L., and Varughese, K. I. (2018) Structure and Inhibitor Specificity of L, D-Transpeptidase (LdtMt2) from Mycobacterium tuberculosis and Antibiotic Resistance: Calcium Binding Promotes Dimer Formation, *The AAPS journal 20*, 44.

[39] Brammer, B. L., Ghosh, A., Pan, Y., Jakoncic, J., Lloyd, E., Townsend, C., Lamichhane, G., and Bianchet, M. (2015) Loss of a Functionally and Structurally Distinct ld-Transpeptidase, LdtMt5, Compromises Cell Wall Integrity in Mycobacterium tuberculosis, *The Journal of Biological Chemistry 290*, 25670-25685.

[40] Hett, E. C., Chao, M. C., Deng, L. L., and Rubin, E. J. (2008) A mycobacterial enzyme essential for cell division synergizes with resuscitation-promoting factor, *PLoS pathogens 4*, e1000001.

[41] Shah, I. M., Laaberki, M.-H., Popham, D. L., and Dworkin, J. (2008) A eukaryotic-like Ser/Thr kinase signals bacteria to exit dormancy in response to peptidoglycan fragments, *Cell 135*, 486-496.

[42] Squeglia, F., Marchetti, R., Ruggiero, A., Lanzetta, R., Marasco, D., Dworkin, J., Petoukhov, M., Molinaro, A., Berisio, R., and Silipo, A. (2011) Chemical basis of peptidoglycan discrimination by PrkC, a key kinase involved in bacterial resuscitation from dormancy, *Journal of the American Chemical Society 133*, 20676-20679.

[43] Tipper, D. J., and Strominger, J. L. (1965) Mechanism of action of penicillins: a proposal based on their structural similarity to acyl-D-alanyl-D-alanine, *Proceedings of the National Academy of Sciences 54*, 1133-1141.

[44] Kastrinsky, D. B., and Barry III, C. E. (2010) Synthesis of labeled meropenem for the analysis of M. tuberculosis transpeptidases, *Tetrahedron letters 51*, 197-200.

[45] Finn, R. D., Mistry, J., Schuster-Böckler, B., Griffiths-Jones, S., Hollich, V., Lassmann, T., Moxon, S., Marshall, M., Khanna, A., and Durbin, R. (2006) Pfam: clans, web tools and services, *Nucleic acids research 34*, D247-D251.

[46] Biarrotte-Sorin, S., Hugonnet, J.-E., Delfosse, V., Mainardi, J.-L., Gutmann, L., Arthur, M., and Mayer, C. (2006) Crystal structure of a novel β-lactam-insensitive peptidoglycan transpeptidase, *Journal of molecular biology 359*, 533-538.

[47] Magnet, S., Arbeloa, A., Mainardi, J.-L., Hugonnet, J.-E., Fourgeaud, M., Dubost, L., Marie, A., Delfosse, V., Mayer, C., and Rice, L. B. (2007) Specificity of L, D-transpeptidases from gram-positive bacteria producing different peptidoglycan chemotypes, *Journal of Biological Chemistry 282*, 13151-13159.

[48] Betts, J. C., Lukey, P. T., Robb, L. C., McAdam, R. A., and Duncan, K. (2002) Evaluation of a nutrient starvation model of Mycobacterium tuberculosis persistence by gene and protein expression profiling, *Molecular microbiology 43*, 717-731.

[49] Bielnicki, J., Devedjiev, Y., Derewenda, U., Dauter, Z., Joachimiak, A., and Derewenda, Z. S. (2006) B. subtilis ykuD protein at 2.0 Å resolution: insights into the structure and function of a novel,

ubiquitous family of bacterial enzymes, *Proteins: Structure, Function, and Bioinformatics 62*, 144-151.

[50] Li, W.-J., Li, D.-F., Hu, Y.-L., Zhang, X.-E., Bi, L.-J., and Wang, D.-C. (2013) Crystal structure of L, D-transpeptidase Ldt Mt2 in complex with meropenem reveals the mechanism of carbapenem against Mycobacterium tuberculosis, *Cell research 23*, 728.

[51] Lecoq, L., Dubée, V., Triboulet, S. b., Bougault, C., Hugonnet, J.-E., Arthur, M., and Simorre, J.-P. (2013) Structure of Enterococcus faecium L, D-transpeptidase acylated by ertapenem provides insight into the inactivation mechanism, *ACS chemical biology 8*, 1140-1146.

[52] Brennan, P. J. (2003) Structure, function, and biogenesis of the cell wall of Mycobacterium tuberculosis, *Tuberculosis 83*, 91-97.

[53] Moraes, G. L., Gomes, G. C., De Sousa, P. R. M., Alves, C. N., Govender, T., Kruger, H. G., Maguire, G. E., Lamichhane, G., and Lameira, J. (2015) Structural and functional features of enzymes of Mycobacterium tuberculosis peptidoglycan biosynthesis as targets for drug development, *Tuberculosis 95*, 95-111.

[54] Fakhar, Z., Naiker, S., Alves, C. N., Govender, T., Maguire, G. E., Lameira, J., Lamichhane, G., Kruger, H. G., and Honarparvar, B. (2016) A comparative modeling and molecular docking study on Mycobacterium tuberculosis targets involved in peptidoglycan biosynthesis, *Journal of Biomolecular Structure and Dynamics 34*, 2399-2417.

[55] Mainardi, J.-L., Hugonnet, J.-E., Rusconi, F., Fourgeaud, M., Dubost, L., Moumi, A. N., Delfosse, V., Mayer, C., Gutmann, L., and Rice, L. B. (2007) Unexpected inhibition of peptidoglycan ld-transpeptidase from Enterococcus faecium by the β-lactam imipenem, *Journal of Biological Chemistry 282*, 30414-30422.

[56] Dodson, G., and Wlodawer, A. (1998) Catalytic triads and their relatives, *Trends in biochemical sciences 23*, 347-352.

[57] Silva, J. R. A., Govender, T., Maguire, G. E., Kruger, H. G., Lameira, J., Roitberg, A. E., and Alves, C. N. (2015) Simulating the inhibition reaction of Mycobacterium tuberculosis L, D-transpeptidase 2 by carbapenems, *Chemical Communications 51*, 12560-12562.

[58] Silva, J. R. r. A., Roitberg, A. E., and Alves, C. u. N. (2014) Catalytic mechanism of L, D-transpeptidase 2 from Mycobacterium tuberculosis described by a computational approach: insights for the design of new antibiotics drugs, *Journal of Chemical Information and Modeling 54*, 2402-2410.

[59] Waksman, S. A. (1949) Streptomycin. Nature and practical applications, *Streptomycin. Nature and practical applications.*

[60] Lehmann, J. (1964) Twenty years afterward: historical notes on the discovery of the antituberculosis effect of para-aminosalicylic acid (PAS) and the first clinical trials, Am Thoracic Soc.

[61] Verma, A. K., and Kalra, O. P. (2012) Discovery of New Drugs Against Tuberculosis: History Guides, *Archives of Clinical Infectious Diseases 7*, 109-112.

[62] Waksman, S. A. (1950) Streptomycin and Neomycin, *British medical journal 2*, 595.

[63] Organization, W. H., and Initiative, S. T. (2010) *Treatment of tuberculosis: guidelines*, World Health Organization.

[64] Benson, C. A., Brooks, J. T., Holmes, K. K., Kaplan, J. E., Masur, H., and Pau, A. (2009) Guidelines for prevention and treatment opportunistic infections in HIV-infected adults and adolescents; recommendations from CDC, the National Institutes of Health, and the HIV Medicine Association/Infectious Diseases Society of America.

[65] Chetty, S., Ramesh, M., Singh-Pillay, A., and Soliman, M. E. (2017) Recent advancements in the development of anti-tuberculosis drugs, *Bioorganic & medicinal chemistry letters 27*, 370-386.

[66] Ma, Z., Lienhardt, C., McIlleron, H., Nunn, A. J., and Wang, X. (2010) Global tuberculosis drug development pipeline: the need and the reality, *The Lancet 375*, 2100-2109.

[67] Papp-Wallace, K. M., Endimiani, A., Taracila, M. A., and Bonomo, R. A. (2011) Carbapenems: past, present, and future, *Antimicrobial agents and chemotherapy 55*, 4943-4960.

[68] Shaikh, S., Fatima, J., Shakil, S., Rizvi, S. M. D., and Kamal, M. A. (2015) Antibiotic resistance and extended spectrum beta-lactamases: types, epidemiology and treatment, *Saudi journal of biological sciences 22*, 90-101.

[69] Birnbaum, J., Kahan, F. M., Kropp, H., and Macdonald, J. S. (1985) Carbapenems, a new class of beta-lactam antibiotics: Discovery and development of imipenem/cilastatin, *The American journal of medicine 78*, 3-21.

[70] Baughman, R. P. (2009) The use of carbapenems in the treatment of serious infections, *Journal of intensive care medicine 24*, 230-241.

[71] Livermore, D. M. (2001) Of Pseudomonas, porins, pumps and carbapenems, *Journal of Antimicrobial Chemotherapy 47*, 247-250.

[72] Jaganath, D., Lamichhane, G., and Shah, M. (2016) Carbapenems against Mycobacterium tuberculosis: a review of the evidence, *The International Journal of Tuberculosis and Lung Disease 20*, 1436-1447.

[73] England, K., Boshoff, H. I., Arora, K., Weiner, D., Dayao, E., Schimel, D., Via, L. E., and Barry, C. E. (2012) Meropenem-clavulanic acid shows activity against Mycobacterium tuberculosis in vivo, *Antimicrobial agents and chemotherapy 56*, 3384-3387.

[74] Tremblay, L. W., Fan, F., and Blanchard, J. S. (2010) Biochemical and structural characterization of Mycobacterium tuberculosis β-lactamase with the carbapenems ertapenem and doripenem, *Biochemistry 49*, 3766-3773.

[75] Schurek, K. N., Wiebe, R., Karlowsky, J. A., Rubinstein, E., Hoban, D. J., and Zhanel, G. G. (2007) Faropenem: review of a new oral penem, *Expert review of anti-infective therapy 5*, 185-198.

[76] Dubée, V., Triboulet, S., Mainardi, J.-L., Ethève-Quelquejeu, M., Gutmann, L., Marie, A., Dubost, L., Hugonnet, J.-E., and Arthur, M. (2012) Inactivation of Mycobacterium tuberculosis L, D-transpeptidase LdtMt1 by carbapenems and cephalosporins, *Antimicrobial agents and chemotherapy 56*, 4189-4195.

[77] Schoonmaker, M. K., Bishai, W. R., and Lamichhane, G. (2014) Nonclassical transpeptidases of Mycobacterium tuberculosis alter cell size, morphology, the cytosolic matrix, protein localization, virulence, and resistance to β-lactams, *Journal of bacteriology 196*, 1394-1402.

[78] Kaushik, A., Makkar, N., Pandey, P., Parrish, N., Singh, U., and Lamichhane, G. (2015) Carbapenems and rifampin exhibit synergy against Mycobacterium tuberculosis and Mycobacterium abscessus, *Antimicrobial agents and chemotherapy 59*, 6561-6567.

[79] Dhar, N., Dubée, V., Ballell, L., Cuinet, G., Hugonnet, J.-E., Signorino-Gelo, F., Barros, D., Arthur, M., and McKinney, J. D. (2015) Rapid cytolysis of Mycobacterium tuberculosis by faropenem, an orally bioavailable β-lactam antibiotic, *Antimicrobial agents and chemotherapy 59*, 1308-1319.

[80] Cynamon, M. H., Speirs, R. J., and Welch, J. T. (1998) In vitro antimycobacterial activity of 5-chloropyrazinamide, *Antimicrobial agents and chemotherapy 42*, 462-463.

[81] Acevedo, O., and Jorgensen, W. L. (2009) Advances in quantum and molecular mechanical (QM/MM) simulations for organic and enzymatic reactions, *Accounts of chemical research 43*, 142-151.

[82] Silva, J. R. A., Bishai, W. R., Govender, T., Lamichhane, G., Maguire, G. E., Kruger, H. G., Lameira, J., and Alves, C. N. (2016) Targeting the cell wall of Mycobacterium tuberculosis: a molecular modeling investigation of the interaction of imipenem and meropenem with L, D-transpeptidase 2, *Journal of Biomolecular Structure and Dynamics 34*, 304-317.

[83] Miller III, B. R., McGee Jr, T. D., Swails, J. M., Homeyer, N., Gohlke, H., and Roitberg, A. E. (2012) MMPBSA. py: an efficient program for end-state free energy calculations, *Journal of chemical theory and computation 8*, 3314-3321.

[84] Naïm, M., Bhat, S., Rankin, K. N., Dennis, S., Chowdhury, S. F., Siddiqi, I., Drabik, P., Sulea, T., Bayly, C. I., and Jakalian, A. (2007) Solvated interaction energy (SIE) for scoring protein− ligand binding affinities. 1. Exploring the parameter space, *Journal of chemical information and modeling 47*, 122-133.

[85] Fakhar, Z., Govender, T., Lamichhane, G., Maguire, G. E., Kruger, H. G., and Honarparvar, B. (2017) Computational model for the acylation step of the β-lactam ring: Potential application for l, d-transpeptidase 2 in mycobacterium tuberculosis, *Journal of Molecular Structure 1128*, 94-102.

[86] Fakhar, Z., Govender, T., Maguire, G. E., Lamichhane, G., Walker, R. C., Kruger, H. G., and Honarparvar, B. (2017) Differential flap dynamics in l, d-transpeptidase2 from mycobacterium tuberculosis revealed by molecular dynamics, *Molecular BioSystems 13*, 1223-1234.

[87] Billones, J. B., Carrillo, M. C. O., Organo, V. G., Macalino, S. J. Y., Sy, J. B. A., Emnacen, I. A., Clavio, N. A. B., and Concepcion, G. P. (2016) Toward antituberculosis drugs: in silico screening of synthetic compounds against Mycobacterium tuberculosis l, d-transpeptidase 2, *Drug design, development and therapy 10*, 1147.

[88] Cheng, F., Li, W., Zhou, Y., Shen, J., Wu, Z., Liu, G., Lee, P. W., and Tang, Y. (2012) admetSAR: a comprehensive source and free tool for assessment of chemical ADMET properties, ACS Publications.

[89] Baldin, S., Misiura, N., and Švedas, V. (2017) Building a Full-Atom Model of L, Dtranspeptidase 2 from Mycobacterium tuberculosis for Screening New Inhibitors, *Acta naturae 9*, 44.

[90] Ntombela, T., Fakhar, Z., Ibeji, C. U., Govender, T., Maguire, G. E., Lamichhane, G., Kruger, H. G., and Honarparvar, B. (2018) Molecular insight on the non-covalent interactions between carbapenems and l, d-transpeptidase 2 from Mycobacterium tuberculosis: ONIOM study, *Journal of Computer-Aided Molecular Design*, 1-15.

[91] Hugonnet, J.-E., Tremblay, L. W., Boshoff, H. I., Barry, C. E., and Blanchard, J. S. (2009) Meropenem-clavulanate is effective against extensively drug-resistant Mycobacterium tuberculosis, *Science 323*, 1215-1218.

[92] Cohen, K. A., El-Hay, T., Wyres, K. L., Weissbrod, O., Munsamy, V., Yanover, C., Aharonov, R., Shaham, O., Conway, T. C., and Goldschmidt, Y. (2016) Paradoxical hypersusceptibility of drug-resistant mycobacteriumtuberculosis to β-lactam antibiotics, *EBioMedicine 9*, 170-179.

CHAPTER THREE

The manuscript in chapter three has been accepted in ChemistrySelect

Inhibition of *Mycobacterium Tuberculosis* L,D-transpeptidase 5 by carbapenems: MD and QM/MM Mechanistic Studies

Gideon F. Tolufashe,[1] Thavendran Govender,[1] Amit K. Halder,[1] Collins U. Ibeji[1], Monsurat M. Lawal[1], Thandokuhle Ntombela[1], Glenn E. M. Maguire,[1,2] Gyanu Lamichhane[3], Hendrik G. Kruger[1,*] and Bahareh Honarparvar[1,*]

[1]Catalysis and Peptide Research Unit, School of Health Sciences, University of KwaZulu-Natal, Durban 4001, South Africa.

[2]School of Chemistry and Physics, University of KwaZulu-Natal, 4001 Durban, South Africa.

[3]Division of Infectious Diseases, School of Medicine, Johns Hopkins University, Baltimore, MD 21205, USA.

*Corresponding authors: baha.honarparvar@gmail.com, Honarparvarb@ukzn.ac.za (Dr Bahareh Honarparvar), (Prof. Hendrik G. Kruger) kruger@ukzn.ac.za, Telephone: + 27 31 2601845, Fax: +27 31 2603091, Catalysis and Peptide Research Unit, School of Health Sciences, University of KwaZulu-Natal, Durban 4041, South Africa.

Abstract

Peptidoglycan is the exoskeleton of bacterial cells and is required for their survival and growth. In *Mycobacterium tuberculosis* (*Mtb*), the bacteria that currently claims the most number of human lives each year, the final step of peptidoglycan synthesis involves generation of 4→3 and 3→3 transpeptide crosslinks catalyzed by D,D-transpeptidase and L,D-transpeptidase (Ldt) enzymes, respectively. Unlike in most other bacteria, for Mtb, the majority of the cross-links are generated by L,D-transpeptidases. Any *Mtb* strain that lacks a functional copy of an Ldt, namely Ldt$_{Mt5,}$ displays aberrant growth phenotype and is more susceptible to killing by cell wall perturbing agents including carbapenems which are considered the last resort antibiotics to treat resistant bacterial infections in humans. Here, we used molecular dynamics (MD) and Quantum Mechanical (QM) simulations to probe the molecular interactions of Ldt$_{Mt5}$ with carbapenems. Ldt$_{Mt5}$ complexes with three carbapenems, ertapenem (ERT), imipenem (IMI) and meropenem (MERO) were simulated. The binding free energies (with entropy contributions) of the selected complexes were calculated from the MD trajectories using the MM/GBSA approach, the theoretical results revealed higher ΔG_{bind} for ERT—Ldt$_{Mt5}$ and IMI—Ldt$_{Mt5}$ than MERO—Ldt$_{Mt5}$. In comparison with Ldt$_{Mt2}$

(experimental and computational results), it is clear that the corresponding interactions of these drugs are much weaker with Ldt$_{Mt5}$. To further understand the catalytic reaction mechanism of Ldt$_{Mt5}$ with the selected carbapenems, the possible reaction pathway (thermodynamics and kinetics) was investigated using a two-layered ONIOM [B3LYP/6-31+g(d,p):Amber] model. The high free energies of activation (ΔG) for imipenem and meropenem, explain the reason behind inefficient binding of these carbapenems to Ldt$_{Mt5}$. The inhibitor—enzyme precomplex computational model for L,D-transpeptidase 5 correctly reflects experimental observations. This is the first computational project focusing on the elucidation of the interactions between carbapenems and Ldt$_{Mt5}$. These results provide a better understanding of how the antibacterial agents function and will potentially contribute to the discovery of more potent Ldt$_{Mt5}$ inhibitors.

Keywords: L,D-Transpeptidase 5 (Ldt$_{Mt5}$); *Mycobacterium tuberculosis* (*Mtb*); Carbapenems; Molecular docking; Molecular dynamics (MD); Quantum Mechanical (QM).

3.1 Introduction

Mycobacterium tuberculosis (*Mtb*), the bacteria that causes tuberculosis (TB), kills more people today than any other single bacteria[1], killing about 2 million people annually and is the direct cause of death for many HIV patients[2]. About one-third of the human population is sub-clinically infected with *Mtb*[3]. *Mtb* is much more resistant to antibiotics than most other bacteria[4, 5] and thus require the design of new and efficient drug regimens. After entering into the lung, the bacteria often remains in a dormant state until the host's immune system is compromised and activation of the disease occur[6].

Peptidoglycan is a major component of the *Mtb* cell wall. It is a macromolecule composed of *cis*-linked glycan chain with short peptide side chains that are crosslinked by transpeptide bridges[7]. In addition to conferring cell shape, mechanical strength and integrity of the cell wall, peptidoglycan is vital for the normal physiology of the bacterial cell. The final step of peptidoglycan biosynthesis involves bonding peptide sidechains with transpeptide linkages. Mtb peptidoglycan contains both the classical 4→3 linkages and the non-classical 3→3 linkages, which are formed by D,D and L,D-transpeptidases, respectively[8, 9]. Carbapenems belong to the *β*-lactam family, the most widely used class of antibiotics to treat infections in humans. Recent studies have demonstrated that carbapenems selectively inhibit the 3→3 crosslinks[11], while classical penicillins inhibit 4→3 crosslinks[10]. The combination of carbapenems and penicillins is speculated to result in coordinated disruption of the mycobacterial cell wall and subsequent killing of the pathogen[7].

The 3→3 crosslink L,D-transpeptidases (Ldts) by-pass the classical penicillin binding proteins (PBPs)[11] thus making them attractive targets for the development of new drugs for the treatment of multidrug-

resistant tuberculosis[11-13]. In *Mtb*, 80% of the peptidoglycan layer has been reported [14, 15] to be crosslinked by L,D-transpeptidases. Therefore, Ldts that generate these linkages are potentially attractive targets against which to develop new drugs to treat drug-resistant TB.

Mtb genome encodes five Ldt paralogs, namely Ldt_{Mt1} to Ldt_{Mt5}. Except for Ldt_{Mt3}, these proteins were found to be active *in vitro* peptidoglycan crosslinking assays. Ldt_{Mt2} has been extensively studied experimentally[16-19] as well as computationally[20-27]. However, very little is known about the activity and interactions of Ldt_{Mt5} with inhibitors. It was experimentally observed that in terms of the binding affinities of the selected carbapenems, carbapenems are weaker binders against Ldt_{Mt5}[28] in comparison to Ldt_{Mt2}[16, 24, 25, 29, 30]. Herein, our group is attempting to unravel these differences, using a computational comparison between these two enzymes.

The reaction mechanism of Ldt_{Mt2} with its natural substrate was investigated using hybrid quantum mechanics/molecular mechanic (QM/MM) molecular dynamic (MD) simulations, followed by umbrella sampling[23]. It was concluded that the mechanistic process for joining of the m-A^{2}pm^3 residue with m-A^{2}pm$^{3'}$, involves two stages: acylation and deacylation[16]. During the acylation stage, two steps were observed: the first is a thiolate/imidazole ion-pair in the zwitterionic form and the second a nucleophilic attack on the carboxyl carbon of the substrate along with the breaking of the peptide bond. In the deacylation stage, the acyl-enzyme undergoes a nucleophilic attack on the carboxyl carbon by the amine group of the second substrate. The free energy calculations confirmed the experimentally proposed mechanism and identified[16] the acylation as the rate-limiting step.

The inhibition of Ldt_{Mt2} by carbapenems was subsequently studied using hybrid quantum mechanics/molecular mechanics (QM/MM) molecular dynamics (MD) simulations and an umbrella sampling approach[22] to investigate the inactivation of Ldt_{Mt2} by the carbapenems, meropenem and imipenem. They studied a four-membered ring transition state and the theoretical energetics obtained from the study followed the same trend of reported experimental data[31]. This activity order was confirmed by using density functional tight binding/molecular mechanics (DFTB/MM) to calculate the potential free energy surface for the reaction mechanism described[22].

Later, the mode of interactions of several carbapenem inhibitors inside the active pocket of Ldt_{Mt2} targeting the cell wall of *Mtb* was theoretically studied using MM/GBSA and SIE binding free energy methods[21]. The average ligand-protein binding free energies in these pre-covalent complexes calculated from their MD simulation followed the same order as the experimental bioactivity data. The isothermal titration calorimetry experiments (ITC) revealed[16, 21] free binding energies for the covalently bonded inhibitors of 9.97 and 8.30 kcal mol^{-1} for imipenem and meropenem against Ldt_{Mt2}, respectively. In other words, these

studies demonstrated that there is a direct correlation between the binding energies calculated in the pre-covalent complexes and the free energies of the subsequent covalently bonded inhibitor—Ldt$_{Mt2}$ complexes. A mechanistic study and acylation step model of the β-lactam ring of the carbapenems with Ldt$_{Mt2}$ was performed by Fakhar et al.[24] using DFT methods. Four possible reaction pathways with different transition states (TS) models were proposed as four membered-rings (TS-4, TS-4-His and TS-4-water) and a six-membered ring (TS-6-water). The thermochemical quantities for the proposed models indicated that the activation barrier of TS-6-water model was considerably lower and therefore more favourable than the other TS models[24].

Subsequently, the flap dynamics of Ldt$_{Mt2}$ and the impact of induced conformational changes of flap region within the binding process was studied using molecular dynamics simulations [24] in explicit solvent. Dynamic cross-correlation matrix (DCCM) analysis demonstrated significant anti-correlated motions in imipenem/LDT$_{Mt2}$ flap whereas ertapenem and meropenem binding induced a shift to correlation motion within flap units. The MM-GBSA method [25] revealed lower values of ΔG_{bind} for MERO—Ldt$_{Mt2}$ and ERT—Ldt$_{Mt2}$ than IMI—Ldt$_{Mt2.}$

Despite several theoretical studies on Ldt$_{Mt2,}$ to the best of our knowledge, there has been no computational study on the inhibition mechanism of Ldt$_{Mt5}$ in the presence of carbapenems. For the first time, Brammer and co-workers reported [28] the crystal structures of Ldt$_{Mt5}$ with meropenem (PDB code:4ZFQ[28] and its apo form (PDB code: 4Z7A[28]. This crystal structure showed that a covalent bond has formed between Cys360 and the β-lactam ring of carbapenems. An experimental study using ITC demonstrated that the interaction of meropenem with Ldt$_{Mt5}$ is not associated with significant heat exchange[28]. Similar results were observed for imipenem and ertapenem. No adduct was detected by mass spectrometry after 5 hours incubation of meropenem and Ldt$_{Mt5}$. It was concluded that meropenem will acylate Ldt$_{Mt5}$ over an extended incubation period as the X-ray structure of covalently bonded meropenem—Ldt$_{Mt5}$ complex was reported[28]. They did not rule out the possibility that Ldt$_{Mt5}$ is more rapidly inactivated by this class of β-lactams in $vivo$, particularly in the event of Ldt$_{Mt5}$ requiring a protein-protein interaction for productive catalysis[28]. It is notable that the meropenem—adduct Ldt$_{Mt5}$ structure[28], the hairpin and loop (**Figure 3.1**) are partially disordered, so modelling of the missing portion was performed. The modeled structure of the Ldt$_{Mt5}$ in complex with meropenem use for this study is presented in **Figure 3.1**.
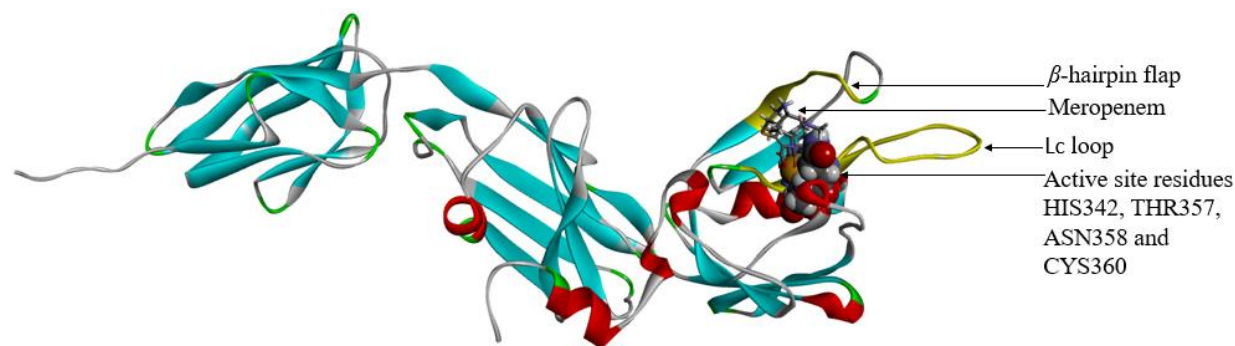
Figure 1 The modelled structure of MERO—Ldt$_{Mt5}$ with displaying active site residues and loop regions. The *β*-hairpin flap (312-330) and Lc loop (338-358) are highlighted in yellow and active site pocket in CPK form [HIS342 (287), THR357 (302), ASN358 (303) and CYS360 (305)] and meropenem (inhibitor) are presented in stick form.

Despite inefficient *in vitro* inactivation of Ldt$_{Mt5}$ by carbapenems, Ldt$_{Mt5}$ knock-out strains of Mtb displayed aberrant growth, and are susceptibility to crystal violet, osmotic shock, and selected carbapenem antibiotics,[28] making this enzyme also an important target for drug development against TB. Ldt$_{Mt5}$ is the only paralog of Ldt$_{Mt2}$ that is not instantly inhibited *in vitro* by carbapenems[28, 32].

The weaker inhibition of Ldt$_{Mt5}$ by carbapenems (compared to other L,D-transpeptidases) has not been addressed at the molecular level; this motivated us to undertake the present study. It is likely that the reduced suceptibilty[13] can be understood from the comparison of the dynamic behaviour of carbapenem-enzyme complexes[25]. The chemical structures of the selected carbapenems are presented in **Figure 3.2**.
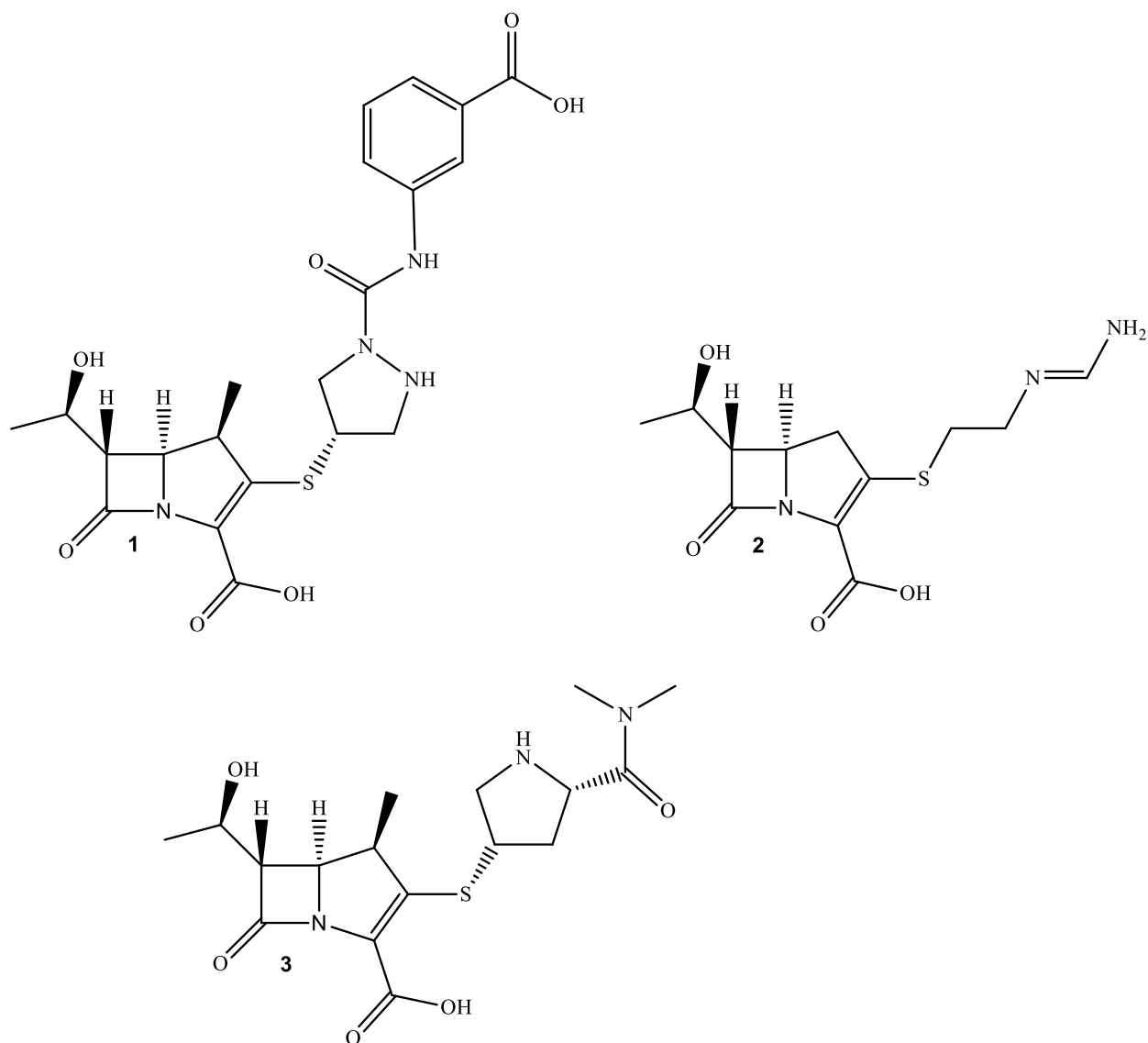
Figure 3.2 Chemical structures of the selected carbapenems; **1**: ertapenem, **2**: imipenem and **3**: meropenem.

Herein, the dynamics of the selected carbapenem derivatives (ertapenem, imipenem and meropenem) complexed with Ldt$_{Mt5}$ were investigated by performing 60 ns MD simulations in an explicit solvation model. The binding energies of the carbapenems to the Ldt$_{Mt5}$ were calculated using MMGBSA binding free energy method. The involvement of the β-hairpin flap[28] and Lc loop[28] present in the enzyme and potential relationship of the flap dynamics to the binding affinities of the compounds in the Ldt$_{Mt5}$ active site, were also analyzed.

Since studies in our laboratory revealed a six-membered ring transition state including one water molecule (TS-6-water) for the inactivation of lactams by transpeptidase[24], a TS-6-water reaction pathway for Ldt$_{Mt5}$ with meropenem and imipenem was also investigated. The choice of these two carbapenems for the

mechanistic study was based on the reported inhibitory function and known experimental binding affinities for Ldt$_{Mt2}$[33]. In order to probe the presumed natural substrate (SUB) for Ldt$_{Mt5,}$ we used the native tetrapeptide substrate L-Ala^1-D-iso-Glu^2-*meso*DAP^3-D-ala^4,[34] the substrate known for Ldt$_{Mt2}$[16].

3.2 Materials and methods

The following approaches were used to investigate the inhibition mechanism of L,D-transpeptidase 5 from *Mycobacterium tuberculosis* in the presence of the selected *β*-lactam carbapenems (**Figure 3.2**). The inhibitor/enzyme complex was prepared using a docking method, followed by visual inspection of the inhibitor pose and comparison to the meropenem/Ldt$_{Mt5}$ crystal structure[28]. This was followed by molecular dynamics simulations/MD trajectory analyses and QM/MM mechanistic studies. Furthermore, the dynamics[35] of the *β*-hairpin flap (312-330) and Lc loop (338-358) (**Figure 3.1**) on the catalytic binding mechanism of Ldt$_{Mt5}$ were analyzed to assess whether there is a correlation between flap/loop opening and closing and the observed binding affinities of the different inhibitors. Note that the flap/loop regions form part of the active pocket[28].

To achieve these objectives we determined the root mean square deviation (RMSD) to ascertain the stability of the system during the simulation. The root mean square fluctuation (RMSF) was calculated to give the flexibility of the residues over the simulation period.

3.2.1 Inhibitor/Enzyme structural preparation

The 3D crystal structure of the Ldt$_{Mt5}$ in complex with meropenem (PDB code:4ZFQ[28]) was obtained from the Protein Data Bank[36]. The missing residues of the Ldt$_{Mt5}$ enzyme were modelled using MODELLER v9.15[37]. As for the various protonation states of the enzyme, it was experimentally revealed that the Ldt$_{Mt5}$ optimally hydrolyzes nitrocefin at pH >9[28], however, the difference in its inhibitory activity is insignificant in comparison with that of Ldt$_{Mt2}$, which favourably causes the hydrolysis of nitrocefin at pH 7[16]. An accurate assignment of the protonation states of all the enzyme residues at pH 7 was assigned by recalculating the standard pKa values of the titratable amino acids using the empirical PropKa web server[38]. The protonation states of the titratable residues of the Ldt$_{Mt5}$ at pH 7 which was used for the modelling, were the same as pH 9 (**Table S1**), this was also confirmed [28] by experiments.

3.2.2 Preparation of the inhibitor-enzyme complex

The prepared structure of Ldt$_{Mt5}$ was used as the starting structure for molecular docking, the active site of the enzyme was defined based on the crystal structure of the meropenem adduct[28]. Meropenem, imipenem and ertapenem which were placed in the identified active pocket of Ldt$_{Mt5}$[28] and were then subjected to redocking using flexible AutoDock Tools software[39]. The charges of the ligands were computed with

Gasteiger partial charges for all atoms. The number of rotatable bonds was 7, 9 and 9 for meropenem, imipenem, ertapenem respectively, which are below the cut-off of 10 rotatable bonds[40, 41].

The AutoGrid map was employed to set the proper size of the grid box. AutoDock tools1.5.6[39] was employed to determine the proper size of the grid box for the potential binding site. The grid box was determined as center (X=3.9; Y= -39.5; Z=12.1) and dimension (X=45; Y=45; Z=45) with the grid spacing of 0.375 Å for each of the following atom types: A C H HD N OA and SA representing all probable atom types in the target enzyme for the potential binding site. The Lamarckian Genetic algorithm[42] was used for molecular docking analysis[43] using the AutoDock 4.2 program [39]. The obtained docked poses and binding energies of the selected ligands complexed with Ldt_{Mt5} were visually inspected to ensure the expected drug/enzyme interactions are in accordance with experiment[28].

3.2.3 Molecular dynamics (MD) simulations

The best docked pose of the selected carbapenems in the active site of Ldt_{Mt5}, in terms of the observed interactions and more negative docked binding energies, were subjected to MD calculations. The hydrogen atoms were added to the complexes using the Leap module as implemented in AMBER14 molecular dynamics package[44]. The AMBER force field 99SB[44] and the general AMBER force field (GAFF)[45] were employed to describe the protein and inhibitors, respectively. The complexes were neutralized by adding the required number of ions (Na^+) before solvation. The system (99835 atoms for both ertapenem and imipenem, while 99852 atoms for meropenem complexes) was solvated in a truncated octahedral cell of TIP3P[46] water molecules, extending 10 Å outside the protein on each side, thereafter, the parameter and topology files were saved for molecular dynamics simulations. Using the SHAKE algorithm [47], all bonds were constrained to hydrogen (H) atoms. The two minimization steps were performed using 5000 frames of steepest decent minimization followed by 10000 of conjugated gradient minimization to remove the overlapping of atoms. Afterwards, the minimized systems were heated up from 0 to 300 K with solute restrained during 300 ps and then 50 ps of density equilibration with weak restraints on solutes and 2000 ps of constant pressure equilibration at 300 K were performed. A total of 60 ns MD simulations for each ERT—Ldt_{Mt5}, IMI—Ldt_{Mt5} and MERO—Ldt_{Mt5} complexes were performed at a constant temperature of 300 K and a constant pressure of 1 atm using Particle Mesh Ewald method[48]. The time step of 2 fs was used for all simulations. The MD trajectories were analyzed using CPPTRAJ module[49] implemented in AMBER14 software on GPUs with 24 shared processors using CHPC cluster. To further validate the consistency and reliability of the MD simulations, two more MD runs with different starting structures (random seed and starting from different sets of atomic coordinates and velocities) were performed.

3.2.4 Principal component analysis (PCA)

Principal component analysis (PCA) is a mathematical tool which describes the atomic positional fluctuations during MD trajectories. PCA can be used to separate a protein's conformational space into one subspace which contains only a few degrees of freedom that dictate the motions relevant for protein function and the remaining subspace which contains irrelevant local fluctuations of the protein[50].

The PCA was performed on the backbone atoms of all the 60 ns MD trajectories by constructing the covariance matrix of the C-α atom displacement. The principal component analysis describes the eigenvectors and eigenvalues, which represents the direction of motions and the amplitudes in those directions of the protein, respectively[51]. The ions and solvent molecules were stripped and CPPTRAJ module implemented in AMBER14 suite was used to perform the PCA and the porcupine plot of protein motion was created by NMWiz GUI for ProDyPrody[52] in VMD[53].

3.2.5 Binding free energy calculations

The binding free energy, ΔG_{bind}, of the ligands to their receptors has been calculated with the MM/GBSA method[54, 55]. The MM-GB/SA method applies the Generalized Born (GB)[56] solvation model to compute the electrostatic component of the solvation binding free energies. The binding free energy (ΔG) of the protein-ligand complex is computed as:

$$\Delta G_{bind} = G_{Carbapenems-LdtMt5} - G_{LdtMt5} - G_{carbapenems} \tag{1}$$

In equation **1**, $G_{Carbapenems-LdtMt5}$ is the absolute free energy of the complex, G_{LdtMt5} is the absolute free energy of the protein, and $G_{carbapenems}$ is the absolute free energy of the carbapenems. The individual components of ΔG_{bind} are defined by:

$$\Delta G_{bind} = \Delta E_{MM} + \Delta G_{solv} - T\Delta S \tag{2}$$

Where E_{MM} is the molecular mechanics energy of the system expressed as the sum of the internal energy (bonds, angles, and dihedrals), E_{int}, electrostatic energy, E_{ele}, and van der Waals term, E_{vdw}, as :

$$E_{MM} = E_{int} + E_{ele} + E_{vdw} \tag{3}$$

ΔG_{solv} is the solvation energy which is divided into the polar (ΔG_{GB}) and non-polar (ΔG_{SA}) contributions as follows:

$$\Delta G_{solv} = \Delta G_{GB} + \Delta G_{SA} \tag{4}$$

The ΔG_{GB} is refered to the electrostatic contribution to solvation and is obtained from GB solvation model. The second term, ΔG_{SA}, is the non-polar contribution to solvation-free energy that is linearly dependent on the solvent accessible surface area (SASA) as:

$$\Delta G_{SA} = \gamma \text{SASA} + b \tag{5}$$

ΔG_{SA} was calculated using AMBER14's default parameters for γ and b. The MM-GBSA binding free energies and per residue binding free energy decomposition were determined by extracting 1000 snapshots at 10 ps interval from the last 10 ns production MD trajectories of the simulation for each complex. The entropy contributions were calculated using normal mode analysis[57, 58] by extracting 100 snapshots from the MD trajectories.

3.2.6 Per-residue binding free energy decomposition analysis

Per-residue binding free energy decomposition analysis[21, 59] around 25 Å from the inhibitor was used to measure the detailed contribution of each active residue to the total binding free energy profile between the carbapenem inhibitors and Ldt$_{Mt5}$ at the atomic level.

3.2.7 QM/MM Mechanistic studies

The input structure for QM/MM calculations was taken from the 1000 snapshots from the last 10 ns of the MD simulation. Then, a precomplex system was generated in the presence of a water molecule included in the active site for the 6-membered ring model based on the model reported before[24, 60]. A two-layered ONIOM method[61-63], implemented in Gaussian 09[64] was used for all the QM/MM calculations on GPUs using CHPC cluster. In our ONIOM [B3LYP/6-31+g(d,p):Amber] model, the system was divided into two layers: a "high layer", treated at the QM level, and a "low layer", treated at the classical MM/Amber level. Prior to optimization, QM region, water and all residues within 6 Å around the active pocket were relaxed while others were held fixed[48] using TAO-ONIOM toolkit[65].

The QM (high layer) region comprised of 65 atoms (imipenem, Cys360 of Ldt$_{Mt5}$ and one water molecule) or 54 atoms (meropenem, Cys360 of Ldt$_{Mt5}$ and one water molecule) with B3LYP 6-31G(d) level of theory (**Figure 3.3**). The remaining part of the enzyme was treated as the low (MM) layer with the AMBER force field. B3LYP/6-31+G(d) was used to obtain the 6-membered ring transition state structures and all transition state calculations were confirmed by vibrational frequency calculations using normal mode analysis[66, 67] with one imaginary frequency. The intrinsic reaction coordinates (IRC) calculations [68, 69] were performed to obtain the minimum energy path for the reaction mechanism. Full optimization of the transition state, reactant and products obtained from the IRC calculations were performed using B3LYP/6-31+G(d). Single-point energy calculations with different functionals (B3LYP, MO6, wb97X) and a larger 6-311+G(2d,2p) basis set were then performed on the optimized structures of the transition state, reactant

and product. These functionals were reported to be excellent for thermodynamics and kinetics calculations[70-75].
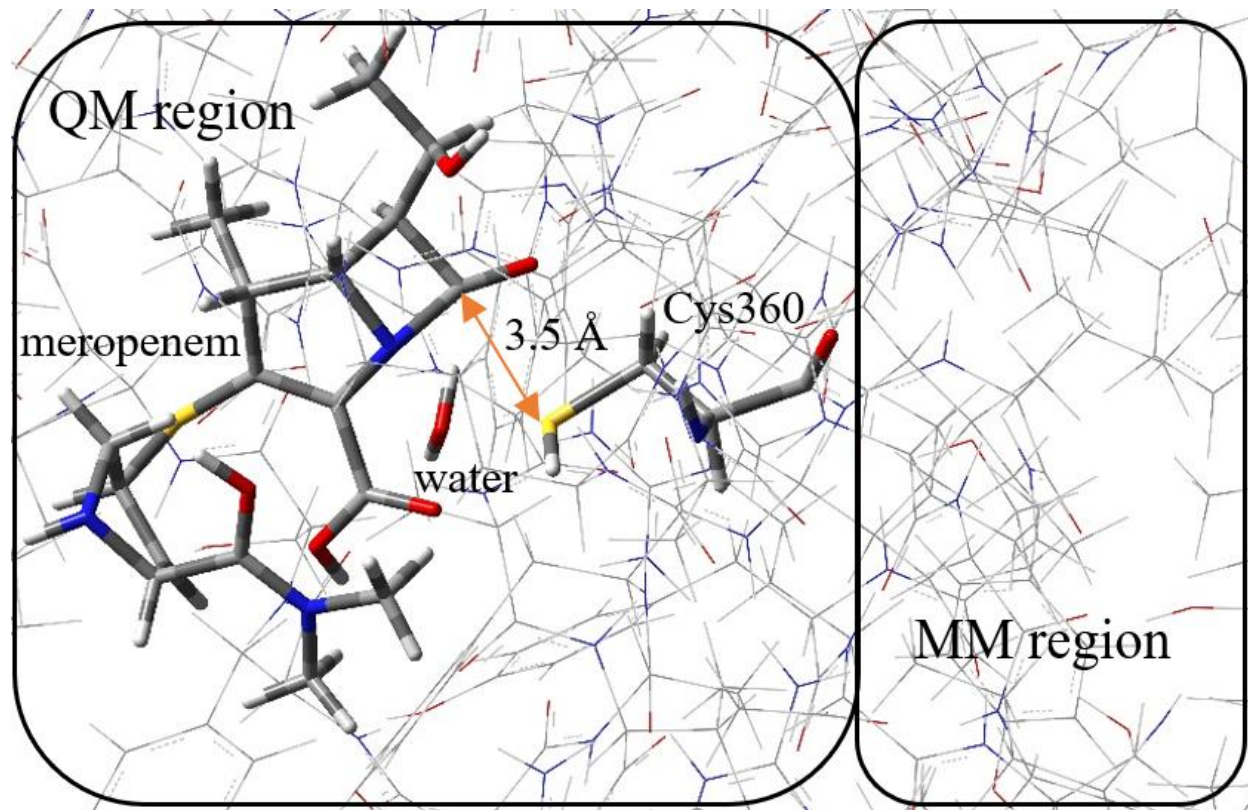
Figure 3.3 3D Structural representation of the meropenem—Ldt$_{Mt5}$ pre-complex system used for ONIOM (B3LYP/6-31+G(d,p):Amber) calculations with the specified QM and MM regions. The atoms in tubes are treated at the QM level, while the atoms in line display style at the MM layer. The distance between the nucleophilic sulfur atom and the electrophilic carbonyl carbon is approximately 3.27 Å. The minimized 3D structures (PDB format) for all inhibitor—Ldt$_{Mt5}$ complexes are provided as supplementary information.

The inclusion of water to facilitate lactam cleavage is transferring the proton from R-SH to the lactam nitrogen. This removes the need for His287 to abstract the proton as is postulated in the literature[16, 24].

3.3 Results and discussion

Starting structures were obtained from a docking procedure, followed by 60 ns MD simulation of the free enzyme and the carbapenem—Ldt$_{Mt5}$ complexes.

3.3.1 Molecular docking

The docked conformations with the most negative binding energies and with a similar pose to the X-ray structure (PDB code: 4ZFQ)[28] (**Figure 3.4**) were used as starting structures for the rest of this study. To ensure the consistency of the selected docked conformations with the experimentally reported crystal structure (4ZFQ)[28], the structural alignment of 4ZFQ with the selected docked complexes were visually compared. The resulting structure in **Figure 3.4** confirms the close proximity of carbonyl group involved in the β-lactam ring of the docked conformer with the sulfur atom (3.27 Å) of the catalytic cysteine residue Cys360 which is comparable with our earlier observation [21] for carbapenem—Ldt$_{Mt2}$ (3.32 Å). The close distance of this carbonyl group to the sulfur atom, indeed, indicates the possibility of a nucleophilic attack followed by subsequent covalent bond formation[16, 21].
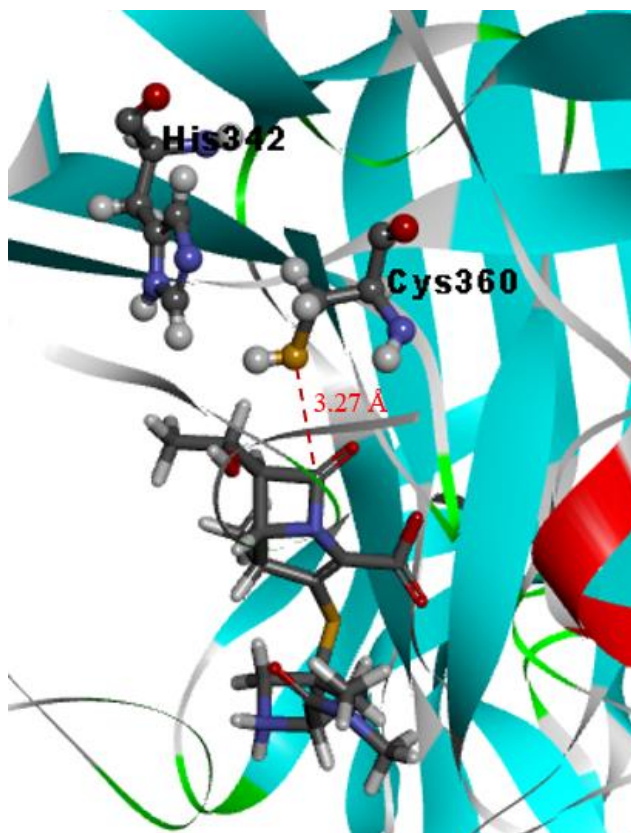
Figure 3.4 The 3D conformation for meropenem in complex with Ldt$_{Mt5}$ enzyme obtained by molecular docking. The 3D conformation for other selected carbapenems is provided in the supplementary information (**Figure S1**). The minimized 3D structures for all inhibitor—Ldt$_{Mt5}$ complexes are provided in the supplementary information.

3.3.2 Molecular dynamics simulations

Analyses were made from the MD trajectories performed.

3.3.3 RMSD analysis

The root mean square deviation with respect to the backbone heavy atoms of the protein structure was used to measure the deviation from the starting structure, as well as the complex stability over 60 ns MD trajectories. The average values of the protein backbone RMSD for ERT—Ldt_{Mt5}, IMI—Ldt_{Mt5} MERO—Ldt_{Mt5} and free—Ldt_{Mt5}, were 1.9, 1.6, 2.8 and 2.3 Å, respectively. Despite the observed variations, reasonable convergence in the RMSD plot was obtained particularly after 40 ns (**Figure 3.5**), which indicates possible conformational changes during the MD trajectories. All four complexes are found to be below this threshold suggesting reasonable stability of the complexes during the MD trajectories.
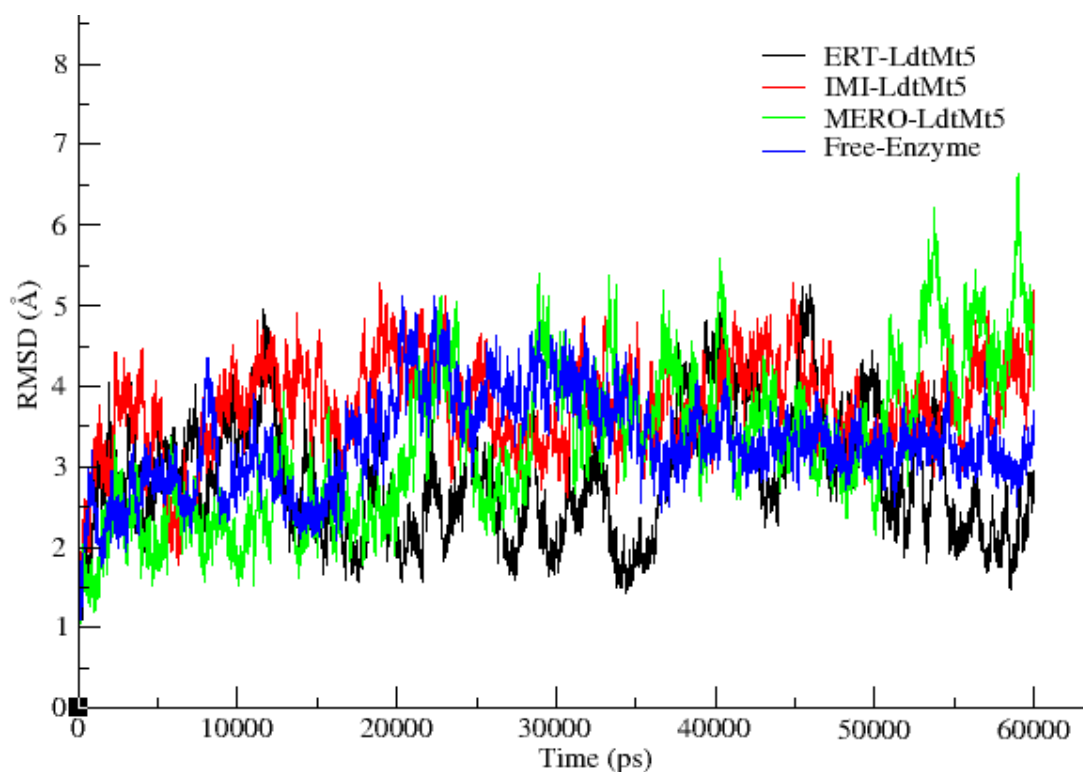
F**igure 3.5** Time evolution of the RMSD from the initial structures in the production MD simulations of Free—Ldt_{Mt5} (blue), ERT—Ldt_{Mt5} (black), IMI—Ldt_{Mt5} (red) and MERO—Ldt_{Mt5} (green) during 60 ns MD simulation time The minimized 3D structures (PDB format) for all inhibitor- Ldt_{Mt5} complexes are provided as supplementary information.

To further validate the consistency and reliability of the MD simulations, two more MD runs with different starting structures (random seed and starting from different sets of atomic coordinates and velocities) were performed (**Figure S8**). The comparable complex fluctuation within these three MD runs confirmed the reliability of the MD simulations to be taken for further trajectory analyses.

3.3.4 RMSF analysis

Given the RMSD result, it is also of interest to assess the RMS per residues, *i.e.*, root mean square fluctuation (RMSF) of the protein backbone. This allows for the evaluation and comparison of the amino acid residue flexibilities (**Figure 3.6**). The nature of these movements is analysed in subsequent sections. Knowing that the *β*-hairpin flap and loop regions display the principal residual fluctuations among *Mtb* L,D-transpeptidases[13], the focus of the RMSF analysis is on these segments of the enzyme. As evident from the RMSF plot (**Figure 3.6**), the residues involved in the *β*-hairpin flap (312-330) and Lc loop (338-358) of Ldt_{Mt5} for ERT—Ldt_{Mt5} and IMI—Ldt_{Mt5} showed higher rigidity around these regions compared to MERO—Ldt_{Mt5}. It can be inferred that the higher residual fluctuations of the MERO—Ldt_{Mt5} leads to the decrease in inhibitor binding. In general, there appears to be no correlation between these results and the calculated binding free energies (**Table 3.1**).
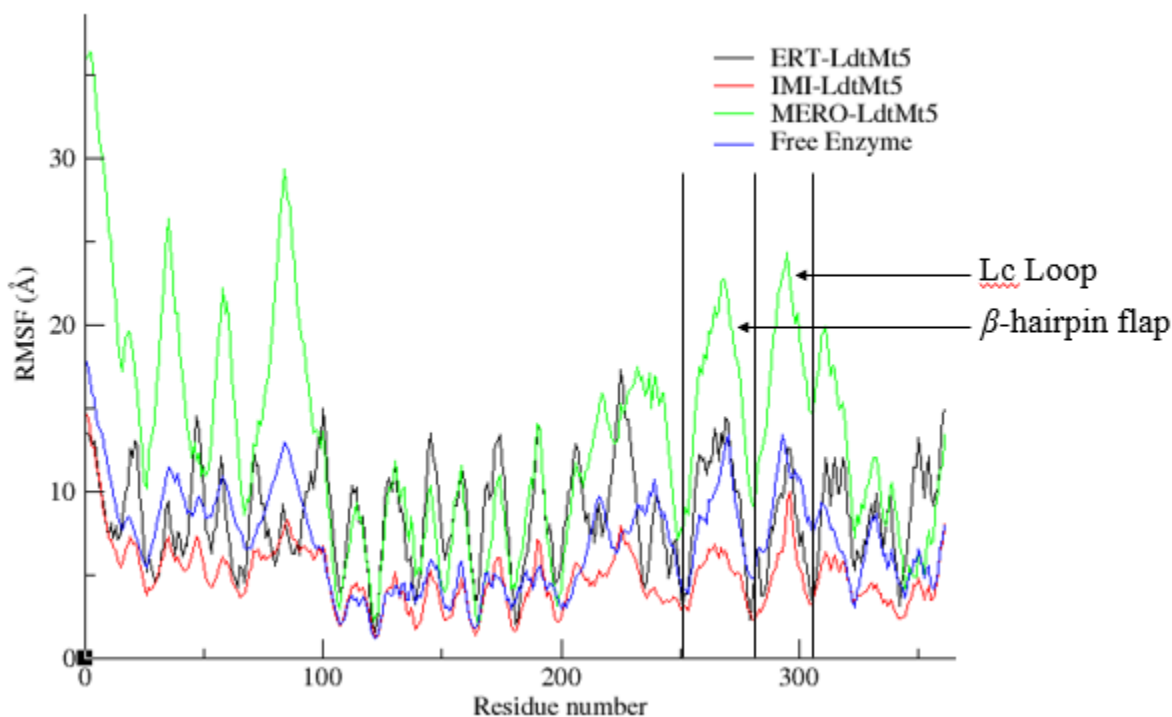
Figure 3.6 RMSF plot of the backbone atoms versus the residue numbers for Free—Ldt_{Mt5} (blue), ERT—Ldt_{Mt5} (black), IMI—Ldt_{Mt5} (red) and MERO—Ldt_{Mt5} (green) during 60 ns MD simulation time. The minimized 3D structures (PDB format) for all inhibitor- Ldt_{Mt5} complexes are provided as supplementary information.

IMI—Ldt_{Mt5} is the only complex that is more rigid than the free enzyme, although IMI—Ldt_{Mt5} is not the best inhibitor based on binding free energies (**Table 3.1**). In previous studies on the flap dynamics study

of Ldt$_{Mt2}$ enzyme complex from *Mtb* with the substrate and the same carbapenems by Fakhar *et al.*[25], the two complexes with the best binding energies (MERO—Ldt$_{Mt2}$ and ERT—Ldt$_{Mt2}$) were more rigid than the free enzyme.

3.3.5 Binding free energy analysis

Previous experimental studies[16] indicated the existence of an inhibitor-enzyme precomplex. Our group has demonstrated before[20, 22, 23, 76] that the calculated energies of these precomplexes are in general agreement with experimental bioactivities[16-18, 29, 32]. As mentioned before, attempts to determine the binding free energies of these carbapenems reacting with Ldt$_{Mt5}$ using ITC, revealed[28] that none of them showed any significant heat exchange upon complexation. Here we report the binding free energy (ΔG$_{bind}$) for the selected inhibitors complexed to Ldt$_{Mt5}$, using the MM-GB/SA method and normal mode analysis with MMPBSA.py[77]. According to the calculated results presented in **Table 3.1**, ΔG_{bind} for ertapenem, imipenem and meropenem in complex with Ldt$_{Mt5}$ were -28.29 kcal/mol, -25.52 kcal/mol and -18.34 kcal/mol respectively. The results for the ERT—Ldt$_{Mt5}$ and IMI—Ldt$_{Mt5}$ complexes demonstrate larger binding free energies compared to MERO—Ldt$_{Mt5}$, which will be further interrogated with per-residue decomposition energy (**Figure 3.7**) and hydrogen bonding analysis (**Table 3.2**).

Table 3.1. Calculated binding free energies and its components for the inhibitors—Ldt$_{Mt5}$ precomplex using MM-GBSA method and normal mode analysis. The energy components are in kcal/mol. The minimized 3D structures (PDB format) for all inhibitors—Ldt$_{Mt5}$ complexes are provided as supplementary information (**Figures S2, S3** and **S4**).

Complex	ΔE_{vdw}	ΔE_{ele}	ΔG_{gas}	ΔG_{polar}	$\Delta G_{nonpolar}$	$\Delta G_{solvation}$	-TΔS	ΔG_{bind}
ERT—Ldt$_{Mt5}$	-28.6	-50.1	-78.6	54.9	-4.6	50.4	28.5	-28.3
IMI—Ldt$_{Mt5}$	-21.6	131.7	110.1	-132.5	-3.1	-135.6	29.1	-25.5
MERO—Ldt$_{Mt5}$	-30.2	-35.7	-65.9	51.2	-3.7	47.6	15.6	-18.3
SUB—Ldt$_{Mt5}$	-32.9	226.2	193.3	-215.3	-5.3	-220.6	23.2	-27.2

ERT—Ldt$_{Mt5}$ and MERO—Ldt$_{Mt5}$ follows the same trends in terms of the energy components (negative and positive values) across the table while the different trends for IMI—Ldt$_{Mt5}$ and SUB—Ldt$_{Mt5}$ may be ascribed to the chemical structure of bulkier cyclo-aliphatic side chains of MERO–Ldt$_{Mt5}$ and ERT–Ldt$_{Mt5}$ in contrast to the linear-aliphatic side chains in IMI–Ldt$_{Mt5}$ and SUB—Ldt$_{Mt5}$, **Figure 3.2**

By decomposing the binding free energy, ERT—Ldt$_{Mt5}$ (-50.07 kcal/mol) and MERO—Ldt$_{Mt5}$ (-35.72 kcal/mol) have the largest electrostatic energy changes upon binding in both gas phase (ΔE_{ele}) and GB solvent (ΔG_{polar}), while IMI—Ldt$_{Mt5}$ (131.68 kcal/mol) has the lowest. Although IMI—Ldt$_{Mt5}$ has the least favourable van der Waals energy change upon binding, the electrostatic energy change compensates significantly. A potential explanation for this is the destabilizing effect of GLU284 as shown in the per-residue energy contribution in **Figure 3.7** for IMI—Ldt$_{Mt5}$. The non-polar contribution to the solvation free energy for ERT—Ldt$_{Mt5}$ (-4.58 kcal/mol) is more negative than that of IMI—Ldt$_{Mt5}$ (-3.09 kcal/mol) and MERO—Ldt$_{Mt5}$ (-3.65 kcal/mol), this correlates with the lipophilic nature (LogP) of these compounds (-1.72, -2.74 and -2.71 respectively) as expected. However, non-polar contributions for all inhibitors are small. This contribution is overcome by the polar contribution of solvation free energy for ERT—Ldt$_{Mt5}$ and MERO—Ldt$_{Mt5}$. The enthalpic and entropic contributions are related. The increase in enthalpy energy of ERT—Ldt$_{Mt5}$ (-56.75 kcal/mol) and IMI—Ldt$_{Mt5}$ (-56.64 kcal/mol) leads to tighter binding, which corresponds to the more negative entropy values observed for ERT—Ldt$_{Mt5}$ (-28.46 kcal/mol) and IMI—Ldt$_{Mt5}$ (-29.12 kcal/mol). This high entropy contribution restricts the mobility of the interacting molecules. The entropy contribution of MERO—Ldt$_{Mt5}$ (15.62 kcal/mol), the lowest, appears to be a result of the shorter and more rigid carbapenem side chain. Also, the binding free energies of the complexes are linked to the SASA (**Figure S7**) which indicates the solvent exposed surface of the protein and hence the folding of exposed parts of the protein[78]. ERT bound Ldt$_{Mt5}$ has a smaller SASA, which could support the highest negative binding free energy observed while the IMI and MERO complexes each demonstrated larger SASA, with weaker binding free energy.

The PCA (**Figure 3.11**) also supports the highest binding free energy observed for ERT—Ldt$_{Mt5}$ with least correlated motion around the β-hairpin flap and Lc loop regions, followed by IMI— Ldt$_{Mt5}$, while the more correlated motion was seen for MERO—Ldt$_{Mt5}$ and consequently, its lower binding free energy. Furthermore, average binding affinities of Ldt$_{Mt5}$ complexes (-28.29 and -25 kcal/mol for Ertapenem and Imipenem respectively Table 2) were found to be less than that for Ldt$_{Mt2}$ complexes [experimental[16, 18, 29] and computational results[20, 22, 76] results (-37.91 and -40.42 kcal/mol for Ertapenem and Imipenem respectively)], as expected.

3.3.6 Per-residue decomposition energy analysis

The key features regarding the residue-based contributions to the binding free energies for the complexes were examined. These results provide a better description of the separate contributions to the total binding free energy. In particular, the per-residue energy decomposition was performed for the inhibitor—Ldt$_{Mt5}$ complexes including the active pocket residues. The β-hairpin flap and L$_C$ loop residues in each complex fall in this range. A total of 1000 snapshots was extracted from the last 10 ns of MD trajectories (at 10 ps

intervals) for all three complexes and were decomposed using per residue decomposition energy analysis implemented in the MMPBSA.py[77] script.   According to **Figure 3.7**, the largest contributions were those of the residues ARG297 and GLU339; ARG297, ARG301 and ASN337; ARG297, PHE340, ASN358 and CYS360 for ERT—Ldt$_{Mt5}$, IMI—Ldt$_{Mt5}$ and MERO—Ldt$_{Mt5}$, respectively.   The X-ray structure of meropenem complexed to Ldt$_{Mt5}$ illustrates the importance of these aforementioned key residues. CYS360, HIS342, ASN358 and THR357 are active site residues, according to previous[13] experimental findings. ARG297, ASN298, ARG301, MET316, ASN318 and GLU328 are residues involved in the *β*-hairpin flap region, while ASN337, GLY338, GLU339 and PHE340 form significant interactions with the meropenem[13]. These interactions for the selected carbapenem complexes were also observed in the per-residue decomposition energy and hydrogen bond analyses (**Table 3.2**, **Figures 3.7, S4, S5** and **S6**).
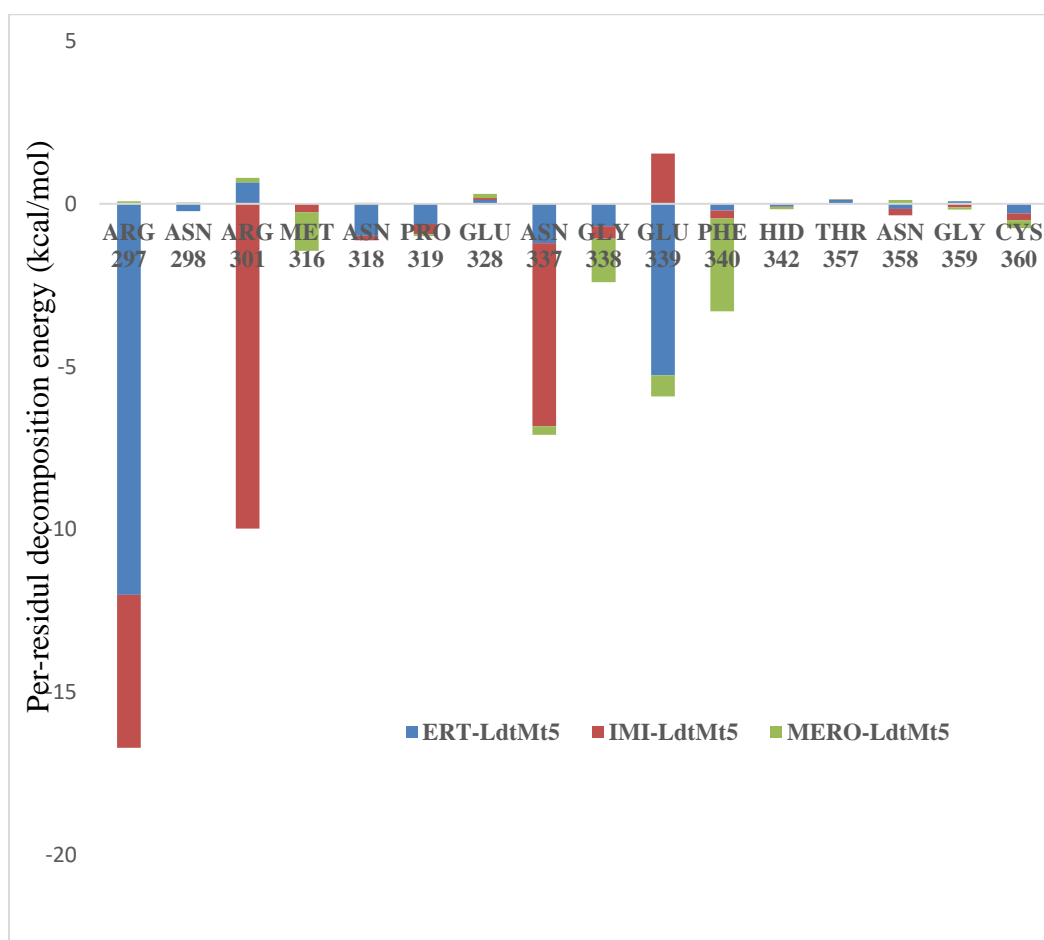
Figure 3.7 The plot of per-residue decomposition analysis for ERT—Ldt$_{Mt5}$, IMI—Ldt$_{Mt5}$ and MERO—Ldt$_{Mt5}$ complex from 1000 snapshots extracted from the last 10 ns MD trajectories. The minimized 3D structures (PDB format) for all inhibitor- Ldt$_{Mt5}$ complexes are provided as supplementary information.

The role of some other important residues was explained[13] from the crystal structure of the meropenem-complex. The two residues at the ends of loop L_C which interact with the PG stem in the outer cavity of Ldt$_{Mt2}$[16], HIS352 and TRP340, are said to be substituted with ASN358 and MET346, respectively, in Ldt$_{Mt5}$. ASN358 replaces this conserved motif histidine, HIS352 in Ldt$_{Mt2}$, that participates in recognition of the donor PG stem[16], and, in Ldt$_{Mt5}$, participates in recognition of the meropenem adduct. The meropenem core[13] lies with its most apolar side facing a hydrophobic patch formed by GLY338, the aliphatic portion of the side chain of GLU339, and PHE340 at the inner cavity. The C-terminal portion of the main chain of loop L_C GLY359 provides apolar contacts with the other side of the carbapenem core. Some hydrophilic interactions were also observed between the carbapenem core and Ldt$_{Mt5}$ which include ASN358, the main chain nitrogen atom of CYS360 hydrogen bond to the carbonyl of the opened penem ring. The GLU328 forms hydrogen bonds to the meropenem hydroxyethyl group and mediates the interaction between the meropenem core carboxylate and the carboxylate of GLU339[13]. Our theoretical result (**Figure 3.13**) aligns with the experimental observations[13] for meropenem in the complex with Ldt$_{Mt5}$. Also, it is interesting to observe that more interactions were seen for ERT—Ldt$_{Mt5}$ and IMI—Ldt$_{Mt5}$ for ARG297, ARG301, ASN337 and GLU339, in comparison to MERO—Ldt$_{Mt5}$. A similar trend was also observed for SUB—Ldt$_{Mt5}$ as represented in **Figure S6**.

3.3.7 Tip-tip distance analysis of the enzymes' hairpin/loop

Tip-tip distance analysis allows for a better understanding of the nature of flexibility in the studied complexes. Due to major structural differences displayed by the β-hairpin and loop L_C among *M. tuberculosis* L,D-transpeptidases[28], and the observed structural changes upon meropenem adduct formation suggest that their mobility and flexibility could play a role in the catalytic mechanism[28]. The flap/loop dynamics during the entire 60 ns MD simulation using the tip-tip center of mass distance analysis between three center of mass tip points on the β-hairpin flap residues (PRO319, ALA320, ALA321) and three facing points at the loop L_C residues (GLY349, ALA350, GLN351) of the enzyme in the four selected complexes and free Ldt$_{Mt5}$ (**Figure S2**) were studied and analyzed.
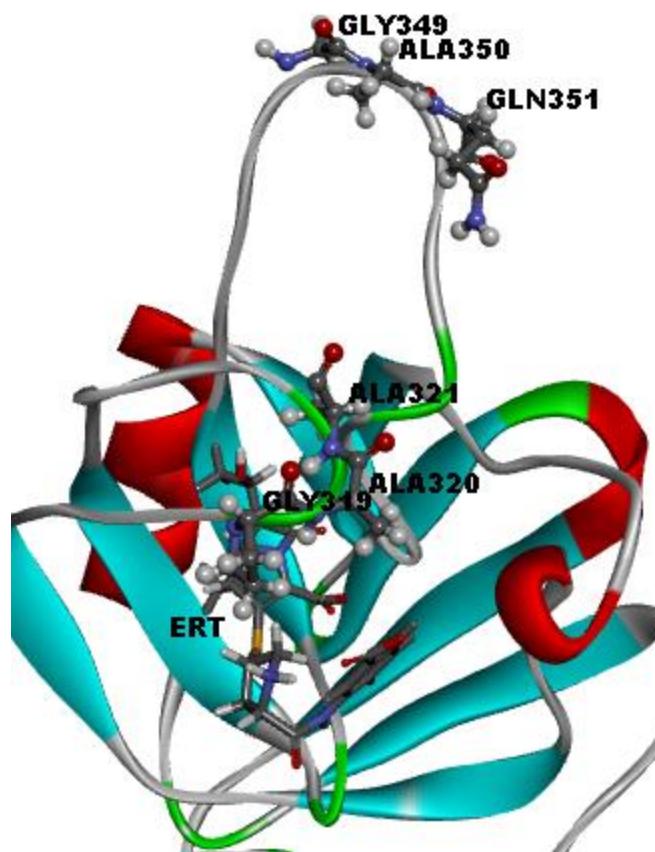
Figure 3.8 The three center of mass tip-tip distances of the *β*-hairpin flap and three facing points at the loop L$_C$ of ERT—Ldt$_{Mt5}$. PRO319-GLY349 D1: 13.32 Å PRO319-ALA350 D2: 13.34 Å PRO319-GLN351 D3: 12.18 Å ALA320-GLY349 D4: 12.77 Å ALA320-ALA350 D5: 13.24 Å ALA320-GLN351 D6: 11.30 Å ALA321-GLY349 D7: 9.37 Å ALA321-ALA350 D8: 10.29 Å ALA321-GLN351 D9: 9.20 Å. The minimized 3D structures (PDB format) for all inhibitor- Ldt$_{Mt5}$ complexes are provided as supplementary information.

Distance analysis enabled us to identify which of the residues best describe the *β*-hairpin and loop L$_C$ dynamics. The same approach[25] was used earlier to study *β*-hairpin flap dynamics of Ldt$_{Mt2}$ from *Mtb*. The present study (**Figure 3.9**) revealed that in the case of ERT—Ldt$_{Mt5}$, the lowest average tip-tip center of mass distances correspond to ALA321—GLN351 D9: (9.20 Å) with the maximum and minimum values, 14.89 Å and 3.5 Å and ALA320-GLN351 D6: (11.30 Å) with the maximum and minimum values, 18.53 Å and 4.1 Å, respectively (**Figure 3.9** and **Table S2)**. Comparing these tip-tip center of mass distances with the open and closed conformations for the different complexes, suggested that these distances [ALA321—GLN351 and ALA320—GLN351] are the most effective tip reference to measure the flap opening (in the range of 10-12 Å) and closure (around 5-7 Å)[25] complex conformations (**Table S2** and **S3)**. Over 60 ns

MD simulation, both the β-hairpin flap and the Lc loop regions reveal flap continuous opening and closing. This suggests the simulation time (60 ns) is long enough. This was also experimentally observed experimentally and is reported to play a significant role in the catalytic mechanism[28].
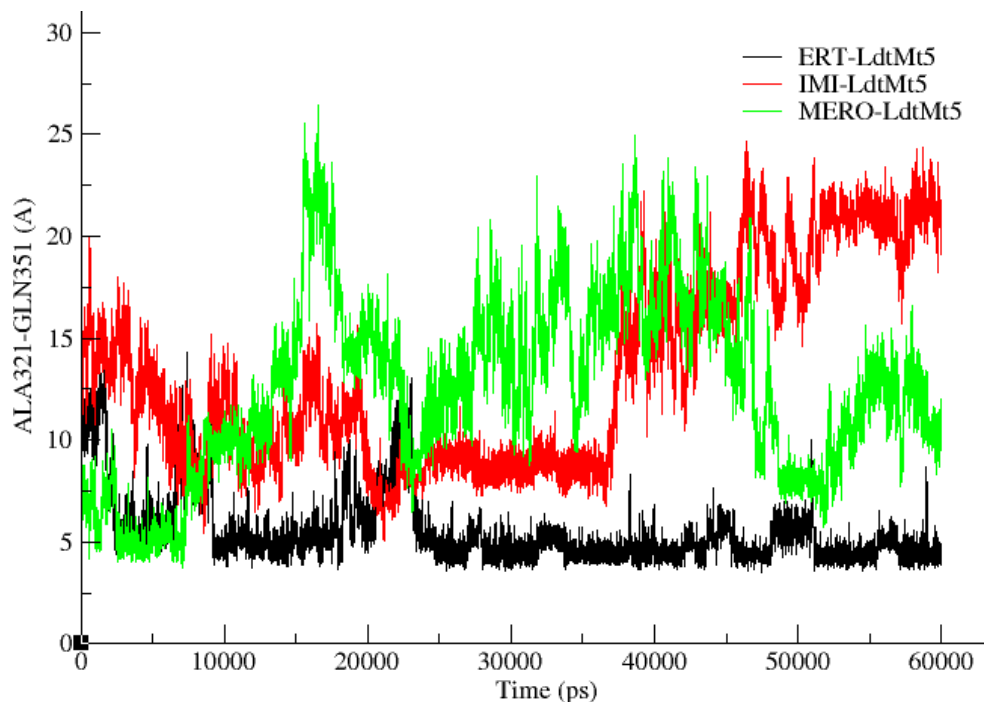
Figure 3.9 The plot of the center of mass tip-tip distances between ALA321—GLN351 residues for the ERT—Ldt_{Mt5}, IMI—Ldt_{Mt5} and MERO—Ldt_{Mt5} over the 60 ns MD simulations. The minimized 3D structures (PDB format) for all inhibitor- Ldt_{Mt5} complexes are provided as supplementary information.

It can be seen in **Figure 3.10** that the average center of mass tip distances between the residues ALA321—GLN351 in ERT—Ldt_{Mt5} is 9.2 Å, IMI—Ldt_{Mt5}, 14.79 Å and MERO—Ldt_{Mt5}, 15.06 Å. This result is in reasonable correlation with the calculated binding free energies; as ertapenem with the best binding affinity adopts the most compact flap conformation, while the weakest inhibitor (meropenem) exhibits the least compact conformation.

70
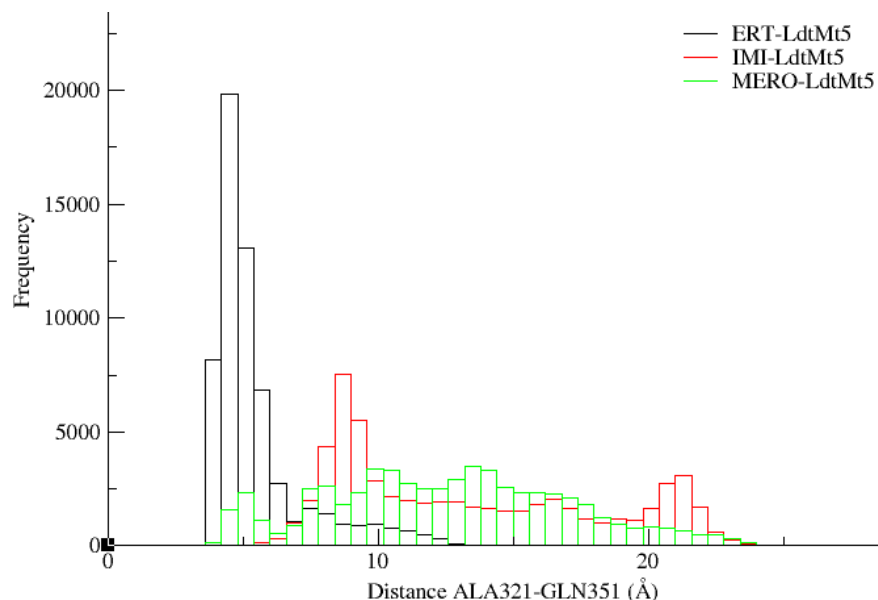
Figure 3.10 Histogram distribution of center of mass tip-tip distance [ALA321-GLN351] distances for ERT—Ldt$_{Mt5}$, IMI—Ldt$_{Mt5}$ and MERO—Ldt$_{Mt5}$ over the 60 ns MD trajectories. The minimized 3D structures (PDB format) for all inhibitor- Ldt$_{Mt5}$ complexes are provided as supplementary information.

Comparison of the average distances for the free Ldt$_{Mt5}$ with the complexes revealed the highest values for all considered tip–tip distances for the free enzyme (**Table S3**). The average distances measured indicates that the ligand binding induces significant flap dynamics towards the formation of closed flap conformation which is insignificant for the free enzyme. This similar phenomenon was also observed in our earlier study[25] on SUB–Ldt$_{Mt2}$ and free Ldt$_{Mt2}$ from *Mycobacterium tuberculosis*.

3.3.8 Principal component analysis (PCA)

PCA is a useful approach in the detection of important motion in biomolecules ranging from proteins to nucleic acids and discovering molecular motions that are biochemically relevant[79]. The concerted conformational motions in ERT—Ldt$_{Mt5}$, IMI—Ldt$_{Mt5}$ and MERO—Ldt$_{Mt5}$ complexes were studied [79] using PC analysis based on eigenvectors and eigenvalues of the covariance matrix. PCA as shown in **Figure 3.11**, revealed that the presence of carbapenems inside the enzyme (Ldt$_{Mt5}$) induce a significant impact on the motions of the *β*-hairpin flap and Lc loop regions (**Figure 3.1**) for the complexes. The ERT—Ldt$_{Mt5}$ complex showed less correlated motion around the flap and Lc loop regions, which can be attributed to its higher binding free energy compared to other complexes. This reduced and correlated motion as compared to IMI—Ldt$_{Mt5}$ and MERO—Ldt$_{Mt5}$ in these regions appears to suggest a more rigid conformation.

ERT-LdtMt5

IMI-LdtMt5
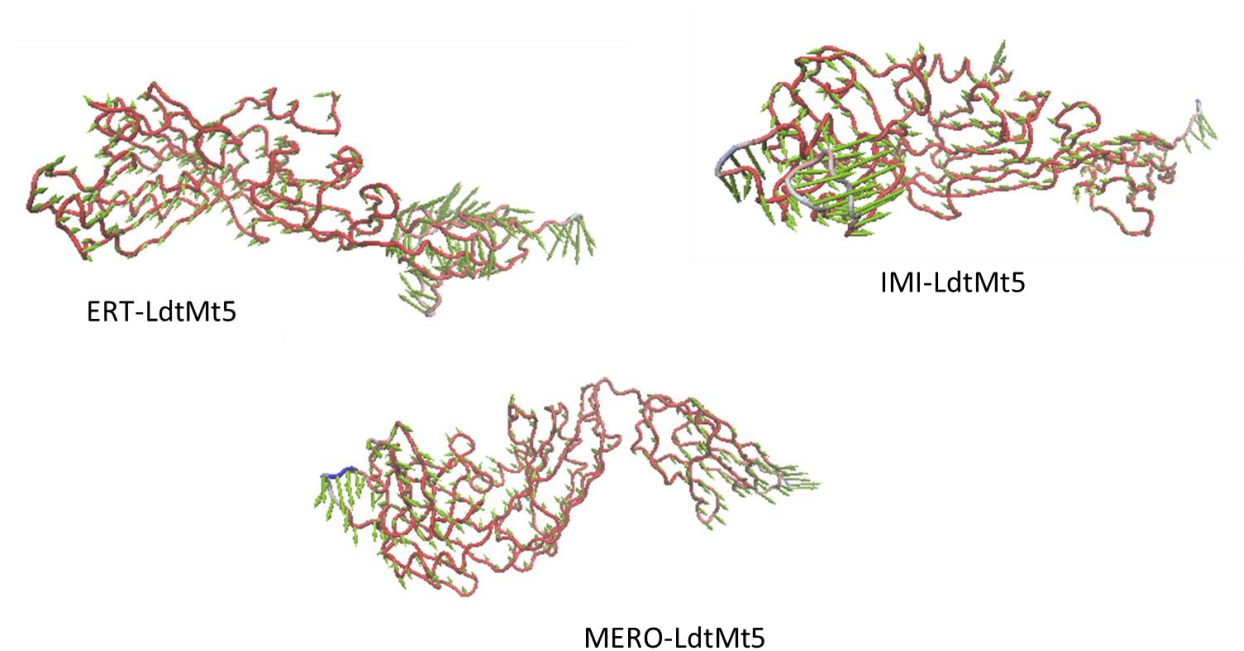
MERO-LdtMt5

Figure 3.11 The first principal components (PC1) collective motions for the obtained predominant eigenvectors using principal component analysis over the 60 ns MD trajectories for ERT— Ldt$_{Mt5}$, IMI— Ldt$_{Mt5}$ and MERO—Ldt$_{Mt5}$. The minimized 3D structures (PDB format) for all inhibitor- Ldt$_{Mt5}$ complexes are provided as supplementary information.

3.3.9 Hydrogen bonding Analysis

Hydrogen bonding interactions are particularly important for proteins, as they provide the organization for distinct folding and the selectivity in the protein-ligand interfacing that supports molecular recognition[80]. The hydrogen bonding interactions between the carbapenems and the active residues of Ldt$_{Mt5}$, their percentage occupancy throughout the MD simulations were investigated and the results listed in **Table 3.2**.

Table 3.2. The hydrogen bonds between carbapenems and active site residues for ERT—Ldt$_{Mt5}$, IMI—Ldt$_{Mt5}$ and MERO—Ldt$_{Mt5}$ complexes over the simulation time.

Complex	Acceptor	Donor	Occupancy (%)	Distance (Å)[a]	Angle (°)[a]
ERT—Ldt$_{Mt5}$	LIG362-O3	ASN358-HD21-ND2	12.8	2.8	156.0
	LIG362-O	ASN358-H-N	4.2	2.9	154.5
	LIG362-O2	ASN358-HD21-ND2	3.3	2.9	151.6
	LIG362-O3	ASN358-HD22-ND2	1.9	2.9	156.2
	LIG362-O	ASN358-HD21-ND2	0.8	2.9	156.0
IMI—Ldt$_{Mt5}$	LIG362-O4	ASN358-HD21-ND2	1.1	3.0	162.0
	ASN358-OD1	LIG362-H2-O2	0.9	2.9	153.7
	LIG362-O2	ASN358-HD21-ND2	0.6	2.9	149.4
	LIG362-O2	ASN358-HD22-ND2	0.6	2.9	153.6
	ASN358-O	LIG362-H2-O2	0.5	2.9	156.3
	ASN358-ND2	LIG362-H2-O2	0.1	2.9	154.3
MERO—Ldt$_{Mt5}$	LIG362-O2	ASN358-HD22-ND2	0.5	2.9	147.5
	LIG362-O3	ASN358-HD21-ND2	0.1	2.9	160.4
	ASN358-OD1	LIG362-H3-O3	0.1	2.9	154.4

[a]The hydrogen bonds were determined by the acceptor…donor atom distance of < 3.0 Å and acceptor…H-donor angle of >140 A˚. LIG362 = ERT, IMI and MERO for each complex. The minimized 3D structures (PDB format) for all inhibitor- Ldt$_{Mt5}$ complexes are provided as supplementary information.

Generally, we observed prevalent hydrogen bond interactions between ASN358 with the ERT—Ldt$_{Mt5}$, IMI—Ldt$_{Mt5}$ and MERO—Ldt$_{Mt5}$ complexes. This contact was also observed between the carbapenem core and Ldt$_{Mt5}$ from experimental findings[13]. The greater occupancy seen in ERT—Ldt$_{Mt5}$ (**Table 3.2**) is in reasonable correlation with its higher binding free energy compared the other two complexes.

3.3.10 Thermochemical analysis

The relative free energies of activation for the reaction mechanism of Ldt$_{Mt5}$ in the presence of imipenem and meropenem are presented in **Table 3.3** for the systems. The reaction energy profile for the obtained activation energies using M06/6-311++G(2d,2p) from **Table 3.3** are presented in **Figure 3.12** and the results will be explained based on this functional. M06 functional gave the lowest ΔG values for enzymatic reactions.[81] ΔG for the 6-membered ring transition state of imipenem and meropenem is 52.23 kcal/mol and 98.96 kcal/mol respectively. This shows that imipenem is more reactive against Ldt$_{Mt5}$ than

meropenem. These results follow the same order as the molecular dynamics calculated binding free energies for the imipenem (-25.52 kcal/mol) and meropenem (-18.34 kcal/mol) precomplexes in this study. The calculated ΔG values for imipenem (-7.43 kcal/mol) and meropenem (-8.65 kcal/mol) with Ldt_{Mt2} obtained by Silva *et al.*[20] also followed the same order. This confirms the experimentally observed result that imipenem reacts faster with Ltd_{Mt2} than meropenem.[24]

The ΔG value for the products (covalently bonded inhibitor complex) of imipenem (4.09 kcal/mol) and meropenem (22.33 kcal/mol) in our study followed the same trend that was experimentally observed for Ldt_{Mt2} against imipenem and meropenem by Erdemli *et al.*[33]

Our results (**Table 3.3**) also reveal that the 6-membered ring transition state mechanism obtained in this study has considerable higher activation energy than that of the 6-membered ring TS of Ldt_{Mt2} obtained previously[24, 60] in our group.

Table 3.3. The thermochemical parameters of 6-membered ring reaction pathways of Ldt$_{Mt5}$ obtained in ONIOM (B3LYP/6-31+g(d,p):Amber) using different density functionals. The ΔE, ΔG, ΔH (kcal/mol) and ΔS (cal/mol/K).

Inhibitors		B3LYP[a]				M06[a]				ωB97X[a]			
		ΔE	ΔG	ΔH	ΔS	ΔE	ΔG	ΔH	ΔS	ΔE	ΔG	ΔH	ΔS
	R	0	0	0	0	0	0	0	0	0	0	0	0
Meropenem	TS	93.77	91.08	91.55	-0.47	101.65	98.96	99.43	-0.47	124.04	121.35	121.82	-0.47
	Pr	17.81	12.14	10.5	1.64	28	22.33	20.67	1.66	31.96	26.29	24.65	1.64
	R	0	0	0	0	0	0	0	0	0	0	0	0
Imipenem	TS	80.07	53.29	47.02	6.27	79.01	52.23	45.96	6.27	85.67	58.89	52.62	6.27
	Pr	30.14	6.16	2.27	3.89	28.07	4.09	0.2	3.89	30.76	6.78	2.89	3.89
	R	0	0	0	0	0	0	0	0	0	0	0	0
Natural substrate	TS	67.04	66.22	64.82	1.39	71.23	70.4	69.01	1.09	76.02	75.19	73.8	1.39
	Pr	14.59	13.42	12.33	1.09	17.65	16.48	15.39	1.39	20.24	19.07	17.98	1.09

[a]Energies relative to reactant for total electronic energy (ΔE) and activation free energy (ΔG, with thermal correction) using B3LYP, M06, ωB97X/6-311++G(d,p):AMBER//B3LYP/6-31G(d,p):AMBER. R = reactant, TS = transition state and P = product. The minimized 3D structures (PDB format) for all inhibitor- Ldt$_{Mt5}$ complexes are provided as supplementary information.

For the activation energies, the entropy contribution of imipenem suggests that it experiences less restriction in the active site, in comparison to the other two cases. Meropenem experiences the largest entropy penalty. This observation is due to the differences in the respective side chains. Imipenem has an aliphatic side which is much less sterically hindered, while the bulky side chain of meropenem is much more restricted in the active site.[20] Also, imipenem has been reported as showing a lower entropy penalty (ΔS) compared to meropenem with Ldt$_{Mt2}$, which is in agreement with Erdemli *et al.*[33].
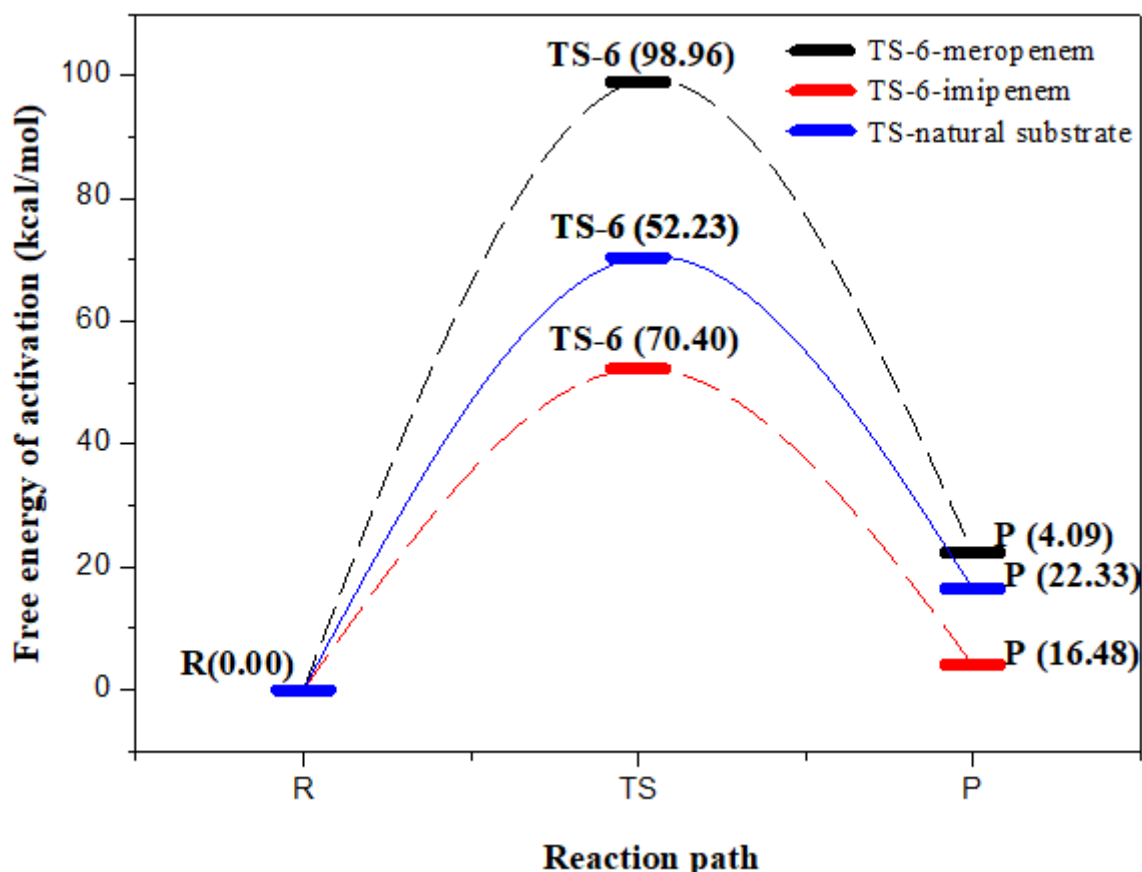
Figure 3.12 Gibbs free energy pathway of 6-membered ring mechanism of inhibition of L,D-transpeptidase (Ld$_{Mt5}$) by meropenem obtained using the ONIOM [M06/6-311++G(2d,2p):Amber] method.

The free energy of activation observed for the natural substrate with Ldt$_{Mt5}$ is 70.4 kcal/mol, which is approximately 40.0 kcal/mol higher than the corresponding activation energy for Ldt$_{Mt2}$[82]. This is an indication that this specific natural substrate is perhaps not the correct one for Ldt$_{Mt5}$. While Ldt$_{Mt2}$ uses the native tetrapeptide substrate L-Ala[1]-D-iso-Glu[2]-*meso*DAP[3]-D-ala[4],[34] the exact substrate for Ldt$_{Mt5}$ is not known. β-lactam antibiotics are known to structural and chemical mimics of peptidoglycan substrates and therefore bind to the enzymes as suicide substrates[83, 84]. The fact the Ldt$_{Mt2}$ binds strongly to carbapenems is indicative of this class of antibiotics closely mimicking the natural substrate of this enzyme. The weaker binding of Ldt$_{Mt5}$ to carbapenems suggests that the native substrate of this enzyme is likely to be different from that of Ldt$_{Mt2}$. While L-Ala[1]-D-iso-Glu[2]-*meso*DAP[3]-D-ala[4] is the most

abundant substrate in the peptidoglycan of Mtb^{14}, bacteria are known to incorporate a range of modification including non-canonical D-amino acids in their peptidoglycan[85]. It is possible that Ldt_{Mt5} is involved in incorporating such amino acids or modifying the peptidoglycan with as yet unknown chemical decorations. Additional studies will be necessary to unveil the native substrates and activity of Ldt_{Mt5}.

3.4 Conclusion

Due to the relatively weak *in vitro* inhibition of Ldt_{Mt5} by carbapenems in comparison to its Ldt_{Mt2} paralog, a theoretical comparative study into the key interactions between active residues of these enzymes with carbapenems is if great importance. Herein, the essential factors that contribute to the binding and inhibition efficiency of the Ldt_{Mt5} in the presence of the three carbapenems, ertapenem, imipenem and meropenem were investigated. Molecular docking was applied for the starting structures of the carbapenems in the active pocket of Ldt_{Mt5} based on the reported single crystal X-ray structure of MERO—Ldt_{Mt5}. Afterwards, the complexes were simulated using the molecular dynamics approach implemented in Amber. The dynamics of *the β*-hairpin flap and Lc loop presence in Ldt_{Mt5} and their effect on the binding free energies were monitored through tip-tip distance analysis. The binding free energies (including entropy contributions) of these complexes were calculated from the MD simulation using MM/GBSA approach, the theoretical results revealed the best ΔG_{bind} for ERT—Ldt_{Mt5} followed by IMI—Ldt_{Mt5} then MERO—Ldt_{Mt5}. Furthermore, per residue free energy decomposition and the hydrogen bonding interactions between the inhibitors and this protein were analysed to identify the essential residual interactions in the carbapenem complexes. The theoretical results revealed interactions between the carbapenems and the following residues are important which were also observed experimentally: ARG297, MET316, GLU328, GLY338, GLU339, CYS360, HIS342, ASN358 and THR357.

It is important to note that a similar previous study with Ldt_{Mt2} with the same inhibitors[25] also did not reveal much correlation between the calculated binding free energies and the quantities calculated (RMSF and Rg). This may also be expected for the current study as efforts to determine the experimental binding free energies[28] with these drugs failed due to weak inhibition of Ldt_{Mt5}. The average tip-tip distances of the *β*-hairpin flap and the Lc loop were analysed. The average tip-tip distances revealed that the distances between ALA321 and GLN351 as well as ALA320 and GLN351 are the most sensitive parameter that appears to correlate with the calculated binding free energies (best binding energy display the most rigid complex structure). Finally, the carbapenem—Ldt_{Mt5} complexes showed similar residual fluctuations from the RMSF analyses to what was reported for Ldt_{Mt2}, despite the fact that carbapenem complexes withLdt_{Mt2}[16, 25] undergo fast acylation (determined with ITC analysis). However, the fluctuations for Ldt_{Mt5} were found to be much larger for Ldt_{Mt5} complexes, especially at the binding site, indicating weaker binding of carbapenems. Furthermore, average binding affinities of Ldt_{Mt5} complexes were found to be less than that for Ldt_{Mt2} complexes, as expected. In

addition to this, the distance analyses suggested that the opening of the flaps in Ldt$_{Mt5}$ complexed with the inhibitor is more pronounced in comparison to that observed for Ldt$_{Mt2}$ complexed form. Overall, the stability of the carbapenem-Ldt$_{Mt5}$ complexes may be perturbed by higher fluctuations of the *β*-hairpin flap and loop L$_C$. Moreover, the interactions of carbapenems with major binding site residues such as HIS342 and CYS360 were found to be weak for Ldt$_{Mt5}$ complexes. The relative higher free energies of activation obtained from the mechanistic studies also support the weak binding of Ldt$_{Mt5}$ against the selected carbapenems. In, addition, this study showed that the existing inhibitors have high activation energies suggesting their poor mode of reaction, and thus a need to find new *β*-lactam compounds against this target. Derivatives of the existing inhibitors will first be subjected computational studies and then validated with experimental bioassays. The higher free energy of activation observed with L-Ala^1-D-iso-Glu^2-*meso*DAP^3-D-ala^4 against Ldt$_{Mt5}$ could suggest that the native substrate of this enzyme is likely to be different from that of Ldt$_{Mt2}$. This study, therefore, confirms that the computational inhibitor-enzyme precomplex model[20, 23, 76] for transpeptidases correctly reflects experimental observations.

Competing interests

The authors declare that they have no competing interests.

Acknowledgement

References

[1] Dye, C., Scheele, S., Dolin, P., Pathania, V., and Raviglione, M. C. (1999) Global burden of tuberculosis: estimated incidence, prevalence, and mortality by country W.H.O. Global Surveillance and Monitoring Project *Jama 282*, 677-686.

[2] Bryce, J., Boschi-Pinto, C., Shibuya, K., Black, R. E., and Group, W. C. H. E. R. (2005) WHO estimates of the causes of death in children, *The Lancet 365*, 1147-1152.

[3] Health, N. I. o. (2012) Research Portfolio Online Reporting Tools (RePORT), 2010, *Available at report. nih. gov/index. aspx.*

[4] Mahindru, S. N. (2009) *Food contaminants-Origin, propagation & analysis*, Vol. 1, APH Publishing.

[5] Kamholz, S. (2002) Drug resistant tuberculosis, *Journal of the Association for Academic Minority Physicians: the official publication of the Association for Academic Minority Physicians 13*, 53-56.

[6] Monack, D. M., Mueller, A., and Falkow, S. (2004) Persistent bacterial infections: the interface of the pathogen and the host immune system, *Nature reviews. Microbiology 2*, 747.

[7] Hugo, W. B., and Russell, A. D. (1998) *Pharmaceutical microbiology*, Blackwell science.

[8] Wietzerbin, J., Das, B. C., Petit, J. F., Lederer, E., Leyh-Bouille, M., and Ghuysen, J. M. (1974) Occurrence of D-alanyl-(D)-meso-diaminopimelic acid and meso-diaminopimelyl-meso-

diaminopimelic acid interpeptide linkages in the peptidoglycan of Mycobacteria, *Biochemistry 13*, 3471-3476.

[9] Moraes, G. L., Gomes, G. C., De Sousa, P. R. M., Alves, C. N., Govender, T., Kruger, H. G., Maguire, G. E., Lamichhane, G., and Lameira, J. (2015) Structural and functional features of enzymes of Mycobacterium tuberculosis peptidoglycan biosynthesis as targets for drug development, *Tuberculosis 95*, 95-111.

[10] Hugonnet, J.-E., and Blanchard, J. S. (2007) Irreversible inhibition of the Mycobacterium tuberculosis β-lactamase by clavulanate, *Biochemistry 46*, 11998-12004.

[11] Mainardi, J.-L., Legrand, R., Arthur, M., Schoot, B., van Heijenoort, J., and Gutmann, L. (2000) Novel mechanism of β-lactam resistance due to bypass of DD-transpeptidation in Enterococcus faecium, *Journal of Biological Chemistry 275*, 16490-16496.

[12] Hugonnet, J.-E., Tremblay, L. W., Boshoff, H. I., Barry, C. E., and Blanchard, J. S. (2009) Meropenem-clavulanate is effective against extensively drug-resistant Mycobacterium tuberculosis, *Science 323*, 1215-1218.

[13] Manina, G., Dhar, N., and McKinney, J. D. (2015) Stress and host immunity amplify Mycobacterium tuberculosis phenotypic heterogeneity and induce nongrowing metabolically active forms, *Cell host & microbe 17*, 32-46.

[14] Lavollay, M., Arthur, M., Fourgeaud, M., Dubost, L., Marie, A., Veziris, N., Blanot, D., Gutmann, L., and Mainardi, J.-L. (2008) The peptidoglycan of stationary-phase Mycobacterium tuberculosis predominantly contains cross-links generated by L, D-transpeptidation, *Journal of Bacteriology 190*, 4360-4366.

[15] Sauvage, E., Kerff, F., Terrak, M., Ayala, J. A., and Charlier, P. (2008) The penicillin-binding proteins: structure and role in peptidoglycan biosynthesis, *FEMS microbiology reviews 32*, 234-258.

[16] Erdemli, S. B., Gupta, R., Bishai, W. R., Lamichhane, G., Amzel, L. M., and Bianchet, M. A. (2012) Targeting the cell wall of Mycobacterium tuberculosis: structure and mechanism of L, D-transpeptidase 2, *Structure 20*, 2103-2115.

[17] Böth, D., Steiner, E. M., Stadler, D., Lindqvist, Y., Schnell, R., and Schneider, G. (2013) Structure of LdtMt2, an L, D-transpeptidase from Mycobacterium tuberculosis, *Acta Crystallographica Section D: Biological Crystallography 69*, 432-441.

[18] Kumar, P., Kaushik, A., Lloyd, E. P., Li, S.-G., Mattoo, R., Ammerman, N. C., Bell, D. T., Perryman, A. L., Zandi, T. A., and Ekins, S. (2017) Non-classical transpeptidases yield insight into new antibacterials, *Nature chemical biology 13*, 54.

[19] Li, W.-J., Li, D.-F., Hu, Y.-L., Zhang, X.-E., Bi, L.-J., and Wang, D.-C. (2013) Crystal structure of L, D-transpeptidase Ldt Mt2 in complex with meropenem reveals the mechanism of carbapenem against Mycobacterium tuberculosis, *Cell research 23*, 728.

[20] Silva, J. R., Bishai, W. R., Govender, T., Lamichhane, G., Maguire, G. E., Kruger, H. G., Lameira, J., and Alves, C. N. (2016) Targeting the cell wall of Mycobacterium tuberculosis: a molecular modeling investigation of the interaction of imipenem and meropenem with L,D-transpeptidase 2, *Journal of biomolecular structure & dynamics 34*, 304-317.

[21] Silva, J. R. A., Bishai, W. R., Govender, T., Lamichhane, G., Maguire, G. E., Kruger, H. G., Lameira, J., and Alves, C. N. (2015) Targeting the cell wall of Mycobacterium tuberculosis: a molecular modeling investigation of the interaction of imipenem and meropenem with L, D-transpeptidase 2, *Journal of Biomolecular Structure and Dynamics 34*, 304-317.

[22] Silva, J. R. A., Govender, T., Maguire, G. E., Kruger, H. G., Lameira, J., Roitberg, A. E., and Alves, C. N. (2015) Simulating the inhibition reaction of Mycobacterium tuberculosis L, D-transpeptidase 2 by carbapenems, *Chemical Communications 51*, 12560-12562.

[23] Silva, J. R. r. A., Roitberg, A. E., and Alves, C. u. N. (2014) Catalytic mechanism of L, D-transpeptidase 2 from Mycobacterium tuberculosis described by a computational approach: insights for the design of new antibiotics drugs, *Journal of Chemical Information and Modeling 54*, 2402-2410.

[24] Fakhar, Z., Govender, T., Lamichhane, G., Maguire, G. E., Kruger, H. G., and Honarparvar, B. (2017) Computational model for the acylation step of the β-lactam ring: Potential application for l, d-transpeptidase 2 in mycobacterium tuberculosis, *Journal of Molecular Structure 1128*, 94-102.

[25] Fakhar, Z., Govender, T., Maguire, G. E., Lamichhane, G., Walker, R. C., Kruger, H. G., and Honarparvar, B. (2017) Differential flap dynamics in l, d-transpeptidase2 from mycobacterium tuberculosis revealed by molecular dynamics, *Molecular BioSystems*.

[26] Billones, J. B., Carrillo, M. C. O., Organo, V. G., Macalino, S. J. Y., Sy, J. B. A., Emnacen, I. A., Clavio, N. A. B., and Concepcion, G. P. (2016) Toward antituberculosis drugs: in silico screening of synthetic compounds against Mycobacterium tuberculosis l, d-transpeptidase 2, *Drug design, development and therapy 10*, 1147.

[27] Baldin, S., Misiura, N., and Švedas, V. (2017) Building a full-atom model of l, dtranspeptidase 2 from Mycobacterium tuberculosis for screening new inhibitors, *Acta Naturae (англоязычная версия) 9*.

[28] Brammer, B. L., Ghosh, A., Pan, Y., Jakoncic, J., Lloyd, E., Townsend, C., Lamichhane, G., and Bianchet, M. (2015) Loss of a Functionally and Structurally Distinct ld-Transpeptidase, LdtMt5, Compromises Cell Wall Integrity in Mycobacterium tuberculosis, *The Journal of Biological Chemistry 290*, 25670-25685.

[29] Bianchet, M. A., Pan, Y. H., Basta, L. A. B., Saavedra, H., Lloyd, E. P., Kumar, P., Mattoo, R., Townsend, C. A., and Lamichhane, G. (2017) Structural insight into the inactivation of Mycobacterium tuberculosis non-classical transpeptidase Ldt Mt2 by biapenem and tebipenem, *BMC biochemistry 18*, 8.

[30] Ntombela, T., Fakhar, Z., Ibeji, C. U., Govender, T., Maguire, G. E., Lamichhane, G., Kruger, H. G., and Honarparvar, B. (2018) Molecular insight on the non-covalent interactions between carbapenems and l, d-transpeptidase 2 from Mycobacterium tuberculosis: ONIOM study, *Journal of Computer-Aided Molecular Design*, 1-15.

[31] Ackerman, S. H., and Gatti, D. L. (2013) Biapenem inactivation by B2 metallo β-lactamases: energy landscape of the hydrolysis reaction, *PloS one 8*, e55136.

[32] Cordillot, M., Dubée, V., Triboulet, S., Dubost, L., Marie, A., Hugonnet, J.-E., Arthur, M., and Mainardi, J.-L. (2013) In vitro cross-linking of Mycobacterium tuberculosis peptidoglycan by l, d-transpeptidases and inactivation of these enzymes by carbapenems, *Antimicrobial agents and chemotherapy 57*, 5940-5945.

[33] Erdemli, S. B., Gupta, R., Bishai, W. R., Lamichhane, G., Amzel, L. M., and Bianchet, M. A. (2012) Targeting the cell wall of Mycobacterium tuberculosis: structure and mechanism of L,D-transpeptidase 2, *Structure 20*, 2103-2115.

[34] Gupta, R., Lavollay, M., Mainardi, J.-L., Arthur, M., Bishai, W. R., and Lamichhane, G. (2010) The Mycobacterium tuberculosis protein LdtMt2 is a nonclassical transpeptidase required for virulence and resistance to amoxicillin, *Nature Medicine 16*, 466-469.

[35] Karubiu, W., Bhakat, S., McGillewie, L., and Soliman, M. E. (2015) Flap dynamics of plasmepsin proteases: insight into proposed parameters and molecular dynamics, *Molecular BioSystems 11*, 1061-1066.

[36] Berman, H. M., Westbrook, J., Feng, Z., Gilliland, G., Bhat, T. N., Weissig, H., Shindyalov, I. N., and Bourne, P. E. (2000) The protein data bank, *Nucleic acids research 28*, 235-242.

[37] Sali, A., and Blundell, T. (1994) Comparative protein modelling by satisfaction of spatial restraints, *Protein structure by distance analysis 64*, C86.

[38] Li, H., Robertson, A. D., and Jensen, J. H. (2005) Very fast empirical prediction and rationalization of protein pKa values, *Proteins: Structure, Function, and Bioinformatics 61*, 704-721.

[39] Morris, G. M., Huey, R., Lindstrom, W., Sanner, M. F., Belew, R. K., Goodsell, D. S., and Olson, A. J. (2009) AutoDock4 and AutoDockTools4: Automated docking with selective receptor flexibility, *Journal of computational chemistry 30*, 2785-2791.

[40] Veber, D. F., Johnson, S. R., Cheng, H.-Y., Smith, B. R., Ward, K. W., and Kopple, K. D. (2002) Molecular properties that influence the oral bioavailability of drug candidates, *Journal of medicinal chemistry 45*, 2615-2623.

[41] Honarparvar, B., Govender, T., Maguire, G. E., Soliman, M. E., and Kruger, H. G. (2013) Integrated approach to structure-based enzymatic drug design: molecular modeling, spectroscopy, and experimental bioactivity, *Chemical reviews 114*, 493-537.

[42] Morris, G. M., Goodsell, D. S., Halliday, R. S., Huey, R., Hart, W. E., Belew, R. K., and Olson, A. J. (1998) Automated docking using a Lamarckian genetic algorithm and an empirical binding free energy function, *Journal of computational chemistry 19*, 1639-1662.

[43] Pandit, A., Sengupta, S., Krishnan, M. A., Reddy, R. B., Sharma, R., and Venkatesh, C. (2018) First report on 3D-QSAR and molecular dynamics based docking studies of GCPII inhibitors for targeted drug delivery applications, *Journal of Molecular Structure 1159*, 179-192.

[44] Wang, J., Wolf, R. M., Caldwell, J. W., Kollman, P. A., and Case, D. A. (2004) Development and testing of a general amber force field, *Journal of computational chemistry 25*, 1157-1174.

[45] Sgrignani, J., Grazioso, G., De Amici, M., and Colombo, G. (2014) Inactivation of TEM-1 by avibactam (NXL-104): insights from quantum mechanics/molecular mechanics metadynamics simulations, *Biochemistry 53*, 5174-5185.

[46] Jorgensen, W. L., Chandrasekhar, J., Madura, J. D., Impey, R. W., and Klein, M. L. (1983) Comparison of simple potential functions for simulating liquid water, *The Journal of chemical physics 79*, 926-935.

[47] Kräutler, V., Van Gunsteren, W. F., and Hünenberger, P. H. (2001) A fast SHAKE algorithm to solve distance constraint equations for small molecules in molecular dynamics simulations, *Journal of computational chemistry 22*, 501-508.

[48] Darden, T., York, D., and Pedersen, L. (1993) Particle mesh Ewald: An N· log (N) method for Ewald sums in large systems, *The Journal of chemical physics 98*, 10089-10092.

[49] Roe, D. R., and Cheatham III, T. E. (2013) PTRAJ and CPPTRAJ: software for processing and analysis of molecular dynamics trajectory data, *Journal of chemical theory and computation 9*, 3084-3095.

[50] Amadei, A., Linssen, A., and Berendsen, H. J. (1993) Essential dynamics of proteins, *Proteins: Structure, Function, and Bioinformatics 17*, 412-425.

[51] Cocco, S., Monasson, R., and Weigt, M. (2013) From principal component to direct coupling analysis of coevolution in proteins: Low-eigenvalue modes are needed for structure prediction, *PLoS Comput Biol 9*, e1003176.

[52] Bakan, A., Meireles, L. M., and Bahar, I. (2011) ProDy: protein dynamics inferred from theory and experiments, *Bioinformatics 27*, 1575-1577.

[53] Humphrey, W., Dalke, A., and Schulten, K. (1996) VMD: visual molecular dynamics, *Journal of molecular graphics 14*, 33-38.

[54] Srinivasan, J., Cheatham, T. E., Cieplak, P., Kollman, P. A., and Case, D. A. (1998) Continuum solvent studies of the stability of DNA, RNA, and phosphoramidate− DNA helices, *Journal of the American Chemical Society 120*, 9401-9409.

[55] Kollman, P. A., Massova, I., Reyes, C., Kuhn, B., Huo, S., Chong, L., Lee, M., Lee, T., Duan, Y., and Wang, W. (2000) Calculating structures and free energies of complex molecules: combining molecular mechanics and continuum models, *Accounts of chemical research 33*, 889-897.

[56] Gohlke, H., and Case, D. A. (2004) Converging free energy estimates: MM-PB (GB) SA studies on the protein–protein complex Ras–Raf, *Journal of computational chemistry 25*, 238-250.

[57] Kassem, S., Ahmed, M., El-Sheikh, S., and Barakat, K. H. (2015) Entropy in bimolecular simulations: A comprehensive review of atomic fluctuations-based methods, *Journal of Molecular Graphics & Modelling 62*, 105-117.

[58] Chiba, S., Harano, Y., Roth, R., Kinoshita, M., and Sakurai, M. (2012) Evaluation of protein-ligand binding free energy focused on its entropic components, *Journal of Computational Chemistry 33*, 550-560.

[59] Xue, W., Jiao, P., Liu, H., and Yao, X. (2014) Molecular modeling and residue interaction network studies on the mechanism of binding and resistance of the HCV NS5B polymerase mutants to VX-222 and ANA598, *Antiviral research 104*, 40-51.

[60] Ibeji, C. G., Thavendran; Ntombela, Thandokuhle; Maguire, Glenn; Lamichhane, Gyanu; Kruger, Hendrik; Honarparvar, Bahareh. Catalytic Role of Water in the Acylation Mechanism of L,D-Transpeptidase 2: A QM/MM (ONIOM) Modeling, *ACS Catalysis (Submitted for publication)*.

[61] Suresh, C. H., Vargheese, A. M., Vijayalakshmi, K. P., Mohan, N., and Koga, N. (2008) Role of structural water molecule in HIV protease-inhibitor complexes: a QM/MM study, *J Comput Chem 29*, 1840-1849.

[62] Svensson, M., Humbel, S., Froese, R. D., Matsubara, T., Sieber, S., and Morokuma, K. (1996) ONIOM: a multilayered integrated MO+ MM method for geometry optimizations and single point energy predictions. A test for Diels− Alder reactions and Pt (P (t-Bu) 3) 2+ H2 oxidative addition, *The Journal of Physical Chemistry 100*, 19357-19363.

[63] Vreven, T., Morokuma, K., Farkas, Ö., Schlegel, H. B., and Frisch, M. J. (2003) Geometry optimization with QM/MM, ONIOM, and other combined methods. I. Microiterations and constraints, *Journal of computational chemistry 24*, 760-769.

[64] Frisch, M., Trucks, G., Schlegel, H. B., Scuseria, G., Robb, M., Cheeseman, J., Scalmani, G., Barone, V., Mennucci, B., and Petersson, G. (2009) Gaussian 09, revision D. 01, Gaussian, Inc., Wallingford CT.

[65] Tao, P., and Schlegel, H. B. (2010) A toolkit to assist ONIOM calculations, *J Comput Chem 31*, 2363-2369.

[66] Coropceanu, V., Malagoli, M., da Silva Filho, D., Gruhn, N., Bill, T., and Brédas, J. (2002) Hole- and electron-vibrational couplings in oligoacene crystals: intramolecular contributions, *Physical review letters 89*, 275503.

[67] Grigorenko, B. L., Khrenova, M. G., Nilov, D. K., Nemukhin, A. V., and Švedas, V. K. (2014) Catalytic cycle of penicillin acylase from Escherichia coli: QM/MM modeling of chemical transformations in the enzyme active site upon penicillin G hydrolysis, *ACS Catalysis 4*, 2521-2529.

[68] Gonzalez, C., and Schlegel, H. B. (1989) An improved algorithm for reaction path following, *The Journal of Chemical Physics 90*, 2154-2161.

[69] Gonzalez, C., and Schlegel, H. B. (1990) Reaction path following in mass-weighted internal coordinates, *Journal of Physical Chemistry 94*, 5523-5527.

[70] Calixto, A. R., Brás, N. F., Fernandes, P. A., and Ramos, M. J. (2014) Reaction Mechanism of Human Renin Studied by Quantum Mechanics/Molecular Mechanics (QM/MM) Calculations, *ACS Catalysis 4*, 3869-3876.

[71] Goerigk, L., and Grimme, S. (2011) A thorough benchmark of density functional methods for general main group thermochemistry, kinetics, and noncovalent interactions, *Physical Chemistry Chemical Physics 13*, 6670-6688.

[72] Neves, R. P., Fernandes, P. A., Varandas, A. n. J., and Ramos, M. J. (2014) Benchmarking of Density Functionals for the Accurate Description of Thiol–Disulfide Exchange, *Journal of chemical theory and computation 10*, 4842-4856.

[73] Sun, Y., and Chen, H. (2014) Performance of density functionals for activation energies of re-catalyzed organic reactions, *Journal of chemical theory and computation 10*, 579-588.

[74] Milhøj, B. O., and Sauer, S. P. (2015) Kinetics and thermodynamics of the reaction between the• OH radical and adenine: a theoretical investigation, *The Journal of Physical Chemistry A 119*, 6516-6527.

[75] Sureshkumar, B., Mary, Y. S., Panicker, C. Y., Resmi, K., Suma, S., Armaković, S., Armaković, S. J., and Van Alsenoy, C. (2017) Spectroscopic analysis of 8-hydroxyquinoline-5-sulphonic acid and investigation of its reactive properties by DFT and molecular dynamics simulations, *Journal of Molecular Structure 1150*, 540-552.

[76] Fakhar, Z., Govender, T., Maguire, G. E., Lamichhane, G., Walker, R. C., Kruger, H. G., and Honarparvar, B. (2017) Differential flap dynamics in l, d-transpeptidase2 from mycobacterium tuberculosis revealed by molecular dynamics, *Molecular BioSystems 13*, 1223-1234.

[77] Miller III, B. R., McGee Jr, T. D., Swails, J. M., Homeyer, N., Gohlke, H., and Roitberg, A. E. (2012) MMPBSA. py: an efficient program for end-state free energy calculations, *Journal of chemical theory and computation 8*, 3314-3321.

[78] Verma, S., Grover, S., Tyagi, C., Goyal, S., Jamal, S., Singh, A., and Grover, A. (2016) Hydrophobic interactions are a key to MDM2 inhibition by polyphenols as revealed by molecular dynamics simulations and MM/PBSA free energy calculations, *PloS one 11*, e0149014.

[79] Stein, S. A. M., Loccisano, A. E., Firestine, S. M., and Evanseck, J. D. (2006) Principal components analysis: a review of its application on molecular dynamics data, *Annual Reports in Computational Chemistry 2*, 233-261.

[80] Hubbard, R. E., and Kamran Haider, M. (2010) Hydrogen bonds in proteins: role and strength, *eLS*.

[81] Bowden, K., and Bromley, K. (1990) Reactions of carbonyl compounds in basic solutions. Part 15. The alkaline hydrolysis of N-methyl, N-phenyl and bicyclo lactams, penicillins and N-alkyl-N-methylacetamides, *Journal of the Chemical Society, Perkin Transactions 2*, 2111-2116.

[82] Ibeji, C. U., Tolufashe, G. F., Ntombela, T., Govender, T., Maguire, G. E., Lamichhane, G., Kruger, H. G., and Honarparvar, B. (2018) The catalytic role of water in the binding site of L, D-Transpeptidase 2 within acylation mechanism: A QM/MM (ONIOM) modeling, *Tuberculosis*.

[83] Park, J. T., and Strominger, J. L. (1957) Mode of action of penicillin. Biochemical basis for the mechanism of action of penicillin and for its selective toxicity, *Science 125*, 99-101.

[84] Waxman, D. J., and Strominger, J. L. (1983) Penicillin-binding proteins and the mechanism of action of beta-lactam antibiotics1, *Annual review of biochemistry 52*, 825-869.

[85] Lam, H., Oh, D.-C., Cava, F., Takacs, C. N., Clardy, J., de Pedro, M. A., and Waldor, M. K. (2009) D-amino acids govern stationary phase cell wall remodeling in bacteria, *Science 325*, 1552-1555.

CHAPTER FOUR

The manuscript in chapter four has been submitted in Journal of Molecular Modelling

Identification of potent L,D-transpeptidase 5 inhibitors for *Mycobacterium tuberculosis* as potential anti-TB leads: Virtual Screening and Molecular Dynamics Simulations

Victor T. Sabe[1], Gideon F. Tolufashe[1], Sibusiso B. Maseko[1], Collins U. Ibeji,[1]

Thavendran Govender [1], Glenn E. M. Maguire[1,2], Gyanu Lamichhane[3], Bahareh Honarparvar[1]* and Hendrik G. Kruger[1]*

[1]Catalysis and Peptide Research Unit, School of Health Sciences, University of KwaZulu-Natal, Durban 4001, South Africa.

[2]School of Chemistry and Physics, University of KwaZulu-Natal, 4001 Durban, South Africa.

[3]Center for Tuberculosis Research, Division of Infectious Diseases, School of Medicine, Johns Hopkins University, Baltimore, MD 21205, USA.

*Corresponding authors: kruger@ukzn.ac.za (Prof. Hendrik G. Kruger), Honarparvarb@ukzn.ac.za (Dr Bahareh Honarparvar), Telephone: + 27 31 2601845, Fax: +27 31 2603091, Catalysis and Peptide Research Unit, School of Health Sciences, University of KwaZulu-Natal, Durban 4041, South Africa.

Abstract

Virtual screening is a useful *in silico* approach to identify potential leads against various targets. It is known that carbapenems (doripenem and faropenem) do not show any reasonable inhibitory activities against L,D-transpeptidase 5 (Ldt_{Mt5}) and also an adduct of meropenem exhibited slow acylation. Since these drugs are active against L,D-transpeptidase 2 (Ldt_{Mt2}), understanding the differences between these two enzymes are essential. In this study, a ligand-based virtual screening of 12766 compounds followed by molecular dynamics (MD) simulations was applied to identify potential leads against Ldt_{Mt5}. To further validate the obtained virtual screening ranking for Ldt_{Mt5}, we screened the same libraries of compounds against Ldt_{Mt2} which had more experimentally reported and calculated binding energies. The observed consistency between the binding affinities of Ldt_{Mt2} validates the obtained virtual screening binding scores for Ldt_{Mt5}. We subjected 37 compounds with docking scores ranging from -7.2 to -9.9 kcal mol^{-1} obtained from virtual screening for further MD analysis. A final set of compounds (n=10) from four antibiotic classes with $\leq$ -30 kcal mol^{-1} Molecular Mechanics/Generalized Born Surface Area (MM-GBSA) binding free energies (ΔG_{bind}) were characterised. The outcome of this study provides insight into the design of potential novel leads for Ldt_{Mt5}.

Keywords: Virtual Screening; Molecular dynamics (MD); *Mycobacterium tuberculosis* (*Mtb*); L,D-transpeptidase 5 (Ldt_{Mt5}); Molecular Mechanics/Generalized Born Surface Area (MM-GBSA).

4.1 Introduction

The alarming rise of multi and extensively drug-resistant tuberculosis (TB) has become a serious global health threat [1]. The emergence of resistant strains is partly due to poor patient compliance with the extensive treatment regimen [2, 3]. Thus, the identification of new anti-TB leads, particularly Ldt_{Mt5}, that can shorten the treatment regimen and target the resistant TB strains are urgently needed. *Mycobacterium tuberculosis* possesses a peptidoglycan (PG) layer that encapsulates the cytoplasmic membrane and is essential for cellular growth and viability [4]. The peptidoglycan structure of *Mtb* from a stationary-phase culture revealed a high content (80%) of nonclassical 3→3 cross-links generated by L,D-transpeptidation [5], whereas the classical 4→3 cross-links are predominantly formed by the D,D-transpeptidation activity of penicillin-binding proteins (PBPs) during the exponential phase of growth [6-9]. L,D-transpeptidases (Ldt) and PBPs are structurally similar [10] and contain the catalytic active-site cysteine and serine residues, respectively [11]. Five Ldt paralogues have been identified for *Mtb*, Ldt_{Mt1} to Ldt_{Mt5}. The reported experimental and theoretical studies revealed that both Ldt_{Mt1} and Ldt_{Mt2} can be inactivated by carbapenems, a class of β-lactam antibiotics [5, 6, 8, 12]. The enzymes, Ldt_{Mt1} and Ldt_{Mt2} also have distinct functions *in vivo* [5, 9] and it has been shown that Ldt_{Mt1} may have a role in adaptation to the non-replicative state of the bacilli [5], while Ldt_{Mt2} is essential for virulence in a mouse model of acute infection [9]. For *Mtb*, Ldt_{Mt5} is required for properly maintaining cell wall integrity [4] and a more recent study also revealed that four L,D paralogues, with the exception of Ldt_{Mt3}, are active in *vitro* peptidoglycan cross-linking assays, and that all but Ldt_{Mt5} are inhibited by carbapenems [7].

The single crystal X-ray structure of the extra-cellular portion of Ldt_{Mt5} was recently published [4]. Modest enhancement in susceptibility of *Mtb* to certain carbapenems (doripenem and faropenem) was observed presumably due to synthetic lethality, as these β-lactams may inactivate other targets. Meanwhile, a meropenem-adduct crystal structure was formed which supports very slow acylation of Ldt_{Mt5} over many days. The structures of apo-Ldt_{Mt5} and its meropenem-Ldt_{Mt5} (**Figure 4.1**) demonstrate that, despite the overall structural similarity to Ldt_{Mt2}, the Ldt_{Mt5} active site residues are different [4].

Figure labels (right side):
β-hairpin
Meropenem
Loop L$_C$
Active site residues HIS287, THR302, ASN303 and CYS305
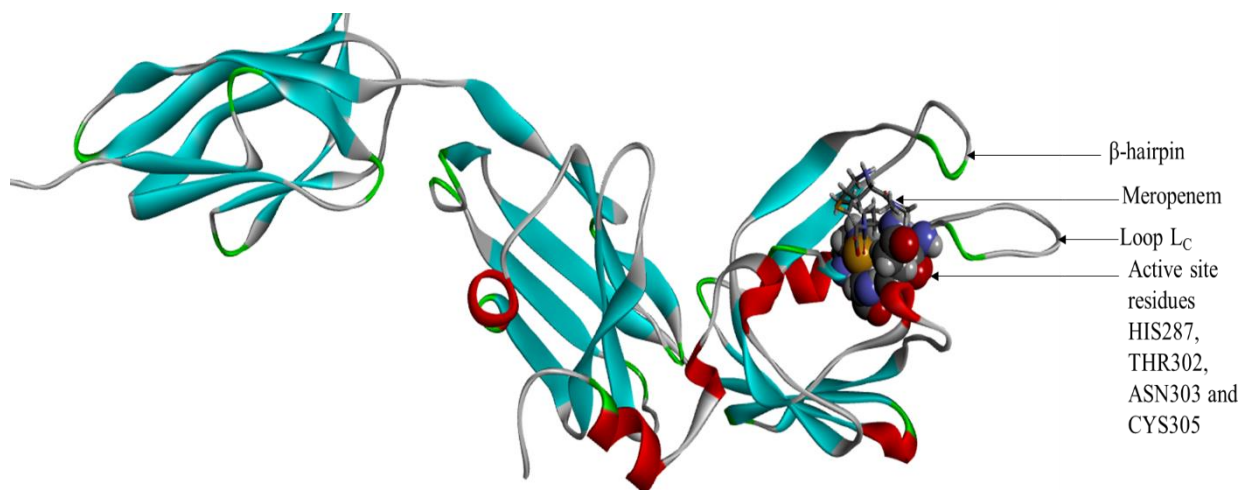
Figure 4.1 The rendering of MERO-Ldt$_{Mt5}$ crystal X-ray structure. Shown is a β-hairpin flap (312-330) and Lc loop (338-358) and active site pocket in CPK form [HIS287 (342), THR302 (357), ASN303 (358) and CYS305 (360)] and meropenem (inhibitor) in stick form [13]

The presence of a structurally divergent catalytic site and a proline-rich C-terminal subdomain suggest that this protein may have a distinct role in PG metabolism, perhaps involving other cell wall anchored proteins. Also, *Mtb* lacking a functional copy of Ldt$_{Mt5}$ displays aberrant growth and is more susceptible to killing by osmotic shock, select carbapenem antibiotics and crystal violet [4]. The *β*-lactam and oxazolidinone compounds will most likely be able to form covalent bonds with the catalytic cysteine of Ldt$_{Mt5}$ probably due to the carbonyl and amide functional group in the structural backbone. Hence, in case any promising inhibitors from the other classes are identified, they will most likely act as competitive [14] inhibitors.
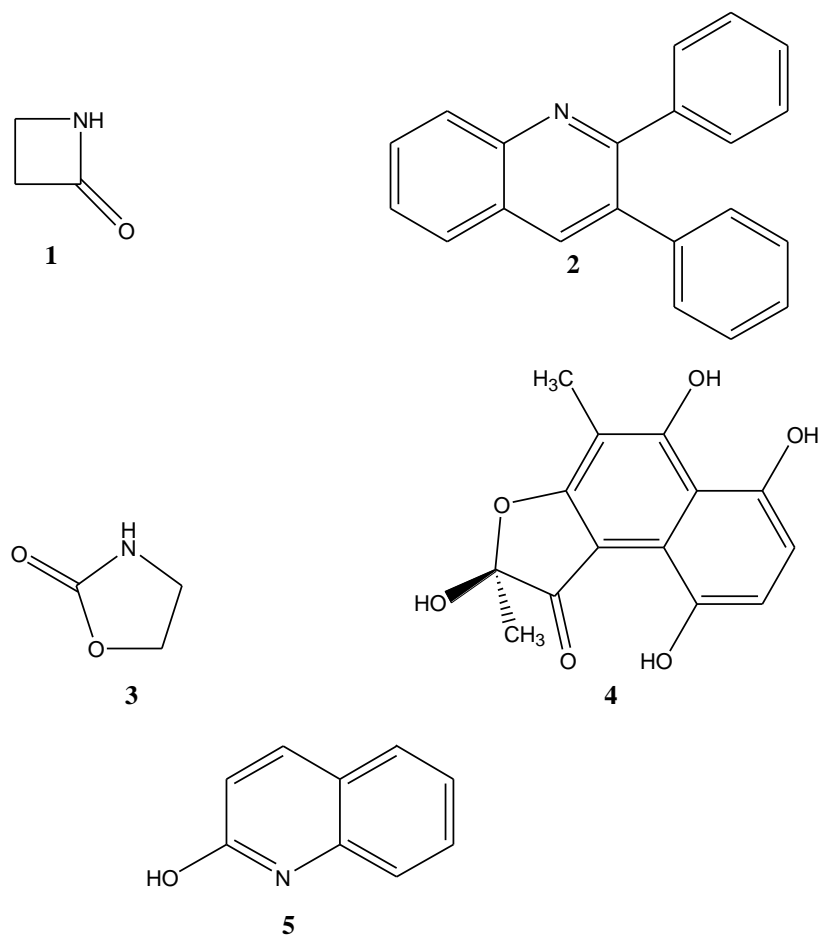
Figure 4.2 2D scaffold structures of (1) *β*-lactam (2) Diarylquinoline (3) Oxazolidinone (4) Rifamycin (5) Quinolone classes of TB antibiotics

Carbapenems gave insignificant binding of Ldt$_{Mt5}$ experimentally using isothermal titration calorimetry (ITC). Carbapenems are considered the last resort antibiotics to treat resistant bacterial infections in humans [15-22]. This fact motivated us to perform a virtual screening of five classes of known TB antibiotics (**Figure 4.2**). Virtual screening with both AutoDock Vina and Schrödinger Maestro software programs was performed as a benchmark for the automated docking. Molecular dynamics and binding free energy studies were performed on each of the screened compounds from the five classes of anti-TB agents. To the best of our knowledge, a computational model to identify and rank the different anti-TB agents against Ldt$_{Mt5}$ has not yet been reported.

4.2 Materials and methods

The following *in silico* approaches were used to screen five classes of known TB antibiotics (**Figure 4.2**) against Ldt$_{Mt5}$. The automated docking process was performed using Autodock Vina [23] and Schrödinger Maestro[24] programs which implement the quasi-flexible docking method to perform the screening [25]. The docked energies followed by visual inspection of the inhibitor pose was performed to ensure the close proximity of the selected compounds with the catalytic cysteine. This was followed by molecular dynamics simulations/MD trajectory analyses using CPPTRAJ module [26] implemented in Amber 14 [27] package on GPU accelerated PMEMD engine.

4.2.1 System preparation

The 3D crystal structure of the meropenem-bound Ldt$_{Mt5}$ (PDB code: 4ZFQ[13]) was retrieved from the Protein Data Bank [28]. The missing residues (the *β*-hairpin flap is missing having the loop LC and the ex-CTSD being disordered)[13] of the Ldt$_{Mt5}$ enzyme were refined using MODELLER v9.15[29]. Assignment of the protonation states of the enzyme residues at pH=7 was performed by recalculating the standard pKa values of the titratable amino acids using the empirical propKa server [30], similar to a study on Ldt$_{Mt2}$ [31]. These protonation states of the titratable residues were used for the virtual screening and for the subsequent modelling.

The chemical compounds used for the screening were retrieved from the ZINC[32] database. This database is available for free download (http://zinc.docking.org) in different formats usable for computational studies[32]. Compounds from five classes of known TB antibiotics were subjected for the initial screening-based on their mode of action. Each scaffold of the five classes was drawn using the 2D Sketcher tool implemented in ZINC GUI. A structural similarity index of 99% was set for all compounds except for rifamycin in which ligand mining could only be performed at a similarity index of 50%. All the screened compounds obeyed Lipinski's rule[33] of drug-likeness to filter the compound molecules and Veber's criteria for oral bioavailability of drug candidates[34]. The considered Lipinski's parameters [33] are as follows: molecular weight; xlogP; net charge; rotatable bonds; polar surface area; hydrogen donors; hydrogen acceptors; polar and apolar solvation (**Table 4.1**).

Table 4.1 Physiochemical properties set for all screened compounds.

Parameter	Minimum	Maximum
Molecular weight (g/mol)	32	500
xlogP	-4.00	5
Net charge	-5	5
Rotatable bonds	0	10
Polar surface area ($\mathring{A}^2$)	0	140
Hydrogen donors	0	5
Hydrogen acceptors	0	10
Polar solvation (kcal mol^{-1})	-400	1
Apolar solvation (kcal mol^{-1})	-100	40

4.2.2 Virtual screening using AutoDock Vina

AutoDock Vina is a program for molecular docking and virtual screening. The prepared 3D structure of Ldt$_{Mt5}$ [13] in PDB format was converted to pdbqt format using raccoon [23], likewise, the library of compounds downloaded from ZINC database in the mol2 format was converted to pdbqt format. Virtual Screening using automated docking involves the preparation of the receptor (this includes assigning of Kollman charges [35] and Gasteiger partial charges [36] to all atoms and assignment of AD4 types to atoms of the protein structure), ligands and a config file in which grid center, a grid box size, and a docking run number are assigned. AutoDock tools1.5.6 [37] was employed to determine the proper size of the grid box for the potential binding site for the lead compounds and the receptor grid center was set on Cys305 (360) (active site reactive residue) [13]. The grid box was determined as a a centre (X=3.9 Y=-39.5 Z=12.1) and dimension (X=45 Y=45 Z=45) with the grid spacing of 0.375 Å were considered for each of the following atom types: A C H HD N OA and SA representing all probable atom types in the target enzyme. Created finally, was a conf.txt file which includes receptor in pdbqt format, a grid center with x, y, z coordinates, a grid box size in Å, and a docking run number of 10. The virtual screening was carried out using the python script, VS.bash executable on AutoDock Vina software on CPU Ubuntu on Dell computer. Docked results were ranked based on the binding affinities and visual inspection to ensure an acceptable drug/enzyme interaction is present. Visual inspection of the selected ligands inside the enzyme was performed using the Discovery Studio [38] software program.

4.2.3 Virtual screening using Schrödinger Maestro

Schrödinger Maestro software program was applied for the docking studies. Protein/ligand preparation and virtual screening were all performed in the Maestro 11.2 graphical user interface [24]. The Protein Preparation Wizard [39] of the Schrödinger Maestro software program was used to prepare the 3D protein

structure. The pre-processing of the protein was performed which includes assigning of bond orders; adding of hydrogens; creating zero-order bonds to metals; creating disulphide bonds; deleting crystallographic waters beyond 5.00 Å from hetero groups and generating hetero states using Epik[40] pH 7.0+/-2.0. In the 3D protein structure refinement, the alignment of H-bonds was done using PROPKA pH: 7.0 and waters with less than three hydrogen bonds to non-waters were removed. Restrained minimization was performed to converge heavy atoms to RMSD of 0.30Å.

The 2D compound sketches were imported onto the Schrödinger Maestro project table and they were converted into a 3D model using the pre-set option. The LigPrep module [24] was used to refine the structures using default parameters. Ionization was performed to generate possible states at target pH:7.0+/-2.0 using Epik [40] and tautomers were generated. The compounds were subjected to OPLS3 [41] (optimized potentials for liquid simulations) force field for energy optimisation. For ligand preparation, the system was set to retain specified chiralities to 10 per ligand and the output format was Maestro from Schrödinger software program. The grid box was positioned at the centre and the receptor grid centre was set on Cys305 (360) (active site reactive residue) [13] with grid spacing minimum distance of 1 Å and a maximum distance of 3.5 Å. The XYZ coordinates were -31.88; 23.5 and -46.48 respectively. Default settings of Maestro 11.2 were used for other parameters such as constraints, rotatable groups, and sites.

Using a predetermined receptor grid, quasi-flexible docking [14, 25, 42] was performed via the Glide [43] mode of Schrödinger Maestro (Schrödinger, Inc). The system was set to resume post-docking minimization, setting the number of poses per ligand to 5. For filtering, default settings were employed and this includes applying the Epik state penalty parameters [24] for docking and the scaling of ligand van der Waals radii for nonpolar atoms using the scaling factor 0.80 [44, 45] and partial charge cut-off 0.15 [44, 45]. Ligand docking was done using the three incremental stages of ranking accuracy *i.e.* high throughput virtual screening (HTVS), Glide simple precision (SP) and Glide extra precision (XP) [24].

The difference with these programs lies in the docking algorithm in which Schrödinger Maestro uses the Glide module which employs the Monte Carlo algorithm [46] that makes random moves and accepts or rejects each conformation based on Boltzmann probability while AutoDock Vina utilizes the AutoDock module. This program applies the genetic algorithm [47], which maintains a selective pressure towards an optimal solution, with randomized information exchange permitting exploration of the search space [25]. However, both software modules (Glide and AutoDock) identify multiple top-ranked docked poses per ligand. They both use hierarchical algorithms that are an exhaustive systematic search for the best ligand conformations within the protein active site, therefore visual inspection for one best conformation per ligand, based on known interactions was performed to identify a single best conformation per ligand for MD simulations.

4.2.4 Molecular dynamics simulation

MD simulations were performed to investigate the stability and dynamics of the 37 complexes using the AMBER 14 package on GPUs with 24 shared processors using CHPC cluster. The ff99SB [48] force field was used to describe the protein whereas the general AMBER force field (GAFF) [49] was used for the ligand. System solvation for the complexes was performed in a 10 Å cubic box using the TIP3P water model. To neutralize the system negative value, sodium ions were added accordingly. The protein-ligand complexes were parametrized by the Leap [49] module of the Amber14 package. All simulations were performed using a 2fs timestep (based on a study with similar protein size) and the rest of the process was also based on the same study [31]. The partial Mesh Ewald (PME) [50] summation method was used to calculate the electrostatic forces with space cut-off of 12 Å. Using the SHAKE algorithm [51], all bonds were constrained to hydrogen (H) atoms. A two-stage energy minimization process, which is characterised by 2500 steps of steepest decent minimization and 2500 steps of the conjugated gradient was carried out to get rid of steric clashes. The solute molecule was first restrained at 500 kcal mol^{-1} whereas the water molecules and the ions were relaxed. The harmonic restraint was removed on the second stage thus the whole system was relaxed. Heating of the system to a constant temperature of 300 K followed with a restraint of 10 kcal mol^{-1} A^{-2} for 200 ps, to keep the solute fixed. Density equilibration for 50 ps was performed and MD simulations ran at a constant temperature and pressure (1atm). The Ldt_{Mt5}-ligand (37 complexes) were simulated for 20 ns [52]. The post-dynamics trajectory analysis including the radius of gyration (Rg) and root mean square deviation (RMSD) was evaluated on the top 5 β-lactams with ≥ 30 kcal/mol. In addition to that, triplicate MD simulations were also performed with varying initial atomic coordinates to validate the simulations.

4.2.5 Binding free energy calculation

MM-GBSA is a widely accepted method to compare the binding affinities and to gain rational insights about inhibitors by analysing the binding mechanism [53]. The average binding free energies (ΔG_{bind}) of the protein-ligand complexes was calculated for the last 10 ns using MM-GBSA method [54]. Counter ions and water molecules were removed. Entropy penalty (-TΔS) for the complexes was obtained using normal mode analysis (nmode). The PTRAJ and CPPTRAJ modules [26] were used to analyse the MD trajectories.

4.3 Results and discussions

4.3.1 Data set preparation

A total of 12766 antibacterial lead compounds in five categories listed in **Table 4.2** were obtained from the ZINC database were screened.

Table 4.2 The selected five categories of antibacterial compounds from the ZINC database

Class	Mode of action	Number of screened compounds
β-lactam	Cell wall biosynthesis (inhibition of transpeptidase and inhibition of β-lactamase by clavulanic acid)	2707
Diarylquinoline	ATP synthesis inhibition (subunit c of ATP synthase)	4309
Oxazolidinone	Protein synthesis inhibition	3065
Rifamycin	RNA synthesis inhibition (inhibition of RNA polymerase).	2678
Quinolone	DNA synthesis inhibition (inhibition of gyrase).	7

4.3.2 Ligand-based virtual screening and docking

Structural parameters were set to filter the compounds for screening based on Lipinski's rule-of-five (**Table 1**). Virtual screening of ligands was performed on a set of 98 docked poses and then considered for further visual inspection of the interaction [14] to determine the optimal ligand conformation per compound in the active pocket of Ldt$_{Mt5}$. A total of 46 top-ranked poses was obtained using AutoDock Vina, (**Table 4.3)** and 52 from Schrödinger Maestro (**Table 4.4**). From there a total of 37 compounds, (13 from AutoDock Vina, **Table 4.3** and 24 from Schrödinger Maestro **Table 4.4**), were selected for MD simulations and binding free energy calculations. Further MD analysis was carried out on the best 5 β-lactams with the binding free energy of ≥ 30.0 kcal/mol. **Figure 4.3** shows the virtual screening workflow down to the final 5 β-lactams compounds.
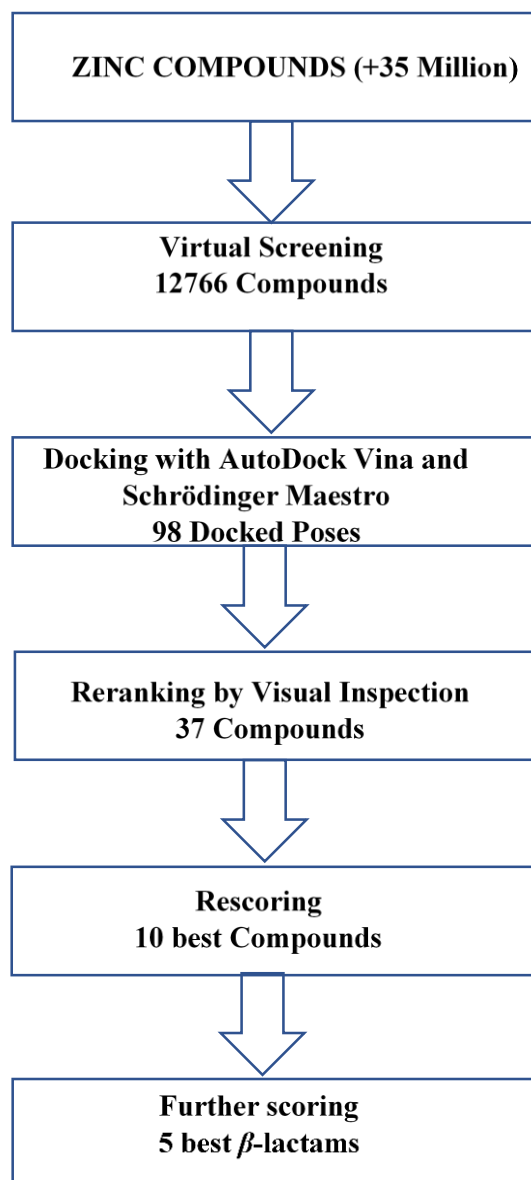
Figure 4.3 Virtual screening workflow to the ten final lead compounds and then more elucidation on five best *β*-lactams.

The docking (consensus) scores for AutoDock Vina of the 10 top-ranked compounds across all classes lie between -7.4 and -9.0 kcal mol^{-1} (**Table 4.3**). The Schrödinger Maestro top-ranked docking scores were also considered, and the values are between -7.2 and -9.9 kcal mol^{-1} (**Table 4.4**). The docking scores of both software programs seem to be within the same range and both software programs optimize the ligand conformation during docking.

Table 4.3 The top 10 ligands per class based on the highest docked energies were chosen for AutoDock Vina against Ldt$_{Mt5}$ (The optimal ligands in the active pocket, highlighted in blue, were selected for further MD analysis)

Antibiotic class	Ligand Identity	Docking score (kcal mol^{-1})
β-lactam		
1	ZINC 01662030	-8.4
2	ZINC 02475683	-8.4
3	ZINC 02475684	-8.4
4	ZINC 01662029	-8.3
5	ZINC 02462884	-8.3
6	ZINC 03791246	-8.3
7	ZINC 01412853	-8.3
8	ZINC 01385054	-8.2
9	ZINC 01412838	-8.2
10	ZINC 01412839	-8.2
Rifamycin		
1	ZINC 19569373	-8.6
2	ZINC 03197606	-8.4
3	ZINC 14828615	-8.4
4	ZINC 01551761	-8.4
5	ZINC 13125731	-8.2
6	ZINC 13125732	-8.2
7	ZINC 14693083	-8.2
8	ZINC 15216498	-8.2
9	ZINC 33832153	-8.2
10	ZINC 39227187	-8.2
Oxazolidinone		
1	ZINC 03921583	-8.7
2	ZINC 03921580	-8.5
3	ZINC 00586642	-8.4
4	ZINC 00003190	-8.3
5	ZINC 00594969	-8.3
6	ZINC 03785925	-8.3
7	ZINC 03921504	-8.3
8	ZINC 05774946	-8.2
9	ZINC 03791902	-8.2
10	ZINC 03921352	-8.2
Diarylquinoline		
1	ZINC 00022457	-9.0
2	ZINC 00022456	-8.7
3	ZINC 00057310	-8.2
4	ZINC 00075863	-8.2
5	ZINC 00097351	-8.2
6	ZINC 00152025	-8.2
7	ZINC 00236246	-8.1
8	ZINC 00254016	-8.1
9	ZINC 00118842	-8.0
10	ZINC 00192295	-8.0
Quinolone		
1	ZINC 80595608	-8.0

2	ZINC 80595598	-7.9
3	ZINC 80595612	-7.9
4	ZINC 78317542	-7.6
5	ZINC 80595606	-7.6
6	ZINC 79236395	-7.4

AutoDock Vina top-ranked docking scores were considered, and the values are between -7.4 and -9.0 kcal mol^{-1}

Table 4.4 The Schrödinger Maestro top ligands per class based on the highest Glide docking score against Ldt$_{Mt5}$ (The optimal ligands in the active pocket, highlighted in blue, were selected for further MD analysis)

Antibiotic class	Ligand Identity	Glide XP GScore (kcal mol^{-1})
β-Lactam		
1	ZINC 03788344	-9.9
2	ZINC 03788344	-9.7
3	ZINC 03788344	-9.4
4	ZINC 03788344	-9.2
5	ZINC 03808350	-8.8
6	ZINC 03788344	-8.9
7	ZINC 03808351	-8.7
8	ZINC 03808352	-8.7
9	ZINC 03826440	-8.4
10	ZINC 03826440	-8.4
11	ZINC 03788344	-8.4
12	ZINC 03785001	-8.2
13	ZINC 03785029	-8.2
14	ZINC 03808350	-8.1
15	ZINC 03784242	-7.9
Rifamycin		
1	ZINC 06483425	-9.3
2	ZINC 06483423	-9.3
3	ZINC 06483425	-9.2
4	ZINC 06483423	-9.2
5	ZINC 13532137	-8.0
6	ZINC 59077219	-7.9
7	ZINC 59077220	-7.9
8	ZINC 59077221	-7.9
9	ZINC 59077222	-7.9
10	ZINC 59077219	-7.9
11	ZINC 59077220	-7.9
12	ZINC 59077221	-7.9
Oxazolidinone		
1	ZINC 00108966	-8.0
2	ZINC 00108966	-8.0
3	ZINC 00108973	-8.0
4	ZINC 00108973	-8.0
5	ZINC 00108966	-7.9
6	ZINC 00108966	-7.9
7	ZINC 00108973	-7.9

8	ZINC 00108973	-7.9
9	ZINC 00052567	-7.5
10	ZINC 00052568	-7.5
11	ZINC 02512954	-7.3
12	ZINC 02512954	-7.2
13	ZINC 00108966	-7.2
14	ZINC 00108966	-7.2
Diarylquinolone		
1	ZINC 00096619	-8.1
2	ZINC 00002447	-7.7
3	ZINC 00002447	-7.7
4	ZINC 00007109	-7.5
5	ZINC 00060410	-7.7
6	ZINC 00060410	-7.7
7	ZINC 00060410	-7.7
8	ZINC 00060410	-7.7
9	ZINC 00060410	-7.7
10	ZINC 00060410	-7.7
Quinolone		
1	ZINC 80595598	-3.6

Schrödinger Maestro top-ranked docking scores were considered, and the values are between -7.2 and -9.9 kcal mol^{-1}. The class Quinolone was eliminated for further MD analysis because of its low docking score of -3.7 kcal mol^{-1}

4.3.3 Binding free energy analysis

Our group has reported that MD studies provide comparable binding free energies for Ldt$_{Mt2}$ with several inhibitors [31] to experiment. Based on the calculated docking scores, the complexes showing the best score and best ligand conformations within the protein active site were subjected to further molecular dynamics simulations using the AMBER14 package. A similar protocol was carried out by John *et al.* and Islam *et al.* [52, 53]. With a cut-off predicted binding energy (ΔG_{bind}) of $\leq$ -30 kcal mol^{-1}, a final set of lead compounds (n=10) (marked in bold) from four antibiotic classes was selected from **Tables 4.5** and **4.6**.

Table 4.5 Binding free energies method and their corresponding components using MM-GBSA method for compounds screened against Ldt_{Mt5} in AutoDock Vina program.

ZINC ID	ΔE_{vdw}	ΔE_{ele}	ΔG_{gas}	ΔG_{polar}	$\Delta G_{nonpolar}$	$\Delta G_{solvation}$	$-T\Delta S$	ΔG_{bind}
β-lactam								
02475683	**-59.68**	**-9.72**	**-69.41**	**27.7**	**-6.82**	**20.88**	**-31.01**	**-48.52**
02462884	**-54.07**	**-8.97**	**-63.03**	**22.7**	**-6.42**	**16.28**	**-27.53**	**-46.75**
03791246	-26.26	-123.11	96.85	-112.62	-3.1	-155.72	-18.6	-18.86
Rifamycin								
14693083	-42.27	-5.81	-48.07	22.49	-3.97	18.52	-2.03	-29.95
13125732	-30.71	-7.55	-38.26	18.27	-2.96	15.31	-15.55	-22.95
13125731	-28.75	-5.52	-34.27	19	-2.92	16.09	-20.68	-18.18
Oxazolidinone								
05774946	-30.17	-0.5	-30.67	8.68	-3.93	4.75	-20.58	-25.92
00003190	-32.67	-4.89	-37.57	15.9	-3.39	12.51	-17.07	-25.06
00594969	-26.73	-0.41	-26.32	9.77	-3.14	6.63	-3.58	-19.7
Diarylquinolone								
00022456	**-47.08**	**-4.08**	**-51.15**	**-14.65**	**-5.36**	**9.28**	**-18.42**	**-41.87**
00022457	**-44.53**	**-5.72**	**-50.25**	**-16.46**	**-5.01**	**11.45**	**-23.61**	**-38.8**
00192295	-35.19	-2.46	-37.65	14.48	-3.22	11.26	-21	-26.39
Quinolone								
78317542	-30.55	-278.11	-308.64	290.44	-3.91	286.52	-18.06	-22.12
79236395	-31.66	-154.13	-185.77	167.67	-3.79	163.88	-14.87	-21.89

Compounds in bold are the best binders within the -30 kcal mol^{-1} ≤ screening threshold and compounds in normal text are below the threshold

Table 4.6 Binding free energies and their corresponding components using MM-GBSA method for compounds screened against Ldt$_{Mt5}$ in Schrödinger Maestro.
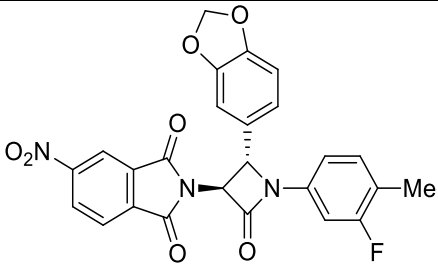
ZINC ID	ΔE_{vdw}	ΔE_{ele}	ΔG_{gas}	ΔG_{polar}	$\Delta G_{nonpolar}$	$\Delta G_{solvation}$	$-T\Delta S$	ΔG_{bind}
β-lactam								
03784242	-28.18	-154.51	-182.69	160.28	-4.08	156.20	-21.11	-26.49
03785029	-27.18	-153.7	-180.88	159.8	-4.03	155.77	-24.48	-25.11
03785344	-19.65	-333.09	-352.74	339.3	-3.43	335.87	-18.24	-16.87
03785001	**-30.57**	**-175.27**	**-205.83**	**179.63**	**-4.48**	**175.15**	**-16.06**	**-30.68**
03808350	-30.12	-136.81	-166.93	150.41	-4.72	145.69	-19.04	-21.23
03808351	**-33.59**	**-188.02**	**-221.61**	**191.16**	**-4.87**	**186.29**	**-27.84**	**-35.32**
03808352	**-34.38**	**-167.3**	**-201.68**	**174.86**	**-5.36**	**169.5**	**-26.19**	**-32.18**
03826440	-26.83	-176.63	-203.45	184.25	-4.36	179.9	-18.32	-23.56
Rifamycin								
06483423	-37.88	-10.71	-48.59	26.03	-4.57	21.45	-17.91	-27.14
06483425	-39.5	-11.34	-50.85	27.31	-4.77	22.53	-11.67	-28.31
13532137	**-46.38**	**-12.24**	**-58.62**	**26.57**	**-5.16**	**21.41**	**-19.39**	**-37.21**
59077219	-9.81	-98.27	-108.1	103.06	-1.73	101.34	-14.14	-6.77
59077220	-17.38	-173.77	-191.17	176.93	-3.29	173.64	-22.4	-17.53
59077221	-20.37	-92.93	-113.32	104.55	-3.23	101.32	-17.38	-11.99
59077222	-33.2	-164.92	-196.14	176.58	-4.28	172.3	-22.59	-23.84
Oxazolidinone								
00052567	-26.43	-304.35	-330.78	315.3	-4.06	311.24	-22.5	-19.54
00052568	-32.74	-307.5	-340.24	316.29	-4.38	311.91	-9.02	-28.33
00108966	-30.59	-4.15	-34.74	12.44	-3.84	8.6	-18.77	-26.13
00108973	**-43.19**	**-3.93**	**-47.12**	**14.93**	**-5.02**	**9.91**	**-23.21**	**-37.21**
02512954	-21.99	-331.59	-353.58	332.66	-3.29	329.37	-20.23	-24.21
Diarylquinolone								
00002447	**-44.45**	**-257.63**	**-302.08**	**270.09**	**-5.69**	**264.4**	**-22.68**	**-37.68**
00007109	-22.67	-3.16	25.83	-3.16	12.22	9.45	-20.51	-16.38
00060410	-28.61	-4.13	-32.74	12.17	-3.48	8.69	-14.97	-24.05
00096619	-34.15	-4.99	-39.13	15.42	-4.18	11.24	-15.17	-27.89

Compounds in bold are the best binders within the -30 kcal mol^{-1} ≤ screening threshold and compounds in normal text are below the threshold

Two different classes of compounds were obtained as the best binders from utilizing the two docking programs. AutoDock Vina identified two lead compounds in terms of highest binding, both

monobactams and these compounds showed greater predicted binding energies compared to the three carbapenems which were identified using Schrödinger Maestro (**Table 4.7).**

Table 4.7 Identified lead compounds with their antibacterial class, ZINC ID, calculated binding energies and the corresponding chemical structure, ten in total

Class	ZINC ID	ΔG_{bind} (kcal mol^{-1})	Structure
β-lactam	**02475683**	**-48.52**	
	02462884	**-46.75**	
	03808351	-35.32	
	03808352	-32.18	
	03785001	-30.68	

Diarylquinolone	**00022456**	**-41.87**	
	00022457	**-38.8**	
	00002447	-37.68	
Oxazolidinone	00108973	-37.21	
Rifamycin	13532137	-37.21	
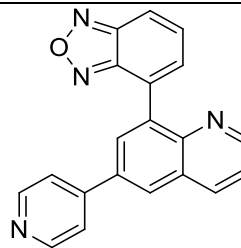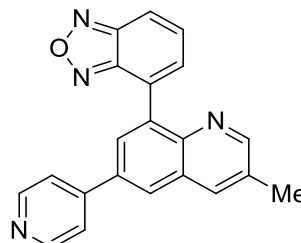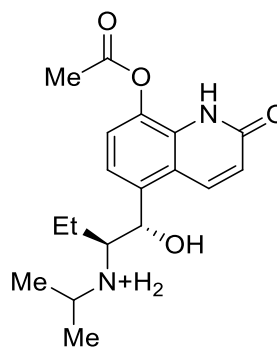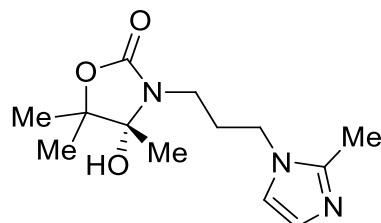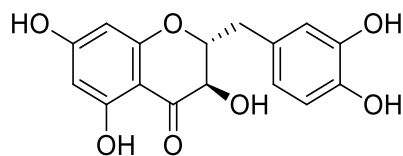
Compounds in bold were screened by AutoDock Vina [23] and compounds in the normal text were screened by Schrödinger Maestro [24]

The final set of compounds (n=10) had all parameters within the Lipinski's and Veber's constraints of drug-likeness (**Table 4.8**). It is noteworthy that all the screened compounds revealed a topological polar surface area (tPSA) > 150 Å^2, which is an indication of a high bioavailability [54].

Table 4.8 Drug-like properties of the 10 potential lead from the ZINC database

ZINC ID	xlogP	Apolar desolvation (kcal mol^{-1})	Polar desolvation (kcal mol^{-1})	H bond donors	H bond acceptors	Net charge	tPSA (Å^2)	Molecular weight (gmol^{-1})	Rotatable bonds
*02475683	4.37	11.33	-14.54	0	10	0	124	489.415	4
*02462884	4.53	12.58	-14.66	0	8	0	105	445.406	4
*03808351	-0.76	-8.64	-92.33	4	7	0	117	342.417	5
*03808352	-0.76	-8.61	-86.43	4	7	0	117	342.417	5
*03785001	4.73	1.62	-34.23	1	3	1	24	384.371	4
ᵞ00022456	4.06	1.31	-14.65	0	5	0	64	324.343	2
ᵞ00022457	4.49	1.62	-14.46	0	5	0	64	338.37	2
ᵞ00108973	0.69	-1.15	-18.45	1	6	0	67	267.329	4
×00002447	1.43	-1.02	-53.74	4	6	1	96	333.408	7
ꜰ13532137	0.92	-3.03	-13.32	5	7	0	127	318.281	2

Compounds in bold were screened by AutoDock Vina and compounds in the normal text were screened by Schrödinger Maestro. Representations: * β-lactam; ᵞ Diarylquinolone; × Oxazolidinone; ꜰ Rifamycin

In light of the experimentally reported covalently bound interactions between L,D-transpeptidases and β-lactams, the subsequent section of this study focuses on better understanding of the binding interactions between the β-lactam class and Ldt$_{Mt5}$. To validate the virtual screening ranking and to compare the binding affinities, selected carbapenems known to inhibit Ldt$_{Mt2}$ were screened for both Ldt$_{Mt2}$ and Ldt$_{Mt5}$ (**Table 4.9**). According to the consistent trend observed in **Table 9** in terms of the binding energies, the docking scores obtained seem to be valid.

Table 4.9 Comparison of the calculated binding energies for carbapenems on Ldt$_{Mt5}$ versus the calculated and experimental [55, 56] binding energies for Ldt$_{Mt2}$

Carbapenem	Ldt$_{Mt2}$ ΔG_{exp} (kcal mol^{-1})	Ldt$_{Mt2}$ ΔG_{docked} (kcal mol^{-1})	Ldt$_{Mt5}$ ΔG_{docked} (kcal mol^{-1})
Biapenem	-9.0[55]	-6.7	-6.2
Imipenem	-9.8[56]	-6.5	-5.5
Meropenem	-8.2[56]	-7.1	-6.3
Tebipenem	-9.4[55]	-6.6	-6.0

The ZINC IDs for biapenem, imipenem, meropenem and tebipenem are 03784073, 03830927, 03808779 and 04072129 respectively

4.3.4 Trajectory analyses of *β*-lactam-Ldt$_{Mt5}$ complexes

4.3.4.1 Root mean square deviation (RMSD) analysis

RMSD is a measure of accuracy, comparing the differences between predicted values and observed values of a model [57]. The average values of the *β*-lactam-Ldt$_{Mt5}$ complexes (A-E) (**Figure 4.4)** are 1.88, 1.75, 1.35, 2.25 and 1.55 Å respectively which lies in the accepted range of <2.5 Å [14] for stable simulation.
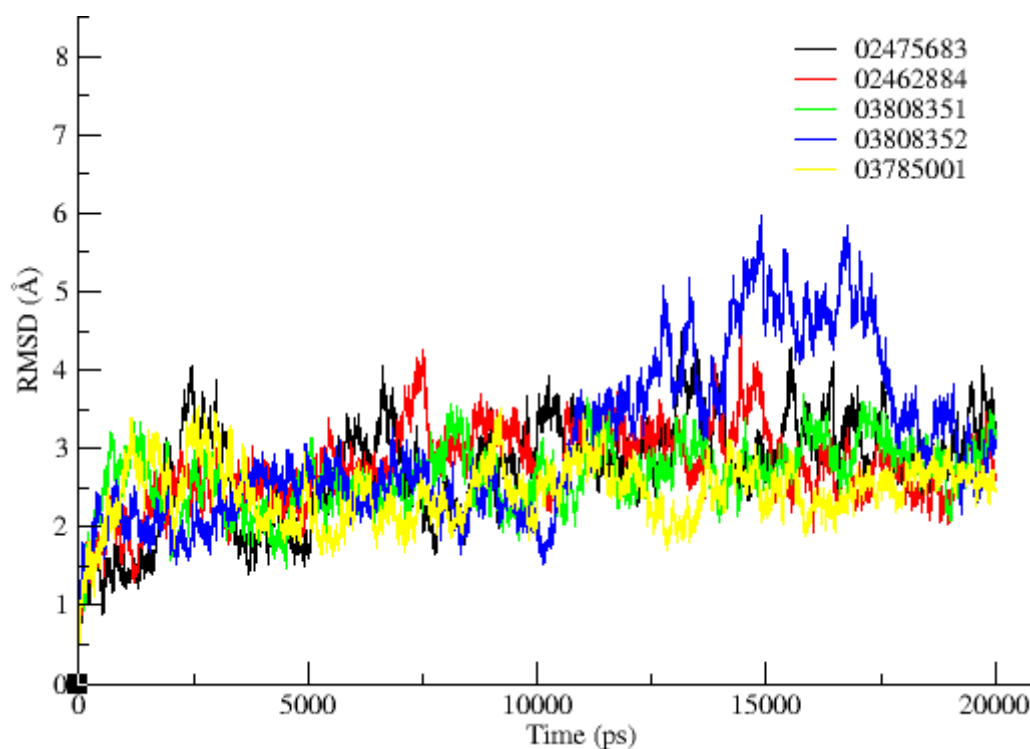
Figure 4.4 Time evolution of the root mean square deviation (RMSD) of the *β*-lactam- Ldt$_{Mt5}$ complexes of **A** 02475683-Ldt$_{Mt5}$ (black), **B** 02462884-Ldt$_{Mt5}$ (red), **C** 03808351-Ldt$_{Mt5}$ (green), **D** 03808352-Ldt$_{Mt5}$ (blue) and **E** 03785001-Ldt$_{Mt5}$ (yellow) during 20 ns MD trajectories

4.3.4.2 Analysis of the radius of gyration (Rg)

The radius of gyration is defined as the moment of inertia of the C-α atoms from its centre of mass and it is used as an indicator of structural compactness of the protein-ligand complex [58, 59]. **Figure 4.5** shows the Rg plots for the β-lactam-Ldt$_{Mt5}$ complexes over a 20 ns trajectory. The average Rg values for complex A (02475683-Ldt$_{Mt5}$), B (02462884-Ldt$_{Mt5}$), C (03808351-Ldt$_{Mt5}$), D (03808352-Ldt$_{Mt5}$) and E (03785001-Ldt$_{Mt5}$) reveal great overall similarity. The values are 29.65 Å, 29.60 Å, 29.83 Å, 30.25Å and 29.60 Å respectively.
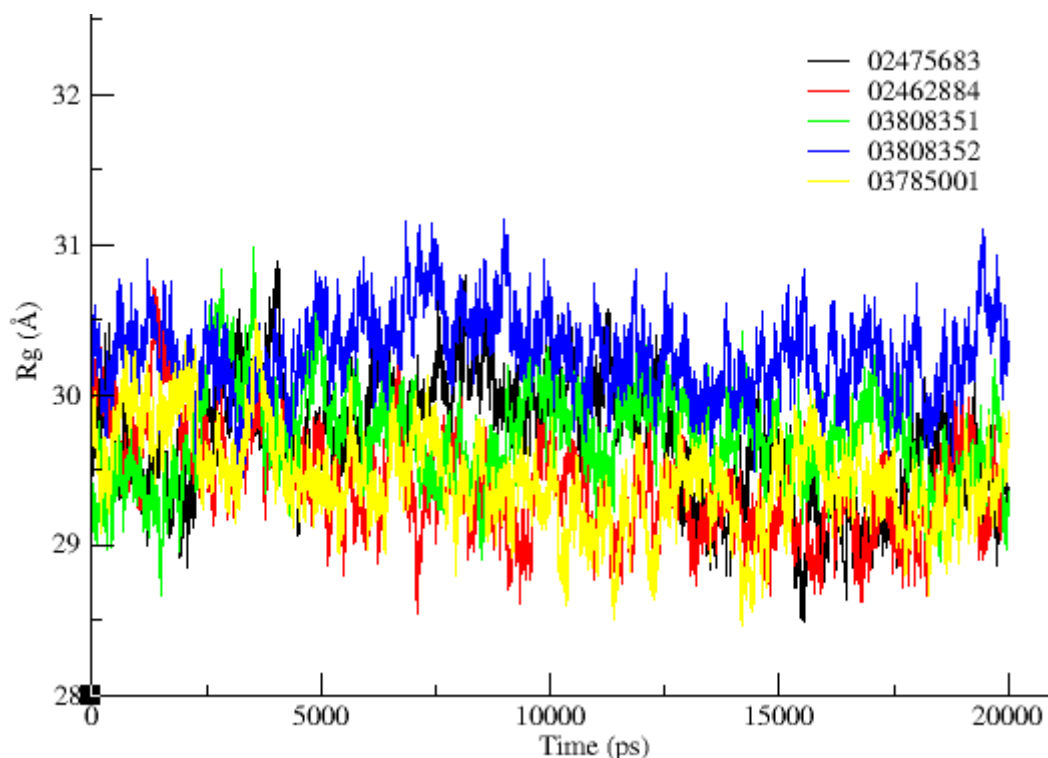
Figure 4.5 The radius of gyration (Rg) of the β-lactam-Ldt$_{Mt5}$ complexes of **A** 02475683-Ldt$_{Mt5}$ (black), **B** 02462884-Ldt$_{Mt5}$ (red), **C** 03808351-Ldt$_{Mt5}$ (green), **D** 03808352-Ldt$_{Mt5}$ (blue) and **E** 03785001-Ldt$_{Mt5}$ (yellow) during 20 ns MD trajectories

4.3.4.3 Binding free energy (ΔG_{bind}) analysis of β-lactam-Ldt$_{Mt5}$ complexes

In this study, the calculated binding energies of β-lactam derivatives (meropenem and imipenem) against Ldt$_{Mt2}$ from previous studies [31, 60] were used to validate the selection of lead compounds which demonstrated the best binding affinity for Ldt$_{Mt5}$. The calculated binding free energies (ΔG_{bind}) of the selected β-lactam-Ldt$_{Mt5}$ complexes were obtained using the MM-GBSA method, 1000 snapshots at 10 ps interval was extracted from the last 10 ns production MD trajectories. The entropy (-TΔS) contributions were calculated using normal mode analysis [61, 62] by extracting 100 snapshots from the MD trajectories due to computa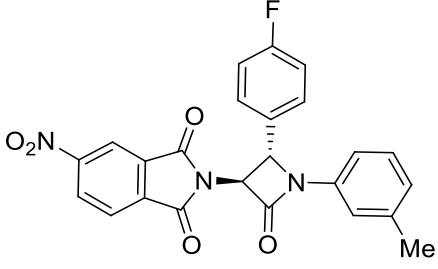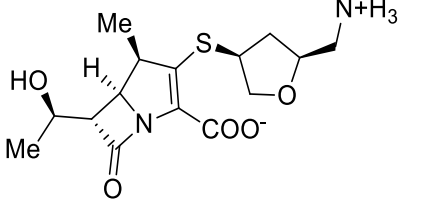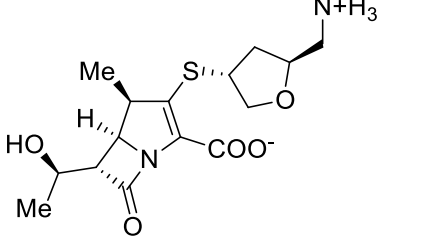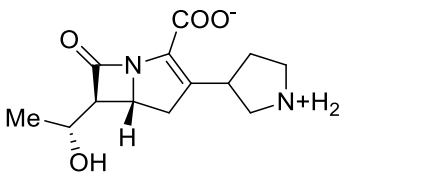tion cost. The contributing binding components upon complexation, namely, ΔE_{vdw}, ΔE_{ele}, ΔG_{gas}, ΔG_{polar}, $\Delta G_{nonpolar}$ and $\Delta G_{solvation}$ are shown in **Table 4.10**. The results reveal the binding free energies (ΔG_{bind}) of -48.52 kcal mol^{-1} and -46.75 kcal mol^{-1} for complex A (02475683-Ldt$_{Mt5}$) and complex B (02462884-Ldt$_{Mt5}$) respectively. The binding free energies of complexes C

(03808351-Ldt$_{Mt5}$), D (03808352-Ldt$_{Mt5}$) and E (03785001-Ldt$_{Mt5}$) are -35.32 kcal mol^{-1}, -32.18 kcal mol^{-1} and -30.68 kcal mol^{-1}, all between -30 kcal mol^{-1} and -40 kcal mol^{-1}. It was observed that compounds with a greater binding affinity (A and B) are characterised by a more negative van der Waals value and they are less electronegative as compared to the other compounds (C-E).

Table 4.10 Calculated binding free energies and their corresponding components using MM-GBSA method for the selected β-lactam-Ldt$_{Mt5}$ complexes.

Compound	ZINC ID	ΔE_{vdw}	ΔE_{ele}	ΔG_{gas}	ΔG_{polar}	$\Delta G_{nonpolar}$	$\Delta G_{solvation}$	-TΔS	ΔG_{bind}
A	**02475683**	**-59.68**	**-9.72**	**-69.41**	**27.7**	**-6.82**	**20.88**	**-31.01**	**-48.52**
B	**02462884**	**-54.07**	**-8.97**	**-63.03**	**22.7**	**-6.42**	**16.28**	**-27.53**	**-46.75**
C	03808351	-33.59	-188.02	-221.61	191.16	-4.87	186.29	-27.84	-35.32
D	03808352	-34.38	-167.3	-201.68	174.86	-5.36	169.5	-26.19	-32.18
E	03785001	-30.57	-175.27	-205.83	179.63	-4.48	175.15	-16.06	-30.68

Compounds in bold were screened by AutoDock Vina and compounds in the normal text were screened by Schrödinger Maestro

4.3.4.4 Residue-inhibitor interaction analysis

To further elucidate the possible intermolecular hydrogen bonding and electrostatic interactions between β-lactam-Ldt$_{Mt5}$ complexes, we used LigPlot program [63]. The active site of Ldt$_{Mt5}$ is defined by four conserved residues (His287 (342), Thr302 (357), Asn303 (358) and Cys305 (360)) [13]. **Figure 4.6** shows the schematic representations of core amino acid residues interaction modes between the β-lactam compounds (A-E) and Ldt$_{Mt5}$. It is important to note that the residue-inhibitor interaction of compound A with Ldt$_{Mt5}$ demonstrates close hydrogen bond interaction between the ligand and two active site residues Asn303 (358) and Cys305 (360), which can be a possible explanation to the highest binding free energy observed. Compound B interact with the residue Asn263 (318) and a water molecule which is within the active site (**Figure 4.6**) and binding free energies (**Table 4.10**) of both compounds (A, B) are within the same range. Common among all 3 compounds (C-E) is the interaction with residue Arg242 (297). Compound C has other interactions with residues Glu284 (339) and Gly304 (359). Val244 (299) is a common residue between compound D and E while each compound interacts with Gly304 (359) and Asn243 (298) respectively. The other 3 compounds (C-E) also fall in a similar binding free energies range (**Table 4.10**) and they are unique in that they interact with different residues, although not with any of the active site residues.

Figure 4.6 2D schematic representations of the hydrogen and hydrophobic interactions between Ldt$_{Mt5}$ residues and the selected β-lactam compounds, ZINC ID (**A**) 02475683, (**B**) 02462884, (**C**) 03808351, (**D**) 03808352, and (**E**) 03785001. All structures are average conformations generated from the last 10 ns snapshots of each MD system
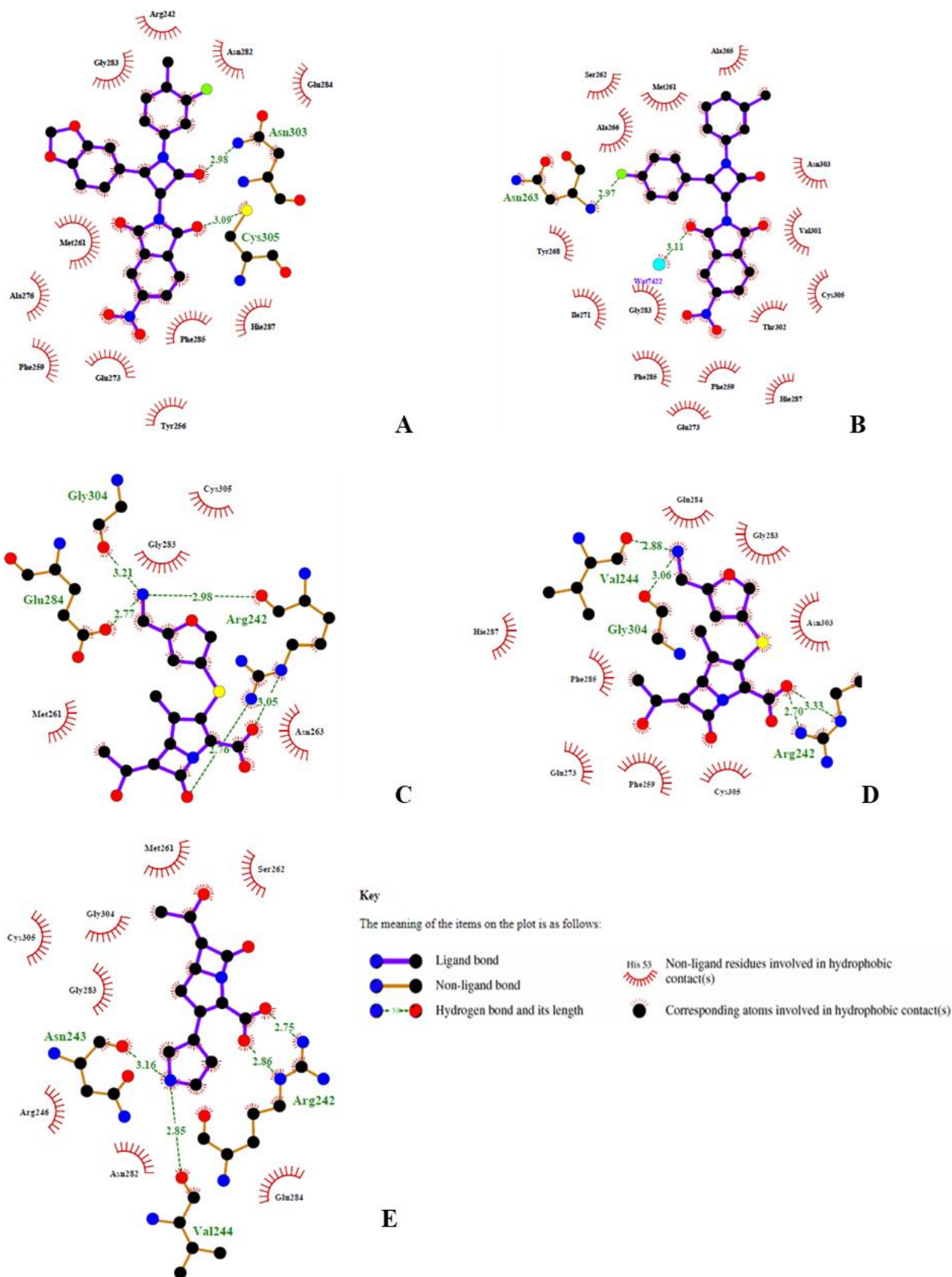
Results from virtual screening and docking studies demonstrated that several lead compounds from different classes of antibiotics potentially tend to bind to the active pocket of Ldt_{Mt5}. The binding free energies also demonstrate the favourable binding potential of our lead compounds to Ldt_{Mt5}. It is known that β-lactams, specifically carbapenems, form covalent bonds with the catalytic cysteine (305) residue of Ldt_{Mt5} due to the carbonyl functional group in the structural backbone. However, results from the model as highlighted by the residue-inhibitor interaction analysis seem to suggest that other compounds may interact differently with Ldt_{Mt5}. Instead of forming covalent interaction, other potential inhibitors of Ldt_{Mt5} may perform competitive inhibition instead. It is also important to note that the closer the inhibitor interacts with the active site residues, the higher the binding affinity it may have as demonstrated compound A (**Figure 4.6**).

4.4 Conclusion

In this study, virtual screening of compounds from ZINC database against Ldt_{Mt5} was investigated with AutoDock Vina and Schrödinger Maestro software programs. The obtained docking scores presented a reasonable number of lead compounds which can be utilised as potential drug candidates against Ldt_{Mt5}. Despite the lack of overlap on the screened compounds using these two different software programs, both provided reasonable binding scores. The observed exclusiveness of each program to a certain class of compounds strongly suggests that the effectiveness of a computational technique is subject to the software program utilised. To improve the chances of getting a 'lead compound', different programs with alternative search algorithms need to be employed for the screening of compound libraries. It is essential to verify virtual screening results with MD free energy calculations as was demonstrated before [14]. The screened lead compounds were subjected to the MM-GBSA approach. A final set of compounds (n=10) from four antibiotic classes with $\leq$ -30 kcal mol^{-1} were obtained.

The computational model presented in this study is robust in that its accuracy was validated on both the docking stage as well as on the MD simulations stage. Such benchmarking offers baseline comparisons of experimental and computational data from a paralog of the enzyme under study which brings about comparable extrapolations applicable to the natural system. The model as expressed through the docking affinities and binding energy calculations from MD simulations demonstrated strong binding ligands. It should also be noted, however, that the residue-inhibitor interaction analysis further revealed that apart from the already known interactions, other compounds interact with other active site residues of the target. This certainly paves the way to explore other β-lactam binding mechanisms and expresses the importance of molecular dynamics simulations in revealing other possible interactions within the active site of other transpeptidases. We, therefore, conclude that pharmacophore-based virtual screening and molecular dynamics simulations are essential tools which will continue to play a significant role in drug design and identification of novel ligands.

Conflict of interest

Authors declare no conflict of interest.

References

[1] Seung, K. J., Keshavjee, S., and Rich, M. L. (2015) Multidrug-resistant tuberculosis and extensively drug-resistant tuberculosis, *Cold Spring Harbor perspectives in medicine*, a017863.

[2] Billones, J. B., Carrillo, M. C. O., Organo, V. G., Macalino, S. J. Y., Sy, J. B. A., Emnacen, I. A., Clavio, N. A. B., and Concepcion, G. P. (2016) Toward antituberculosis drugs: in silico screening of synthetic compounds against Mycobacterium tuberculosis l, d-transpeptidase 2, *Drug design, development and therapy 10*, 1147.

[3] Adewumi, O. A. (2012) Treatment outcomes in patients infected with multidrug resistant tuberculosis and in patients with multidrug resistant tuberculosis coinfected with human immunodeficiency virus at Brewelskloof Hospital.

[4] Brammer, B. L., Ghosh, A., Pan, Y., Jakoncic, J., Lloyd, E., Townsend, C., Lamichhane, G., and Bianchet, M. (2015) Loss of a Functionally and Structurally Distinct ld-Transpeptidase, LdtMt5, Compromises Cell Wall Integrity in Mycobacterium tuberculosis, *The Journal of Biological Chemistry 290*, 25670-25685.

[5] Lavollay, M., Arthur, M., Fourgeaud, M., Dubost, L., Marie, A., Veziris, N., Blanot, D., Gutmann, L., and Mainardi, J.-L. (2008) The peptidoglycan of stationary-phase Mycobacterium tuberculosis predominantly contains cross-links generated by L, D-transpeptidation, *Journal of Bacteriology 190*, 4360-4366.

[6] Dubée, V., Triboulet, S., Mainardi, J.-L., Ethève-Quelquejeu, M., Gutmann, L., Marie, A., Dubost, L., Hugonnet, J.-E., and Arthur, M. (2012) Inactivation of Mycobacterium tuberculosis L, D-transpeptidase LdtMt1 by carbapenems and cephalosporins, *Antimicrobial agents and chemotherapy 56*, 4189-4195.

[7] Cordillot, M., Dubée, V., Triboulet, S., Dubost, L., Marie, A., Hugonnet, J.-E., Arthur, M., and Mainardi, J.-L. (2013) In vitro cross-linking of Mycobacterium tuberculosis peptidoglycan by l, d-transpeptidases and inactivation of these enzymes by carbapenems, *Antimicrobial agents and chemotherapy 57*, 5940-5945.

[8] Lecoq, L., Dubée, V., Triboulet, S. b., Bougault, C., Hugonnet, J.-E., Arthur, M., and Simorre, J.-P. (2013) Structure of Enterococcus faecium L, D-transpeptidase acylated by ertapenem provides insight into the inactivation mechanism, *ACS chemical biology 8*, 1140-1146.

[9] Gupta, R., Lavollay, M., Mainardi, J.-L., Arthur, M., Bishai, W. R., and Lamichhane, G. (2010) The Mycobacterium tuberculosis protein LdtMt2 is a nonclassical transpeptidase required for virulence and resistance to amoxicillin, *Nature Medicine 16*, 466-469.

[10] Biarrotte-Sorin, S., Hugonnet, J.-E., Delfosse, V., Mainardi, J.-L., Gutmann, L., Arthur, M., and Mayer, C. (2006) Crystal structure of a novel β-lactam-insensitive peptidoglycan transpeptidase, *Journal of molecular biology 359*, 533-538.

[11] Mainardi, J.-L., Fourgeaud, M., Hugonnet, J.-E., Dubost, L., Brouard, J.-P., Ouazzani, J., Rice, L. B., Gutmann, L., and Arthur, M. (2005) A novel peptidoglycan cross-linking enzyme for a β-lactam-resistant transpeptidation pathway, *Journal of Biological Chemistry 280*, 38146-38152.

[12] Mainardi, J.-L., Villet, R., Bugg, T. D., Mayer, C., and Arthur, M. (2008) Evolution of peptidoglycan biosynthesis under the selective pressure of antibiotics in Gram-positive bacteria, *FEMS microbiology reviews 32*, 386-408.

[13] Basta, L. A. B., Ghosh, A., Pan, Y., Jakoncic, J., Lloyd, E. P., Townsend, C. A., Lamichhane, G., and Bianchet, M. A. (2015) Loss of a functionally and structurally distinct ld-transpeptidase, LdtMt5, compromises cell wall integrity in mycobacterium tuberculosis, *Journal of Biological Chemistry 290*, 25670-25685.

[14] Honarparvar, B., Govender, T., Maguire, G. E., Soliman, M. E., and Kruger, H. G. (2013) Integrated approach to structure-based enzymatic drug design: molecular modeling, spectroscopy, and experimental bioactivity, *Chemical reviews 114*, 493-537.

[15] Bradley, J., Garau, J., Lode, H., Rolston, K., Wilson, S., and Quinn, J. (1999) Carbapenems in clinical practice: a guide to their use in serious infection, *International journal of antimicrobial agents 11*, 93-100.

[16] Paterson, D. (2000) Recommendation for treatment of severe infections caused by Enterobacteriaceae producing extended-spectrum β-lactamases (ESBLs), *Clinical Microbiology and Infection 6*, 460-463.

[17] Paterson, D. L. (2002) Serious infections caused by enteric gram-negative bacilli--mechanisms of antibiotic resistance and implications for therapy of gram-negative sepsis in the transplanted patient, In *Seminars in respiratory infections*, pp 260-264.

[18] Paterson, D. L., and Bonomo, R. A. (2005) Extended-spectrum β-lactamases: a clinical update, *Clinical microbiology reviews 18*, 657-686.

[19] Torres, J. A., Villegas, M. V., and Quinn, J. P. (2007) Current concepts in antibiotic-resistant gram-negative bacteria, *Expert review of anti-infective therapy 5*, 833-843.

[20] Meletis, G. (2016) Carbapenem resistance: overview of the problem and future perspectives, *Therapeutic advances in infectious disease 3*, 15-21.

[21] Kattan, J., Villegas, M., and Quinn, J. (2008) New developments in carbapenems, *Clinical Microbiology and Infection 14*, 1102-1111.

[22] El-Gamal, M. I., Brahim, I., Hisham, N., Aladdin, R., Mohammed, H., and Bahaaeldin, A. (2017) Recent updates of carbapenem antibiotics, *European journal of medicinal chemistry 131*, 185-195.

[23] Trott, O., and Olson, A. J. (2010) AutoDock Vina: improving the speed and accuracy of docking with a new scoring function, efficient optimization, and multithreading, *Journal of computational chemistry 31*, 455-461.

[24] Schrödinger Release 2018-1: Maestro, S., LLC, New York, NY, 2018.

[25] Reddy, A. S., Pati, S. P., Kumar, P. P., Pradeep, H., and Sastry, G. N. (2007) Virtual screening in drug discovery-a computational perspective, *Current Protein and Peptide Science 8*, 329-351.

[26] Roe, D. R., and Cheatham III, T. E. (2013) PTRAJ and CPPTRAJ: software for processing and analysis of molecular dynamics trajectory data, *Journal of chemical theory and computation 9*, 3084-3095.

[27] Pearlman, D. A., Case, D. A., Caldwell, J. W., Ross, W. S., Cheatham III, T. E., DeBolt, S., Ferguson, D., Seibel, G., and Kollman, P. (1995) AMBER, a package of computer programs for applying molecular mechanics, normal mode analysis, molecular dynamics and free energy calculations to simulate the structural and energetic properties of molecules, *Computer Physics Communications 91*, 1-41.

[28] Berman, H. M., Westbrook, J., Feng, Z., Gilliland, G., Bhat, T. N., Weissig, H., Shindyalov, I. N., and Bourne, P. E. (2006) The protein data bank, 1999–, In *International Tables for Crystallography Volume F: Crystallography of biological macromolecules*, pp 675-684, Springer.

[29] Sali, A. (1994) Modeller. A program for protein structure modeling by satisfaction of spatial restraints, *http://guitar. rockefeller. edu/modiller/modeller. html*.

[30] Li, H., Robertson, A. D., and Jensen, J. H. (2005) Very fast empirical prediction and rationalization of protein pKa values, *Proteins: Structure, Function, and Bioinformatics 61*, 704-721.

[31] Fakhar, Z., Govender, T., Maguire, G. E., Lamichhane, G., Walker, R. C., Kruger, H. G., and Honarparvar, B. (2017) Differential flap dynamics in l, d-transpeptidase2 from mycobacterium tuberculosis revealed by molecular dynamics, *Molecular BioSystems 13*, 1223-1234.

[32] Irwin, J. J., Sterling, T., Mysinger, M. M., Bolstad, E. S., and Coleman, R. G. (2012) ZINC: a free tool to discover chemistry for biology, *Journal of chemical information and modeling 52*, 1757-1768.

[33] Lipinski, C. A., Lombardo, F., Dominy, B. W., and Feeney, P. J. (2001) Experimental and computational approaches to estimate solubility and permeability in drug discovery and development settings1, *Advanced drug delivery reviews 46*, 3-26.

[34] Veber, D. F., Johnson, S. R., Cheng, H.-Y., Smith, B. R., Ward, K. W., and Kopple, K. D. (2002) Molecular properties that influence the oral bioavailability of drug candidates, *Journal of medicinal chemistry 45*, 2615-2623.

[35] Singh, U. C., and Kollman, P. A. (1984) An approach to computing electrostatic charges for molecules, *Journal of Computational Chemistry 5*, 129-145.

[36] Gasteiger, J., and Marsili, M. (1980) Iterative partial equalization of orbital electronegativity—a rapid access to atomic charges, *Tetrahedron 36*, 3219-3228.

[37] Morris, G. M., Huey, R., Lindstrom, W., Sanner, M. F., Belew, R. K., Goodsell, D. S., and Olson, A. J. (2009) AutoDock4 and AutoDockTools4: Automated docking with selective receptor flexibility, *Journal of computational chemistry 30*, 2785-2791.

[38] BIOVIA, D. S. (2017) BIOVIA Discovery Studio 2017 R2: A comprehensive predictive science application for the Life Sciences, *San Diego, CA, USA http://accelrys. com/products/collaborative-science/biovia-discovery-studio*.

[39] Sastry, G. M., Adzhigirey, M., Day, T., Annabhimoju, R., and Sherman, W. (2013) Protein and ligand preparation: parameters, protocols, and influence on virtual screening enrichments, *Journal of computer-aided molecular design 27*, 221-234.

[40] Shelley, J. C., Cholleti, A., Frye, L. L., Greenwood, J. R., Timlin, M. R., and Uchimaya, M. (2007) Epik: a software program for pK a prediction and protonation state generation for drug-like molecules, *Journal of computer-aided molecular design 21*, 681-691.

[41] Harder, E., Damm, W., Maple, J., Wu, C., Reboul, M., Xiang, J. Y., Wang, L., Lupyan, D., Dahlgren, M. K., and Knight, J. L. (2015) OPLS3: a force field providing broad coverage of drug-like small molecules and proteins, *Journal of chemical theory and computation 12*, 281-296.

[42] Jones, G., Willett, P., Glen, R. C., Leach, A. R., and Taylor, R. (1997) Development and validation of a genetic algorithm for flexible docking, *Journal of molecular biology 267*, 727-748.

[43] Friesner, R. A., Murphy, R. B., Repasky, M. P., Frye, L. L., Greenwood, J. R., Halgren, T. A., Sanschagrin, P. C., and Mainz, D. T. (2006) Extra precision glide: Docking and scoring incorporating a model of hydrophobic enclosure for protein− ligand complexes, *Journal of medicinal chemistry 49*, 6177-6196.

[44] Enyedy, I. J., and Egan, W. J. (2008) Can we use docking and scoring for hit-to-lead optimization?, *Journal of computer-aided molecular design 22*, 161-168.

[45] Repasky, M. P., Shelley, M., and Friesner, R. A. (2007) Flexible ligand docking with Glide, *Current Protocols in Bioinformatics*, 8.12. 11-18.12. 36.

[46] Metropolis, N., Rosenbluth, A. W., Rosenbluth, M. N., Teller, A. H., and Teller, E. (1953) Equation of state calculations by fast computing machines, *The journal of chemical physics 21*, 1087-1092.

[47] Taylor, R. D., Jewsbury, P. J., and Essex, J. W. (2002) A review of protein-small molecule docking methods, *Journal of computer-aided molecular design 16*, 151-166.

[48] Hornak, V., Abel, R., Okur, A., Strockbine, B., Roitberg, A., and Simmerling, C. (2006) Comparison of multiple Amber force fields and development of improved protein backbone parameters, *Proteins: Structure, Function, and Bioinformatics 65*, 712-725.

[49] Wang, J., Wolf, R. M., Caldwell, J. W., Kollman, P. A., and Case, D. A. (2004) Development and testing of a general amber force field, *Journal of computational chemistry 25*, 1157-1174.

[50] Harvey, M., and De Fabritiis, G. (2009) An implementation of the smooth particle mesh Ewald method on GPU hardware, *Journal of chemical theory and computation 5*, 2371-2377.

[51] Kräutler, V., Van Gunsteren, W. F., and Hünenberger, P. H. (2001) A fast SHAKE algorithm to solve distance constraint equations for small molecules in molecular dynamics simulations, *Journal of computational chemistry 22*, 501-508.

[52] John, A., Sivashanmugam, M., Umashankar, V., and Natarajan, S. K. (2017) Virtual screening, molecular dynamics, and binding free energy calculations on human carbonic anhydrase IX catalytic domain for deciphering potential leads, *Journal of Biomolecular Structure and Dynamics 35*, 2155-2168.

[53] Islam, M. A., and Pillay, T. S. (2017) Identification of promising DNA GyrB inhibitors for Tuberculosis using pharmacophore-based virtual screening, molecular docking and molecular dynamics studies, *Chemical biology & drug design 90*, 282-296.

[54] Martin, Y. C. (2005) A bioavailability score, *Journal of medicinal chemistry 48*, 3164-3170.

[55] Bianchet, M. A., Pan, Y. H., Basta, L. A. B., Saavedra, H., Lloyd, E. P., Kumar, P., Mattoo, R., Townsend, C. A., and Lamichhane, G. (2017) Structural insight into the inactivation of Mycobacterium tuberculosis non-classical transpeptidase Ldt Mt2 by biapenem and tebipenem, *BMC biochemistry 18*, 8.

[56] Erdemli, S. B., Gupta, R., Bishai, W. R., Lamichhane, G., Amzel, L. M., and Bianchet, M. A. (2012) Targeting the cell wall of Mycobacterium tuberculosis: structure and mechanism of L, D-transpeptidase 2, *Structure 20*, 2103-2115.

[57] Hyndman, R. J., and Koehler, A. B. (2006) Another look at measures of forecast accuracy, *International journal of forecasting 22*, 679-688.

[58] Lobanov, M. Y., Bogatyreva, N., and Galzitskaya, O. (2008) Radius of gyration as an indicator of protein structure compactness, *Molecular Biology 42*, 623-628.

[59] Peterson, K., Zimmt, M., Linse, S., Domingue, R., and Fayer, M. (1987) Quantitative determination of the radius of gyration of poly (methyl methacrylate) in the amorphous solid state by time-resolved fluorescence depolarization measurements of excitation transport, *Macromolecules 20*, 168-175.

[60] Silva, J. R. A., Bishai, W. R., Govender, T., Lamichhane, G., Maguire, G. E., Kruger, H. G., Lameira, J., and Alves, C. N. (2016) Targeting the cell wall of Mycobacterium tuberculosis: a molecular modeling investigation of the interaction of imipenem and meropenem with L, D-transpeptidase 2, *Journal of Biomolecular Structure and Dynamics 34*, 304-317.

[61] Kassem, S., Ahmed, M., El-Sheikh, S., and Barakat, K. H. (2015) Entropy in bimolecular simulations: A comprehensive review of atomic fluctuations-based methods, *Journal of Molecular Graphics & Modelling 62*, 105-117.

[62] Chiba, S., Harano, Y., Roth, R., Kinoshita, M., and Sakurai, M. (2012) Evaluation of protein-ligand binding free energy focused on its entropic components, *Journal of Computational Chemistry 33*, 550-560.

[63] Wallace, A. C., Laskowski, R. A., and Thornton, J. M. (1995) LIGPLOT: a program to generate schematic diagrams of protein-ligand interactions, *Protein engineering, design and selection 8*, 127-134.

CHAPTER FIVE

The manuscript in chapter five has been published in Journal of Molecular Graphics and Modelling

Inhibition Mechanism of L,D-transpeptidase 5 in presence of the *β*-lactams using ONIOM Method

Gideon F. Tolufashe,[a] Victor T. Sabe,[a] Collins U. Ibeji,[a] Monsurat M. Lawal,[a]
Thavendran Govender,[a] Glenn E. M. Maguire,[a,b] Gyanu Lamichhane,[c] Hendrik G. Kruger[a*] and Bahareh Honarparvar[a*]

[1]Catalysis and Peptide Research Unit, School of Health Sciences, University of KwaZulu-Natal, Durban 4001, South Africa.

[2]School of Chemistry and Physics, University of KwaZulu-Natal, 4001 Durban, South Africa.

[3]Center for Tuberculosis Research, Division of Infectious Diseases, School of Medicine, Johns Hopkins University, Baltimore, MD 21205, USA.

*Corresponding authors: kruger@ukzn.ac.za (Prof. Hendrik G. Kruger), Honarparvarb@ukzn.ac.za (Dr Bahareh Honarparvar), Telephone: + 27 31 2601845, Fax: +27 31 2603091, Catalysis and Peptide Research Unit, School of Health Sciences, University of KwaZulu-Natal, Durban 4041, South Africa.

Abstract

Tuberculosis (TB) is one of the world's deadliest diseases caused by the bacterium, *Mycobacterium tuberculosis* (*Mtb*). The L,D-transpeptidase enzymes catalyze the most dominant $3 \rightarrow 3$ peptidoglycan cross-links of the Mtb cell wall and specific *β*-lactam antibiotics have been reported to inhibit its action. Carbapenems inactivate L,D-transpeptidases by acylation, although differences in antibiotic side chains modulate drug binding and acylation rates. Herein, we used a two-layered our Own N-layer integrated Molecular Mechanics ONIOM method to investigate the catalytic mechanism of L,D-transpeptidase 5 (Ldt_{Mt5}) by *β*-lactam derivatives. Ldt_{Mt5} complexes with six *β*-lactams, ZINC03788344 (**1**), ZINC02462884 (**2**), ZINC03791246 (**3**), ZINC03808351 (**4**), ZINC03784242 (**5**) and ZINC02475683 (**6**) were simulated. The QM region (high-level) comprises the *β*-lactam, one water molecule and the Cys360 catalytic residue, while the rest of the Ldt_{Mt5} residues were treated with the AMBER force field. The activation energies ($\Delta G^{\#}$) were calculated with B3LYP, M06-2X and ωB97X density functionals with 6-311++G(2d, 2p) basis set. The $\Delta G^{\#}$ for the acylation of Ldt_{Mt5} by the selected *β*-lactams were calculated as 13.67, 20.90, 22.88, 24.29, 27.86 and 28.26 kcal mol^{-1} respectively. Several of the compounds showed an improved $\Delta G^{\#}$ when compared to the previously calculated for imipenem and meropenem for the acylation step for Ldt_{Mt5}. This model provides further validation of the catalytic inhibition mechanism of LDTs with atomistic detail.

Keywords: *Mycobacterium tuberculosis* (*Mtb*), L,D-transpeptidase 5 (Ldt$_{Mt5}$), QM/MM, ONIOM, Catalytic mechanism.

5.1 Introduction

The understanding of the enzyme-catalysed reactions mechanisms is essential to the study of biochemical processes. Possibly, an improved understanding can add to the development of novel inhibitors with greater therapeutic potential[1]. In *Mtb* Peptidoglycan is required for major cell division, growth and recovery from dormancy. This is a metabolically inactive state that allows the mycobacteria to endure hostile physical-chemical situations or nutrient malnourishment[2]. This inactive state subsequently leads to latent infection which affects one-third of the world's population[2]. The β-lactam antibiotics, an effective therapeutic category of antibacterial[3] agents for the inhibition of transpeptidases, which are required in cell wall biosynthesis[4]. Majority of the cross-linkage has been reported to occur via 3→3 linkages catalysed by L,D-transpeptidases which bypass the D,D-transpeptidase activity of penicillin-binding proteins (PBPs), leading to high-levels of resistance to the drugs[5-8]. The second type of cross-linkage occurs via 4→3 linkages catalysed by D,D-transpeptidase (also PBPs). This group of antibacterial drugs inactivate both transpeptidase enzymes[2, 3, 5, 9-12]. Carbapenems are one group of β-lactam antibiotics showed to have inactivated L,D-transpeptidase activity[2, 5, 10-12]. As is the case for all cysteine proteases[13], L,D-transpeptidases hydrolyse the peptide bonds by two catalytic processes that are required to start enzyme acylation by the second last peptide of the donor stem leading to the release of the C-terminal residue. This is tailed by deacylation of this acyl-enzyme intermediate by an acceptor stem[10, 14].

Unique to *Mtb*, the majority of the cross-links are generated by L,D-transpeptidation reaction, making this enzyme essential in the adaptation of *Mtb* to the stationary phase[5]. Combined inhibition of both transpeptidases (L,D and D,D) will permanently hinder the synthesis of the peptidoglycan sheet and therefore, destroy the bacteria[15]. Erdemli and co-workers[10] proposed mechanism of acylation of L,D-transpeptidase to be built on cysteine protease mechanism. This mechanism for Ldt$_{Mt2}$ proceeds in two phases. Firstly, is the acylation step, where the Cys352 thiolate is produced via abstraction of proton bonds on the acyl carbon of the substrate resulting in a tetrahedral intermediate. Secondly, in the deacylation step, additional peptide stem goes into the catalytic pocket and binds to the residues with the side chain amide of the m-A2pm3′ residue. In this step, His336 plays the role of the catalytic base via abstraction of a proton from the amine group of the mA2pm3′ residue, which in turn makes an attack (nucleophilic) on the carbonyl carbon of the acyl-enzyme[10].

Computational applications have been employed to investigate this mechanism, which corroborates experimental observations for the catalytic mechanism of L,D-transpeptidase 2, a commonly studied enzyme from *Mtb*[16, 17]. The first computational study on the inhibition mechanism of L,D-transpeptidase 2 was carried out using a hybrid DFTB/MM potential[16]. The peptidoglycan fragment bound with the initial coordinates of the extramembrane portion of Ldt$_{Mt2}$ (ex-Ldt$_{Mt2}$) (PDB code:

3TUR) was replaced *in silico*, for the natural substrate. Based on the results obtained, the formation of His336-imidazolium/Cys354-thiolate initiated a four-membered ring acylation step. This is then followed by a single step attack of Cys 354 on the carbonyl carbon of the substrate. The aforementioned is the rate-limiting step, and it agrees with the experimental results for cysteine proteases. The attack on the acyl-enzyme complex by the amine group of the subsequent substrate and results in the formation of 3→3 peptide bond (deacylation step) [16]. Fakhar *et al.*[17] using a *β*-lactam model investigated the acylation of the *β*-lactam ring by Ldt$_{Mt2}$ in *Mtb* with B3LYP/6-31 + G(d). The acylation mechanism employed four-membered and six-membered ring transition states. The calculated thermochemical quantities for the proposed models specified that the activation free energy for the six-membered ring transition states model was significantly lower in comparison to other models[17].

The crystal structure of Ldt$_{Mt5}$ was recently solved both for apo (PDB code: 4Z7A[12]) and meropenem bound (PDB code: 4ZFQ[12]). Any *Mtb* strain with a deletion of Ldt$_{Mt5}$ displays abnormal growth phenotype and is more vulnerable to killing by cell wall perturbing agents including carbapenems which are considered the last resort antibiotics to combat resistant bacterial infections in humans[12].

Herein we have investigated the acylation reaction of some selected *β*-lactam derivatives from our on-going virtual screening against Ldt$_{Mt5}$ *via* a 6-membered ring mechanism. These results we hope will provide a reasonable computational model for designing new anti-Tuberculosis drugs. This present work will adopt the protocol reported by Fakhar *et al.*[17]. The selected *β*-lactams are shown in **Figure 5.1**. A water molecule will be evaluated as well as the active pocket of Ldt$_{Mt5}$ at the quantum mechanical (QM) level, and the other portion of the enzyme at molecular mechanics (MM) level. Compounds **1, 3, 4** and **5** are carbapenems while compounds **2** and **6** are monobactams.
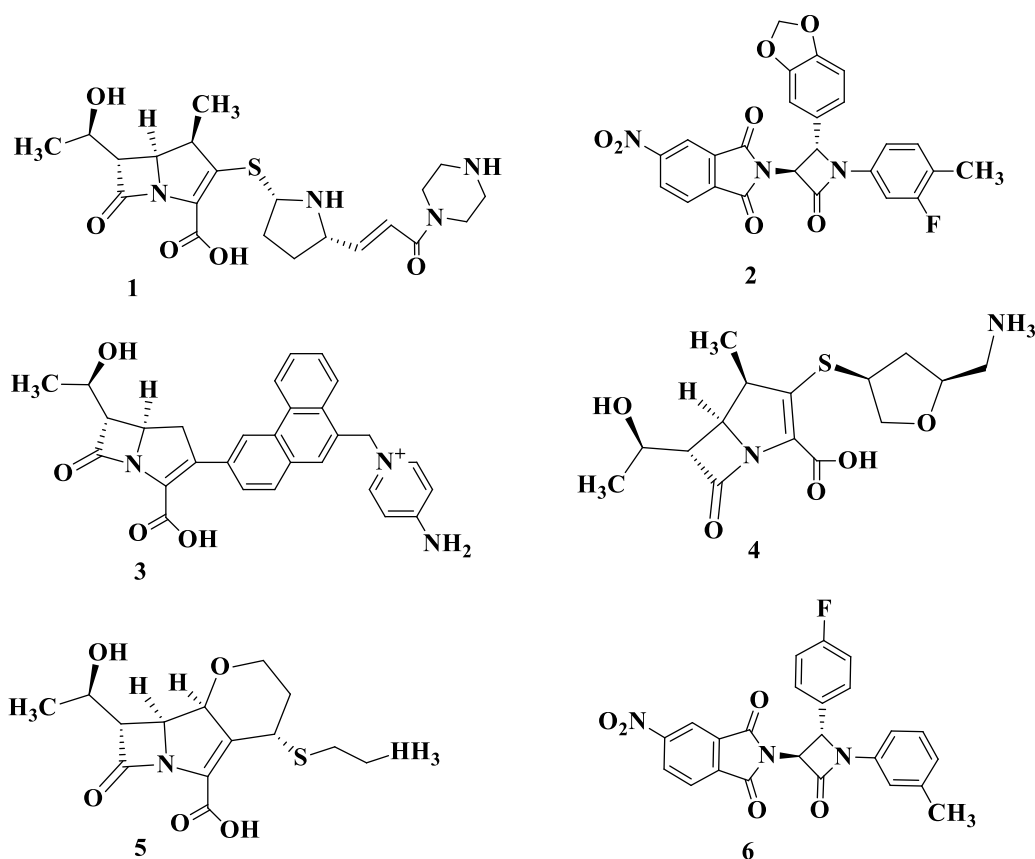
Figure 5.1 2D structures of the selected β-lactam derivatives.

5.2 Computational methods

A 6-membered ring transition state mechanism[18, 19] for the acylation of carbapenems by Ldt$_{Mt5}$ (from *Mtb*) was investigated with a water molecule within the active pocket. QM/MM (ONIOM[20]) method calculations were applied. The influence of catalytic water has been reported to play a vital role in enzymatic reactions[17] using the ONIOM method[20].

5.2.1 System preparation

The crystal structure of meropenem-Ldt$_{Mt5}$ complex (**Figure S1**) was retrieved from protein data bank[21] (PDB code: 4ZFQ, 2.8 Å resolution)[12]. Meropenem was removed and complexed with the selected β-lactam derivatives from the ZINC database[22] as described in our on going virtual screening study. The β-lactams were docked into the active site of Ldt$_{Mt5}$ using AutoDock Vina and Schrodinger Glide programs. The ff99SB [23] force field was applied for the protein whereas the general AMBER force field (GAFF) [24] was used for the ligand. System solvation for the complexes was performed in a 10 Å cubic box using the TIP3P water model. To neutralize the system, counterions were added accordingly. The protein-ligand complexes were parametrized by the Leap [24] module of the Amber14 package. All simulations were performed using a 2fs timestep based on a study with similar protein size [25]. The partial Mesh Ewald (PME) [26] summation method was used to calculate the electrostatic forces with space cut-off of 12 Å. Using the SHAKE algorithm [27], all bonds were constrained to hydrogen (H) atoms. A two-stage energy minimization process, which is characterised by 2500 steps of steepest

decent (partial geometric minimization) and 2500 steps of the conjugated gradient (full geometric minimization) was carried out to eliminate steric clashes. The solute molecule was first restrained at 500 kcal mol^{-1}, whereas the water molecules and the ions were relaxed.

The starting structure was obtained from the previously minimized structure, upon deletion of all water molecules beyond a shell of 6 Å around the inhibitor-enzyme complexes. All counterions that were in far distant from the active site were removed. A similar approach has been reported before [28, 29].

Prior to optimization in ONIOM, the TAO ONIOM toolkit[30, 31] was utilized to generate the starting structure (for each system) containing the Cys360, β-lactams and the water molecule (QM/MM regions) around 6 Å around the active site while others more than 6 Å were held fixed [30, 31]. This was done to prevent fictitious changes and instabilities in the geometries. The obtained structures showed a sufficiently close distance between inhibitor, Cys360 and water molecule for a nucleophilic attack to occur [32]. QM/MM calculations implemented in Gaussian 09[20] were used to investigate the mechanism of the reaction. The cysteine catalytic active site (Cys360), all the selected β-lactams and the water molecule were placed at a high layer [B3LYP/6-31+G(d)4] while the other residues were at the low layer (AMBER) for geometry optimization. To obtain the transition state for each system, constrained interatomic distances (**Figure 5.3**) similar to those previously reported[28] for Ldt$_{Mt2}$ were applied. All transition state calculations were verified by vibrational frequency calculations exhibiting only one imaginary frequency. The intrinsic reaction coordinate (IRC) calculations were computed to determine the reaction pathway. A full unconstrained geometry optimization of the obtained transition states, reactant and product from IRC were performed. Single-point energy calculations were performed on the optimized structures of the transition states, reactant and product, resorting to the electronic embedding scheme with the different functionals (B3LYP, MO6, wb97X) and 6-311+G(2d,2p) basis set. These functionals have been reported to give reproducible results for thermodynamics and kinetics calculations[33-35]. The frontier orbital (HOMO, LUMO) for β-lactams (1-6) complexed with Ldt$_{Mt5}$ were

obtained using B3LYP/6 31G(d,p). The donor-acceptor interactions in the systems were evaluated using the natural bond orbital (NBO) calculations.
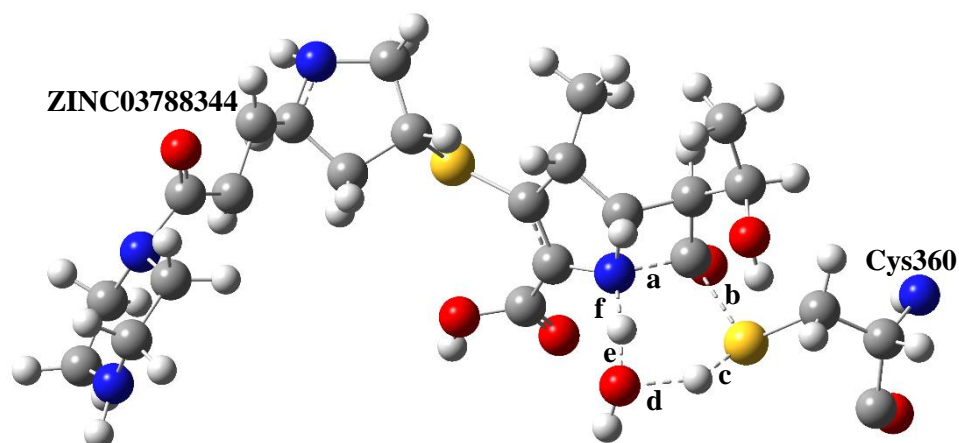
Figure 5.2 2D structure of the 6-membered ring transition states starting structures obtained using constraints with ONIOM (B3LYP/6-31+G(d):AMBER), where a =1.64 Å, b = 2.14 Å, c =1.60 Å, d = 1.58 Å, e = 1.3 Å, f = 1.3 Å. The TS optimized coordinates of all enzyme-inhibitor complexes are provided in the supplementary material)

5.2.3 Second-order perturbation analysis

NBO analysis is used to interpret the extent and function of intermolecular orbital interactions in the molecular system, principally charge transfer[36, 37]. The second-order perturbation theory is applied to estimate the energetic importance of all interactions between filled donor and empty acceptor NBOs. For each donor NBO (*i*) and acceptor NBO (*j*), the stabilization energy *E*(*2*) associated with delocalization is estimated as:

$$E^2 = \Delta E_{ij} = q_j \frac{F(i,j)^2}{\varepsilon_j - \varepsilon_i}$$

Where q_j is the donor orbital occupancy, ε_i and ε_j are diagonal matrix elements and $F(i,j)$ is the off-diagonal Fock matrix element.

5.2.4 Frontier molecular (FMO) orbitals

The electronic interaction between the donor and acceptor as well as the electron transfer in the molecular system principally relies on the spatial position of the FMO[38]. The kinetic characteristics of reactants and reactions are assessed by considering only FMO interactions[39]. To achieve this, the highest occupied molecular orbitals (HOMOs) and lowest unoccupied molecular orbitals (LUMOs) energies and the molecular orbital contributions were calculated using DFT[40-42].

5.3 Results and discussion
5.3.1 Mechanistic study

The activation free energies, enthalpies and entropies of the selected compounds, complexed with Ldt_{Mt5} for the 6-membered ring reaction pathway of the acylation are listed in **Table 5.1**. To investigate the accuracy and sensitivity of different functionals and method used, single point energy calculations of the respective structures (reactants, transition states and products) were performed using electronic embedding with B3LYP, M06-2X and ωB97X with 6-311++G(2d, 2p) basis set which have been reported to perform reasonable for kinetic and thermodynamic analysis[33-35]. In our previous study, the critical catalytic role of water, known to play a vital role in reaction mechanism has been demonstrated[9, 17]. The kinetic parameters obtained from the proposed model with water (TS-6-water) showed a lower activation barrier when compared with the model without water in Ldt_{Mt2}[17]. The catalytic behaviour of the acylation of Cys360 in Ldt_{Mt5} with one water molecule in the binding pocket against the selected β-lactams compounds was investigated. As shown in **Table 5.1**, the lowest activation energy ($\Delta G^{\#}$) is obtained with B3LYP/6-311++G(2d,2p) basis set, and thus our elucidation will be based on the results from this functional. The 6-membered ring transition state $\Delta G^{\#}$ of compounds **2-6** differs by about 1 kcal mol^{-1} while compound **1** showed the lowest activation barrier (**Table 5.1**). A comparison of the ΔH values of the transition states for compounds **1-6** revealed that they are consistent with the results obtained for the calculated $\Delta G^{\#}$.

Our results also reveal that our proposed 6-membered ring transition state mechanism is comparable to the activation energies of the 6-membered ring TS of Ldt_{Mt2} achieved previously[28] in our group using the same functional and basis set. In addition, the results revealed that this TS model with thermal corrections has a smaller value (between 14 and 28 kcal mol^{-1}) for Ldt_{Mt5} compared to the $\Delta G^{\#}$ 19.98 and 24.55 kcal mol^{-1} for a similar concerted pathway for imipenem and meropenem complexed with Ldt_{Mt2}[28]. Meanwhile, a higher $\Delta G^{\#}$ 53.29 and 91.08 kcal mol^{-1} for imipenem and meropenem against Ldt_{Mt5} respectively was previously observed[43]. Meropenem and imipenem were tested experimentally against $Ldt_{Mt5,}$ both drugs were reported to show slow acylation which indicates possibly higher activation energies.

Table 5.1 Relative energy, ΔH (kcal mol^{-1}) and ΔS (kcal mol^{-1}) of Ldt$_{Mt5}$ for the 6-membered ring reaction pathway of the acylation step obtained in ONIOM model using different density functionals at 6-311++G(2d,2p):AMBER.

Compounds		B3LYP[a]				M06[a]				ωB97X[a]			
	R	ΔE	$\Delta G^{\#}$	ΔH	ΔS	ΔE	$\Delta G^{\#}$	ΔH	ΔS	ΔE	$\Delta G^{\#}$	ΔH	ΔS
1		0	0	0	0	0	0	0	0	0	0	0	0
	TS	17.36	13.67	13.41	0.26	21.71	18.03	17.77	0.26	23.08	19.39	19.13	0.26
	Pr	-19.39	-19.36	-18	-1.36	-18.75	-18.72	-17.35	-1.37	-18.94	-18.91	-17.54	-1.37
2	R	0	0	0	0	0	0	0	0	0	0	0	0
	TS	22.62	20.9	18.75	2.15	25.89	23.02	22.02	1.00	28.19	26.46	24.32	2.14
	Pr	-19.66	-16.79	-19.75	2.96	12.12	14.99	12.03	2.96	13.66	16.54	13.57	2.97
3	R	0	0	0	0	0	0	0	0	0	0	0	0
	TS	23.65	22.88	18.9	3.98	27.5	26.73	28.78	-2.05	28.69	27.92	23.95	3.97
	Pr	-14.23	-12.96	-14.28	1.32	-11.6	-10.32	-11.65	1.33	-13.74	-12.47	-13.79	1.32
4	R	0	0	0	0	0	0	0	0	0	0	0	0
	TS	25.01	24.29	21.68	2.61	27.33	26.62	24.01	2.61	30.77	30.05	27.44	2.61
	Pr	-6.26	-4.69	-4.93	0.24	-4.48	-2.91	-3.16	0.25	-5.26	-3.68	-3.93	0.25
5	R	0	0	0	0	0	0	0	0	0	0	0	0
	TS	29.3	27.86	25.62	2.24	32.15	30.71	28.47	2.24	34.12	32.69	30.44	2.25
	Pr	-9.88	-8.46	-8.41	-0.05	-7.69	-6.27	-6.22	-0.05	-9.11	-7.68	-7.64	-0.04
6	R	0	0	0	0	0	0	0	0	0	0	0	0
	TS	28.33	28.26	21.54	6.72	33	32.91	26.2	6.71	38.22	38.14	31.42	6.72
	Pr	-24.68	-23.23	-22.06	-1.17	-21.83	-20.38	-19.22	-1.16	-20.18	-18.73	-17.57	-1.16

[a]Energies relative to reactant for total electronic energy (ΔE) and activation free energy ($\Delta G^{\#}$, with thermal correction) using B3LYP, M06, ωB97X/6-311++G(d,p):AMBER//B3LYP/6-31G(d,p):AMBER. R = reactant, TS = transition state and Pr = product. (The TS optimized coordinates of enzyme-inhibitor complexes are provided in the supplementary material)

Based on the results shown in **Table 5.1** and **Figure 5.3**, compound **1** is the most reactive inhibitor in comparison to the other compounds.
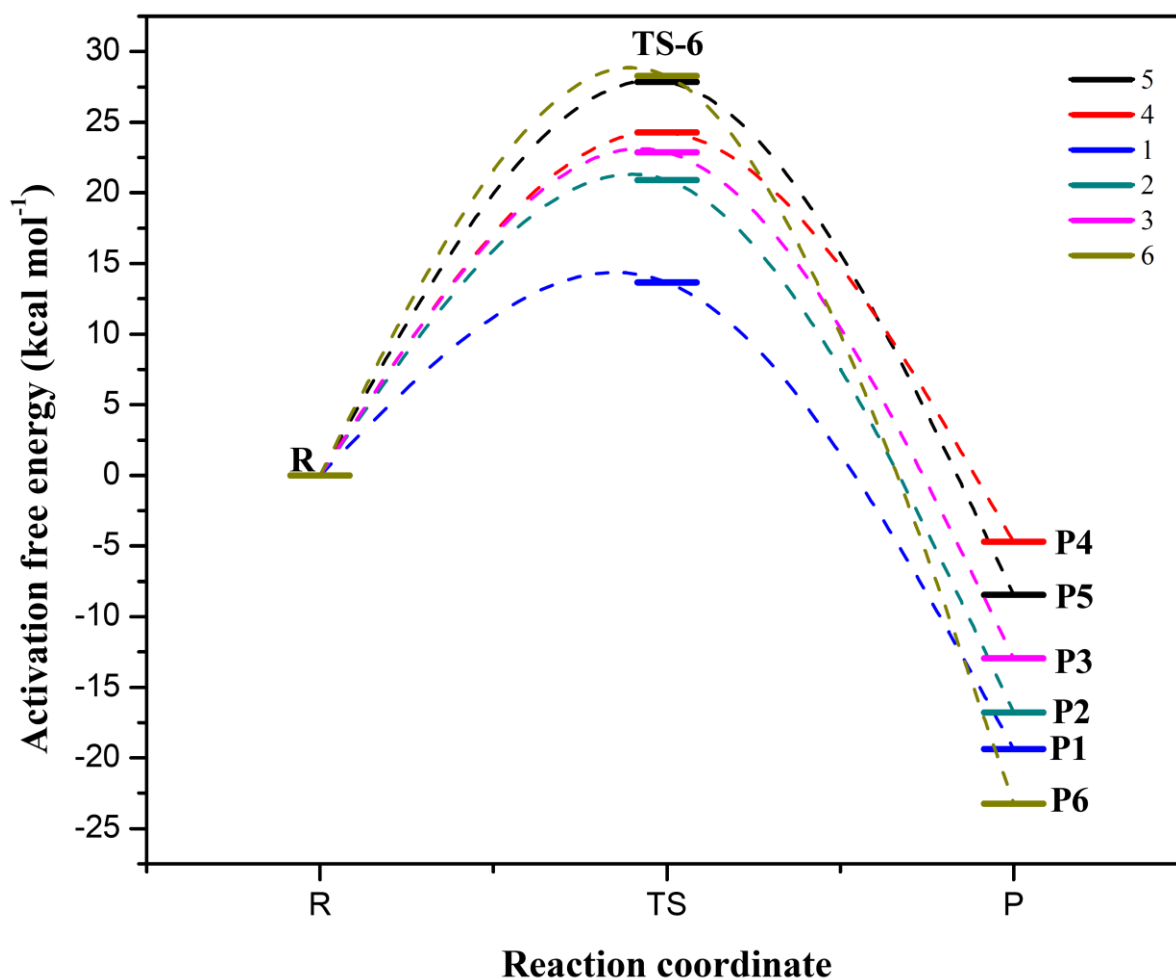
Figure 5.3 Gibbs free energy pathway for the 6-membered ring mechanism of inhibition of L,D-transpeptidase (Ldt$_{Mt5}$) by the β-lactams compounds obtained at (ONIOM) B3LYP/6-311++G(2d,2p):AMBER, extrapolated from **Table 1**. See **Fig. 1** for the structure of the inhibitors.

5.3.2 Frontier molecular orbitals and electrostatic potential mapping

The difference in the LUMO-HOMO, also known as the energy gap helps to characterize the chemical reactivity and kinetic stability of a molecule[44]. The frontier molecular orbitals (LUMO-HOMO) of the β-lactams plot is shown in **Figure S3**. This energy gap for the studied compounds calculated by B3LYP/6-31G(d,p) is presented in **Table S1**. The order of reactivity ranges from the lowest to highest in the order **2** < **1** < **3** < **4** < **5** < **6**. This order relatively follows the same order base on the $\Delta G^{\#}$ of the covalently bonded product formed after the acylation (**Table 5.1**), which indicates how fast or slow the kinetics of the reaction are. Molecular electrostatic potential (ESP) calculations of the transition states structures were surface mapped and this parameter was then used to depict the size, shape, charge density and reactive sites of the molecules[45, 46]. The mapped surface of the different compounds is presented in **Figure 5.4**. The values of the electrostatic potential are signified by various colours; red denotes the regions of the most negative electrostatic potential, blue signifies the regions of the most

positive electrostatic potential and green represents the region of zero potential[47]. **Figure 5.4** gives a pictorial representation of the nucleophilic sites and relative reactivity of atoms. It is evident in all the compounds that the site of nucleophilic attack between the Sγ and C3 atoms (red region) of cysteine and lactam ring respectively react with the electrophilic sites.
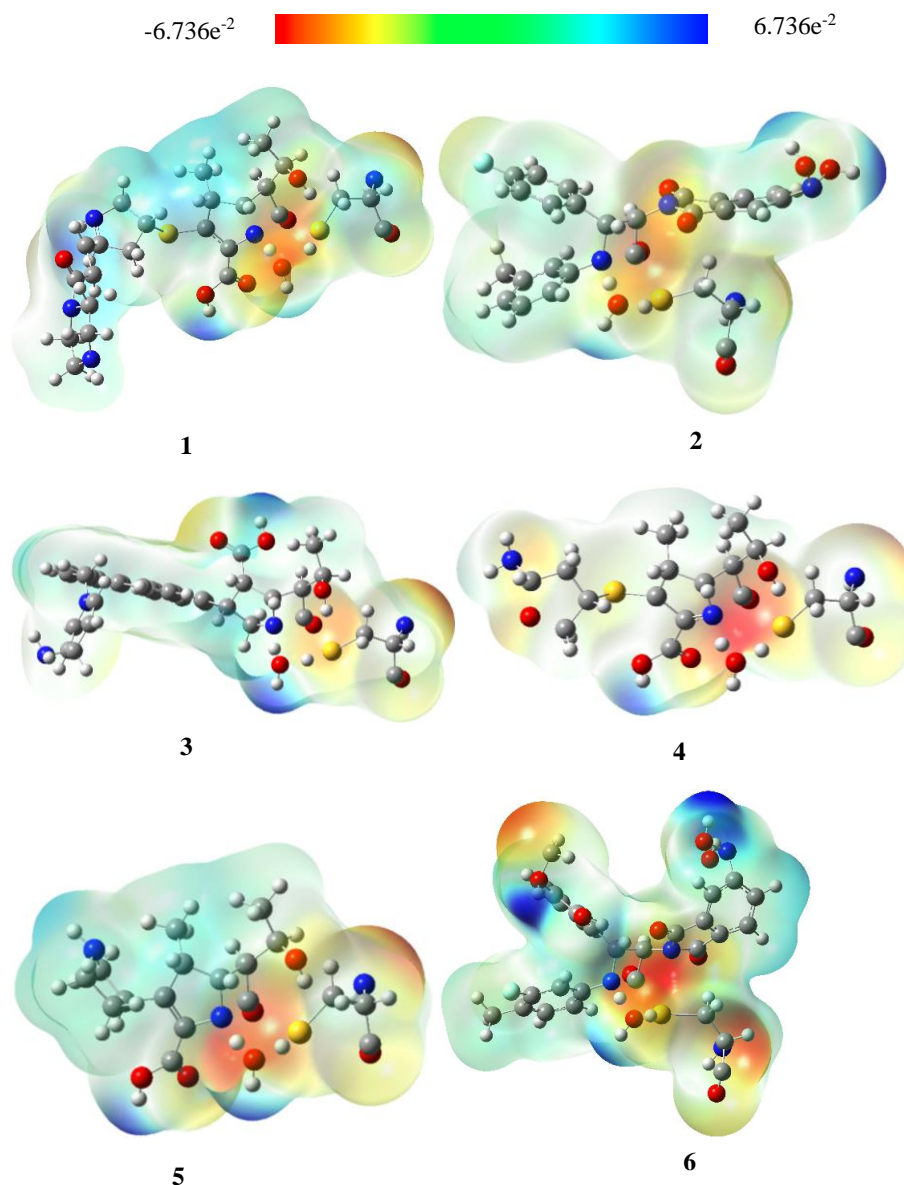
Figure 5.4 Molecular electrostatic potential surface of the selected β-lactams—Ldt$_{Mt5}$ calculated at the B3LYP/6-31 + G(d,p), mapped onto electron density (0.004 electrons per Å3) isosurfaces. The red regions correspond to the site most susceptible to nucleophilic attack. Blue and red regions represent positive and negative potential areas, respectively.

5.3.3 Natural bond orbital (NBO) analysis

Charge transfer, viz from a donor (bond or lone pair) to acceptor corresponding to a stabilizing donor-acceptor interaction can be calculated using NBO analysis. The charge transfer between the β-lactam-

Ldt$_{Mt5}$ complexes is of paramount importance. The resulted donor, acceptor orbitals and energy of stabilization E^2 is derived from the second-perturbation theory[48, 49]. A larger E^2 value indicates a stronger interaction between the electron-donors and electron-acceptors, *i.e.* the more donating tendency from donors to acceptors the greater the extent of conjugation of the whole system[50]. In other words, a larger E^2 value contributes to a lower energy. The pictorial representation of the electron transfer for lactams—Ldt$_{Mt5}$ complexes derived from this analysis is shown in **Figure 5.5**.
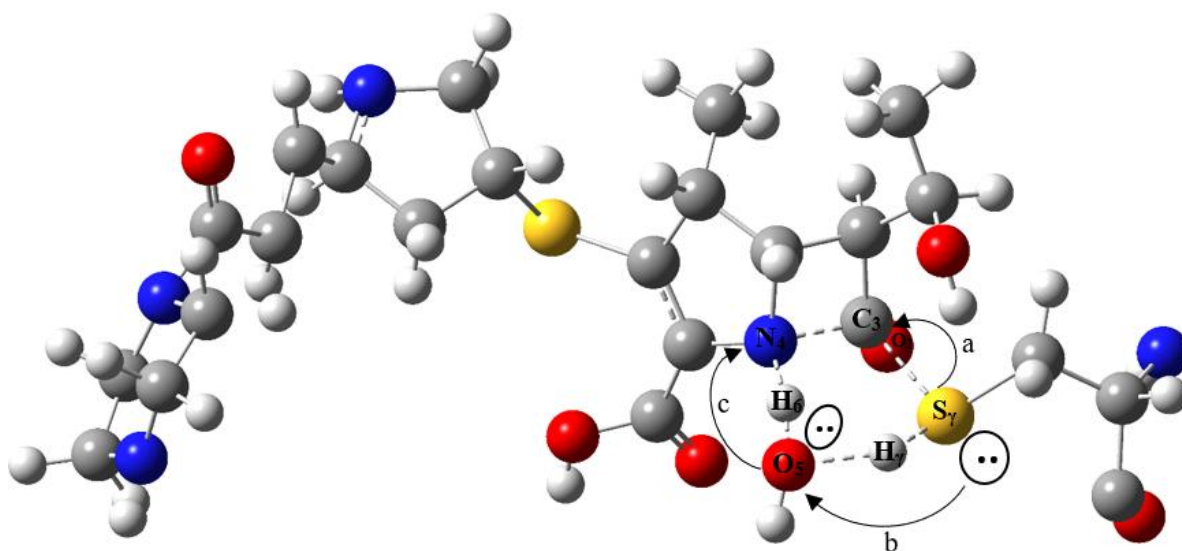
Figure 5.5 Depiction of electron transfer for β-lactams/Ldt$_{Mt5}$ complexes derived from second-order perturbation theory of NBO analysis. The curved arrows (a, b and c) depict the direction of charge transfer from lone pair to antibonding (LP→σ*). (The TS optimized coordinates are provided in the supplementary material)

As presented in **Table 5.2**, the 6-membered ring, stabilization energy E^2 for the nucleophilic attack on the carbonyl group of compounds **4**, **3**, **5**, **6**, **2** and **1** by the thiol group of Cys360 are 8.01, 6.16, 5.49, 3.40, 1.87 and 0.91 kcal mol^{-1} respectively. These values showed that the carbapenems have a more nucleophilic attack in comparison to the monobactam. The E^2 value of the 6-membered ring transition states for each complex from a lone pair (LP) of the Sγ atom of the donor to the acceptor (C3). The concerted proton transfer to the *β*-lactam nitrogen (LP(N$_β$)-LP*(H$_e$)) revealed compound **5** and **6** (1.64 and 1.49 kcal mol^{-1}, respectively) as the highest while compound **2** (1.00 kcal mol^{-1}) the lowest. The result follows a similar trend with the activation energies of compound **5** and **6** having lower activation energies.

Table 5.2 Second-order perturbation stabilization energies corresponding to the core intermolecular charge transfer interaction (Donor to Acceptor) of the Ldt_{Mt5} for 6-membered transition states of carbapenems obtained at B3LYP/6-311++G(d,p).

Donor	Acceptor	E2(kcal/mol)
1		
LP (Sγ)	δ*(C3-O2)	0.91
LP (H42)	δ*(N6-C7)	1.06
2		
LP (Sγ)	δ*(C3-O2)	1.87
LP*(H21)	δ*(N2-C3)	1
3		
LP (Sγ)	δ*(C3-O2)	6.16
LP*(H21)	δ*(N2-C30)	1.17
4		
LP (Sγ)	δ*(C3-O2)	8.01
LP*(O-H21)	δ*(N2-C3)	0.14
5		
LP (Sγ)	δ*(C3-O2)	5.49
LP (H41)	δ*(N5-C9)	1.64
6		
LP (Sγ)	δ*(C3-O2)	3.4
LP* (H20)	δ*(N1-C4)	1.49

5.4 Conclusion

Due to the relatively weak *in vitro* inhibition of Ldt_{Mt5} by the carbapenems drugs currently employed, we used the *β*-lactam ring as a scaffold to screen similar compounds in the ZINC database to see their kinetic behaviour with this enzyme. In this study, we investigated the acylation step of Ldt_{Mt5} by employing QM/MM (ONIOM) calculations. The 6-membered ring mechanisms were investigated for the acylation reaction path of Ldt_{Mt5} with six selected *β*-lactams from the ZINC database. The activation free energy ($\Delta G^{\#}$) obtained from the 6-membered ring TS reveal that all the *β*-lactams were thermodynamically favourable than previously calculated $\Delta G^{\#}$ for imipenem and meropenem complexed with Ldt_{Mt5}. Meropenem and imipenem were tested experimentally against Ldt_{Mt5}, both drugs were reported to show slow acylation which indicates possibly higher activation energies. The obtained results are comparable to that observed for Ldt_{Mt2} albeit, for compound **1** the activation energy is considerably lower than that obtained for meropenem and imipenem in complexed with Ldt_{Mt2}. This suggests that compound 1 should, in theory, be a very potent inhibitor of Ldt_{Mt5}.

The LUMO-HOMO energy gap values of the compounds are small suggestive of their structural stability. ESP revealed that the site of reaction is chemically active sites viz the interaction of the lactam ring with the cysteine of Ldt_{Mt5}. It is important to stress that this study has in addition to the previous efficacy reported for carbapenems, the selected β-lactam derivatives showed a lower energy barrier difference found in acylation with these new derivatives against Ldt_{Mt5}. Consequently, these findings should be subject to experimental bioactivities of this enzyme, more specific binding thermodynamics assays i.e. isothermal titration calorimetry. Feedback from that will assist us to better validate our theoretical model and aid rational design of new compounds and potential drug candidates with higher inhibitory activity against *Mtb*.

Competing interests

The authors declare no competing interests.

References

[1] Lonsdale, R., Harvey, J. N., and Mulholland, A. J. (2012) A practical guide to modelling enzyme-catalysed reactions, *Chemical Society Reviews 41*, 3025-3038.

[2] Correale, S., Ruggiero, A., Capparelli, R., Pedone, E., and Berisio, R. (2013) Structures of free and inhibited forms of the L, D-transpeptidase LdtMt1 from Mycobacterium tuberculosis, *Acta Crystallographica Section D: Biological Crystallography 69*, 1697-1706.

[3] Fisher, J. F., Meroueh, S. O., and Mobashery, S. (2005) Bacterial resistance to β-lactam antibiotics: compelling opportunism, compelling opportunity, *Chemical reviews 105*, 395-424.

[4] Hugonnet, J.-E., Tremblay, L. W., Boshoff, H. I., Barry, C. E., and Blanchard, J. S. (2009) Meropenem-clavulanate is effective against extensively drug-resistant Mycobacterium tuberculosis, *Science 323*, 1215-1218.

[5] Lavollay, M., Arthur, M., Fourgeaud, M., Dubost, L., Marie, A., Veziris, N., Blanot, D., Gutmann, L., and Mainardi, J.-L. (2008) The peptidoglycan of stationary-phase Mycobacterium tuberculosis predominantly contains cross-links generated by L, D-transpeptidation, *Journal of Bacteriology 190*, 4360-4366.

[6] Mainardi, J.-L., Fourgeaud, M., Hugonnet, J.-E., Dubost, L., Brouard, J.-P., Ouazzani, J., Rice, L. B., Gutmann, L., and Arthur, M. (2005) A novel peptidoglycan cross-linking enzyme for a β-lactam-resistant transpeptidation pathway, *Journal of Biological Chemistry 280*, 38146-38152.

[7] Mainardi, J.-L., Hugonnet, J.-E., Rusconi, F., Fourgeaud, M., Dubost, L., Moumi, A. N., Delfosse, V., Mayer, C., Gutmann, L., and Rice, L. B. (2007) Unexpected inhibition of peptidoglycan ld-transpeptidase from Enterococcus faecium by the β-lactam imipenem, *Journal of Biological Chemistry 282*, 30414-30422.

[8] Mainardi, J.-L., Villet, R., Bugg, T. D., Mayer, C., and Arthur, M. (2008) Evolution of peptidoglycan biosynthesis under the selective pressure of antibiotics in Gram-positive bacteria, *FEMS microbiology reviews 32*, 386-408.

[9] Tipper, D. J., and Strominger, J. L. (1965) Mechanism of action of penicillins: a proposal based on their structural similarity to acyl-D-alanyl-D-alanine, *Proceedings of the National Academy of Sciences 54*, 1133-1141.

[10] Erdemli, S. B., Gupta, R., Bishai, W. R., Lamichhane, G., Amzel, L. M., and Bianchet, M. A. (2012) Targeting the cell wall of Mycobacterium tuberculosis: structure and mechanism of L, D-transpeptidase 2, *Structure 20*, 2103-2115.

[11] Gupta, R., Lavollay, M., Mainardi, J.-L., Arthur, M., Bishai, W. R., and Lamichhane, G. (2010) The Mycobacterium tuberculosis protein LdtMt2 is a nonclassical transpeptidase required for virulence and resistance to amoxicillin, *Nature Medicine 16*, 466-469.

[12] Brammer, B. L., Ghosh, A., Pan, Y., Jakoncic, J., Lloyd, E., Townsend, C., Lamichhane, G., and Bianchet, M. (2015) Loss of a Functionally and Structurally Distinct ld-Transpeptidase, LdtMt5, Compromises Cell Wall Integrity in Mycobacterium tuberculosis, *The Journal of Biological Chemistry 290*, 25670-25685.

[13] Vicik, R., Busemann, M., Baumann, K., and Schirmeister, T. (2006) Inhibitors of cysteine proteases, *Current topics in medicinal chemistry 6*, 331-353.

[14] Cordillot, M., Dubée, V., Triboulet, S., Dubost, L., Marie, A., Hugonnet, J.-E., Arthur, M., and Mainardi, J.-L. (2013) In vitro cross-linking of Mycobacterium tuberculosis peptidoglycan by l, d-transpeptidases and inactivation of these enzymes by carbapenems, *Antimicrobial agents and chemotherapy 57*, 5940-5945.

[15] Kohanski, M. A., Dwyer, D. J., and Collins, J. J. (2010) How antibiotics kill bacteria: from targets to networks, *Nature Reviews Microbiology 8*, 423.

[16] Silva, J. R. r. A., Roitberg, A. E., and Alves, C. u. N. (2014) Catalytic mechanism of L, D-transpeptidase 2 from Mycobacterium tuberculosis described by a computational approach: insights for the design of new antibiotics drugs, *Journal of Chemical Information and Modeling 54*, 2402-2410.

[17] Fakhar, Z., Govender, T., Lamichhane, G., Maguire, G. E., Kruger, H. G., and Honarparvar, B. (2017) Computational model for the acylation step of the β-lactam ring: Potential application for l, d-transpeptidase 2 in mycobacterium tuberculosis, *Journal of Molecular Structure 1128*, 94-102.

[18] Fakhar, Z., Govender, T., Lamichhane, G., Maguire, G. E. M., Kruger, H. G., and Honarparvar, B. (2017) Computational model for the acylation step of the β-lactam ring: Potential application for l,d-transpeptidase 2 in mycobacterium tuberculosis, *Journal of Molecular Structure 1128*, 94-102.

[19] Silva, J. R., Roitberg, A. E., and Alves, C. N. (2014) Catalytic mechanism of L,D-transpeptidase 2 from Mycobacterium tuberculosis described by a computational approach: insights for the design of new antibiotics drugs, *Journal of chemical information and modeling 54*, 2402-2410.

[20] Dapprich, S., Komáromi, I., Byun, K. S., Morokuma, K., and Frisch, M. J. (1999) A new ONIOM implementation in Gaussian98. Part I. The calculation of energies, gradients, vibrational frequencies and electric field derivatives, *Journal of Molecular Structure: THEOCHEM 461*, 1-21.

[21] Berman, H. M., Westbrook, J., Feng, Z., Gilliland, G., Bhat, T. N., Weissig, H., Shindyalov, I. N., and Bourne, P. E. (2006) The protein data bank, 1999–, In *International Tables for Crystallography Volume F: Crystallography of biological macromolecules*, pp 675-684, Springer.

[22] Irwin, J. J., and Shoichet, B. K. (2005) ZINC− A free database of commercially available compounds for virtual screening, *Journal of chemical information and modeling 45*, 177-182.

[23] Hornak, V., Abel, R., Okur, A., Strockbine, B., Roitberg, A., and Simmerling, C. (2006) Comparison of multiple Amber force fields and development of improved protein backbone parameters, *Proteins: Structure, Function, and Bioinformatics 65*, 712-725.

[24] Wang, J., Wolf, R. M., Caldwell, J. W., Kollman, P. A., and Case, D. A. (2004) Development and testing of a general amber force field, *Journal of computational chemistry 25*, 1157-1174.

[25] Fakhar, Z., Govender, T., Maguire, G. E., Lamichhane, G., Walker, R. C., Kruger, H. G., and Honarparvar, B. (2017) Differential flap dynamics in l, d-transpeptidase2 from

mycobacterium tuberculosis revealed by molecular dynamics, *Molecular BioSystems 13*, 1223-1234.

[26] Harvey, M., and De Fabritiis, G. (2009) An implementation of the smooth particle mesh Ewald method on GPU hardware, *Journal of chemical theory and computation 5*, 2371-2377.

[27] Kräutler, V., Van Gunsteren, W. F., and Hünenberger, P. H. (2001) A fast SHAKE algorithm to solve distance constraint equations for small molecules in molecular dynamics simulations, *Journal of computational chemistry 22*, 501-508.

[28] Ibeji, C. U., Tolufashe, G. F., Ntombela, T., Govender, T., Maguire, G. E., Lamichhane, G., Kruger, H. G., and Honarparvar, B. (2018) The catalytic role of water in the binding site of L, D-Transpeptidase 2 within acylation mechanism: A QM/MM (ONIOM) modeling, *Tuberculosis*.

[29] Calixto, A. R., Brás, N. r. F., Fernandes, P. A., and Ramos, M. J. (2014) Reaction mechanism of human renin studied by quantum mechanics/molecular mechanics (QM/MM) calculations, *Acs Catalysis 4*, 3869-3876.

[30] Zhou, J., Tao, P., Fisher, J. F., Shi, Q., Mobashery, S., and Schlegel, H. B. (2010) QM/MM studies of the matrix metalloproteinase 2 (MMP2) inhibition mechanism of (S)-SB-3CT and its oxirane analogue, *Journal of chemical theory and computation 6*, 3580-3587.

[31] Cao, Y., Han, S., Yu, L., Qian, H., and Chen, J.-Z. (2014) MD and QM/MM studies on long-chain L-α-hydroxy acid oxidase: substrate binding features and oxidation mechanism, *The Journal of Physical Chemistry B 118*, 5406-5417.

[32] Silva, J. R. A., Bishai, W. R., Govender, T., Lamichhane, G., Maguire, G. E., Kruger, H. G., Lameira, J., and Alves, C. N. (2016) Targeting the cell wall of Mycobacterium tuberculosis: a molecular modeling investigation of the interaction of imipenem and meropenem with L, D-transpeptidase 2, *Journal of Biomolecular Structure and Dynamics 34*, 304-317.

[33] Ribeiro, A. J., Yang, L., Ramos, M. J., Fernandes, P. A., Liang, Z.-X., and Hirao, H. (2015) Insight into enzymatic nitrile reduction: QM/MM study of the catalytic mechanism of QueF nitrile reductase, *ACS Catalysis 5*, 3740-3751.

[34] Milhøj, B. O., and Sauer, S. P. (2015) Kinetics and thermodynamics of the reaction between the• OH radical and adenine: a theoretical investigation, *The Journal of Physical Chemistry A 119*, 6516-6527.

[35] Goerigk, L., and Grimme, S. (2011) A thorough benchmark of density functional methods for general main group thermochemistry, kinetics, and noncovalent interactions, *Physical Chemistry Chemical Physics 13*, 6670-6688.

[36] Gangadharan, R. P., and Krishnan, S. S. (2014) Natural Bond Orbital (NBO) Population Analysis of 1-Azanapthalene-8-ol, *Acta Physica Polonica, A. 125*.

[37] Glendening, E. D., Landis, C. R., and Weinhold, F. (2012) Natural bond orbital methods, *Wiley interdisciplinary reviews: computational molecular science 2*, 1-42.

[38] Sitha, S., and Bhanuprakash, K. (2006) Role of aromatic π-bridge on electron transport property in a donor–bridge–acceptor system: A computational study on frontier molecular orbitals, *Journal of Molecular Structure: THEOCHEM 761*, 31-38.

[39] Bradley, J., and Gerrans, G. (1973) Frontier molecular orbitals. A link between kinetics and bonding theory, *Journal of Chemical Education 50*, 463.

[40] Runge, E. (1985) 52 (1984) 997; EK Gross, W. Kohn, *Phys. Rev. Lett 55*, 2850.

[41] Suendo, V., and Viridi, S. (2011) Ab initio calculation of UV-Vis absorption spectra of a single molecule chlorophyll a: Comparison study between RHF/CIS, TDDFT, and semi-empirical methods, *arXiv preprint arXiv:1105.3766*.

[42] Adejoro, I., Tolufashe, F., and Ibeji, C. Density Functional Theory (DFT) Study of a new 4-[(Z)-phenyldiazenyl]-2H-Chromen-2-one Dye for Its Use as Sensitizer in Molecular Photovoltaics.

[43] Gideon F. Tolufashe, T. G., Amit K. Halder, Collins U. Ibeji1, Monsurat M. Lawal, Thandokuhle Ntombela, Glenn E. M. Maguire, Gyanu Lamichhane, Hendrik G. Kruger and Bahareh Honarparvar. (2018) Inhibition of Mycobacterium tuberculosis L,D-transpeptidase 5 by carbapenems: MD and QM/MM Mechanistic Studies *Journal of Computer-aided Molecular Design, Submitted for publication*.

[44] Uesugi, Y., Mizuno, M., Shimojima, A., and Takahashi, H. (1997) Transient resonance Raman and ab initio MO calculation studies of the structures and vibrational assignments of the T1

state and the anion radical of coumarin and its isotopically substituted analogues, *The Journal of Physical Chemistry A 101*, 268-274.

[45] Alkorta, I., and Perez, J. J. (1996) Molecular polarization potential maps of the nucleic acid bases, *International Journal of Quantum Chemistry 57*, 123-135.

[46] Murray, J. S., and Politzer, P. (2003) Molecular electrostatic potentials, In *Computational Medicinal Chemistry for Drug Discovery*, pp 231-254, CRC Press.

[47] Sethi, A., and Prakash, R. (2015) Novel synthetic ester of Brassicasterol, DFT investigation including NBO, NLO response, reactivity descriptor and its intramolecular interactions analyzed by AIM theory, *Journal of Molecular Structure 1083*, 72-81.

[48] James, C., Raj, A. A., Reghunathan, R., Jayakumar, V., and Joe, I. H. (2006) Structural conformation and vibrational spectroscopic studies of 2, 6-bis (p-N, N-dimethyl benzylidene) cyclohexanone using density functional theory, *Journal of Raman Spectroscopy 37*, 1381-1392.

[49] Liu, J.-n., Chen, Z.-r., and Yuan, S.-f. (2005) Study on the prediction of visible absorption maxima of azobenzene compounds, *Journal of Zhejiang University. Science. B 6*, 584.

[50] Balachandran, V., and Parimala, K. (2012) Tautomeric purine forms of 2-amino-6-chloropurine (N 9 H 10 and N 7 H 10): Structures, vibrational assignments, NBO analysis, hyperpolarizability, HOMO–LUMO study using B3 based density functional calculations, *Spectrochimica Acta Part A: Molecular and Biomolecular Spectroscopy 96*, 340-351.

CHAPTER SIX

Conclusion

Tuberculosis is one of the most deadly human infectious diseases and research in the area has led to significant and promising insights into combating this devastating disease[1]. The incidence of the epidemics of HIV/AIDS, diabetes, and multidrug resistance have contributed to the susceptibility of TB globally. Transpeptidases catalyze the polymerization of the peptidoglycan cell wall of *Mtb* and since mycobacteria cannot survive without PG, inhibiting its synthesis can be a powerful way to kill *Mtb*. The genome of *Mtb* encodes five Ldt paralogs, namely Ldt$_{Mt1}$ to Ldt$_{Mt5}$. Any *Mtb* strain that lacks a functional copy of an Ldt, namely L,D-transpeptidase 5 (Ldt$_{Mt5}$), displays aberrant growth and this phenotype is more susceptible to killing by cell wall perturbing agents. These include carbapenems, which are considered the last resort antibiotics to treat resistant bacterial infections in humans. Carbapenems, a class of β-lactams, are more effective against LDTs responsible for the synthesis of PG in *Mtb*. Despite incredible contributions worldwide on understanding the mechanism of L,D-transpeptidases inhibition (from *Mtb*) with respect to carbapenems, there are significant gaps yet to be addressed by researchers.

In this thesis, the introductory chapter provides a summary of the necessary background for the rest of the thesis (Chapter one). A detailed literature review (up to date) on the structure and function of L,D- and D,D-transpeptidase family of enzymes from *Mycobacterium tuberculosis* was presented in Chapter two. The study summarizes the experimental and computational studies on L,D transpeptidases in *Mtb* that have been identified and validated. The reported structures of L,D- and D,D-transpeptidases, as well as their functionalities, were reviewed and the proposed enzymatic mechanisms for L,D-transpeptidases were summarized. In addition, we provided bioactivities of known *M. tuberculosis* drugs against these enzymes based on both experimental and computational approaches. In *Mtb*, 80% of the peptidoglycan layer has been reported [2, 3] to be crosslinked by L,D-transpeptidases. Peptidoglycan is the exoskeleton of bacterial cells required for their survival and growth, therefore, Ldts that generate these linkages are potentially attractive targets for the development of new drugs to treat drug-resistant TB. Among the five paralogs of Ldts present in *Mtb*, Ldt$_{Mt2}$ is the commonly investigated. Ldt$_{Mt5}$ has been reported to be essential for proper maintenance of cell wall integrity of the bacteria but carbapenems showed negligible activity against it.

Our group has previously studied the mechanism of carbapenems against Ltd$_{Mt2}$[4-6]. In contrast to Ldt$_{Mt5}$, carbapenems are very effective against Ldt$_{Mt2}$. This prompted us to investigate the inhibition mechanism of Ldt$_{Mt5}$ against carbapenems using molecular dynamics and hybrid QM/MM methods. The acylation mechanism of carbapenem—Ldt$_{Mt5}$ in which the process occurs *via* a cyclic transition state (TS) as proposed earlier for L,D-transpeptidases[7] was adopted for this study[4].

The first computational study was targeted at understanding the inhibition mechanism of carbapenems against Ldt$_{Mt5}$ (Chapter three). The binding free energies (including entropy contributions) of these complexes were calculated from the MD simulation using an MM/GBSA approach, the theoretical results revealed the best ΔG_{bind} for ERT—Ldt$_{Mt5}$ followed by IMI—Ldt$_{Mt5}$ then MERO—Ldt$_{Mt5}$. The

theoretical results revealed important interactions between the carbapenems on the following residues ARG297, MET316, GLU328, GLY338, GLU339, CYS360, HIS342, ASN358 and THR357 by per residue free energy decomposition and the hydrogen bonding analysis. These interactions were also observed experimentally[8]. In addition, the average binding affinities of Ldt_{Mt5} complexes were found to be less than that for Ldt_{Mt2} complexes, as expected. Furthermore, the relative higher free energies of activation obtained from the mechanistic studies also support the weak binding of Ldt_{Mt5} against the selected carbapenems. This study, therefore, confirms that the computational inhibitor-enzyme pre-complex model for L,D-transpeptidase 5 correctly reflects experimental observations[8] in terms of the activity and the free binding energies.

In the second investigation, virtual screening of compounds from the ZINC database against Ldt_{Mt5} was investigated with AutoDock Vina and Schrödinger Maestro software programs (Chapter Four). The obtained docking scores gave a reasonable number of potential lead compounds, which can be utilized as potential drug candidates against Ldt_{Mt5}. Despite the lack of overlap on the screened compounds using these two different software programs, both provided reasonable binding scores. The two docking programs gave completely different results in terms of the specific drugs that were identified based on the respective scoring functions[9]. Similar variations have been previously reported[9-11]. In order to validate the docking results against a better method, the screened lead compounds were subjected to molecular dynamics simulations and free binding energies calculated using the MM-GBSA approach. The free binding energies of these compounds in this study against Ldt_{Mt5} showed better binding compared to meropenem and imipenem and are also comparable to those reported for Ldt_{Mt2} experimentally[7, 12, 13]. The outcome of this study provides insight into the design of potential novel leads for Ldt_{Mt5}.

The 6-membered ring mechanisms were investigated for the acylation reaction path of Ldt_{Mt5} with six selected β-lactams from the previous study (Chapter 4) using hybrid QM/MM calculations (Chapter five). The activation free energy ($\Delta G^{\#}$) obtained from the 6-membered ring TS reveal that all the β-lactams were more thermodynamically favourable than previously calculated $\Delta G^{\#}$ for imipenem and meropenem complexed with Ldt_{Mt5}. Meropenem and imipenem were tested experimentally against Ldt_{Mt5}[8], and both drugs were reported to show slow acylation, which indicates possibly higher activation energies. The selected β-lactam derivatives against Ldt_{Mt5} showed a lower energy barrier difference for the acylation step than that calculated for meropenem and imipenem. Consequently, these findings mean that bioactivity experiments on this enzyme, more specific binding thermodynamics assays (isothermal titration calorimetry) need to be undertaken. This will assist in further validation of our theoretical model and aid rational design of new compounds and potential drug candidates with higher inhibitory activity against *Mtb*. The entire work is thus summarized in this section (Chapter six) to provide an overall conclusion on the present study.

Future studies should include an adequately long molecular dynamics study of the enzyme with carbapenems to explore the significant loop regions responsible for the catalytic mechanism of the target as well as target-inhibitor interactions at the atomic level. In addition, new β-lactams compounds should be computed against this enzyme with lower activation energies leading to improved bioactivity. The computational model should be improved by introducing more water molecules around the active site of the Cys360 catalytic residues that will be treated at least at semi-empirical level.

References

[1] Comas, I., and Gagneux, S. (2009) The past and future of tuberculosis research, *PLoS pathogens 5*, e1000600.

[2] Lavollay, M., Arthur, M., Fourgeaud, M., Dubost, L., Marie, A., Veziris, N., Blanot, D., Gutmann, L., and Mainardi, J.-L. (2008) The peptidoglycan of stationary-phase Mycobacterium tuberculosis predominantly contains cross-links generated by L, D-transpeptidation, *Journal of Bacteriology 190*, 4360-4366.

[3] Sauvage, E., Kerff, F., Terrak, M., Ayala, J. A., and Charlier, P. (2008) The penicillin-binding proteins: structure and role in peptidoglycan biosynthesis, *FEMS microbiology reviews 32*, 234-258.

[4] Fakhar, Z., Govender, T., Lamichhane, G., Maguire, G. E., Kruger, H. G., and Honarparvar, B. (2017) Computational model for the acylation step of the β-lactam ring: Potential application for l, d-transpeptidase 2 in mycobacterium tuberculosis, *Journal of Molecular Structure 1128*, 94-102.

[5] Ntombela, T., Fakhar, Z., Ibeji, C. U., Govender, T., Maguire, G. E., Lamichhane, G., Kruger, H. G., and Honarparvar, B. (2018) Molecular insight on the non-covalent interactions between carbapenems and l, d-transpeptidase 2 from Mycobacterium tuberculosis: ONIOM study, *Journal of Computer-Aided Molecular Design*, 1-15.

[6] Ibeji, C. U., Tolufashe, G. F., Ntombela, T., Govender, T., Maguire, G. E., Lamichhane, G., Kruger, H. G., and Honarparvar, B. (2018) The catalytic role of water in the binding site of L, D-Transpeptidase 2 within acylation mechanism: A QM/MM (ONIOM) modeling, *Tuberculosis*.

[7] Erdemli, S. B., Gupta, R., Bishai, W. R., Lamichhane, G., Amzel, L. M., and Bianchet, M. A. (2012) Targeting the cell wall of Mycobacterium tuberculosis: structure and mechanism of L, D-transpeptidase 2, *Structure 20*, 2103-2115.

[8] Brammer, B. L., Ghosh, A., Pan, Y., Jakoncic, J., Lloyd, E., Townsend, C., Lamichhane, G., and Bianchet, M. (2015) Loss of a Functionally and Structurally Distinct ld-Transpeptidase, LdtMt5, Compromises Cell Wall Integrity in Mycobacterium tuberculosis, *The Journal of Biological Chemistry 290*, 25670-25685.

[9] Huang, S.-Y., Grinter, S. Z., and Zou, X. (2010) Scoring functions and their evaluation methods for protein–ligand docking: recent advances and future directions, *Physical Chemistry Chemical Physics 12*, 12899-12908.

[10] Bissantz, C., Folkers, G., and Rognan, D. (2000) Protein-based virtual screening of chemical databases. 1. Evaluation of different docking/scoring combinations, *Journal of Medicinal Chemistry 43*, 4759-4767.

[11] Cummings, M. D., DesJarlais, R. L., Gibbs, A. C., Mohan, V., and Jaeger, E. P. (2005) Comparison of automated docking programs as virtual screening tools, *Journal of Medicinal Chemistry 48*, 962-976.

[12] Gupta, R., Lavollay, M., Mainardi, J.-L., Arthur, M., Bishai, W. R., and Lamichhane, G. (2010) The Mycobacterium tuberculosis protein LdtMt2 is a nonclassical transpeptidase required for virulence and resistance to amoxicillin, *Nature Medicine 16*, 466-469.

[13] Böth, D., Steiner, E. M., Stadler, D., Lindqvist, Y., Schnell, R., and Schneider, G. (2013) Structure of LdtMt2, an L, D-transpeptidase from Mycobacterium tuberculosis, *Acta Crystallographica Section D: Biological Crystallography 69*, 432-441.

Appendix 1. Supplementary material for Chapter 3

Table S1 The protonation states of the titratable Ldt$_{Mt5}$ residues at pH=7.

Residues	pKa
GLU 58	4.56
LYS 59	10.44
ARG 60	12.42
ARG 66	13.07
ARG 70	13.17
ASP 73	2.59
ASP 77	4.04
GLU 87	3.88
ASP 90	2.49
ARG 95	12.33
LYS 104	10.58
TYR 110	10.18
ARG 112	12.5
ASP 113	2.46
ARG 114	12.67
TYR 117	11.28
GLU 121	3.81
TYR 125	11.47
ASP 126	4.03
TYR 129	10.64
HIS 138	7.16
ASP 139	3.76
LYS 141	10.64
LYS 148	10.54
LYS 156	10.29
ASP 157	3.36
ASP 181	3.06
ASP 186	3.32
LYS 187	10.63
GLU 191	4.96
ASP 199	4.03
GLU 203	4.25

ASP 211	3.28
GLU 212	4.77
HIS 219	6.52
GLU 224	4.62
TYR 225	14.16
TYR 226	13.69
ASP 233	3.18
ASP 235	4.26
LYS 237	10.86
ASP 245	3.14
TYR 248	10.64
ASP 252	3.63
HIS 256	7.41
ARG 261	13.52
ARG 262	13
ARG 273	13.1
ASP 279	3.94
ASP 285	2.52
CYS 288	11.22
ASP 294	2.28
ARG 297	12.26
ARG 301	12.54
HIS 305	6.54
GLU 309	3.8
LYS 310	9.26
ASP 313	3.6
TYR 315	10.27
TYR 323	9.5
HIS 325	6.17
GLU 328	4.67
GLU 338	5.08
HIS 342	**6.48**
CYS 360	**12.67**
GLU 366	4.65
GLU 369	3.95
TYR 371	13.94
TYR 372	10.66
TYR 377	12.18
ASP 379	5.29
GLU 382	4.62
TYR 392	10.29

ASP 394	3.15
ASP 396	3.84
ASP 399	4.86
ASP 403	2.37
ASP 405	4.03
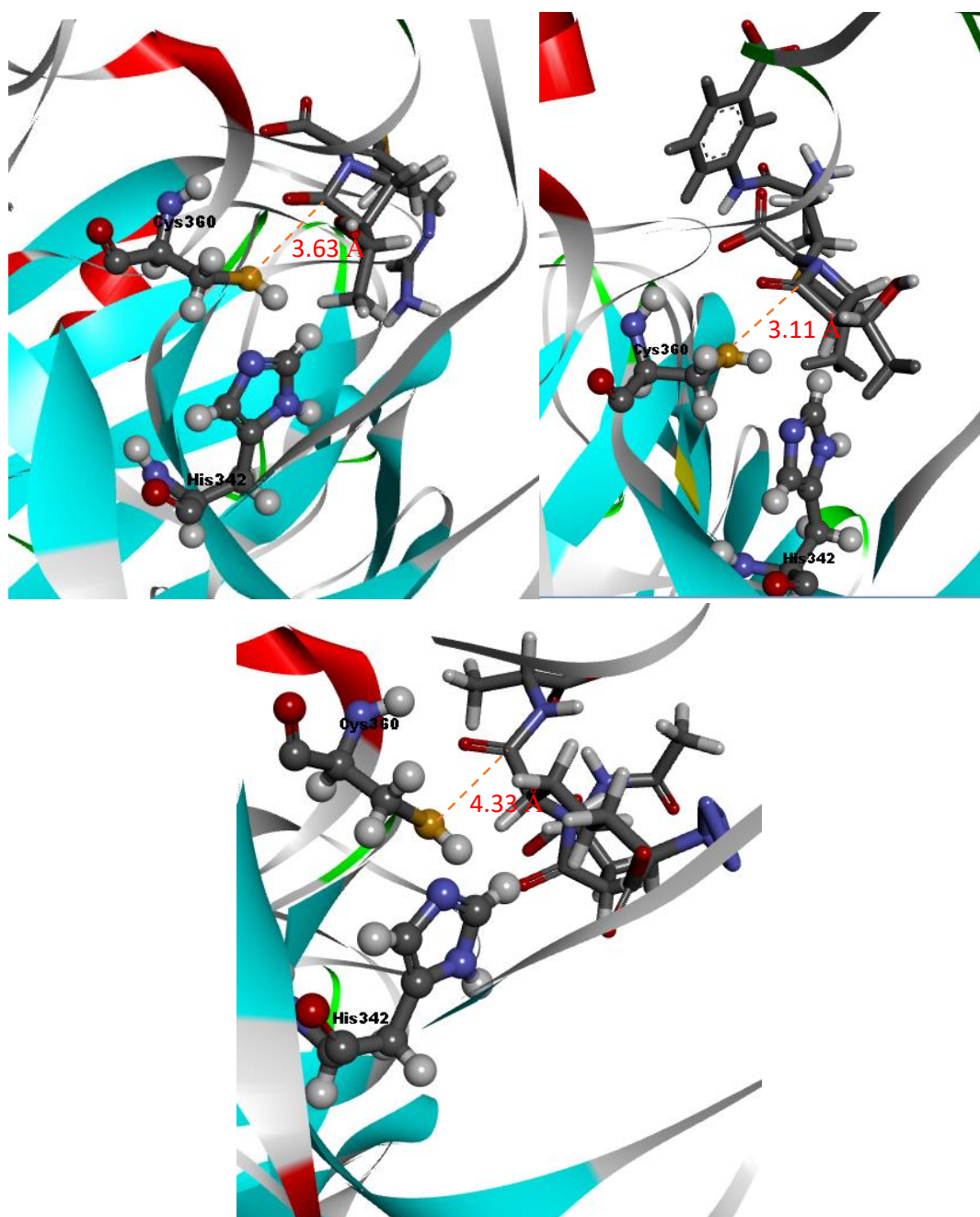
Figure S1 The 3D conformations for (A) Imipenem and (B) Ertapenem (C) Natural substrate in complex with Ldt_Mt5 enzyme obtained by molecular docking.
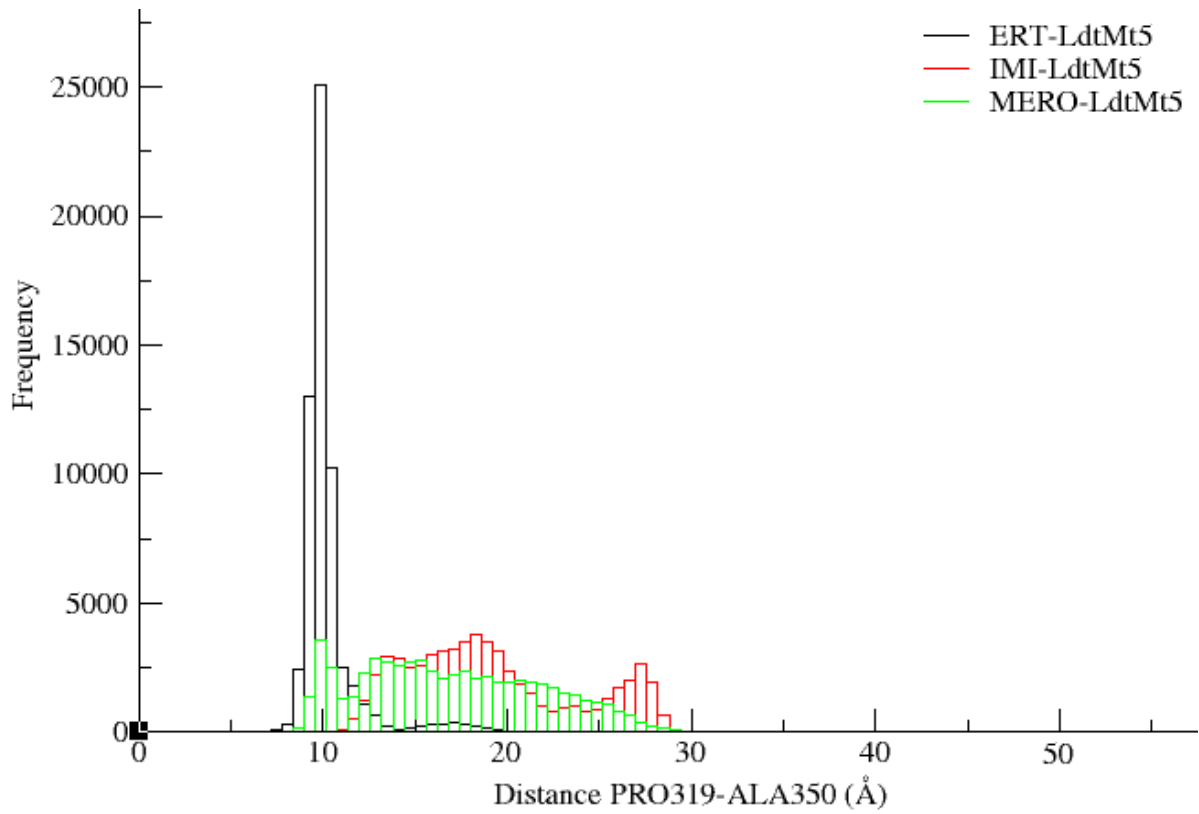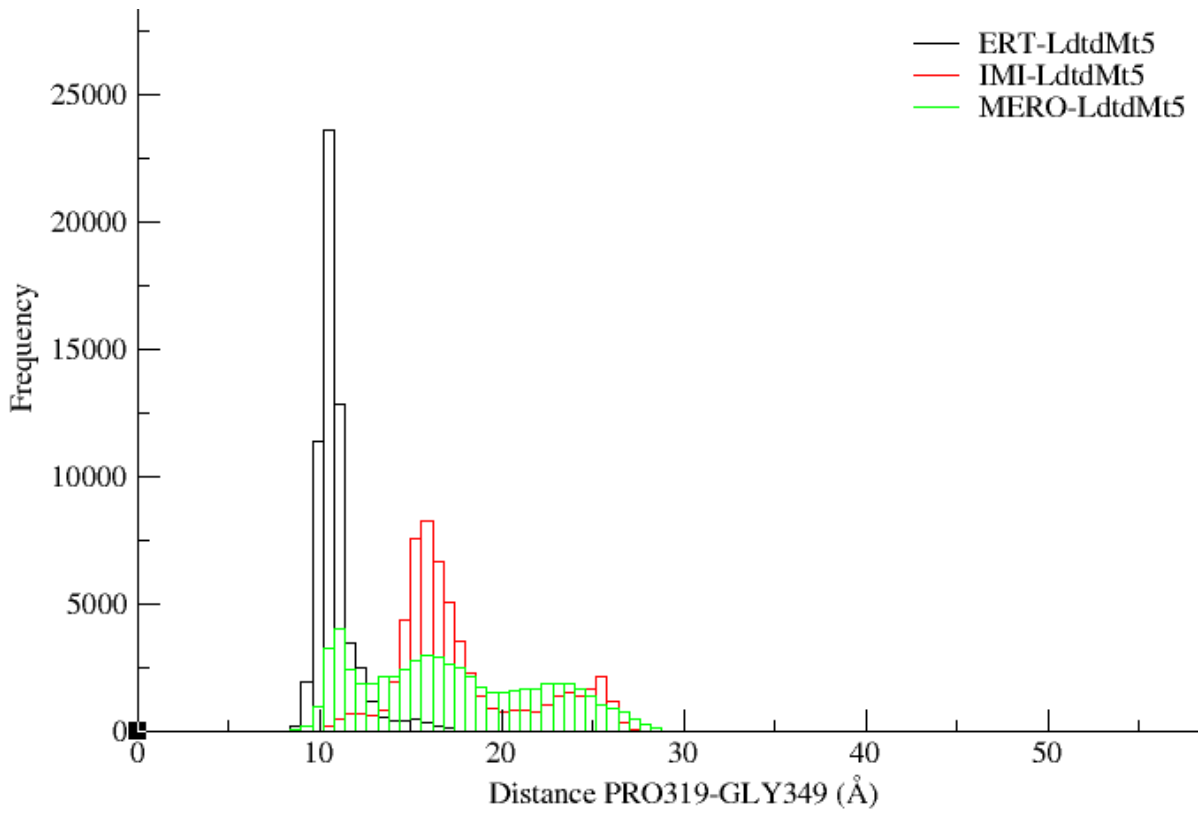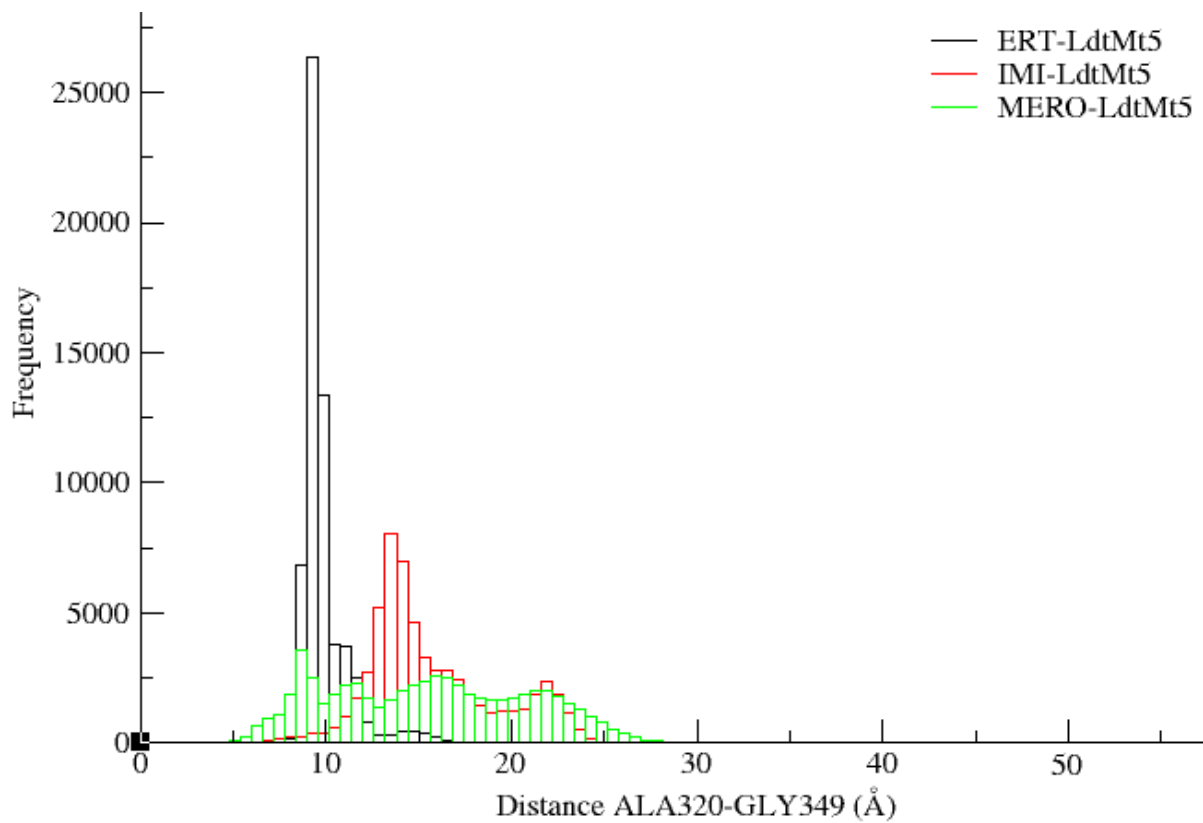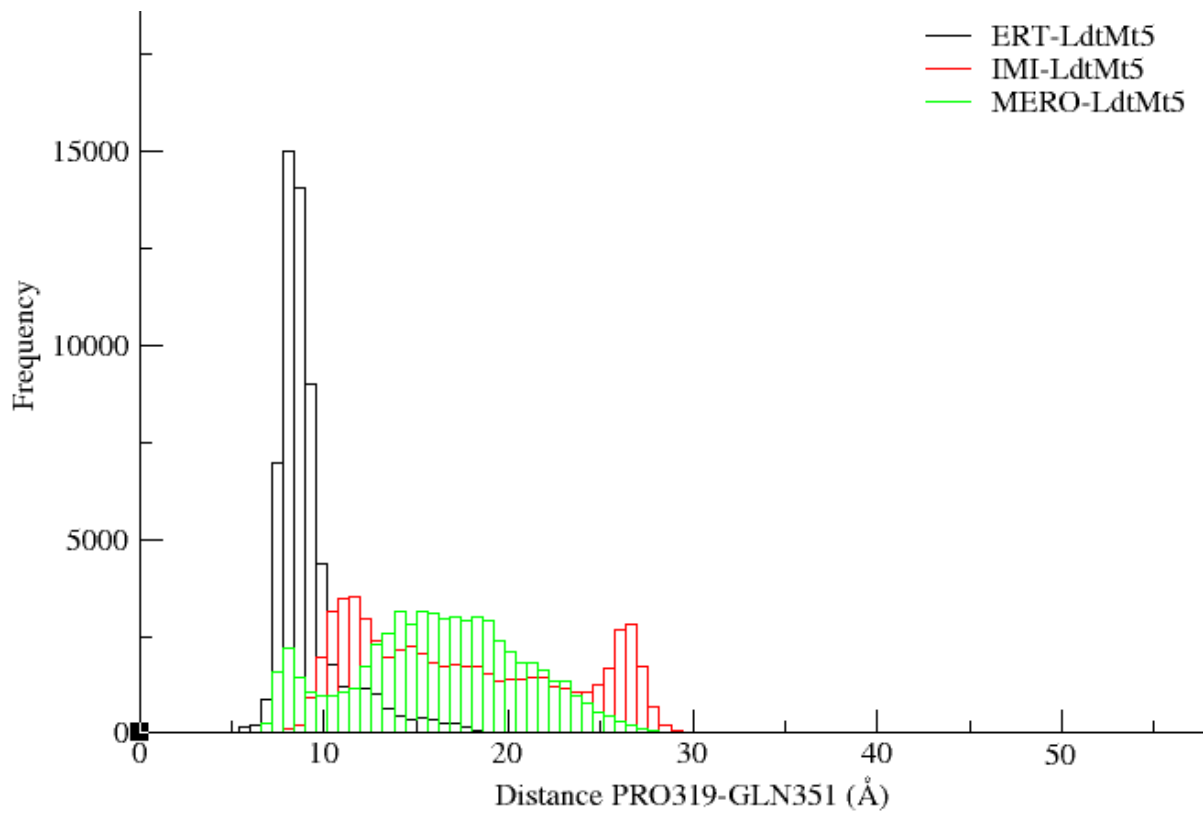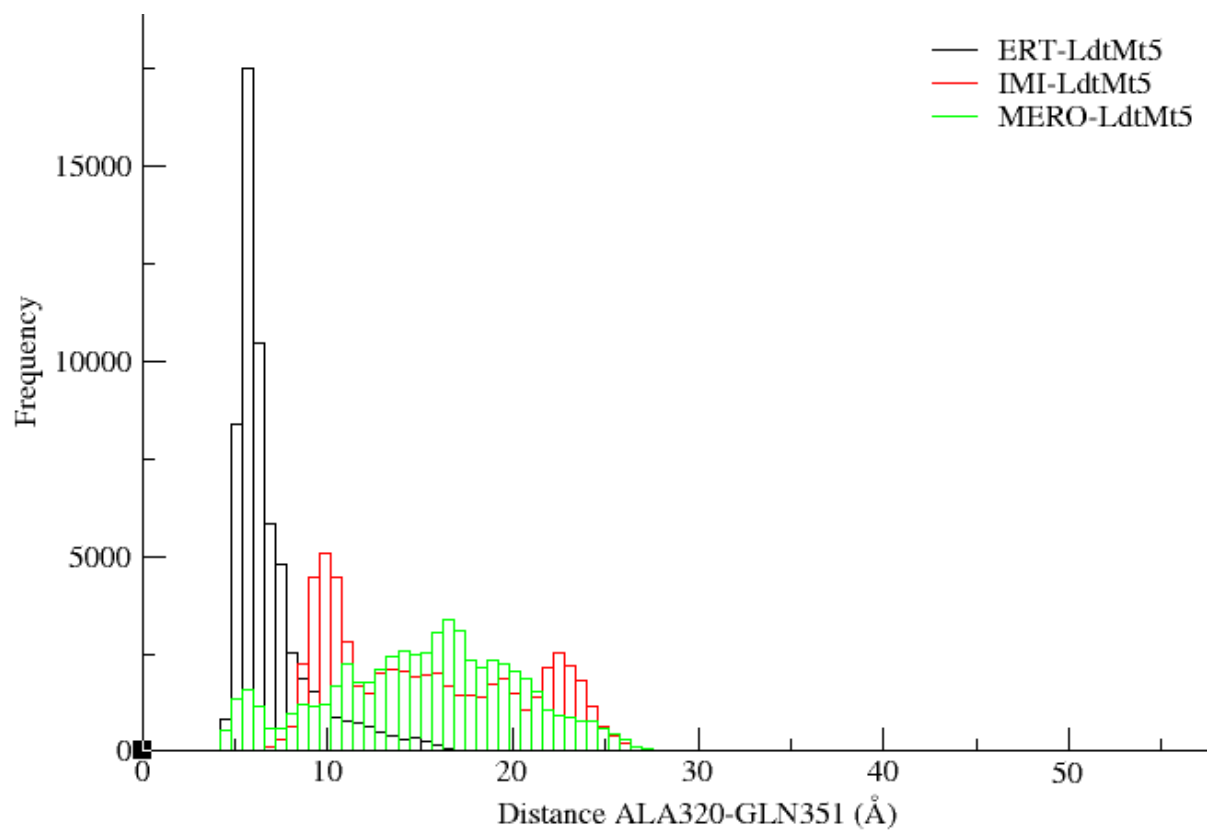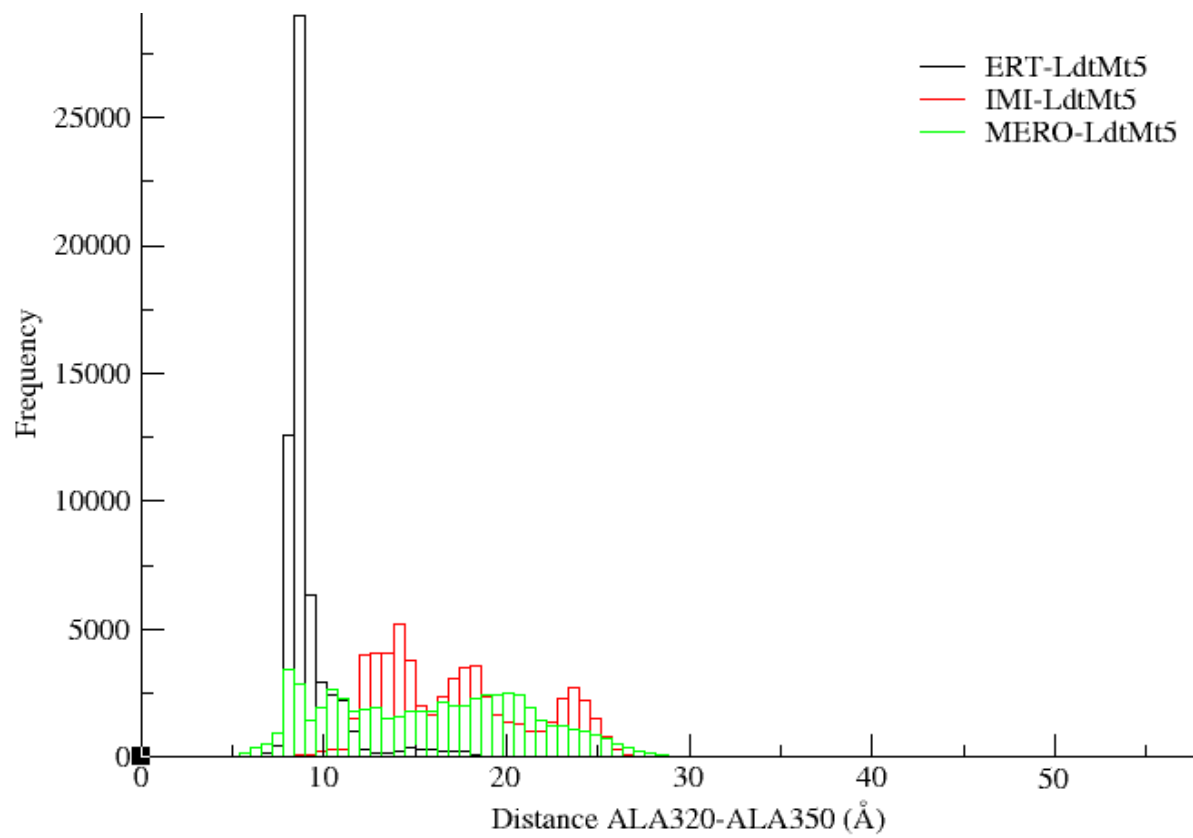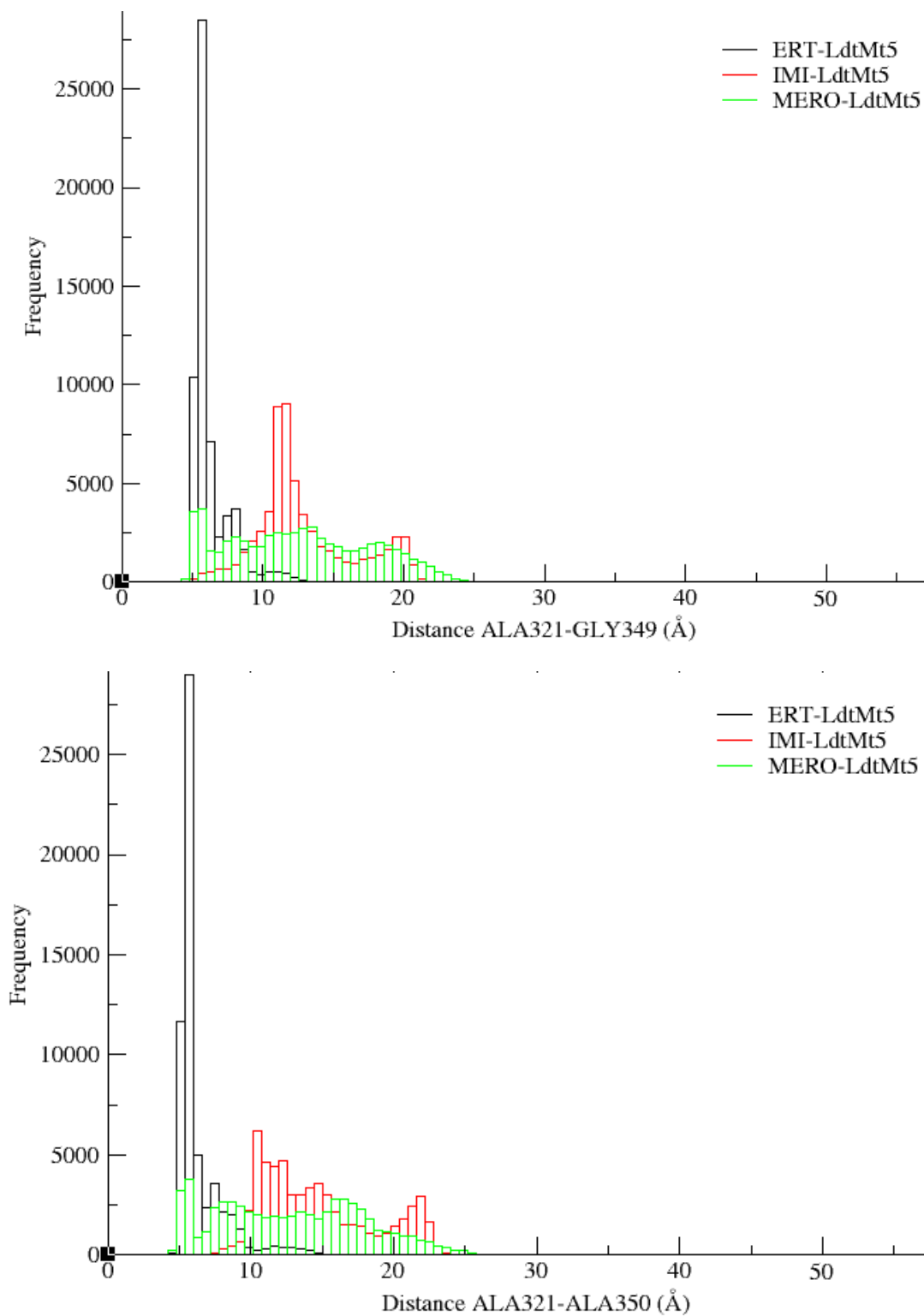
Figure S2 Histogram distribution of the tip-tip distances for ERT-LdtMt5, IMI-LdtMt5 and MERO-LdtMt5 over the 60 ns MD trajectories: D1: PRO319-GLY349 D2: PRO319-ALA350 D3: PRO319-GLN351 D4: ALA320-GLY349 D5: ALA320-ALA350 D6: ALA320-GLN351 D7: ALA321-GLY349 D8: ALA321-ALA350 D9: ALA321-GLN351.

Table S2 Average, maximum and minimum values for the tip-tip distances for ERT-LdtMt5, IMI-LdtMt5 and MERO-LdtMt5 over the 60 ns MD trajectories.

ERT-Ldt$_{Mt5}$	Flap tips	Average distance(Å)	Max. value	Min. value
	PRO319-GLY349	13.31875	18.5441	8.0934
	PRO319-ALA350	13.3411	21.2384	5.4438
	PRO319-GLN351	12.17885	19.5449	4.8128
	ALA320-GLY349	12.76815	18.1888	7.3475
	ALA320-ALA350	13.23585	20.3587	6.113
	ALA320-GLN351	11.3033	18.5327	4.0739
	ALA321-GLY349	9.369	14.3144	4.4236
	ALA321-ALA350	10.29375	16.5666	4.0209
	ALA321-GLN351	9.2049	14.8925	3.5173
IMI-Ldt$_{Mt5}$	**Flap tips**	**Average distance(Å)**	**Max. value**	**Min. value**
	PRO319-GLY349	18.74675	28.1251	9.3684
	PRO319-ALA350	20.2258	29.9013	10.5503
	PRO319-GLN351	18.6594	30.0674	7.2514
	ALA320-GLY349	16.01705	25.9577	6.0764
	ALA320-ALA350	17.74735	28.4055	7.0892
	ALA320-GLN351	16.9422	28.4003	5.4841
	ALA321-GLY349	13.4909	22.4313	4.5505
	ALA321-ALA350	15.83605	24.7497	6.9224
	ALA321-GLN351	14.7909	24.6841	4.8977
MERO-Ldt$_{Mt5}$	**Flap tips**	**Average distance(Å)**	**Max. value**	**Min.value**
	PRO319-GLY349	19.63605	31.2853	7.9868
	PRO319-ALA350	19.9922	31.7357	8.2487
	PRO319-GLN351	17.4153	29.4292	5.4014

	ALA320-GLY349	17.03175	29.4106	4.6529
	ALA320-ALA350	17.66495	30.8501	4.4798
	ALA320-GLN351	16.9422	28.4003	5.4841
	ALA321-GLY349	15.65435	26.8576	4.4511
	ALA321-ALA350	16.22155	28.1441	4.299
	ALA321-GLN351	15.06445	26.4135	3.7154

Table S3 Average, maximum and minimum values for the tip-tip distances for Free-LdtMt5 over the 60 ns MD trajectories.

Free- Ldt_{Mt5}	**Flap tips**	**Average distance (Å)**	**Max. value**	**Min. value**
	PRO319-GLY349	20.30075	27.7099	12.8916
	PRO319-ALA350	17.34275	24.6979	9.9876
	PRO319-GLN351	16.49245	22.8007	10.1842
	ALA320-GLY349	19.93465	27.7383	12.131
	ALA320-ALA350	17.46865	24.5619	10.3754
	ALA320-GLN351	16.06805	22.8366	9.2995
	ALA321-GLY349	16.62965	24.41	8.8493
	ALA321-ALA350	14.41665	21.1822	7.6511
	ALA321-GLN351	13.102	19.5415	6.6625
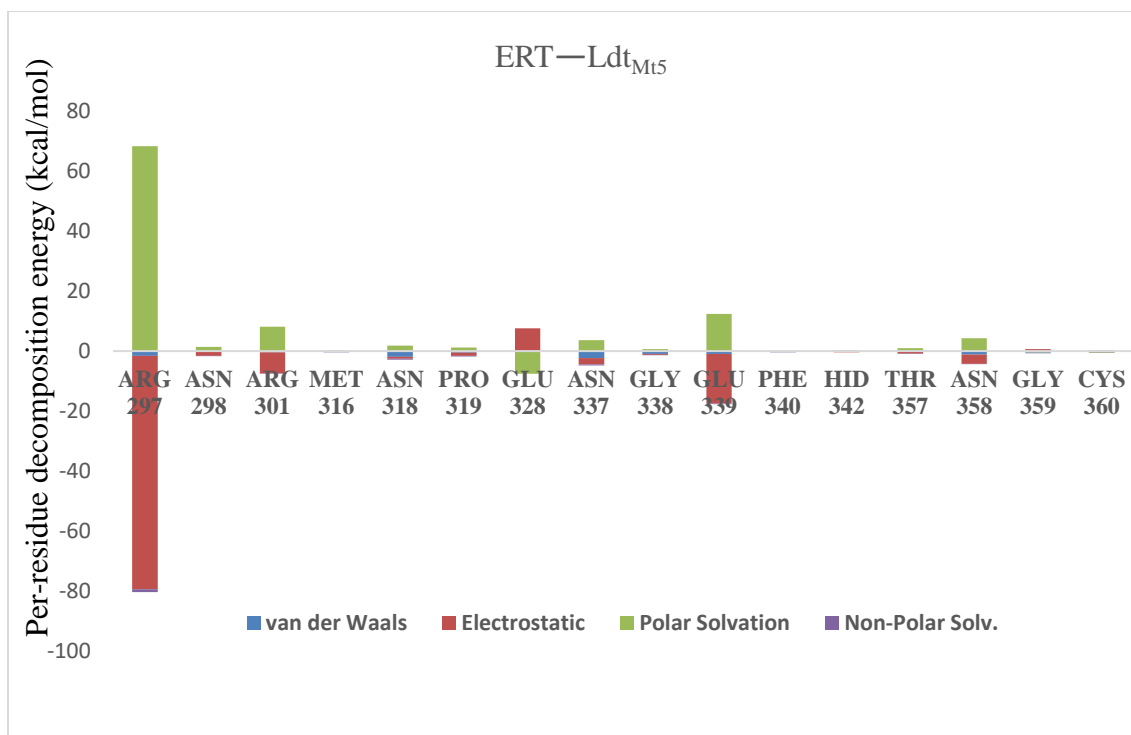
Figure S3 The plot of per residue decomposition analysis of ERT—Ldt$_{Mt5}$ complex.
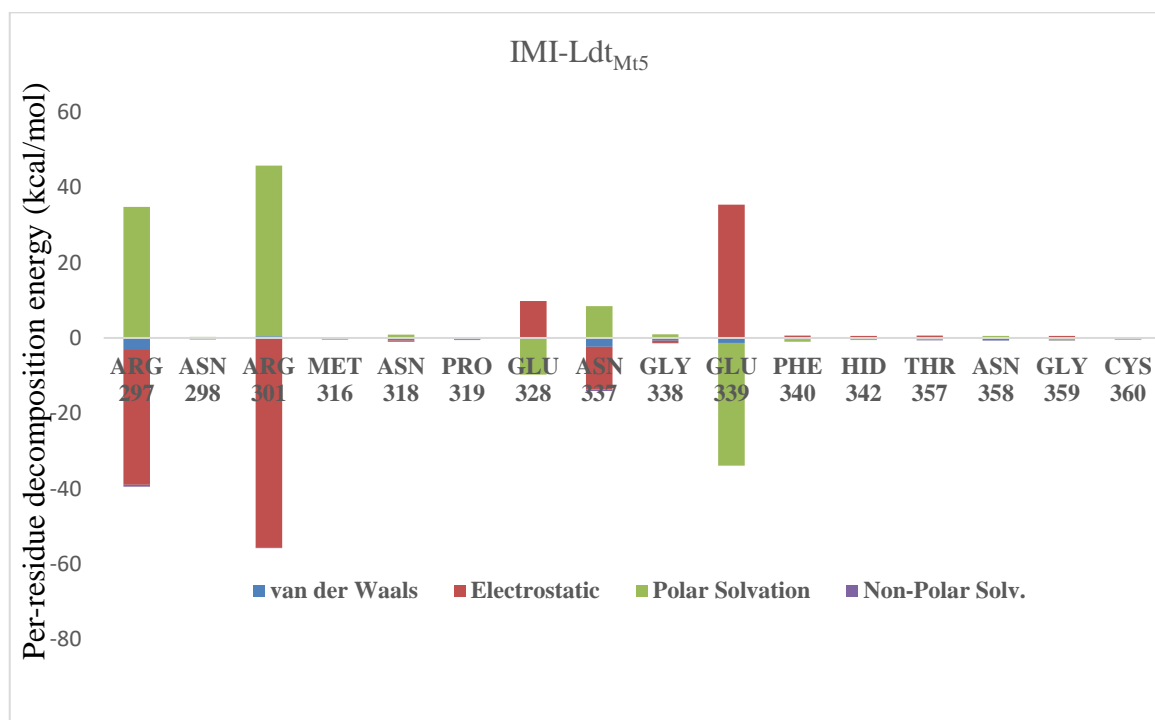
Figure S4 The plot of per-residue decomposition analysis of IMI—Ldt$_{Mt5}$ complex.
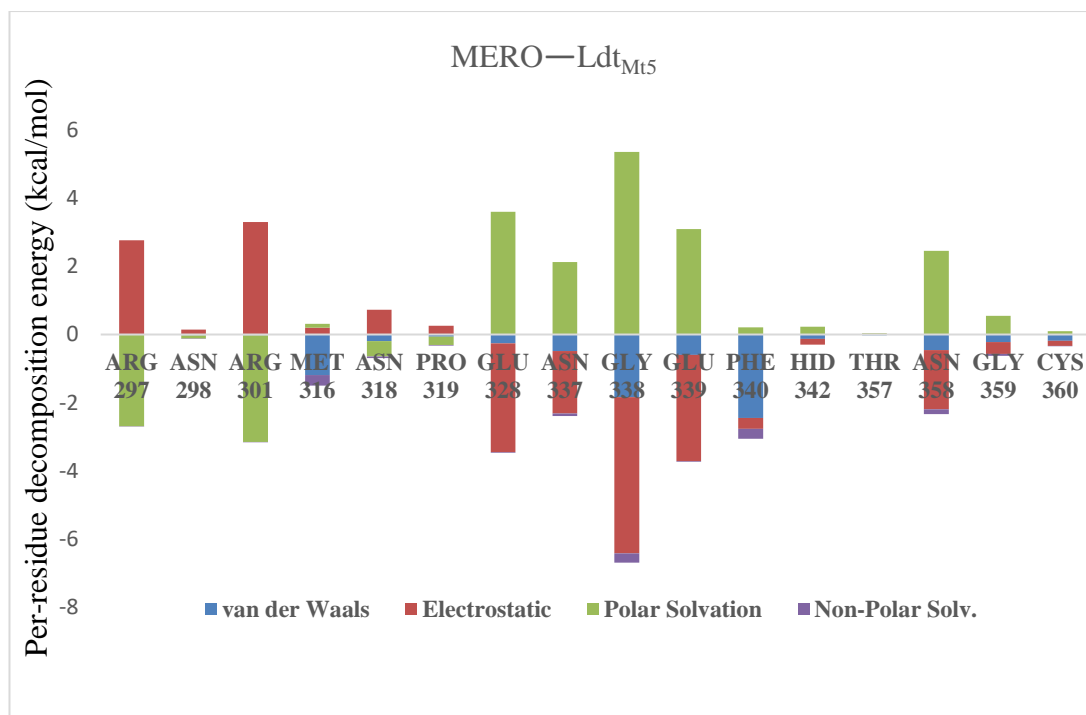
Figure S5 The plot of per-residue decomposition analysis of MERO—Ldt$_{Mt5}$ complex.
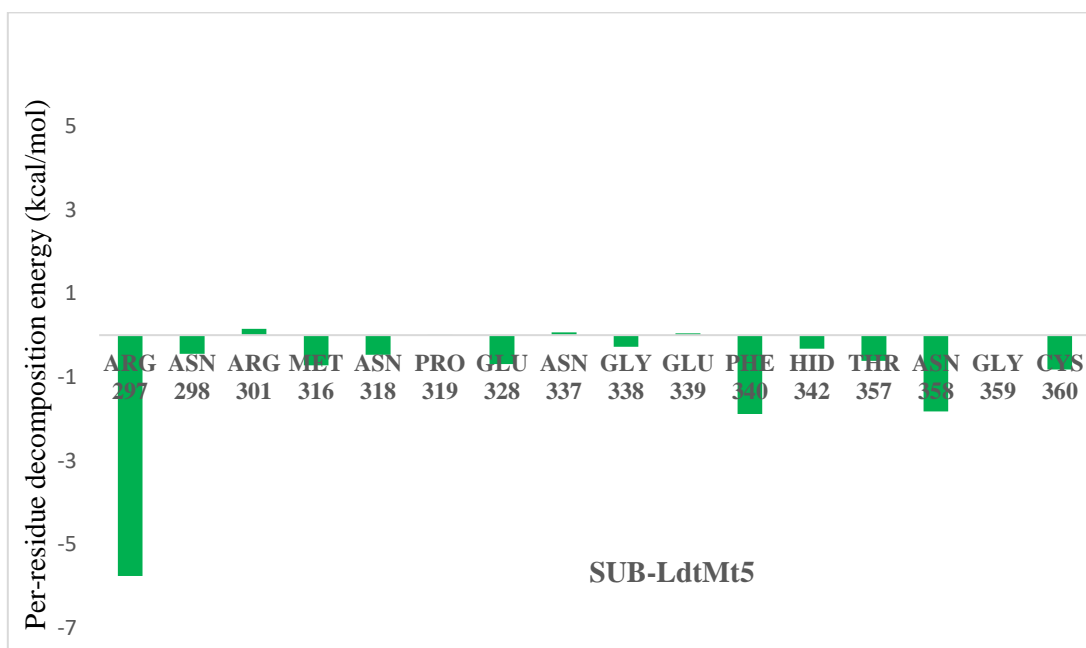
Figure S6 The plot of per-residue decomposition analysis of SUB—Ldt$_{Mt5}$ complex.
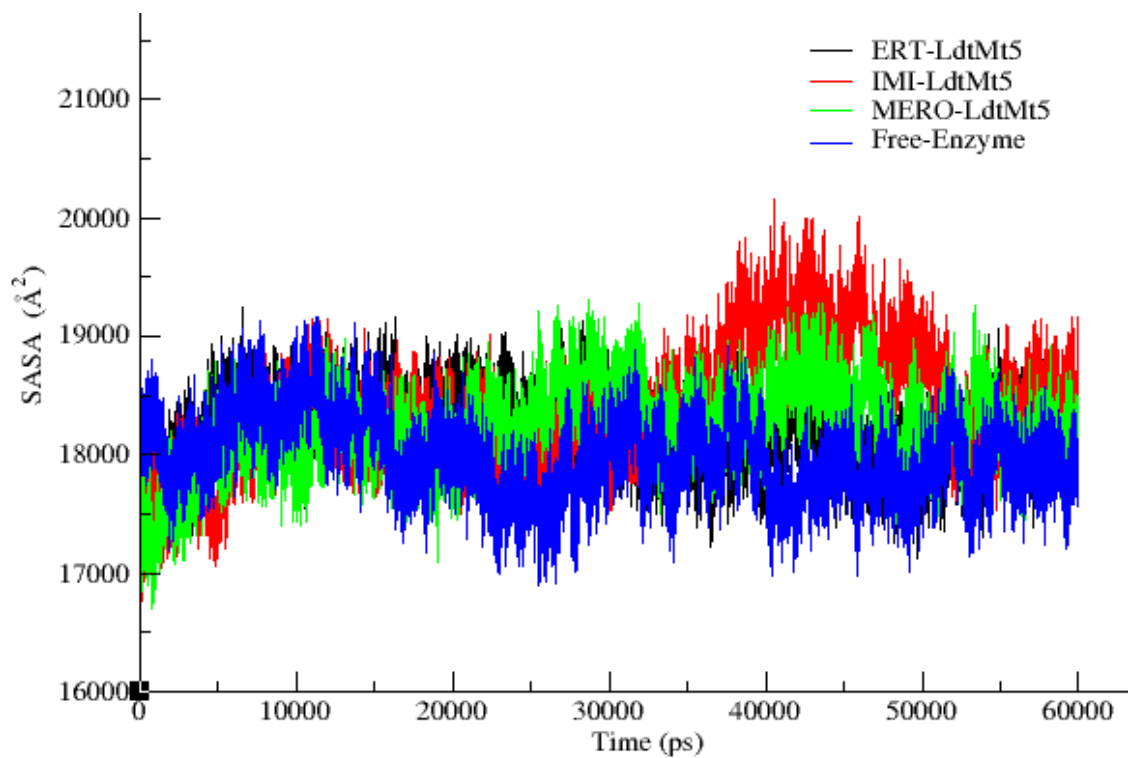
Figure S7 Solvent accessible surface area (SASA) of Free—Ldt$_{Mt5}$ (blue), ERT—Ldt$_{Mt5}$ (black), IMI—Ldt$_{Mt5}$ (red) and MERO—Ldt$_{Mt5}$ (green) over the 60 ns simulation time.
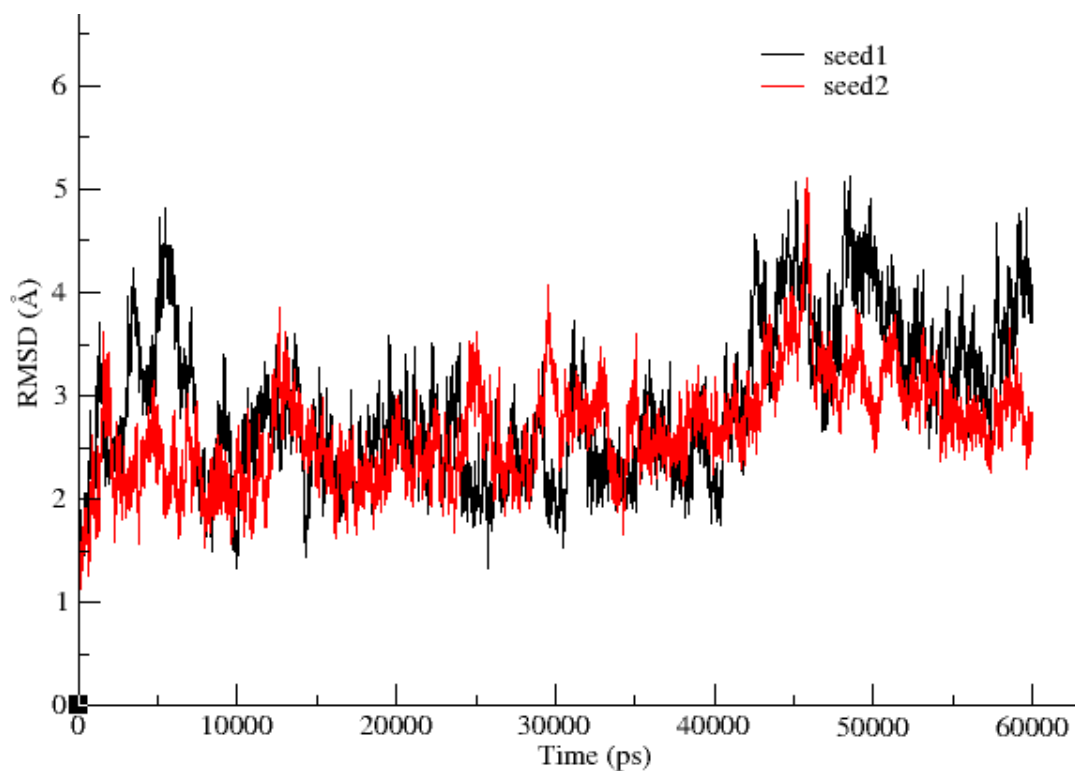
Figure S8 RMSD plot of backbone atoms of Ldt$_{Mt5}$ over three 60 ns MD trajectories.

(A)

(B)

(C)

(D)
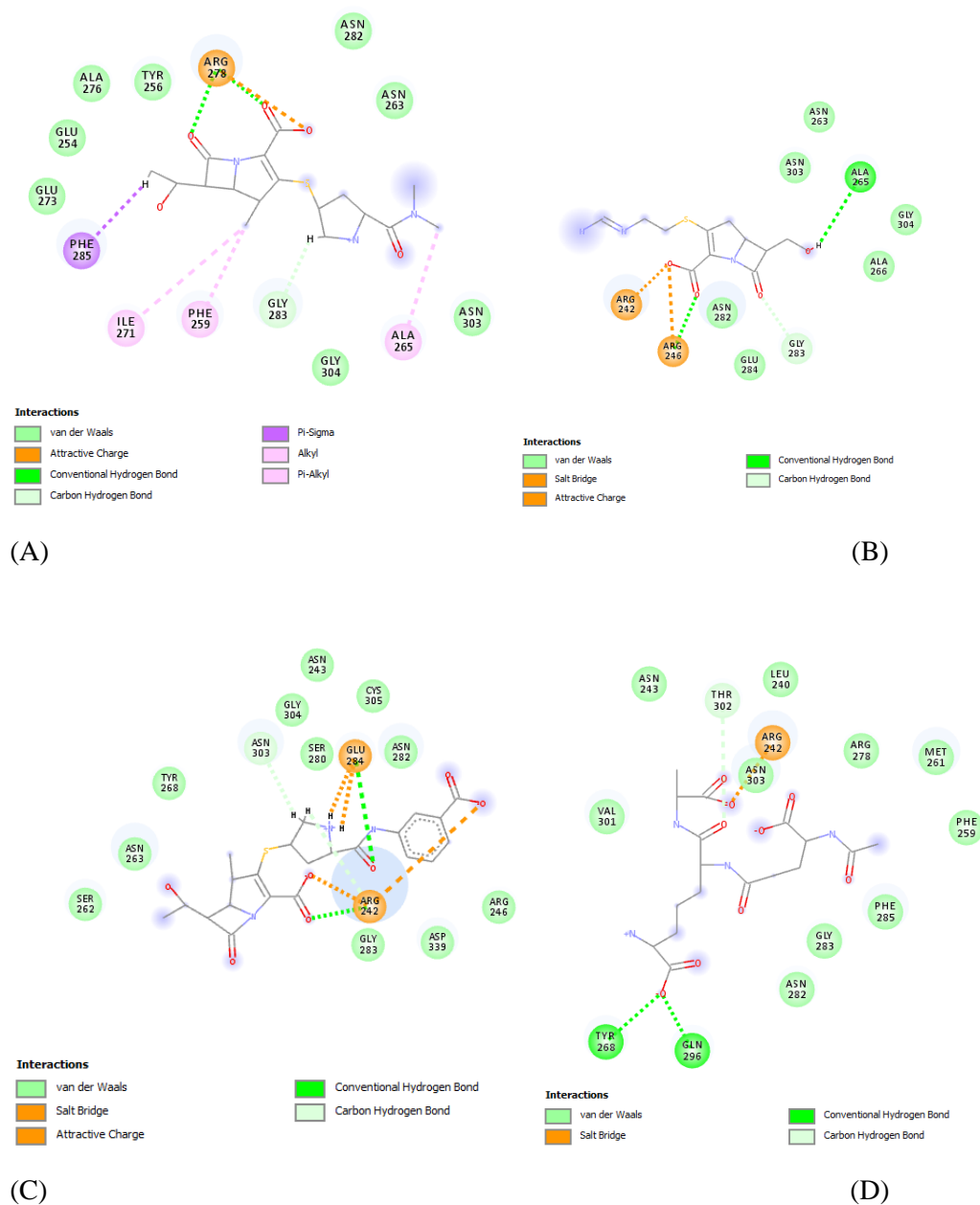
Figure S9 View of the binding site interactions observed for the minimized highest scoring MM-GBSA representative complex of each ligand: (A) meropenem, (B) imipenem, (C) ertapenem and (D) natural substrate. Where the protein residues numbers are in parenthesis as follows; LEU240(295), ARG242(297), ASN243(298), ARG246(301), GLU254(309), TYR256(311), PHE259(314), MET261(316), SER262(317), ASN263(318), ALA265(320), ALA266(321), ILE271(326), GLU273(328), ALA276(331), ARG278(333), SER280(335), ASN282(337), GLY283(338), GLU284(339), PHE285(340), GLN296(351), VAL301(356), ASN303(358), GLY304(359), CYS305(360), ASP339(394).
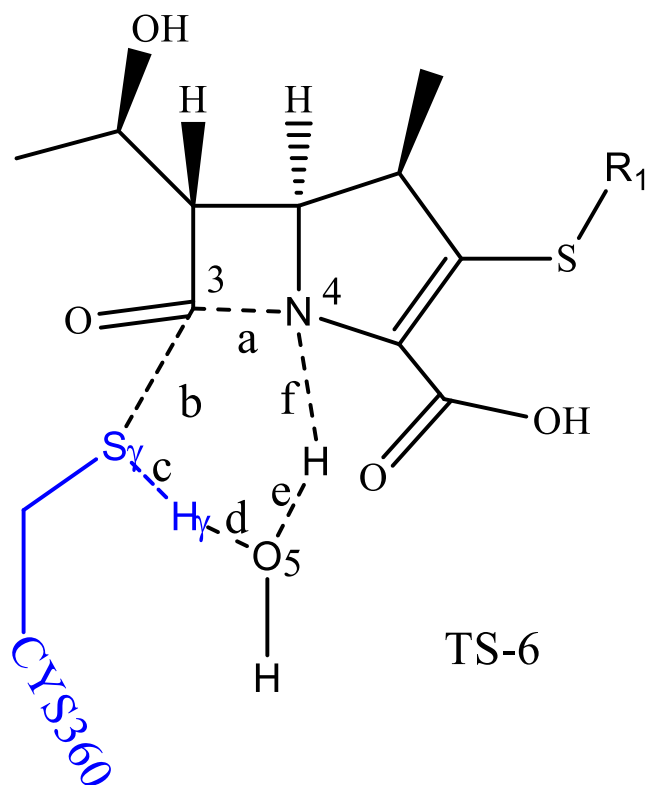
Figure S10 2D structure of the 6-membered ring transition states obtained using constraints with ONIOM (B3LYP/6-31+G(d): AMBER). (1): Carbapenem. R_1 = imipenem side chain, a =1.58 Å, b = 2.32 Å, c =1.64 Å, d = 1.25 Å, e = 1.12 Å, f = 1.42 Å. (2): Carbapenem. R_1 = meropenem side chain, a =1.60 Å, b =2.52 Å, c =1.82 Å, d = 1.13 Å, e = 1.00 Å, f = 1.79 Å.
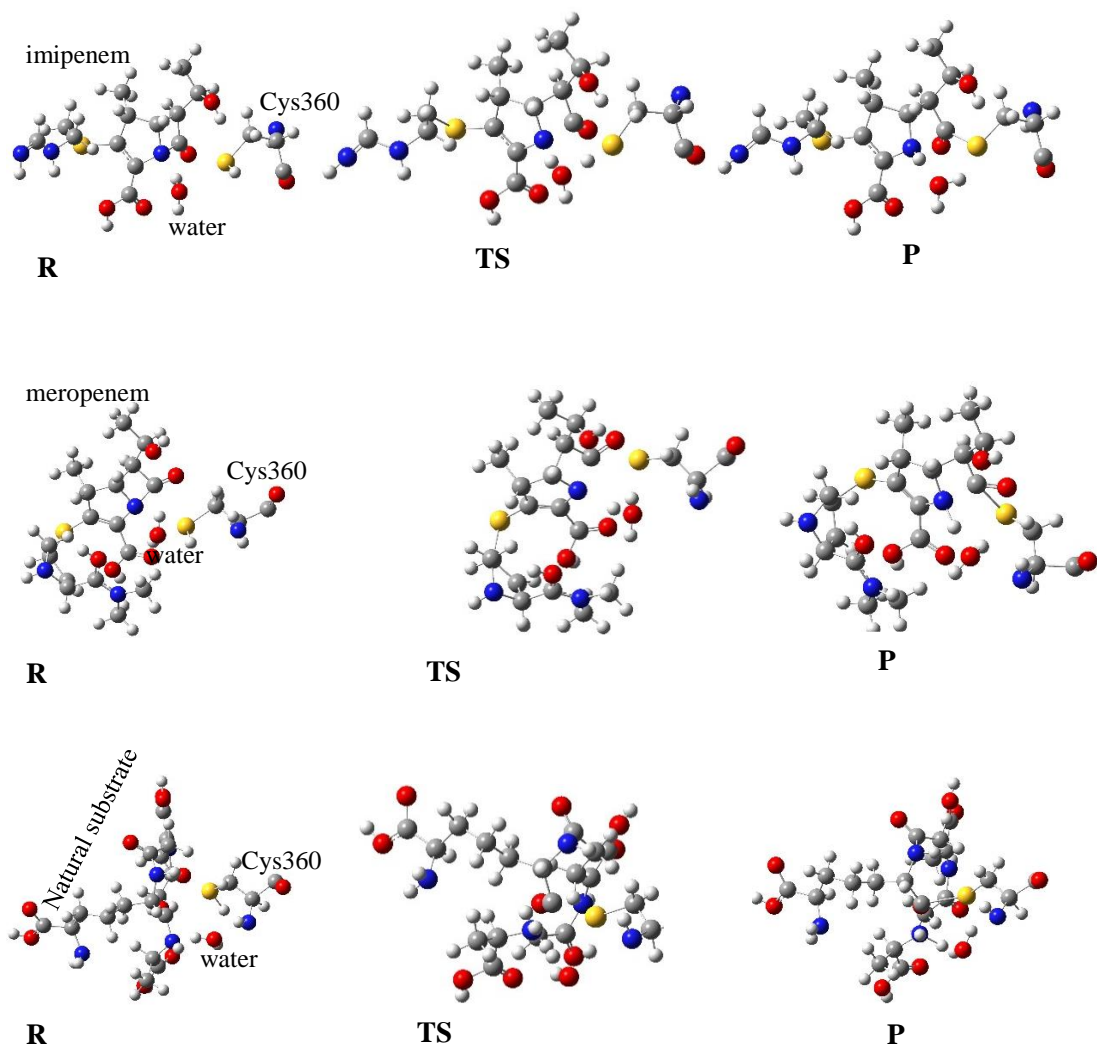
Figure S11   A pictorial representation describing the reactants, transition states and products of the complexes.
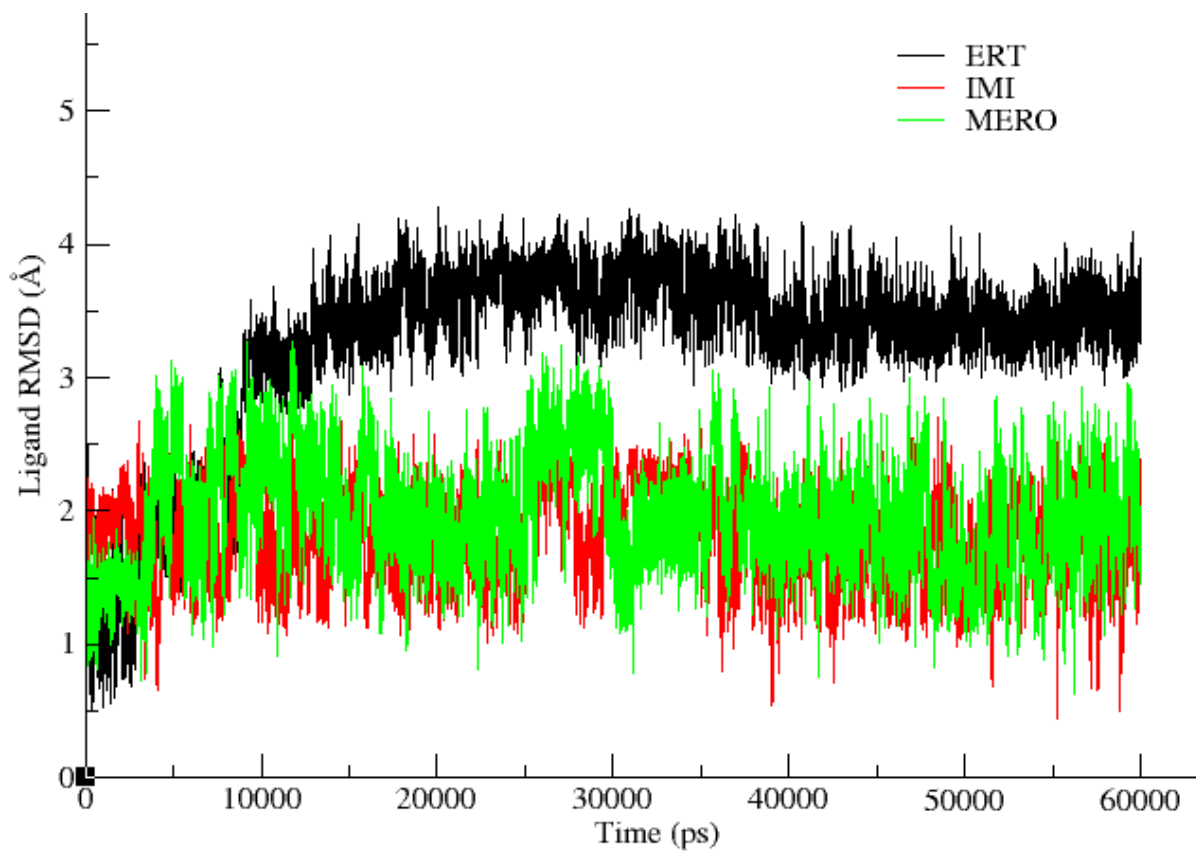
Fig. S12 Ligand RMSD plot for ertapenem (ERT), imipenem (IMI) and meropenem (MERO) over 60 ns MD trajectories.

Appendix 2. Supplementary material for Chapter 4

Table S1: A detailed summary of the binding energy calculations for the compounds in the other antibiotic classes

ZINC ID	ΔE_{vdw}	ΔE_{ele}	ΔG_{gas}	ΔG_{polar}	$\Delta G_{nonpolar}$	$\Delta G_{solvation}$	$-T\Delta S$	$-\Delta G_{bind}$
Diarylquinolone								
00022456	**-47.08**	**-4.08**	**-51.15**	**14.65**	**-5.36**	**9.28**	**-18.42**	**-41.87**
00022457	**-44.53**	**-5.72**	**-50.25**	**-16.46**	**-5.01**	**11.45**	**-23.61**	**-38.8**
00002447	-44.45	-257.63	-302.08	270.09	-5.69	264.4	-22.68	-37.68
Oxazolidinone								
00108973	-43.19	-3.93	-47.12	14.93	-5.02	9.91	-23.21	-37.21
Rifamycin								
13532137	-46.38	-12.24	-58.62	26.57	-5.16	21.41	-19.39	-37.21

Compounds in bold were screened by AutoDock Vina, and compounds in the normal text were screened by Schrödinger Maestro.

Table S2: Distances in angstroms (Å) between the carbon atom of the carbonyl group of the β-lactam and the sulphur atom of the cysteine (CYS305 (360)) residue of the Ldt_{Mt5} active site

β-lactam compound	Distance before MD simulation (Å)	Distance after MD simulation (Å)
A	7.164	5.442
B	7.456	8.276
C	4.077	7.929
D	4.077	5.158
E	5.327	5.486

Triplicate MD simulations with varying initial atomic coordinates to confirm the stability of the initial simulation are shown in the figure below.
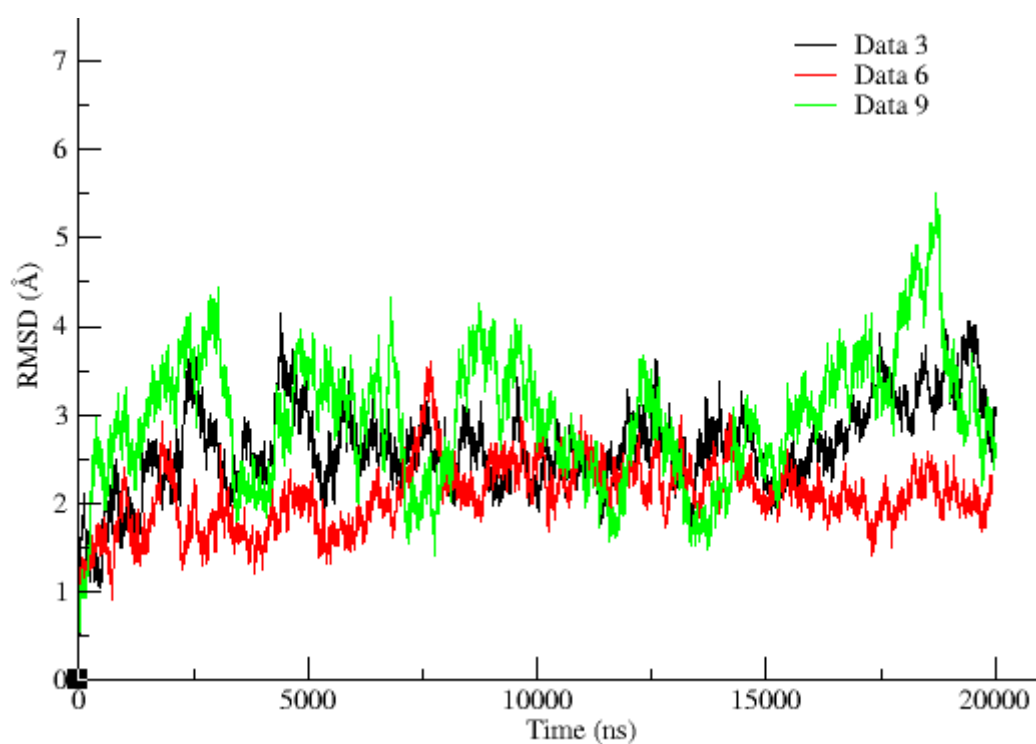
Figure S1: Time evolution of the root mean square deviation (RMSD) from MD simulations of one complexed structure at different velocities the during 20 ns MD simulation trajectory at 6ns (Data 3); 12ns (Data 6) and 18ns (Data 9).

Appendix 3. Supplementary material for Chapter 5
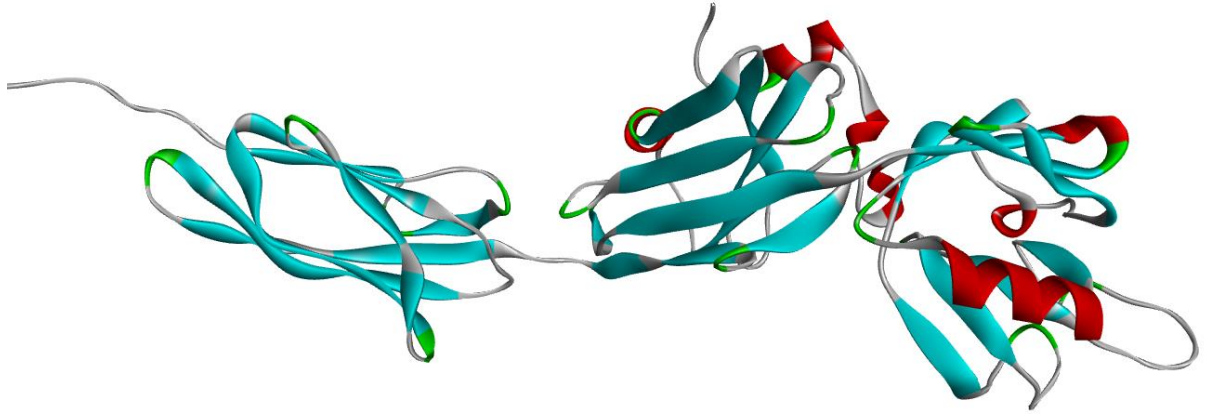
Figure S1 The 3D crystal structure of Ldt$_{Mt5}$ (PDB code: 4ZFQ).

1

2

3

4

5

6
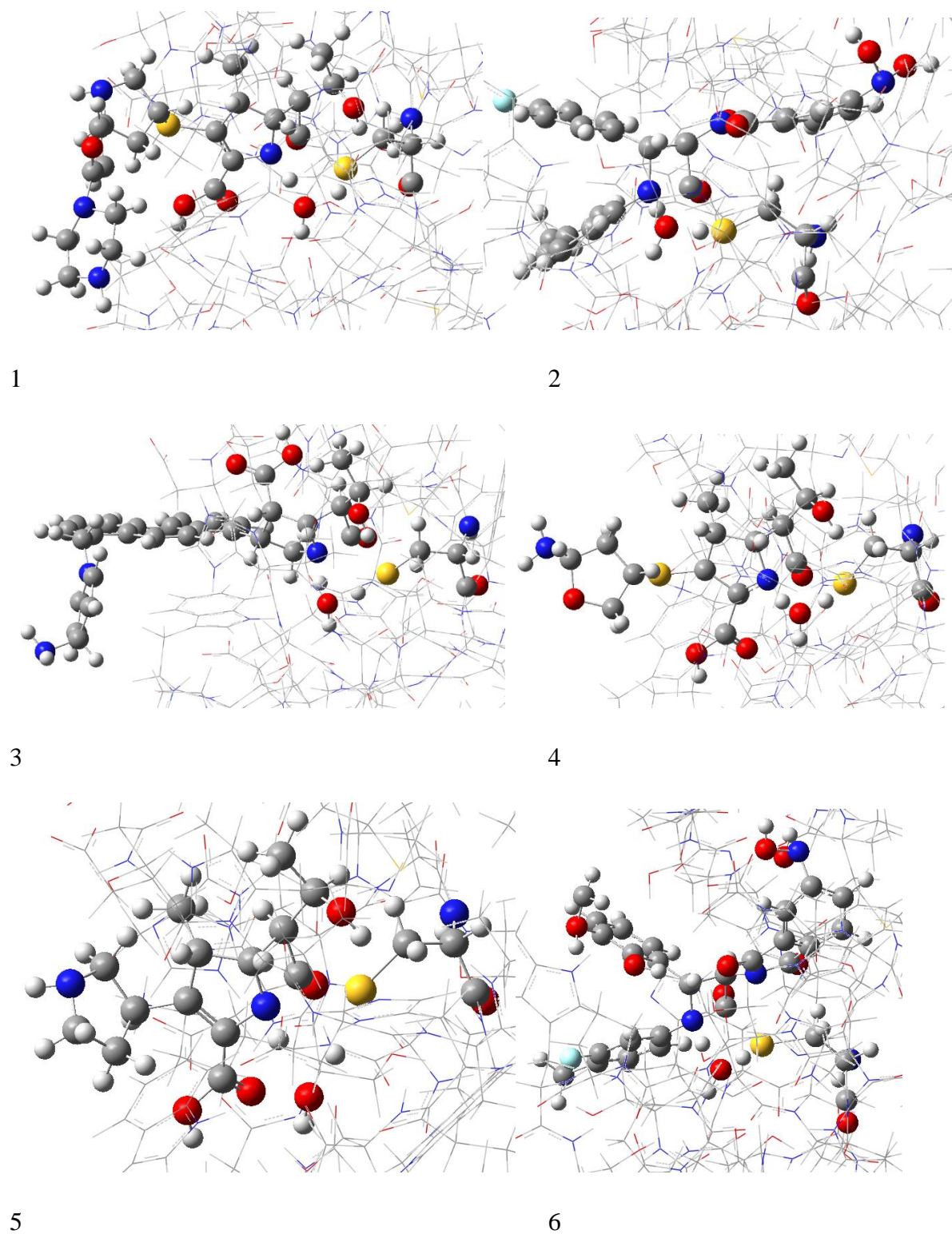
Figure S2. Optimized TS structures of (1) TS-6- ZINC03788344 and (2) TS-6-ZINC02462884 (3) TS-6-ZINC03791246 and (4) TS-6-ZINC03808351 (5) TS-6-ZINC03784242 (5) TS-6-ZINC02475683 obtained from an ONIOM (B3LYP/631+G(d): AMBER) calculation.

Compound 1 (TS Coordinate)

0 1

S-S	-1	2.73513600	-9.15245600	3.49405400	H
O-O	-1	0.11249900	-4.25111200	3.07908900	H
O-OH	-1	3.72473600	-2.47535800	1.72353400	H
O-OH	-1	0.09483700	-9.09991900	1.47570200	H
O-O	-1	-1.02610700	-7.30258100	1.86093000	H
N-N	0	1.72557300	-5.64749900	1.81104400	H
C-CM	0	3.14120000	-5.33838200	2.39501500	H
C-CT	0	2.63834400	-4.14055300	3.19443800	H
C-CT	-1	3.77939100	-6.54285600	3.09743400	H
C-C	0	1.20545300	-4.30674600	2.60110300	H
C-CA	-1	2.55633800	-7.48333500	2.82903500	H
C-CA	-1	1.40186500	-7.04480800	2.10807100	H
C-CT	-1	3.48809400	-2.85922300	3.06382600	H
C-CT	-1	4.09411300	-6.32786800	4.56735200	H
C-CT	-1	4.86675100	-3.13482900	3.66682500	H
C-C	-1	0.08172400	-7.79688700	1.84161600	H
H-HC	-1	3.76495000	-5.07157300	1.57085900	H
H-HC	-1	2.58484000	-4.39143500	4.28425600	H
H-HC	-1	4.68754300	-6.94193700	2.58158700	H
H-H1	-1	2.97024600	-2.02622700	3.59999000	H
H-HC	-1	4.37307800	-7.26556300	5.06441600	H
H-HC	-1	4.92333600	-5.61131400	4.69088800	H
H-HC	-1	3.22950500	-5.90434500	5.10586200	H
H-HC	-1	5.56219300	-3.51969400	2.90940800	H
H-HC	-1	5.30594300	-2.23101800	4.08969200	H
H-HC	-1	4.82846800	-3.88819900	4.47251800	H
H-HO	-1	2.87235600	-2.35896700	1.31844700	H
H-HO	-1	-0.79978100	-9.37150500	1.29060300	H
N-N	0	-0.11312600	0.15687800	2.87825400	H
H-H	-1	-0.91468300	-0.34106400	3.21799500	H
C-CT	0	0.33856400	-0.25048700	1.54053600	H
H-H1	-1	0.82349400	0.64867600	1.11962300	H
C-CT	-1	1.42545800	-1.37318200	1.45960200	H
H-H1	-1	1.99376900	-1.22304000	0.52385500	H
H-H1	-1	2.15066000	-1.14671300	2.26605900	H
S-SH	0	0.67383700	-2.95520900	1.02469900	H
H-H	0	1.28334100	-3.61273100	-0.25078500	H
C-C	0	-0.93400900	-0.46572200	0.65541200	H
O-O	0	-2.01671200	-0.40674200	1.18507500	H
O-O	0	1.60638200	-5.08340500	-0.72162200	H
H-H	-1	0.90381600	-5.35754400	-1.30954200	H
H-H	-1	1.63845000	-5.27921000	0.56347900	H
C-CT	-1	4.41201900	-9.64444500	3.15580800	H
C-CT	-1	4.44650900	-10.76822500	2.10968100	H
C-CT	-1	5.07653000	-10.20933700	4.41985100	H
H-H1	-1	4.96427400	-8.74637200	2.78797200	H
C-CT	-1	5.11670000	-11.91815800	2.79861300	H
H-HC	-1	5.02224000	-10.45941100	1.20183800	H
H-HC	-1	3.41482700	-11.04886100	1.78146900	H
H-H1	-1	5.97779600	-9.61189700	4.70563700	H
H-H1	-1	4.37073100	-10.20041300	5.28742100	H
H-H1	-1	4.44805800	-12.75340200	2.81219600	H

```
N-N        -1   5.46084600  -11.61298300   4.06144100 H
H-H        -1   5.02388400  -12.42584700   4.44656100 H
C-CM       -1   6.38408800  -12.30313000   2.01304100 H
H-HC        0   7.39819200  -12.27169000   2.40319400 H
C-CM       -1   6.01227500  -12.58642000   0.54569600 H
H-HC       -1   5.01435500  -12.96956600   0.49820500 H
C-C         0   7.14253900  -13.22244300  -0.20465000 H
C-CT       -1   5.74820000  -14.75354200  -2.00158700 H
H-H1       -1   6.05194100  -15.70658700  -1.62165800 H
C-CT        0   7.51011800  -13.58157200  -3.88271600 H
H-H1        0   7.67684100  -12.78208600  -4.62996700 H
H-H        -1   5.98033600  -14.27526300  -5.24085800 H
C-C         0   7.60440800  -13.01444800  -2.47554600 H
N-N         0   6.96396900  -13.94259400  -1.51270300 H
N-N        -1   6.18591900  -14.14340800  -4.16560100 H
C-CT        0   5.46885300  -15.07693600  -3.39750000 H
O-O        -1   8.33197300  -13.16554500   0.13551300 H
H-H1        0   8.69067300  -12.94469600  -2.24349100 H
H-H1        0   5.58816000  -16.14529500  -3.66490100 H
H-H1       -1   4.44691800  -14.73809100  -3.47276100 H
H-H1        0   4.84991300  -14.39489200  -1.46535000 H
H-H        -1   7.19945300  -12.00584100  -2.14567100 H
H-H1        0   8.31823700  -14.33102800  -4.03191600 H
```

Compound 2 (TS Coordinate)

```
0 1
O     -1   1.50123800   -4.02014100   4.20143800
N      0   2.01921200   -5.95468800   2.42811400
C      0   3.54932600   -5.83623500   2.62400500
C      0   3.43705500   -4.49487200   3.32771600
C      0   1.92226800   -4.42987800   3.14878900
H     -1   3.95112300   -5.59141500   1.65578200
H     -1   3.26584700   -4.51816300   4.41139400
N      0   0.01271200   -0.20750000   2.63002500
H     -1  -0.89064200   -0.44390600   2.95226500
C      0   0.36120500   -0.64076300   1.33060000
H     -1   0.86550200    0.10703400   0.71247000
C     -1   1.35829400   -1.87116200   1.35912500
H     -1   1.91878000   -1.89939500   0.40579900
H     -1   2.10814300   -1.56376000   2.11375900
S      0   0.61744600   -3.46643500   1.69515700
H      0   0.92802300   -4.40313100   0.51133300
C      0  -0.96133000   -0.86531100   0.53882200
O      0  -2.02257000   -0.67746000   1.09204300
O      0   1.25530500   -5.62944300   0.05237100
H      0   0.42302800   -6.11903800  -0.04833600
H      0   1.67595100   -5.83159200   1.09393800
C      0   1.29948800   -7.17796900   2.71564400
C      0   1.01261900   -8.05096500   1.64609200
C      0   0.87377900   -7.53505100   3.99505600
C      0   0.26256600   -9.20355000   1.85942400
H      0   1.39886300   -7.84967500   0.65387000
C      0   0.16319900   -8.72323100   4.23008800
```

H	0	1.13743700	-6.88138800	4.81061600
C	0	-0.16620600	-9.53799400	3.14232900
H	0	0.01871400	-9.84739000	1.02048900
H	0	-0.74352700	-10.44531700	3.30388100
C	0	-0.22084200	-9.13611900	5.62883900
H	0	0.65645500	-9.46501800	6.20026800
H	0	-0.67657100	-8.30375600	6.16804500
H	0	-0.93698300	-9.96417100	5.61680600
C	0	4.08976600	-7.04102400	3.35333700
C	0	4.43762800	-8.19614100	2.63496800
C	0	4.04929100	-7.11681100	4.75472200
C	0	4.73987700	-9.39300500	3.28583500
H	0	4.47377700	-8.15543900	1.54981500
C	0	4.32750800	-8.31011200	5.42467100
H	0	3.78359400	-6.24641000	5.34578900
C	0	4.66384400	-9.42748300	4.67203500
H	0	5.01637300	-10.28943000	2.74203300
H	0	4.29428600	-8.37297600	6.50780100
F	0	4.93830900	-10.59446100	5.31395500
C	0	3.87761100	-2.39591500	4.32087000
C	0	3.92707500	-1.02373700	3.82732800
C	0	4.33520800	-2.47920200	2.03568200
C	0	4.28670100	-1.04208700	2.48130600
N	0	4.14302100	-3.24612200	3.19503300
O	0	4.51809100	-2.92151300	0.91981400
O	0	3.67211200	-2.78909000	5.44527500
C	0	4.63325500	0.13245800	1.83444000
H	0	4.94692200	0.16938300	0.79887100
C	0	3.73111900	0.15248800	4.52306300
H	0	3.28324400	0.13248700	5.50907200
C	0	4.18485500	1.32999900	3.93259300
H	0	4.16108900	2.27209600	4.46058000
N	0	5.48292500	2.36267800	2.12624700
O	0	5.76565000	3.25959200	3.17273600
H	0	5.86569500	4.11294500	2.71593300
C	0	4.73565200	1.27698300	2.64686800
O	0	6.70961500	1.87414400	1.60802600
H	0	7.16889600	1.42442800	2.35198

Compound 3 (TS Coordinate)

0 1

O	-1	1.06484900	-4.43612200	2.82225100	H
N	0	2.90408400	-5.52374100	1.66931200	H
C	0	4.24262000	-5.02273200	2.16740000	H
C	0	3.57058800	-3.86971500	2.94664300	H
C	0	2.18567600	-4.36792200	2.38620100	H
H	-1	4.80524400	-4.60380800	1.31737500	H
H	-1	3.51837300	-4.04043300	4.00851400	H
N	0	0.05904100	-0.16766500	2.43907200	H
H	-1	-0.75476900	-0.70210100	2.67819400	H
C	0	0.48136800	-0.41936900	1.08738800	H
H	-1	0.75695800	0.50695600	0.52017600	H
C	-1	1.73935300	-1.34247600	0.94590600	H
H	-1	2.26712600	-1.12866000	-0.00160700	H

H	-1	2.40748500	-0.94287000	1.73389200 H
S	0	1.49421900	-3.09011100	0.57341200 H
H	0	2.44389000	-3.84070600	-0.47149900 H
C	0	-0.77852100	-0.88489800	0.30785600 H
O	0	-1.81662300	-1.07695300	0.89898300 H
O	0	2.89069300	-5.00836100	-0.78602100 H
H	0	2.18087800	-5.43788600	-1.29406900 H
H	0	2.86185400	-5.40023600	0.27565000 H
C	0	4.25124200	-2.49936600	2.84584400 H
H	0	3.53939700	-1.74170300	3.20421000 H
C	0	5.49055000	-2.45776000	3.73723300 H
H	0	5.25024600	-2.76071100	4.75675200 H
H	0	6.25695400	-3.13520300	3.34802100 H
H	0	5.90666900	-1.44951000	3.74991500 H
O	0	4.72175400	-2.18819600	1.54639600 H
H	0	3.97807100	-2.27541000	0.92819400 H
C	0	2.64631500	-6.85142000	2.25930400 H
H	0	2.12149500	-6.71909100	3.21147600 H
H	0	2.00813000	-7.45589000	1.60856800 H
C	0	4.97512200	-6.23648500	2.81362600 H
C	0	4.04638400	-7.46551100	2.41523100 H
H	0	5.92622300	-6.37517200	2.29214800 H
H	0	4.39545400	-7.68372400	1.41169800 H
C	0	4.09255200	-8.79149100	3.16085200 H
C	0	5.17358300	-9.70814300	2.95113600 H
C	0	3.01849800	-9.19366600	3.93801600 H
C	0	5.13860700	-11.00330800	3.55158700 H
C	0	6.29663700	-9.38011700	2.12271500 H
C	0	2.98900700	-10.45902900	4.54672400 H
H	0	2.16376500	-8.54216400	4.07599100 H
C	0	6.22650500	-11.94543600	3.31072300 H
C	0	4.02736600	-11.34371300	4.35873600 H
C	0	7.30259500	-10.26411400	1.87897600 H
H	0	6.35374300	-8.39960600	1.66529600 H
H	0	2.13465100	-10.74069800	5.15572400 H
C	0	7.31145000	-11.57249600	2.46165700 H
C	0	6.24512100	-13.23502700	3.89504700 H
H	0	3.97123700	-12.31727700	4.83065100 H
H	0	8.11231300	-9.97560000	1.21893200 H
C	0	8.37877800	-12.49160700	2.22599900 H
C	0	7.28134500	-14.11434800	3.65980100 H
H	0	5.43845900	-13.55075300	4.54583900 H
C	0	8.34802100	-13.73919800	2.82559600 H
H	0	7.27465100	-15.09794000	4.12084300 H
H	0	9.16362200	-14.43612800	2.64851100 H
C	0	9.57401300	-12.13212600	1.36426400 H
H	0	9.99056800	-11.16832400	1.67987800 H
H	0	10.36011000	-12.88322800	1.53597300 H
C	0	10.10806100	-11.22284200	-0.86135700 H
C	0	8.52539000	-12.98894400	-0.72221000 H
C	0	10.16420100	-11.32213600	-2.20176600 H
H	0	10.68153500	-10.47896800	-0.31382500 H
C	0	8.53034300	-13.15542100	-2.05574700 H
H	0	7.88684900	-13.57709000	-0.07246900 H
C	0	9.44840700	-12.40104700	-2.98387400 H

153

H	0	10.78391800	-10.61444900	-2.74750900 H
H	0	7.87941800	-13.90521100	-2.49424600 H
N	0	9.28211800	-12.01598500	-0.06890600 H
C	0	5.42003000	-6.26574700	4.27122300 H
O	0	4.96338700	-5.27415900	5.07262000 H
H	0	5.35056100	-5.45449900	5.95168500 H
O	0	6.16314800	-7.12259300	4.69318100 H
N	0	10.35259000	-13.36875300	-3.65908800 H
H	0	10.90915500	-12.88063100	-4.36303500 H
H	0	11.01663000	-13.71870200	-2.96755400 H
H	0	8.86833200	-11.95723100	-3.80740600 H

Compound 4 (TS Coordinate)

0 1

O	-1	0.13421400	-4.31300500	3.12795300
O	-1	3.74123500	-2.52915900	1.77849900
O	-1	0.11187900	-9.15373300	1.53073600
O	-1	-1.00906600	-7.35639900	1.91597900
N	0	1.80833000	-5.53082000	1.76046200
C	0	3.18591300	-5.34134800	2.45151400
C	0	2.65971800	-4.16812500	3.26857600
C	-1	3.79592800	-6.59663500	3.15262000
C	0	1.22619200	-4.30120200	2.65775400
C	-1	2.57342500	-7.53724800	2.88407200
C	-1	1.45355200	-6.76152600	2.13657200
C	-1	3.50518300	-2.91284800	3.11881300
C	-1	4.11120600	-6.38171200	4.62238500
C	-1	4.88410100	-3.18899800	3.72100100
C	-1	0.09882400	-7.85077700	1.89657700
H	-1	3.78185200	-5.12521700	1.62600700
H	-1	2.60104000	-4.44471100	4.33985600
H	-1	4.70460500	-6.99574600	2.63665600
H	-1	2.98774800	-2.08021500	3.65574100
H	-1	4.39021400	-7.31936300	5.11943300
H	-1	4.94035700	-5.66510600	4.74592900
H	-1	3.24654400	-5.95817000	5.16090400
H	-1	5.57919700	-3.57363600	2.96447700
H	-1	5.32301600	-2.28481900	4.14466800
H	-1	4.84547200	-3.94182700	4.52773200
H	-1	2.88941300	-2.41262900	1.37352500
H	-1	-0.78273900	-9.42532100	1.34564300
N	0	-0.07217700	0.12781000	2.86281200
H	-1	-0.93172200	-0.28723700	3.16295900
C	0	0.33372300	-0.16551900	1.53508800
H	-1	0.80645900	0.70249400	1.06460300
C	-1	1.40840000	-1.31943400	1.40453600
H	-1	1.97672400	-1.16920900	0.46881600
H	-1	2.13361900	-1.09286600	2.21101100
S	0	0.70744100	-2.93586500	0.98470200
H	0	0.97774200	-5.32091200	-1.20989100
C	0	-0.95429700	-0.39328100	0.69435900
O	0	-2.03191200	-0.35100400	1.24113200
O	0	1.69798300	-4.91233500	-0.70100500
H	0	1.75644400	-5.34826400	0.29446700

H	0	1.36953700	-3.83445700	-0.26776800
S	-1	2.74966200	-9.18262200	3.53962700
C	-1	4.03820200	-10.03827800	2.65884400
C	-1	5.14185200	-10.46875900	3.61419500
C	-1	3.48646300	-11.28721300	1.98602200
H	-1	4.44017100	-9.32810000	1.89303800
C	-1	5.34059500	-11.96919300	3.45525300
H	-1	4.86015100	-10.22338600	4.66926700
H	-1	6.09114100	-9.92051000	3.39121700
H	-1	3.58126700	-11.20567100	0.87401600
H	-1	2.39781200	-11.40701200	2.21518100
H	-1	6.36118900	-12.18553200	3.05000800
O	-1	4.27270000	-12.48438300	2.50100200
N	-1	5.24035300	-12.64491000	4.75688900
H	-1	5.07771600	-13.62119400	4.61399600
H	-1	6.09311000	-12.51975800	5.26398100

Compound 5 (TS Coordinate)

0 1

O	-1	0.11611000	-4.25863600	3.07358000
O	-1	3.72473600	-2.47535800	1.72353400
O	-1	0.09483700	-9.09991900	1.47570200
O	-1	-1.02610700	-7.30258100	1.86093000
N	0	1.71771700	-5.64349300	1.80765400
C	0	3.13962500	-5.33624500	2.38077600
C	0	2.63219100	-4.14987900	3.19871800
C	-1	3.77939100	-6.54285600	3.09743400
C	0	1.20905300	-4.42316100	2.63601000
C	-1	2.55633800	-7.48333500	2.82903500
C	-1	1.40186500	-7.04480800	2.10807100
C	-1	3.48809400	-2.85922300	3.06382600
C	-1	4.09411300	-6.32786800	4.56735200
C	-1	4.86675100	-3.13482900	3.66682500
C	-1	0.08172400	-7.79688700	1.84161600
H	-1	3.76495000	-5.07157300	1.57085900
H	-1	2.58484000	-4.39143500	4.28425600
H	-1	4.68754300	-6.94193700	2.58158700
H	-1	2.97024600	-2.02622700	3.59999000
H	-1	4.37307800	-7.26556300	5.06441600
H	-1	4.92333600	-5.61131400	4.69088800
H	-1	3.22950500	-5.90434500	5.10586200
H	-1	5.56219300	-3.51969400	2.90940800
H	-1	5.30594300	-2.23101800	4.08969200
H	-1	4.82846800	-3.88819900	4.47251800
H	-1	2.87235600	-2.35896700	1.31844700
H	-1	-0.79978100	-9.37150500	1.29060300
N	0	-0.05550000	0.07324400	2.91133600
H	-1	-0.91468300	-0.34106400	3.21799500
C	0	0.34966800	-0.22120000	1.57806100
H	-1	0.82349400	0.64867600	1.11962300
C	-1	1.42545800	-1.37318200	1.45960200
H	-1	1.99376900	-1.22304000	0.52385500
H	-1	2.15066000	-1.14671300	2.26605900

S	0	0.69711000	-2.95922200	0.86192200
H	0	1.45198100	-3.87670100	-0.26460600
C	0	-0.93979400	-0.43099100	0.72922300
O	0	-2.01826400	-0.40233300	1.28060800
O	0	1.62604500	-5.06703500	-0.64287400
H	0	0.80271400	-5.35607600	-1.07356500
H	0	1.64423500	-5.43966100	0.42499600
C	0	2.73760000	-8.98752200	3.05648600
C	0	3.30019300	-9.48238800	4.41689000
C	0	3.77780700	-9.58152800	2.03175900
H	0	1.77790700	-9.47548000	2.89470700
H	0	2.82965400	-10.45775000	4.64102000
H	0	3.09283700	-8.82291100	5.26125700
C	0	4.85484500	-10.28088400	2.88571700
H	0	3.28648600	-10.28061300	1.35073500
H	0	4.22222100	-8.79095300	1.42063000
H	0	4.63535600	-11.36184900	2.95772600
N	0	4.74117100	-9.60273600	4.18314200
H	0	5.21247500	-10.11348900	4.92756300
H	0	5.86484300	-10.16828100	2.47671300

Compound 6 (TS Coordinate)

0 1
N	0	2.43367500	-6.52887600	1.44291700
C	0	3.93374700	-6.59846400	1.26380300
C	0	4.04278400	-5.15322500	1.76688500
C	0	2.59708500	-5.13199200	2.29225500
H	-1	4.36465800	-6.57051800	0.22666700
H	-1	4.32826900	-4.88622700	2.75245700
N	0	0.06476100	-0.45786300	2.48974900
H	-1	-0.78677700	-0.89086400	2.77499800
C	0	0.46908800	-0.80651800	1.13032000
H	-1	0.95140000	0.09887600	0.67662500
C	-1	1.55336500	-1.92298200	1.01660600
H	-1	2.12167600	-1.77284100	0.08085900
H	-1	2.27856500	-1.69651200	1.82306300
S	0	1.26172700	-3.92746900	1.39631000
H	0	1.25859200	-4.84964500	0.00460600
C	0	-0.83293300	-0.95648500	0.27720600
O	0	-1.89812100	-0.87950300	0.84591300
O	0	1.06193300	-5.80268500	-0.64227100
H	0	0.25563600	-6.31160000	-0.69801600
H	0	1.82294400	-6.33192800	0.34715900
C	0	1.73280000	-7.68643000	2.01469800
C	0	1.85749200	-8.92189900	1.36732000
C	0	0.98112400	-7.57056400	3.17823800
C	0	1.25716300	-10.03619500	1.94459500
H	0	2.43381500	-9.03261300	0.44786500
C	0	0.43344200	-8.71425500	3.75120900
H	0	0.84704100	-6.58996800	3.62080500
C	0	0.55951000	-9.97035200	3.15699200
C	0	4.46739600	-2.77253600	1.25694600
C	0	5.35597700	-2.12701500	0.29478500

C	0	5.15527200	-4.39223300	-0.31005000
C	0	5.91615700	-3.16524700	-0.46084000
N	0	4.29911400	-4.13344400	0.78564300
O	0	5.23285000	-5.42323200	-0.96420200
O	0	4.05129100	-2.34631200	2.31442400
C	0	7.20738300	-3.12514100	-0.89882600
H	0	7.66870500	-4.01000300	-1.32998800
C	0	5.93061000	-0.85677500	0.26369700
H	0	5.38576500	0.02459900	0.59987800
C	0	7.28730600	-0.82041100	-0.06656200
H	0	7.88627000	0.08340700	0.03655800
N	0	9.12871200	-2.39437200	0.29864700
C	0	7.91416400	-2.04074200	-0.36649500
C	0	-0.04768100	-11.19855400	3.75942100
H	0	-0.94228700	-11.50627100	3.20202900
H	0	0.65328900	-12.04143700	3.73981600
H	0	-0.34367800	-11.02981400	4.80060100
H	0	-0.11730200	-8.62073200	4.68399800
F	0	1.35849100	-11.22523500	1.31666700
C	0	4.68650000	-7.67400000	2.00239800
C	0	5.29314900	-8.71400800	1.27888400
C	0	4.80484800	-7.67740600	3.39878200
C	0	5.94355500	-9.74181900	1.96922500
C	0	5.44857500	-8.71407600	4.06824400
H	0	4.37032300	-6.84278700	3.94324000
C	0	6.01407700	-9.76953300	3.35337500
H	0	5.10124900	-7.99479600	-0.49608300
H	0	5.51052600	-8.70313500	5.15549500
H	0	6.51985100	-10.59312200	3.85326200
H	0	6.00656300	-10.96338900	0.44980000
O	0	6.56341800	-10.80106600	1.23263700
O	0	5.28854800	-8.84580700	-0.08283900
C	0	7.90566800	-10.55420700	0.74368800
H	0	7.89418100	-10.00170300	-0.19483600
O	0	9.45371100	-3.68489800	-0.10395600
H	0	10.40217700	-3.66181700	-0.25672100
O	0	8.55520500	-2.76932900	1.56710100
H	0	9.20081400	-2.44590900	2.20522400
H	0	8.46445800	-10.08478600	1.54649600
O	0	2.68948400	-5.02350800	3.56081600

ΔE = 1.76 eV ΔE = 1.75 eV ΔE = 1.09 eV

ZINC03784242 ZINC03808351 ZINC03788344

ΔE = 1.27 eV ΔE = 1.53 eV ΔE = 0.23 eV

ZINC03791246 ZINC02462884 ZINC02475683
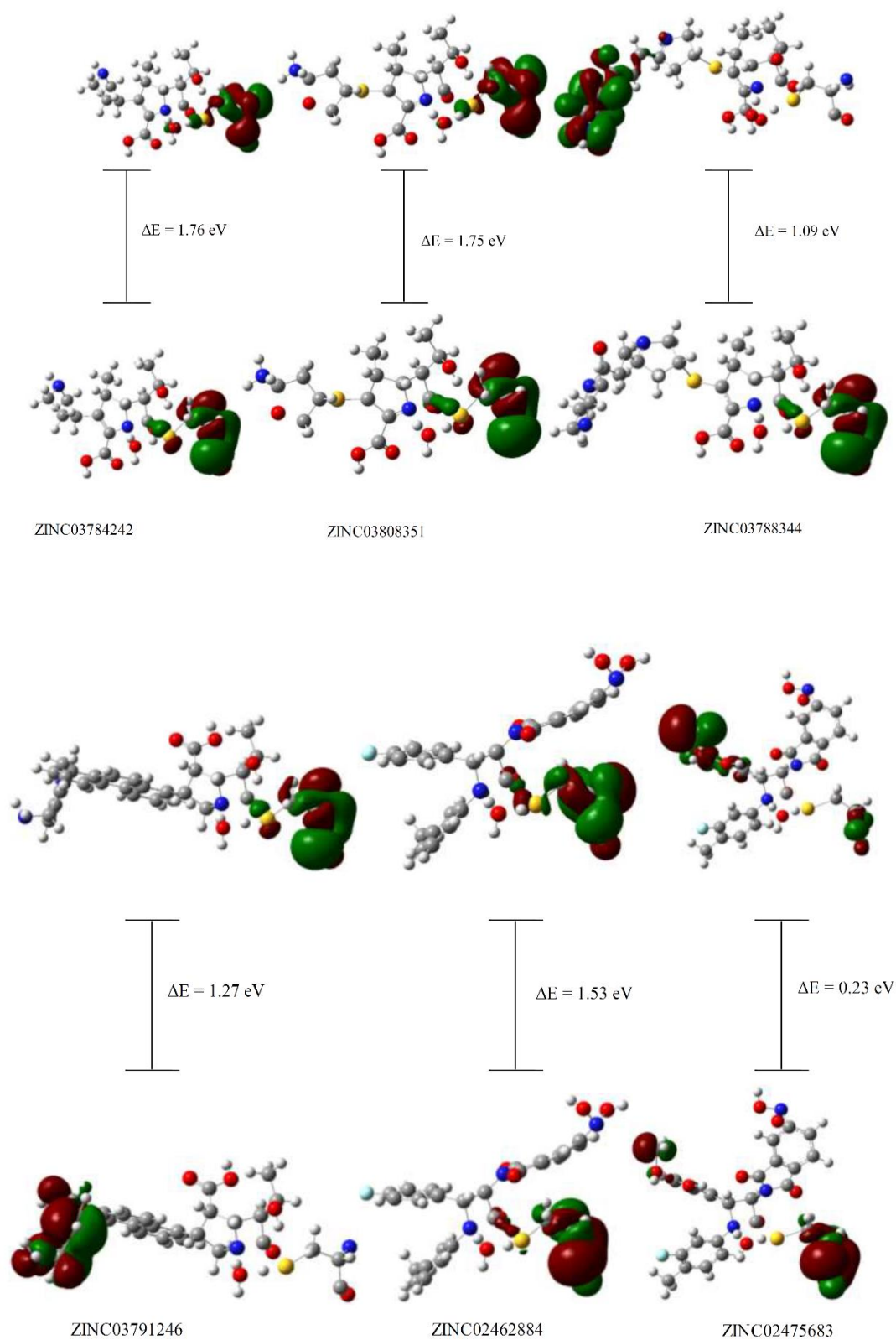
Figure S3. The frontier molecular orbital (FMO) representing the LUMO-HOMO orbitals for 6-membered ring mechanisms obtained using TDDFT/6-311++G(2d,2p). The energy difference between LUMO and HOMO (energy gap) is represented in eV.

Table S1. Energetic parameters for the 6-membered ring mechanism obtained using TDDFT/6-311++G(2d,2p). The energy gap is represented in eV.

Compounds	E_{HOMO} (eV)	E_{LUMO} (eV)	ΔE_{gap} (eV)
1	-5.39	-4.3	1.09
2	-5.85	-4.32	1.53
3	-5.32	-4.05	1.27
4	-5.83	-4.08	1.75
5	-5.46	-3.7	1.76
6	-4.19	3.96	0.23